Dissertations and Theses

6-2020

Development of a State-Space Aeroelastic Model of a Flexible T-Tail Aircraft for Flutter Analysis

Patrick S. Downs

DEVELOPMENT OF A STATE-SPACE AEROELASTIC MODEL OF A

FLEXIBLE T-TAIL AIRCRAFT FOR FLUTTER ANALYSIS

By

Patrick S. Downs

A Thesis Submitted to the Faculty of Embry-Riddle Aeronautical University

In Partial Fulfillment of the Requirements for the Degree of

Master of Science in Aerospace Engineering

June 2020

Embry-Riddle Aeronautical University

Daytona Beach, Florida

DEVELOPMENT OF A STATE-SPACE AEROELASTIC MODEL OF A FLEXIBLE T-TAIL AIRCRAFT FOR FLUTTER ANALYSIS

By

Patrick S. Downs

This Thesis was prepared under the direction of the candidate's Thesis Committee Chair and Co-Chair, Dr. Richard Prazenica and Professor Glenn Greiner, Department of Aerospace Engineering, and has been approved by the members of the Thesis Committee. It was submitted to the Office of the Senior Vice President for Academic Affairs and Provost, and was accepted in partial fulfillment of the requirements for the degree of Master of Science in Aerospace Engineering.

THESIS COMMITTEE

Richard J. Prazenica
Digitally signed by Richard J. Prazenica
Date: 2020.06.04 00:54:21 -04'00'

Chairman, Dr. Richard Prazenica

Prof. Glenn P. Greiner
Digitally signed by Prof. Glenn P. Greiner
Date: 2020.06.04 15:42:31 -04'00'

Co-Chairman, Professor Glenn Greiner

Hever Moncayo
Digitally signed by Hever Moncayo
Date: 2020.06.04 14:00:29 -04'00'

Member, Dr. Hever Moncayo

Dr. Magdy S. Attia
Digitally signed by Dr. Magdy S. Attia
Date: 2020.06.04 16:29:44 -04'00'

Graduate Program Coordinator,
Dr. Magdy Attia

6/4/2020

Date

Dean of the College of Engineering,
Dr. Maj Mirmirani

6/5/2020

Date

Christopher Grant
Digitally signed by Christopher Grant
Date: 2020.06.08 08:32:38 -04'00'

Associate Provost of Academic Support,
Dr. Christopher Grant

6/8/2020

Date

ACKNOWLEDGMENTS

ABSTRACT

Flutter prediction is an important part of the preliminary design process of any new aircraft. Current analysis methods include coupled fluid structure interaction codes and doublet lattice panel codes. The computation resources and time required for CFD solutions makes them unattractive for preliminary design and doublet lattice models require considerable pre and post processing to provide satisfactory results. Thus, a process for developing an analytical model to facilitate rapid design changes and the implementation of active control systems is the main motivation of this thesis. An analytical model is developed by first deriving the equations of motion of the structure for unforced vibration. Then the generalized aerodynamic forcing functions for incompressible, compressible subsonic, and supersonic flow are derived. Next, Roger's Approximation is used to form a state-space model that describes the forced vibration of the system. The results of the normal mode calculations show that the process used to model the T-tail can accurately predict the unforced vibrational characteristics of the system. The flutter results show that the process developed in this thesis yields a conservative estimation of the flutter dynamic pressure while still capturing the behavior of the transonic dip.

TABLE OF CONTENTS

LIST OF FIGURES

LIST OF TABLES

SYMBOLS

μ	mass ratio
h	plunge (bending) deflection
α	pitch (torsion) angular deflection
β	control surface angular deflection
L	aerodynamic lift force
K_α	airfoil pitching stiffness
K_h	airfoil plunging stiffness
K_β	airfoil control surface stiffness
M_α	aerodynamic pitching moment
M_β	aerodynamic hinge moment
b	airfoil semi-chord length
a	non-dimensional distance from mid-chord to the elastic axis
x_w	non-dimensional distance from mid-chord to the airfoil center of mass
e	non-dimensional distance from mid-chord to the flap break
c	non-dimensional distance from mid-chord to the hinge line
x_β	non-dimensional distance from mid-chord to the flap center of mass
p	local static pressure
p_∞	freestream static pressure
γ	ratio of specific heats
w	piston velocity
a_∞	freestream speed of sound
ρ_∞	freestream density

U_∞ freestream velocity

M Mach number

q dynamic pressure

k reduced frequency

ω circular frequency

$C(k)$ Theodorsen's Function

NOMENCLATURE

AC   Advisory Circular

AIAA   American Institute of Aeronautics and Astronautics

DOF   Degree of Freedom

CG   Center of Gravity

CFR   Code of Federal Regulations

CR   Contractor Report

EA   Elastic Axis

FAA   Federal Aviation Administration

HL   Hinge Line

HT   Horizontal Tail

LE   Leading Edge

NACA   National Advisory Committee for Aeronautics

NASA   National Aeronautics and Space Administration

SHM   Simple Harmonic Motion

TE   Trailing Edge

TM   Technical Manual

TR   Technical Report

VT   Vertical Tail

1. Introduction

Aeroelasticity is defined as the the study of the interaction between aerodynamic forces and structural forces. Aeroelastic effects can be broken down into static phenomena and dynamic phenomena. A.R. Collar (1978) introduced the triangle of forces as a way to show how different engineering disciplines overlap to form the study of aeroelasticity. Figure 1.1 shows the aeroelastic triangle of forces, with the study of dynamics, fluid mechanics, and structural mechanics combined to form the study of aeroelasticity.

Dynamics
Inertial Forces

Dynamic Stability

Mechanical Vibrations

Aeroelasticity
Flutter and Buffetting

Fluid Mechanics
Aerodynamic Forces

Divergence

Structural Mechanics
Elastic Forces
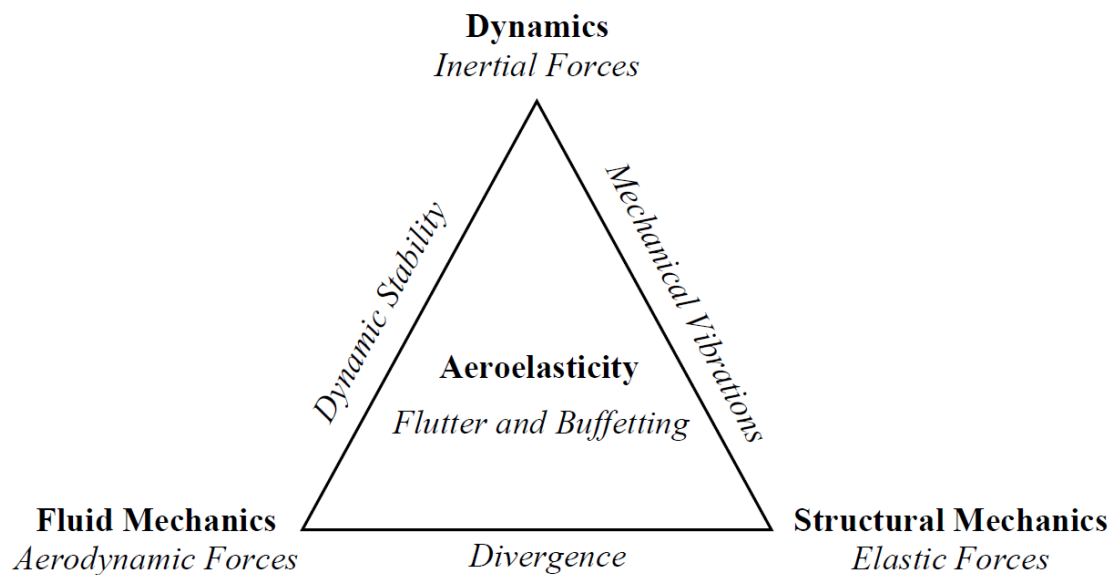
Figure 1.1 The Aeroelastic Triangle of Forces (Palazzo, 2017)

Some examples of static aeroelastic phenomena are divergence and control reversal. Dynamic aeroelastic phenomena include flutter and buffeting. Flutter is a self-excited, dynamic instability in which structural oscillations become out of phase with oscillatory airloads, meaning the airflow is adding energy into the system rather than acting as a source of damping. As the airspeed increases, the inherent damping of the structure is not able to remove all of the energy being added and the system becomes neutrally stable. The

airspeed that corresponds to the neutrally stable system is known as the flutter speed. When the flutter speed is exceeded, the oscillations diverge and can lead to structural failure.

Aeroelastic phenomena such as flutter were observed in aircraft as early as the 1917 Handley Page 0/400 bomber of World War I (WWI). The elevators oscillated 180 degrees out of phase with each other, causing violent tail oscillations. While there are documented observations of flutter occurring in these aircraft, aeroelasticity only became an important consideration in the design process of an aircraft in the early stages of World War Two (WWII) (Bisplinghoff, Ashley, & Halfman, 1996).

1.1. Motivation

In 1977, Mykytow presented the theory of the transonic flutter dip. As an aircraft approaches the speed of sound, the flutter speed begins to decrease. This decrease in flutter speed is exacerbated by an increase in mass ratio. As the flight speed surpasses Mach 1, the flutter speed begins to increase (Mykytow, 1977). Figure 1.2 shows the non-dimensional flutter velocity parameter versus the Mach number for a swept wing with varying mass ratios. The region above the curves is unstable and the region below the curves is free from flutter. This illustrates the phenomenon where a dip occurs in the transonic region at or near the speed of sound. Aeroelastic phenomena such as flutter become more prevalent in high-speed aircraft configurations due to the transonic dip, as well as other characteristics common to high speed aircraft such as thin and flexible structures. When analyzing the aeroelastic response of a typical commercial aircraft, the focus is primarily on the lifting surfaces; most commercial aircraft have long, slender, high aspect ratio wings, while the fuselage diameter is large, usually providing a higher bending and torsional stiffness compared to the wing. Supersonic aircraft wings have a much lower

$$\frac{V_{\cos \Lambda}}{b \omega_\alpha \sqrt{\mu}}$$
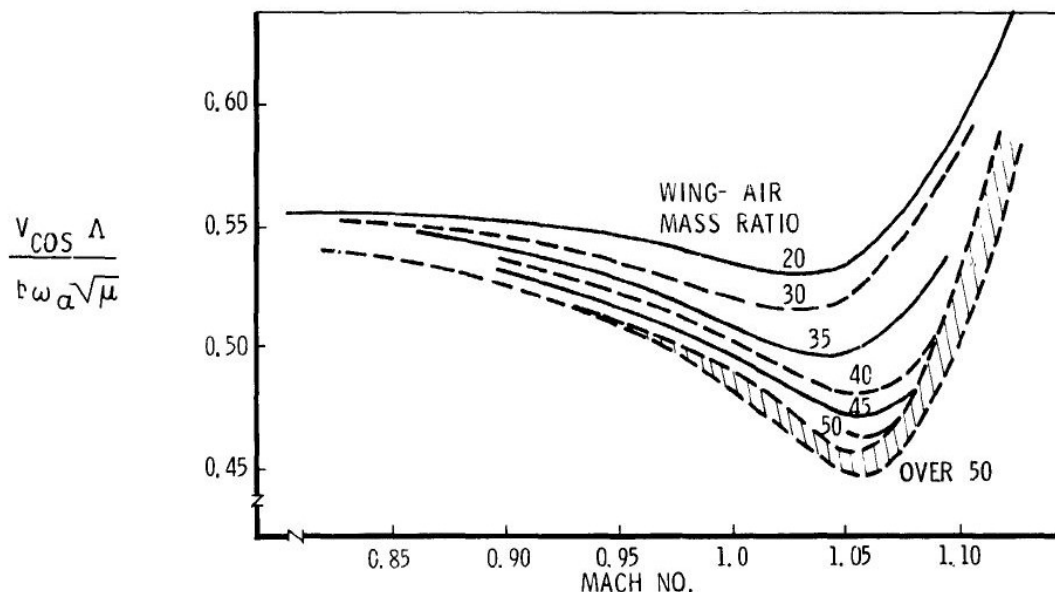
Figure 1.2 Transonic Dip (Mykytow, 1977)

aspect ratio and the application of the area rule results in reduced fuselage stiffness, thereby reducing its structural frequencies. As a result, body bending and torsion are important considerations in aeroelastic analysis of a supersonic aircraft.

To design a flutter-free airframe, the structure must be adequately stiff or balance masses must be added, both of which have an associated weight penalty. If an active control system is used to provide stability, it is possible that the weight of the airframe could be reduced. Active controls add artificial stiffness to the system such that the flutter speed is increased. Reduction in structural weight can provide improvements in performance such as reduced fuel consumption, increased range, and longer endurance.

In the current environment, aeroelastic stability design requirements for commercial aircraft are governed by 14 CFR 25.629 and AC 25.629-1B. These airworthiness regulations state: "the airplane must be designed to be free from aeroelastic instability for all design conditions within the stability aeroelastic stability envelope", (FAA, 1992). The

aeroelastic stability envelope is defined in 14 CFR 25.629. The Federal Aviation

Administration (FAA) permits the use of control systems to improve aeroelastic stability as

long as the actuation system continuously provides at least the minimum stiffness or

damping required to show aeroelastic stability (FAA, 1992). Other methods of flutter

prevention include mass balancing, changing the stiffness of the structure, using hydraulic

dampers, and implementing tailored composite structures to change bending

characteristics (Ramsey, 2006).

Active flutter suppression systems have been demonstrated in a variety of different

flight tests. In the early 1970s, a B-52 was retrofitted with extra control surfaces, external

stores, and ballasts to reduce the flutter speed for use in the Control Configured Vehicle

(CCV) program. The B-52CCV program showed the ability of an active control system to

control flutter modes, maneuver loads, and stability augmentation. However, one

important distinction is that the flutter instability of the B-52CCV was considered mild to

moderate, where the decline in damping is very gradual with increasing speed. In 1977, a

study of a German F-4F using its own control surfaces showed that structural

non-linearities affect the performance of the control law (Livne, 2018).

1.2. Objectives

The main objective of this research is to develop a state-space aeroelastic model of a

supersonic T-tail passenger jet configuration for rapid flutter estimation in a preliminary

design environment. An analytical model is developed by first deriving the equations that

describe the structural dynamics of the system, and then developing the aerodynamic

forcing functions for three different speed regimes: incompressible, compressible

subsonic, and supersonic. The aerodynamic forces are derived using Theodorsen's

method, Possio's integral equations using acceleration potential doublets, and first-order

Piston Theory, respectively.

To determine the flutter speed, the aerodynamic loads are adapted to a system whose

displacement is a superposition of its normal modes of vibration. The bending, torsional,

and rotational influence coefficients are calculated using Euler-Bernoulli beam theory and

unit load analysis. Flomenhoft's matrix iteration method is used to determine the

approximate coupled frequencies and mode shapes. These are then used to develop a

system of mass, stiffness, and damping matrices. Next, the two dimensional aerodynamic

loads are integrated over the lifting surfaces providing the three-dimensional aerodynamic

forces and moments. Finally, Roger's Approximation is used to determine a rational

function approximation of the airloads so that an eigenvalue solution can be used to

determine the flutter speed.

An MSC Nastran model is created to validate the normal modes and frequencies of the

structure on the ground, as well as, the open loop flutter frequencies and mode shapes. The

implementation of such an analysis allows for rapid design changes, as well as, real time

simulation of open-loop and closed-loop flutter characteristics. This model will be used to

compare the results from the matrix iteration process and eigenvalue solution with the

Nastran output, which is a commonly used tool in the aerospace industry.

The remainder of this thesis is organized as follows: Chapter 2 presents the relevant

literature in each of the areas of study; Chapter 3 presents the physical system being

analyzed; Chapter 4 derives the flexibility influence coefficients for the empennage,

discusses the process for finding the normal modes using matrix iteration, and formulates

the homogeneous equations of motion; Chapter 5 derives the incompressible,

compressible subsonic, and supersonic aerodynamic forces to utilize Roger's

Approximation; Chapter 6 shows the common solution methods used in aeroelastic

analysis and how they are applied to this problem formulation; Chapter 7 presents the

comparison of the results of the analytical models to the Nastran model; and Chapter 8

provides the conclusion and recommendations.

   This research focuses on the aft portion of the aircraft, as there exists very little

literature on the modeling and analysis of tail flutter while wing flutter is relatively well

understood. Figure 1.3 shows the workflow for modeling and analyzing the tail flutter of a

supersonic T-tail passenger jet.
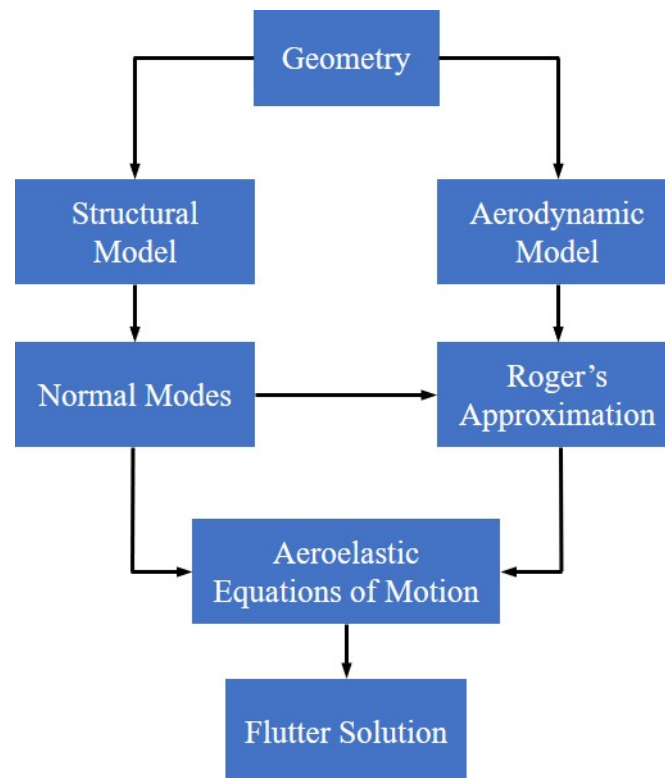
Figure 1.3 Modeling Workflow

The geometric properties are are used to define the structural model which is then solved

to determine the normal modes of vibration. The geometric properties are also used to

calculate the generalized aerodynamic forcing functions which are then used in combination with normal modes to develop a rational function approximation of the airloads. Once the rational function approximation is determined, a system of N equations is defined that represent the forced vibration of the aircraft. Once the aeroelastic equations of motion are known, an eigenvalue flutter solution was used to determine the flutter speed.

This research utilizes existing knowledge in: unforced vibration of one-dimensional structures; unsteady aerodynamics of an aeroelastic typical section; rational function approximations of unsteady aerodynamic loads; and eigenvalue analysis. The new contributions include: the application of Bernoulli-Euler beam bending to calculate the flexibility influence coefficients of a three-dimensional structure; the use of matrix iteration to calculate the normal modes of a three-dimensional structure; using Possio's integral equation for find three-dimensional aerodynamic loads; the derivation of three-dimensional, three degree-of-freedom unsteady supersonic aerodynamic loads using Piston Theory.

2. Literature Review

This chapter reviews the literature in several key areas of relevance to this thesis: the equations of motion of a tapered beam, the generalized aerodynamic forces for subsonic and supersonic flow, the fundamentals of aeroelastic modeling, and solutions methods for the flutter determinant.

2.1.   Beam Equations of Motion

Bisplinghoff, Ashley, and Halfman (1996) present the use of Euler-Bernoulli beam deflection theory to derive the matrix of flexibility influence coefficients for a tapered beam. The bending influence coefficients for a uniform cantilevered beam are defined as displacement and rotation of a given point on the beam due to a unit load or unit moment applied to another point on the beam. The procedure can be applied to a tapered beam by treating it as a finite number of uniform sections, each with different mass and stiffness properties.

The use of matrix iteration to determine uncoupled mode shapes and frequencies is also discussed by Bisplinghoff et al. (1996). However, the matrix iteration method was originally presented by Flomenhoft (1950) who theorized that the determination of mode shapes and frequencies can be reduced to an eigenvalue problem. The solution to the eigenvalue problem is further discussed by Clough and Penzien (2010) who state that a sweeping matrix process can be used to determine the first four or five modes (p. 267).

Scanlan and Rosenbaum (1968) show the process for deriving a system of mass, stiffness, and damping matrices. The typical section equations of motion of a pitch-plunge-flap airfoil are extended into three dimensions by weighting the section properties by the mode shapes and then integrating over the semi-span. This gives the

mass, stiffness, and damping matrices for a three dimensional lifting surface. The three

dimensional aerodynamic forces are found using a similar process (Scanlan & Rosenbaum,

1968).

2.2.   Generalized Aerodynamic Forces

In 1936, Theodorsen first presented the solution of an oscillating airfoil in

incompressible flow in NACA TR 496. Theodorsen developed the equations for unsteady

aerodynamic forces using potential flow theory satisfying the Kutta condition. The

velocity potentials were divided into circulatory flow potentials and non-circulatory flow

potentials. The non-circulatory contributions satisfy the flow tangency condition while the

circulatory flow potentials satisfy the Kutta condition (Theodorsen, 1936).

This work was expanded upon by Theodorsen and Garrick (1942) in NACA TR 736 to

include an aerodynamically balanced flap. Around the same time, Küssner and Schwartz

independently derived their own solution pertaining to the airfoil-flap problem, which is

published in NACA TM 991 (Kussner & Schwarz, 1941). Both works describe the

aerodynamic forces and moments for a typical section in terms of T-functions in NACA

TR 736 and Küssner functions in NACA TM 991.

Smilg and Wasserman (1942) expanded on the works of Theodorsen, Garrick,

Küssner, and Schwartz and applied them to an airfoil-flap system with an unsealed gap.

An assumption of simple harmonic motion was applied so the equations can be

represented in terms of complex coefficients that are a function of reduced frequency

(Smilg & Wasserman, 1942).

Compressible, subsonic, unsteady flow is discussed by Bisplingohff et. al. (1996)

through the use of kernel functions to solve Possio's integral equation. In NASA

CR-148019, Edwards mentions the use of kernel function codes to solve the hyperbolic

partial differential equation for perturbation velocity potential (Edwards, 1977). Bland

(1982) presents a computational solution for Possio's integral equation using three

different kernel functions.

In 1956, Ashley and Zartarian created Piston Theory, a method used to derive the

airloads for an airfoil oscillating in supersonic flow. Piston Theory treats the airfoil surface

as the head of a piston that oscillates within a fluid slab and generates isentropic pressure

waves. The pressure waves are integrated over the surface of the airfoil to determine the

unsteady aerodynamic forces acting on the airfoil in supersonic flow (Ashley & Zartarian,

1956).

Karpel (1982) discusses the use of rational function approximations (RFAs) to model

unsteady aerodynamic loads in the Laplace domain so the system can subsequently be

modeled in the time domain. Roger and Hodges (1975) outline the use of common

denominator coefficients in rational function approximations to reduce the number of lag

states. The use of rational function approximations eliminates the assumption of simple

harmonic motion in the solution of the aeroelastic equations. This method provides the

frequency and damping of the oscillations at each airspeed, whereas a solution method like

the k-method flutter solution is only valid at the flutter speed.

2.3.   Aeroelastic Modeling

Bisplinghoff et al. (1996) outline the basics of aeroelastic modeling using matrix

differential equations. A two dimensional airfoil is presented, the structural equations of

motion and the quasi-steady airloads are derived, and the flutter determinant is presented.

Fung (2008) gives a similar, numerical example for finding the flutter speed of a two

dimensional airfoil using the k-method solution. Scanlan and Rosenbaum (1968) show a

method to extend the two-dimensional flutter problem to represent a three-dimensional

wing in incompressible flow.

2.4. Flutter Determinant

Edwards summarizes four of the most common methods to solve the flutter

determinant for the flutter speed and how to formulate the equations of motion for each

solution type. The four solution methods for aeroelastic equations are the p-method,

k-method, pk-method, and the augmented states method (Edwards, 1977). Fung (2008)

shows in detail how the equations for the k-method flutter solution are derived and a

numerical example is provided. The k-method assumes the system is oscillating with

simple harmonic motion and the flutter determinant is solved for a range of reduced

frequencies. The p-method assumes an eigenvalue solution of the form $p = \gamma + ik$. The

pk-method assumes the structural dynamics have a p-method type solution and the

aerodynamics have a k-method type solution.

Karpel (1981) shows how to apply rational function approximations to develop a root

locus type solution to the flutter determinant. Using rational function approximations

allows for direct computation of airloads at a given reduced frequency and Mach number.

Therefore, the frequency of each point on the root locus is valid for all airspeeds at the

given Mach numbers (Karpel, 1981).

3. Aeroelastic System

The geometry that is analyzed in this research is a generic T-tail aircraft with a long, narrow fuselage and low aspect ratio wings. The global coordinate system is a standard aircraft model axis system with the origin at the nose, positive X_G pointing aft and positive Y_G out the starboard side. The elastic analysis for the empennage is carried out in a body fixed frame whose origin is fixed at the rear spar of the wing and the centerline of the fuselage with positive X pointing aft and positive Y out the right wing. Figure 3.1 shows the global coordinate frame and the body fixed frame.
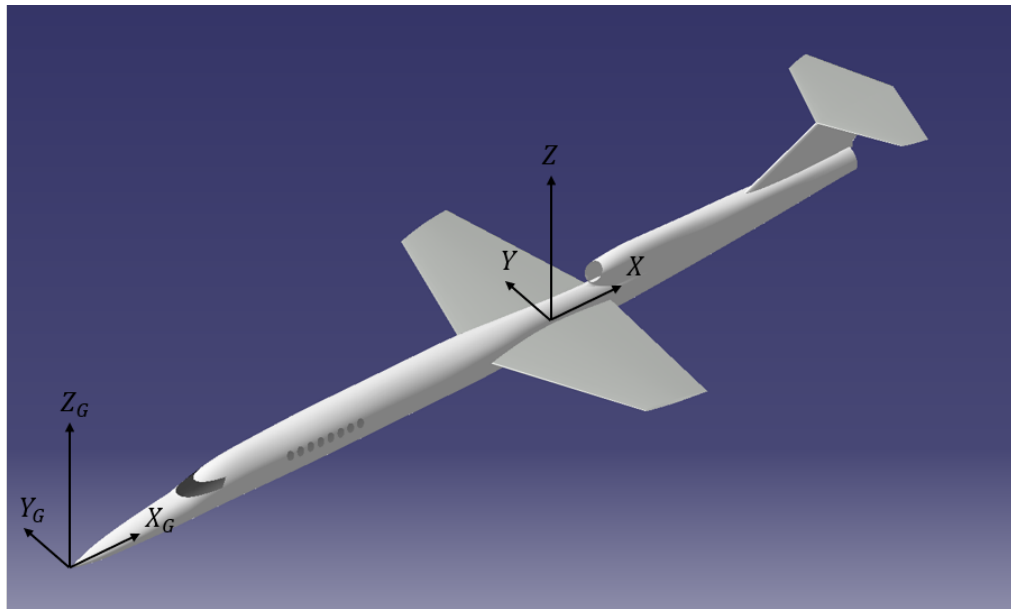
Figure 3.1 Axis System Definitions

Throughout this thesis, all forces, moments, and deflections referring to a point on the fuselage are denoted by a subscript F. All forces, moments, and deflections referring to a point on the vertical tail are denoted by a subscript V. All forces, moments, and deflections referring to a point on the starboard (right) side of the horizontal tail are denoted by a subscript HS. All forces, moments, and deflections referring to a point on the port (left) side of the horizontal tail are denoted by a subscript HP. In Nastran, the empennage

structure is idealized as a series of straight beams, cantilevered at the rear spar of the

aircraft. The fuselage is treated as a constant cross section beam while the lifting surfaces

are treated as tapered beams. Figure 3.2 shows the idealized model in the Nastran work

space. The triangular symbols represent the lumped masses of the model and the structure
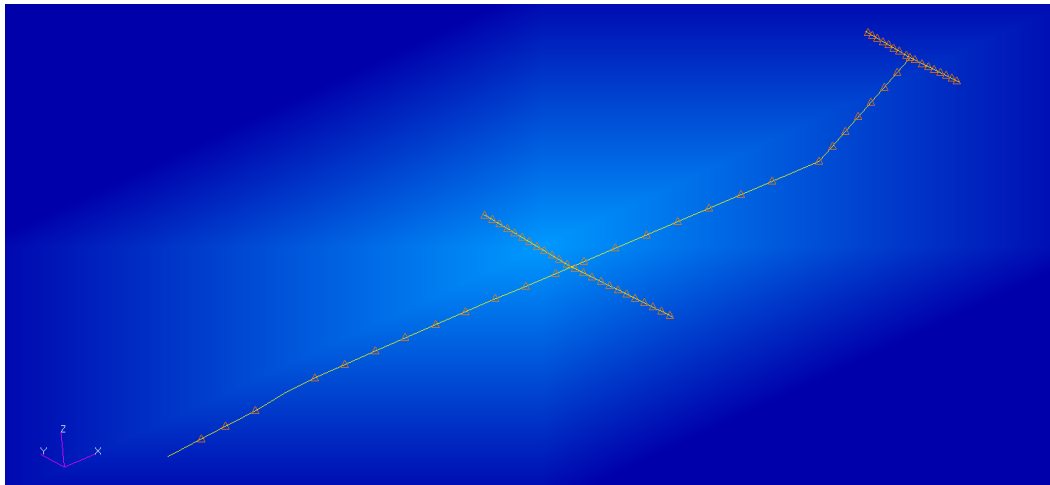
Figure 3.2 Idealized Structural Stick Model

is built using tapered beam elements. When analyzing the tail modes, the model is reduced

to the aft fuselage and empennage fixed in space. Figure 3.3 shows the tail structural stick
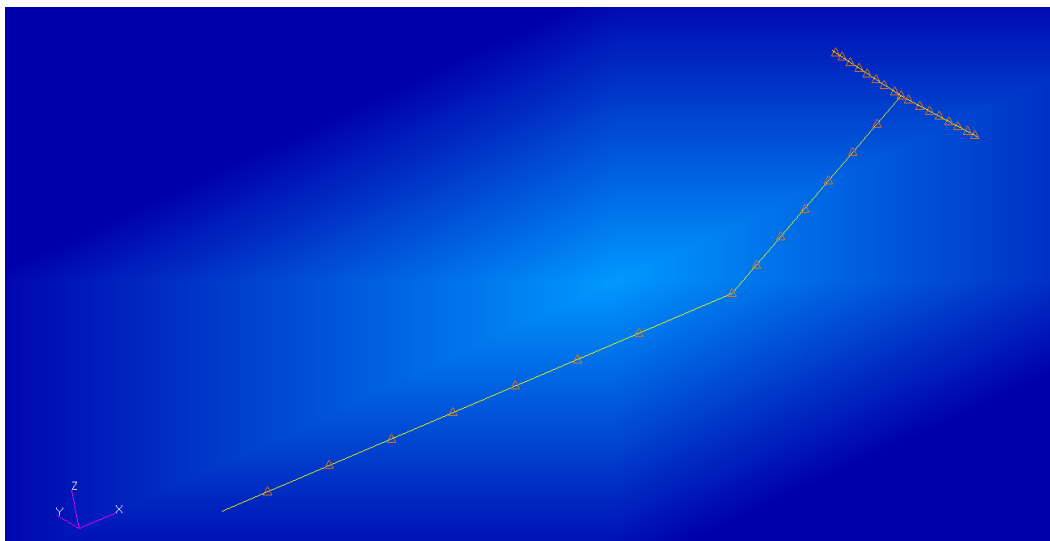
model.

Figure 3.3 Tail Structural Stick Model

The input data used to build the structural model are given in Table 3.1.

Table 3.1

Fuselage Model Data

N	Weight	X	Y	Z	I_{xx}	I_{yy}	I_{zz}
-	(lb_f)	(in)	(in)	(in)	(in^4)	(in^4)	(in^4)
1	0.0	1112.9	0.0	112.0	79410.5	41461.1	37949.4
2	1443.0	1177.3	0.0	112.0	79410.5	41461.1	37949.4
3	1524.0	1265.8	0.0	112.0	79410.5	41461.1	37949.4
4	1537.5	1354.2	0.0	112.0	79410.5	41461.1	37949.4
5	1527.5	1442.7	0.0	112.0	79410.5	41461.1	37949.4
6	1492.6	1531.2	0.0	112.0	79410.5	41461.1	37949.4
7	1299.1	1619.7	0.0	112.0	79410.5	41461.1	37949.4
8	1181.1	1708.2	0.0	112.0	79410.5	41461.1	37949.4
9	892.5	1841.0	0.0	112.0	79410.5	41461.1	37949.4

The values of X, Y, and Z are the coordinates of the lumped mass in the global coordinate system and the area moments of inertia I_{xx}, I_{yy}, and I_{zz} are given in the Nastran beam axis system. The data used to build the structural model of the vertical tail are given in Table 3.2. The data used to build the structural model of the starboard horizontal tail are given in Table 3.3.

The mass of the structure is reduced to a series of points along the elastic axis that have mass, moments of inertia, and static moments representative of the three-dimensional structure. For the left side of the horizontal tail, the data given in Table 3.3 are used changing Y to a negative value. For the vibrational analysis of the empennage, the model is assumed to be fixed in space at the origin of the body fixed coordinate frame. From here, the flexibility influence coefficients are derived.

Table 3.2

Vertical Tail Model Data

N	Weight	X	Y	Z	I_{xx}	I_{yy}	I_{zz}
-	(lb_f)	(in)	(in)	(in)	(in^4)	(in^4)	(in^4)
1	0.0	1841.0	0.0	112.00	283381.1	4767.41	94606.9
2	579.0	1880.1	0.0	134.57	283381.1	4767.41	94606.9
3	375.3	1919.2	0.0	157.14	249442.5	4246.39	84945.3
4	257.3	1958.3	0.0	179.71	219900.9	3791.18	76479.2
5	193.0	1997.4	0.0	202.29	194032.3	3390.33	68988.8
6	115.5	2036.5	0.0	224.86	171145.4	3032.86	62265.0
7	117.9	2075.6	0.0	247.43	150719.9	2710.72	56155.1
8	53.6	2114.7	0.0	270.00	132242.9	2415.91	50508.2

Table 3.3

Starboard Horizontal Tail Model Data

N	Weight	X	Y	Z	I_{xx}	I_{yy}	I_{zz}
-	(lb_f)	(in)	(in)	(in)	(in^4)	(in^4)	(in^4)
1	0.0	2114.7	0.0	270.0	32827.1	1402.5	81172.9
2	224.6	2115.2	16.1	270.0	29483.9	1252.3	70447.0
3	140.1	2116.2	42.8	270.0	21053.1	877.31	45730.9
4	102.3	2116.9	64.2	270.0	16655.6	684.6	34601.7
5	80.1	2117.7	85.7	270.0	11529.1	463.8	23867.0
6	66.7	2118.5	107.1	270.0	8914.1	353.9	19684.9
7	55.6	2119.3	128.5	270.0	6819.6	276.2	17209.6
8	35.6	2120.1	149.9	270.0	4480.6	170.9	15685.7
9	11.1	2120.7	166.0	270.0	3881.0	146.9	15565.6

The MSC Nastran model is used to validate the normal modes and flutter modes of the
system. MSC Nastran is a commonly used tool in the aerospace industry for static and
dynamic aeroelastic analysis. Nastran employs a conventional finite element structural
solver in conjunction with an aerodynamic panel method solver. The aerodynamic model

employs doublet-lattice aerodynamics for subsonic flows and a variety of different methods for supersonic flight. The most commonly used supersonic method is the ZONA51, which uses the doublet-lattice panel model. Since the panel model is a linear flat plate solution, Navier-Stokes solvers can be used to determine the pressure and lift curve slope of the true wing, which can then be mapped to the aerodynamic panels for improved fidelity. A Nastran aeroelastic model is composed of an elastic structural model and an aerodynamic panel model that are splined together. Splines are used to interpolate between the motion of the structure and the motion of the aerodynamic panels. MSC Nastran treats the structural DOFs as independent and the aerodynamic DOFs as dependent. Figure 3.4 shows the aeroelastic model used for validation.
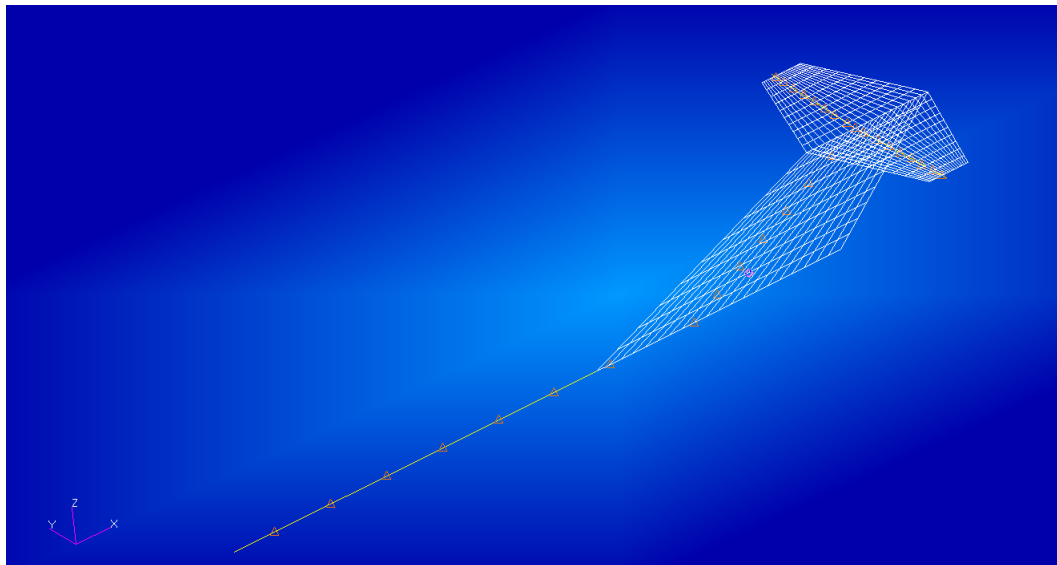
Figure 3.4 Nastran Aeroelastic Model

For analysis in Nastran, it was assumed that the elastic axis of the vertical tail was at 40% of the chord along its entire span. In addition, it was assumed that the flap was 20% of the mass of that strip and the flap chord length was 25% of the airfoil chord length. Table 3.4 gives the data used to create the panel model of the vertical tail.

Table 3.4

Vertical Tail Aerodynamic Model Data

N	b	a	x_w	c	x_β
-	(*in*)	-	-	-	-
1	130.0	-0.2	0.2	0.5	0.55
2	125.1	-0.2	0.2	0.5	0.55
3	120.3	-0.2	0.2	0.5	0.55
4	115.4	-0.2	0.2	0.5	0.55
5	110.6	-0.2	0.2	0.5	0.55
6	105.7	-0.2	0.2	0.5	0.55
7	100.9	-0.2	0.2	0.5	0.55
8	96.0	-0.2	0.2	0.5	0.55

Table 3.5 gives the data used to create the aerodynamic model for the left and right sides of

the horizontal tail.

Table 3.5

Horizontal Tail Aerodynamic Model Data

N	b	a	x_w	c	x_β
-	(*in*)	-	-	-	-
1	96.0	-0.2	0.2	0.5	0.55
2	89.7	-0.2	0.2	0.5	0.55
3	79.1	-0.2	0.2	0.5	0.55
4	70.7	-0.2	0.2	0.5	0.55
5	62.2	-0.2	0.2	0.5	0.55
6	53.7	-0.2	0.2	0.5	0.55
7	45.3	-0.2	0.2	0.5	0.55
8	36.9	-0.2	0.2	0.5	0.55
9	30.5	-0.2	0.2	0.5	0.55

Nastran has the capability to perform k-method and pk-method flutter solutions. A common approach to Nastran flutter analysis is determining the pk-method flutter solution for a specified Mach number for a range of altitudes, which provides different densities and speeds of sound.

Throughout this thesis, the derivations refer to "segments" of structure. A segment is defined as length of the structure with constant structural and geometric properties. The mass properties given in Tables 3.1, 3.2, and 3.3 are representative of the centroid of the segment. The geometric data, which was used in the computation of the aerodynamic loads, was calculated using the centroid of each segment as a reference point.

4. Structural Dynamics

The following section outlines the process used to develop the system dynamic equations of motion for the aft fuselage and empennage of a T-tail aircraft. The aft fuselage is assumed to be fixed in space. To develop the equations of motion for a three dimensional flutter problem, a number of simplifications are required. Since a three dimensional continuous structure has an infinite number of degrees of freedom, the flutter mode is represented by an infinite series of normal modes, neglecting aerodynamic damping and stiffness (Scanlan & Rosenbaum, 1968). The dynamics of a finite span wing are determined by first deriving the equations of motion for an oscillating flat plate and then using strip theory to extend the results into three dimensions. The same can be said for the aft fuselage and empennage of an aircraft.

The first step in determining the structural dynamics of the tail is understanding the dynamics of an airfoil-flap section that is elastically restrained in space. For this, a typical aeroelastic wing section is used to define the common nomenclature and sign conventions. Then, the three degree-of-freedom equations of motion are derived using Lagrange's Equations.

Next, the method of influence coefficients is used to determine the global bending, torsion, and bending-torsion coupling effects using influence coefficients for the T-tail geometry. The Bernoulli-Euler beam bending theorem is used to determine the bending influence coefficients of the structure due to an applied load. Strain energy is used to find the torsional deformation of the structure due to an applied moment. The bending-torsion coupling influence coefficients are also found using the Bernoulli-Euler beam bending theorem.

Then, matrix iteration is used to find the coupled frequencies and mode shapes of the tail. The calculated modes are then used to find the equations of motion for the structure, as well as, derive the three-dimensional aerodynamic forcing functions used in the flutter analysis. For this analysis, Lagrange's Equations take the form:

$$\frac{d}{dt}\left(\frac{\partial \mathcal{L}}{\partial \dot{\xi}_i}\right) - \left(\frac{\partial \mathcal{L}}{\partial \xi_i}\right) = Q_i \qquad (4.1)$$

where $\mathcal{L}$ is the Lagrangian of the system, ξ_i are the generalized coordinates, and Q_i are generalized non-conservative forces or moments. The Lagrangian $\mathcal{L}$ is defined as the difference between the kinetic energy T of the system and the potential energy V of the system.

$$\mathcal{L} = T - V \qquad (4.2)$$

Since the kinetic energy of the system is purely dependent on generalized rates and the potential energy is purely dependent on generalized displacements, Equation (4.1) can be written as,

$$\frac{d}{dt}\left(\frac{\partial T}{\partial \dot{\xi}_i}\right) + \left(\frac{\partial V}{\partial \xi_i}\right) = Q_i \qquad (4.3)$$

The results of applying Lagrange's Equations are N linear differential equations that can be written in matrix form and reduced to the form of a mass-spring-damper system. The eigenvalues of the homogeneous equations of motion correspond to the normal modes of the aircraft aft fuselage and empennage in the absence of aerodynamic effects. These modes are known as the "on ground" modes and will match the output from the matrix iteration solution.

4.1. Airfoil Dynamics

Understanding the dynamics of a typical aeroelastic section is vital when deriving the equations of motion for a more complex system. Theodorsen (1936) introduced the typical section in NACA TR-496. He presented the solution to the unsteady aerodynamic forcing functions of a flat plate oscillating in incompressible, inviscid flow (Theodorsen, 1936). The typical section defines the common nomenclature and sign conventions for aeroelastic analysis. Theodorsen's original derivation was for a flat plate with a flap that rotates about its leading edge. Smilg and Wasserman (1942) extended Theodorsen's work to include a flap with an unsealed gap. The typical section is used as the reference section in aeroelastic problems much like the mean geometric chord is taken as the reference section for classical aerodynamic problems. The typical section is most commonly chosen to be located at 75% of the semispan of the lifting surface. Figure 4.1 shows the typical section in its local coordinate frame.
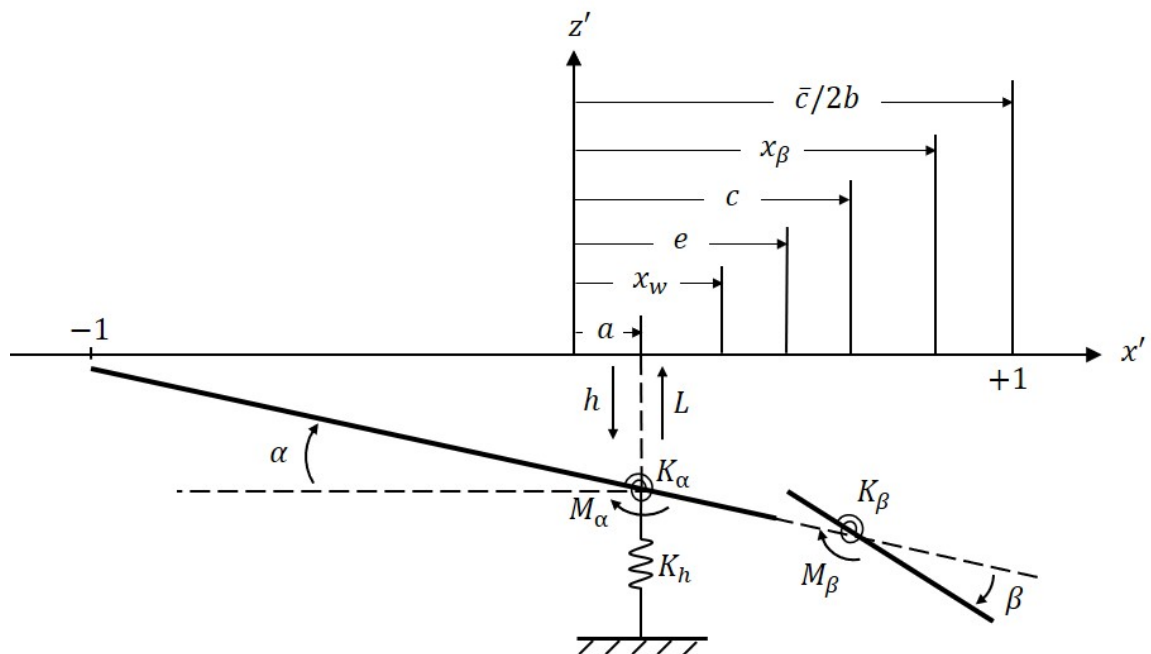
Figure 4.1 Flat Plate Typical Section with Unsealed Gap

The origin of the typical section is at the midchord such that the leading edge is $-b$ in the negative x' direction and the trailing edge is b in the positive x' direction. All of the lengths in Figure 4.1 are non-dimensionalized with the semichord b. The non-dimensional parameters in Figure 4.1 are listed below:

a = the non-dimensional distance from the origin to the elastic axis

x_w = the non-dimensional distance from the origin to the center of gravity of the wing-flap system

e = the non-dimensional distance from the origin to the flap break point

c = the non-dimensional distance from the origin to the hinge line

x_β = the non-dimensional distance from the origin to the center of gravity of the flap

The typical section is fixed in space with a spring such that it is free to oscillate in the z' direction. A spring is fixed to the typical section at its elastic axis and is used to simulate structural bending stiffness, describing its plunging motion. The airfoil is also constrained in rotation by a torsional spring such that it can oscillate in pitch about its elastic axis. This spring is used to simulate structural torsional stiffness. The flap is connected to the wing section with a torsional spring such that it can oscillate about the hinge line. This spring is used to simulate the stiffness of the actuation device. The K_α is the pitching stiffness about the elastic axis, K_h is the plunging stiffness, and K_β is the flap stiffness about the hinge line.

A positive pitch angle α is defined as the angle the wing section makes with the horizontal when the leading edge is deflected upwards. Positive plunge h is defined in the negative z' direction. A positive flap deflection angle β is defined as the angle the flap makes with respect to the chord line of the wing section when the trailing edge is deflected downwards.

The position of a point on the wing section in the airfoil coordinate frame is given by,

$$z_w = -(h\,b) - b\,(x' - a)\,\alpha \tag{4.4}$$

The position of a point on the flap section in the airfoil coordinate frame is given by,

$$z_f = -(h\,b) - b\,(c - a)\,\alpha - b\,(x' - c)(\alpha + \beta) \tag{4.5}$$

The kinetic energy of the wing section is:

$$T_w = \int_0^{be} \rho_w(x')\,\dot{z}_w^2\,dx' \tag{4.6}$$

and the kinetic energy of the flap section is:

$$T_f = \int_{be}^{b} \rho_\beta(x')\,\dot{z}_f^2\,dx' \tag{4.7}$$

Then the total kinetic energy of the typical section is found by adding the kinetic energy of the wing section and flap section. This is found by substituting Equation (4.4) and Equation (4.5) into Equation (4.6) and Equation (4.7) respectively.

$$T_{total} = T_w + T_f \tag{4.8}$$

The potential energy is:

$$V = \tfrac{1}{2}K_h\,h^2 + \tfrac{1}{2}K_\alpha\,\alpha^2 + \tfrac{1}{2}K_\beta\,\beta^2 \tag{4.9}$$

The equations of motion for the typical section are most simply derived using Lagrange's

Equations, a process that is discussed in detail in the following section. The results of

applying Lagrange's Equations are three coupled second order differential equations as

follows:

$$mb\ddot{h} + S_\alpha\ddot{\alpha} + S_\beta\ddot{\beta} + K_h bh = -L \tag{4.10}$$

$$S_\alpha b\ddot{h} + I_\alpha\ddot{\alpha} + \left[I_\beta + S_\beta b(c-a)\right]\ddot{\beta} + K_\alpha\alpha = M_\alpha \tag{4.11}$$

$$S_\beta b\ddot{h} + \left[I_\beta + S_\beta b(c-a)\right]\ddot{\alpha} + I_\beta\ddot{\beta} + K_\beta\beta = M_\beta \tag{4.12}$$

where L is the section lift, M_α is the section pitching moment, and M_β is the section hinge

moment. These equations are the basis for deriving the aeroelastic equations of motion for

a three dimensional structure. The parameters in Equation (4.10) through Equation (4.12)

are calculated using the following integrals. The wing section mass per unit span is

defined as:

$$m'_w = \int_{-b}^{be} \rho_w(x')\, dx' \tag{4.13}$$

The wing static moment per unit span about the elastic axis is defined as:

$$S'_w = \int_{-b}^{be} b\,(x'-a)\rho_w(x')\, dx' \tag{4.14}$$

The wing section mass moment of inertia per unit span about the elastic axis is defined as:

$$I'_w = \int_{-b}^{be} b^2\,(x'-a)^2\rho_w(x')\, dx' \tag{4.15}$$

The flap section mass per unit span is defined as:

$$m'_\beta = \int_{be}^{b} \rho_\beta(x')\,dx' \tag{4.16}$$

The flap section static moment per unit span about the hinge line is defined as:

$$S'_\beta = \int_{be}^{b} b\,(x'-c)\,\rho_\beta(x')\,dx' \tag{4.17}$$

The flap section mass moment of inertia per unit span about the hinge line is defined as:

$$I'_\beta = \int_{be}^{b} b^2\,(x'-c)^2\,\rho_\beta(x')\,dx' \tag{4.18}$$

The flap section static moment per unit span about the elastic axis is defined as:

$$S'_f = \int_{be}^{b} b\,[(c-a)+(x'-c)]\rho_\beta(x')\,dx' \tag{4.19}$$

or,

$$S'_f = \int_{be}^{b} b\,(x'-a)\rho_\beta(x')\,dx' \tag{4.20}$$

The flap mass moment of inertia per unit span about the elastic axis is given by:

$$I'_f = \int_{be}^{b} b^2\,[(c-a)+(x'-c)]^2\rho_\beta(x')\,dx' \tag{4.21}$$

or,

$$I'_f = \int_{be}^{b} b^2\,(x'-a)\rho_\beta(x')\,dx' \tag{4.22}$$

The total typical section mass per unit span is given by:

$$m' = m'_w + m'_f \tag{4.23}$$

The total typical section static moment per unit span about the elastic axis is given by:

$$S'_\alpha = S'_w + S'_f \tag{4.24}$$

The total typical section mass moment of inertia per unit span about the elastic axis is given by:

$$I'_\alpha = I'_w + I'_f \tag{4.25}$$

4.2. Mode Shape Determination

The coupled frequencies and mode shapes of the structure are determined using the matrix iteration method for a lumped parameter system developed by Flomenhoft (1950). To determine the modes using this method, the flexibility influence coefficients of each structural component are required. Bisplinghoff, Ashley, and Halfman (1996) present the process for deriving the influence coefficients as they discuss the deformation of an elastic airplane under static loads. The following section outlines their method for determining the flexibility influence coefficients of an elastic airplane subjected to a combination of generalized forces. For an airplane, under the assumption that the structure is perfectly elastic, the deflections of the aircraft under static load can be represented by the linear system,

$$q = CQ \tag{4.26}$$

where Q is an applied force, C is a proportionality constant, and q are the resulting

deflections. Since the system is linear, superposition applies. This means the total

deflection of a given point can be written as the sum of deflections caused by the

individual forces and moments. Under the assumption of superposition, Q now represents

generalized forces and q represents generalized coordinates. Equation (4.26) can then be

written as a summation of n generalized forces weighted by their corresponding flexibility

influence coefficients, C_{ij}, as follows:

$$q_i = \sum_{j=1}^{n} C_{ij} Q_j \qquad (i = 1, 2, \cdots, n) \qquad (4.27)$$

Alternately, the forces can be expressed as functions of displacement by,

$$Q_i = \sum_{j=1}^{n} k_{ij} q_j \qquad (i = 1, 2, \cdots, n) \qquad (4.28)$$

where k_{ij} are known as stiffness influence coefficients. Equation (4.27) and Equation

(4.28) can be written in matrix notation as follows:

$$\{q\} = [C]\{Q\} \qquad (4.29)$$

$$\{Q\} = [k]\{q\} \qquad (4.30)$$

Thus, the stiffness influence coefficients and flexibility influence coefficients are related by

the following:

$$[k] = [C]^{-1} \qquad (4.31)$$

In most cases, finding the stiffness influence coefficients is a much more involved process

than that of finding the flexibility influence coefficients; thus determining the flexibility

influence coefficients is the more common method (Bisplinghoff et al., 1996).

The flexibility influence coefficients of a slender wing, as described by Bisplinghoff et

al. (1996), are found by applying a unit load and unit torque along the structure's elastic

axis at location η and measuring the response at location y. Figure 4.2 shows the variable

designations for a straight tapered wing. For a straight tapered wing with loads applied to
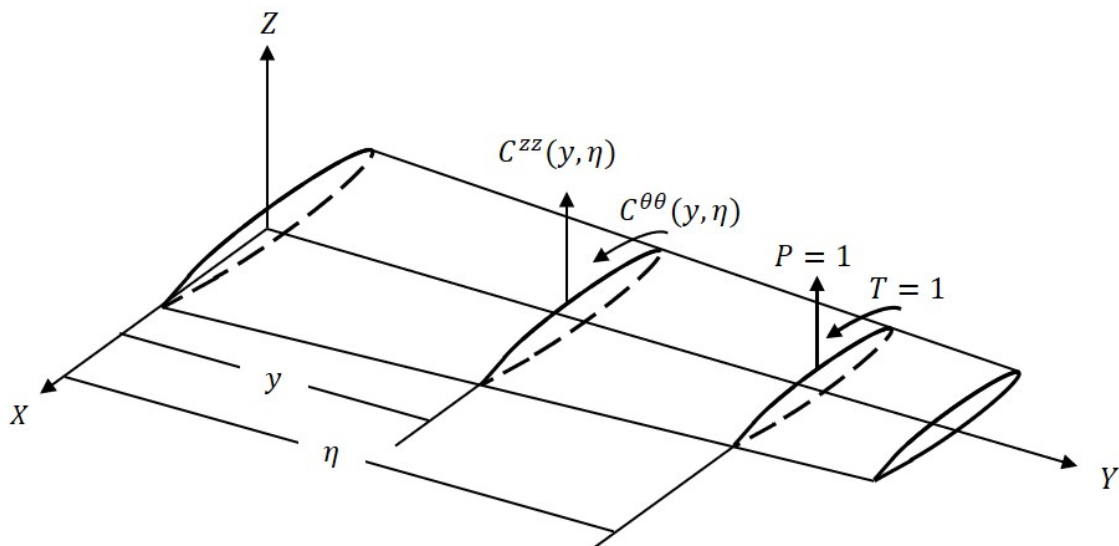
Figure 4.2 Straight Wing Subjected to Unit Load and Torque (Bisplinghoff et al., 1996)

the elastic axis, it is known that there i s no bending deflection due to an applied torque

and no torsion due to an applied point load. Therefore, the only influence coefficients that

need to be calculated are $C^{zz}(y,\eta)$ and $C^{\theta\theta}(y,\eta)$, where $C^{zz}(y,\eta)$ is the bending influence

coefficient at y due to a unit load at η and $C^{\theta\theta}(y,\eta)$ is the torsional influence coefficient at

y due to a unit torque at η. Bisplinghoff et al. derived the influence coefficients for a

straight tapered wing using strain energy. For the case of $\eta \geq y$, the bending influence

coefficients are:

$$C^{zz}(y,\eta) = \int_0^y \frac{(\eta - \lambda)(y - \lambda)}{EI} d\lambda + \int_0^y \frac{d\lambda}{GK} \qquad (\eta \geq y) \qquad (4.32)$$

and when $y \geq \eta$,

$$C^{zz}(y,\eta) = \int_0^\eta \frac{(\eta - \lambda)(y - \lambda)}{EI} d\lambda + \int_0^\eta \frac{d\lambda}{GK} \qquad (y \geq \eta) \qquad (4.33)$$

Next, the torsional influence coefficients are found. For the case of $\eta \geq y$, the torsional

influence coefficients are:

$$C^{\theta\theta}(y,\eta) = \int_0^y \frac{d\lambda}{GJ} \qquad (\eta \geq y) \qquad (4.34)$$

and when $y \geq \eta$,

$$C^{\theta\theta}(y,\eta) = \int_0^\eta \frac{d\lambda}{GJ} \qquad (y \geq \eta) \qquad (4.35)$$

where in Equation (4.32) through Equation (4.35), EI represents the bending stiffness of

the structure at location y, GJ represents the torsional stiffness, and GK represents the

shear stiffness of the structure at location y. In Equations. (4.32) and (4.33), the first

integral represents the deflection due to bending stress and the second integral represents

the deflection due to transverse shear stress.

While Equations (4.32) through (4.35) are useful for the analysis of a tapered wing,

more generality must be considered when investigating empennage flutter. The approach

used to derive the flexibility influence coefficients for the tail is the same as that of a wing.

For a straight, tapered beam with varying bending stiffness $EI(x)$, a force P applied at

location ξ will result in a deflection w and slope w' at location x. Figure 4.3 shows the

bending and slope at x due to a load at ξ. For a straight, tapered beam with varying
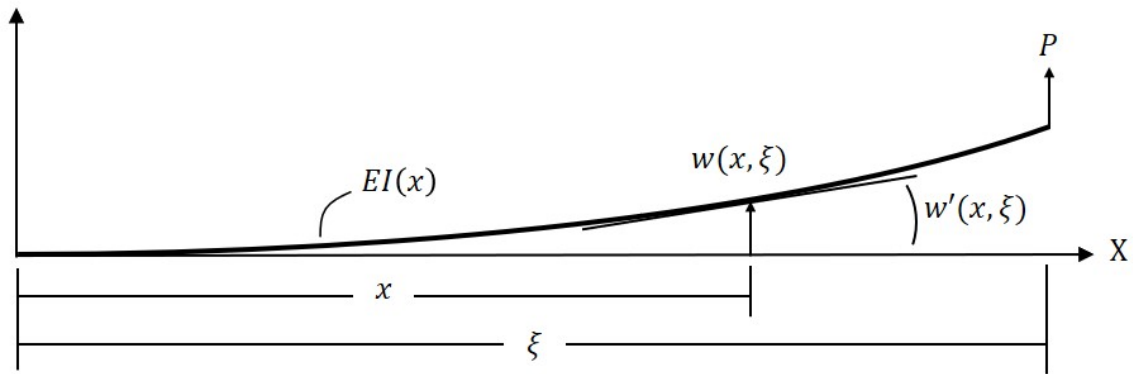
Figure 4.3 Displacement and Slope due to an Applied Load

torsional stiffness $GJ(x)$, a torque T applied at location ξ will result in a rotation θ at

location x. Figure 4.4 shows the rotation at x due to a torque at ξ. When determining the
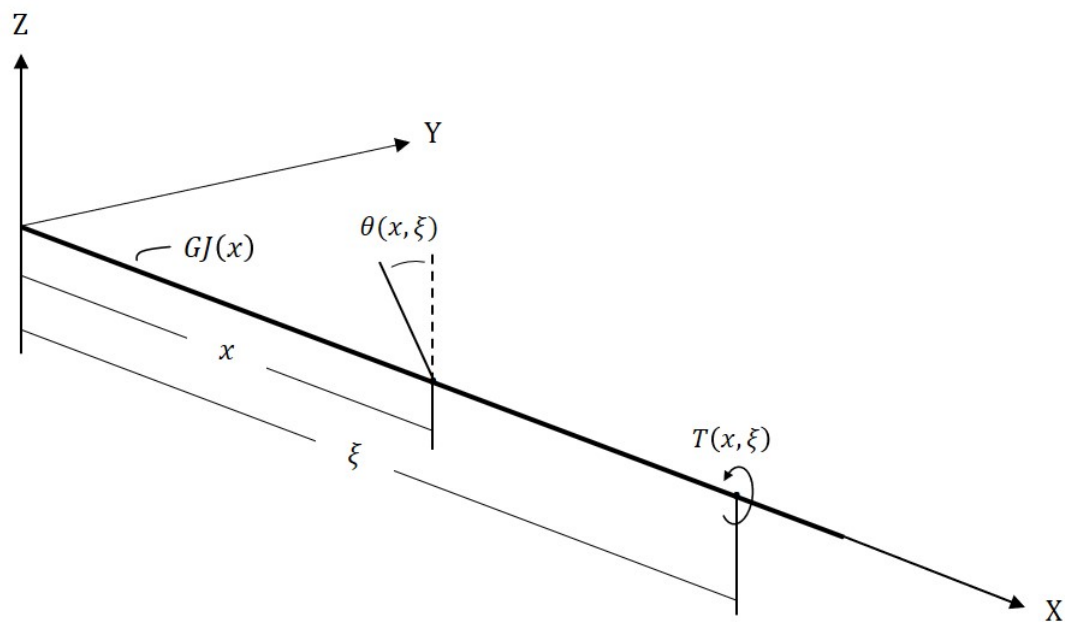
Figure 4.4 Rotation due to an Applied Torque

bending influence coefficients, Euler-Bernoulli beam theory is used. For simplicity, deformations due to shear are neglected and the relationship between bending deflection and applied moment becomes:

$$w''(x,\xi) = \frac{1}{EI(x)}M(x,\xi) \tag{4.36}$$

where $w''(x,\xi)$ is the second derivative of the deflection at point x due to a point load at ξ, $M(x,\xi)$ is the bending moment at point x due to a point load at ξ, and $EI(x)$ is the bending stiffness of the beam at point x. The angular rotation of that beam due to an applied torque is given by:

$$\theta'(x,\xi) = \frac{1}{GJ(x)}T(x,\xi) \tag{4.37}$$

where $\theta'(x,\xi)$ is the first derivative of the rotation of the beam at point x due to a torque applied at ξ, $T(x,\xi)$ is the torque applied to point ξ, and $GJ(x)$ is the torsional rigidity of the beam at point x.

In the following sections, the processes for deriving the influence coefficients for the fuselage, vertical tail, and horizontal tail are given. A subscript F will designate deflections or loads applied to the fuselage. A subscript V, HS, or HP will designate deflections or loads applied to the vertical tail, starboard horizontal tail, or port horizontal tail respectively. The numbers 1 through 6 indicate the direction of the deflection or applied load. Each number indicates the following:

1   Deflection or Load Applied in X Direction

2   Deflection or Load Applied in Y Direction

3   Deflection or Load Applied in Z Direction

4   Rotation or Moment Applied About the X Axis

5   Rotation or Moment Applied About the Y Axis

6   Rotation or Moment Applied About the Z Axis

Finally, the first subscript refers to the deflection or rotation and the second subscript refers to the applied load or moment. For example, C_{F_3,V_1} represents the deflection of the fuselage in the Z direction due to an applied load to the vertical tail in the X direction and C_{V_6,HS_2} represents the rotation of the vertical tail about the Z axis due to an applied load to the starboard horizontal tail in the Y direction.

Fuselage Influence Coefficients

The fuselage influence coefficients are determined by finding the deflections of the fuselage due to loads and moments applied to the fuselage, vertical tail, starboard horizontal tail, and port horizontal tail independently of one another. This is done by determining the bending and torsional moments that result from a point load and applying Equation (4.36) and Equation (4.37).

The deflections due to a load applied to the fuselage will be investigated. Two cases must be considered when formulating the moment: $\xi \geq x$ and $x > \xi$. Figure 4.5 shows the internal moment for the case of $\xi \geq x$.
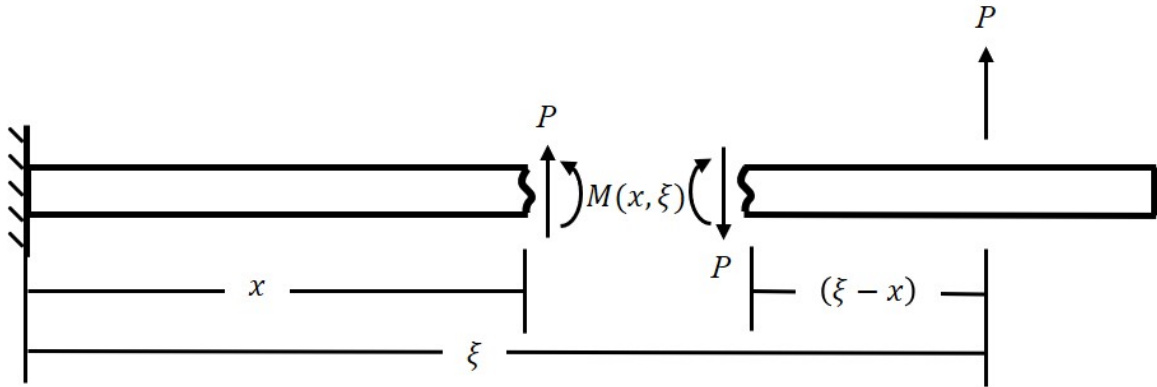
Figure 4.5 Bending Moment at x Due to an Applied Load at ξ

For this unit load case, the bending moment is:

$$M(x,\xi) = (1)(\xi - x) \tag{4.38}$$

which when substituted into Equation (4.36) gives:

$$w''(x,\xi) = \frac{1}{EI(x)}(\xi - x) \tag{4.39}$$

For simplicity, the bending stiffness is treated as constant along the domain of integration, a segment of the fuselage. Integrating once leads to the slope of the beam at point x due to a point load at ξ. This slope is given by:

$$w'(x,\xi) = \frac{1}{EI(x)}\left(\xi x - \tfrac{1}{2}x^2 + C_1\right) \tag{4.40}$$

where C_1 is a constant of integration that is determined by evaluating the slope at a boundary. Applying Equation (4.40) in the same way gives the rotational influence coefficients of the fuselage, which are useful in calculating the influence coefficients of the

vertical tail and horizontal tail. For fuselage bending in the Y direction, Equation (4.40) is written as:

$$C_{F_6,F_2}(x,\xi) = \frac{1}{EI_{zz}(x)}\left(\xi x - \tfrac{1}{2}x^2 + C_1\right) \tag{4.41}$$

For fuselage bending in the Z direction, Equation (4.40) is written as:

$$C_{F_5,F_3}(x,\xi) = -\frac{1}{EI_{yy}(x)}\left(\xi x - \tfrac{1}{2}x^2 + C_1\right) \tag{4.42}$$

Integrating the slope leads to the deflection of the beam at point x due to a point load at ξ. The deflection is given by:

$$w(x,\xi) = \frac{1}{EI(x)}\left(\tfrac{1}{2}\xi x^2 - \tfrac{1}{6}x^3 + C_1 x + C_2\right) \tag{4.43}$$

where C_2 is a constant of integration that is determined by evaluating the deflection at a boundary. Since Equations. (4.40) and (4.43) are only valid for beams with a constant flexural rigidity, a beam with varying section properties must be treated as a series of sections with constant properties where the slope and deflection are evaluated at the boundaries. Recall that the bending influence coefficients are defined as the deflection of the structure at point x due to a unit load applied at ξ. So, for fuselage bending in the Y direction, the bending influence coefficients are:

$$C_{F_2,F_2}(x,\xi) = \frac{1}{EI_{zz}(x)}\left(\tfrac{1}{2}\xi x^2 - \tfrac{1}{6}x^3 + C_1 x + C_2\right) \tag{4.44}$$

For fuselage bending in the Z direction, the bending influence coefficients are:

$$C_{F_3,F_3}(x,\xi) = \frac{1}{EI_{yy}(x)}\left(\tfrac{1}{2}\xi x^2 - \tfrac{1}{6}x^3 + C_1 x + C_2\right) \tag{4.45}$$

Next an applied torque is considered. Figure 4.6 illustrates the internal torsion resulting from an applied torque.
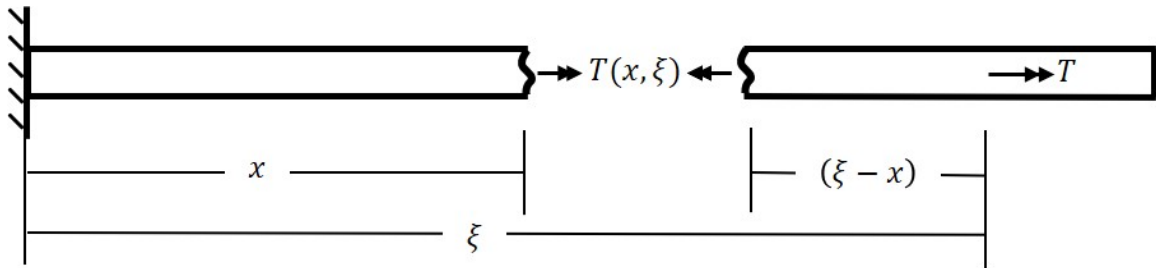
Figure 4.6 Torsion at x Due to an Applied Torque at ξ

For this case, the torsional moment is:

$$T(x,\xi) = 1 \tag{4.46}$$

For simplicity, the torsional stiffness is treated as a constant along the domain of integration. Then, for a constant torsional stiffness, Equation (4.37) becomes:

$$\theta'(x,\xi) = \frac{1}{GJ(x)}(1) \tag{4.47}$$

Integrating once gives the rotation of the fuselage at point x due to a unit torsion at ξ. This is expressed as,

$$\theta(x,\xi) = \frac{1}{GJ(x)}(x + C_1) \tag{4.48}$$

where C_1 is a constant of integration that is determined by evaluating the rotation of the

fuselage at the boundary. Therefore, the torsional influence coefficients of the fuselage are:

$$C_{F_4,F_4}(x,\xi) = \frac{1}{GJ(x)}(x+C_1) \tag{4.49}$$

Next, for the case of $x > \xi$, there is no bending moment at the location where the

displacement is being measured. Therefore,

$$M(x,\xi) = 0 \tag{4.50}$$

Then, Equation (4.36) becomes:

$$w''(x,\xi) = 0 \tag{4.51}$$

The slope is:

$$w'(x,\xi) = \frac{1}{EI}C_1 \tag{4.52}$$

and the deflection becomes,

$$w(x,\xi) = \frac{1}{EI}(C_1 x + C_2) \tag{4.53}$$

where C_1 and C_2 are again found by evaluating the slope and deflection at the boundary.

Then, for fuselage bending in the Y direction, the bending influence coefficients are:

$$C_{F_2,F_2}(x,\xi) = \frac{1}{EI_{zz}(x)}(C_1 x + C_2) \tag{4.54}$$

For fuselage bending in the Z direction, the bending influence coefficients are:

$$C_{F_3,F_3}(x,\xi) = \frac{1}{EI(x)}(C_1 x + C_2) \qquad (4.55)$$

For this case, the torsional moment is also zero when $x > \xi$,

$$T(x,\xi) = 0 \qquad (4.56)$$

Equation (4.37) becomes:

$$\theta'(x,\xi) = 0 \qquad (4.57)$$

and integrating shows that the rotation of the fuselage at point x due to a unit torsion at ξ is equal to a constant for the case of $x > \xi$. Expressed mathematically,

$$\theta(x,\xi) = C_1 \qquad (4.58)$$

Next, the fuselage deflections and slopes due to an applied moment about Y and Z are both considered for the case of $\xi > x$. In both cases,

$$M_y(x,\xi) = M_z(x,\xi) = 1 \qquad (4.59)$$

For a moment about the Y axis, Equation (4.36) gives:

$$C_{F_3,F_5}(x,\xi) = -\frac{1}{EI_{yy}(x)}\left(\xi x - \tfrac{1}{2}x^2 + C_1\right) \qquad (4.60)$$

and Equation (4.40) gives:

$$C_{F_5,F_5}(x,\xi) = \frac{1}{EI_{yy}(x)}(x+C_1) \tag{4.61}$$

For a moment about the Z axis, Equation (4.36) gives:

$$C_{F_2,F_6}(x,\xi) = \frac{1}{EI_{zz}(x)}\left(\xi x - \tfrac{1}{2}x^2 + C_1\right) \tag{4.62}$$

and Equation (4.40) gives:

$$C_{F_6,F_6}(x,\xi) = \frac{1}{EI_{zz}(x)}(x+C_1) \tag{4.63}$$

Although Equations (4.60) through (4.63) are not directly needed, their understanding is required in deriving the influence coefficients the vertical and horizontal tail have upon the fuselage.

To begin, the deflections of the fuselage due to a load on a segment of the vertical tail are considered. Applying a unit load to the vertical tail in the X direction (drag) results in a bending moment at fuselage station x that is equal to the difference in Z between the location where the load is applied and where the internal load is to be determined, represented by ζ. Figure 4.7 shows the moment generated at x due to a load in the X direction on a vertical tail segment. The resulting moment is:

$$M(z,\zeta) = \zeta(1) \tag{4.64}$$
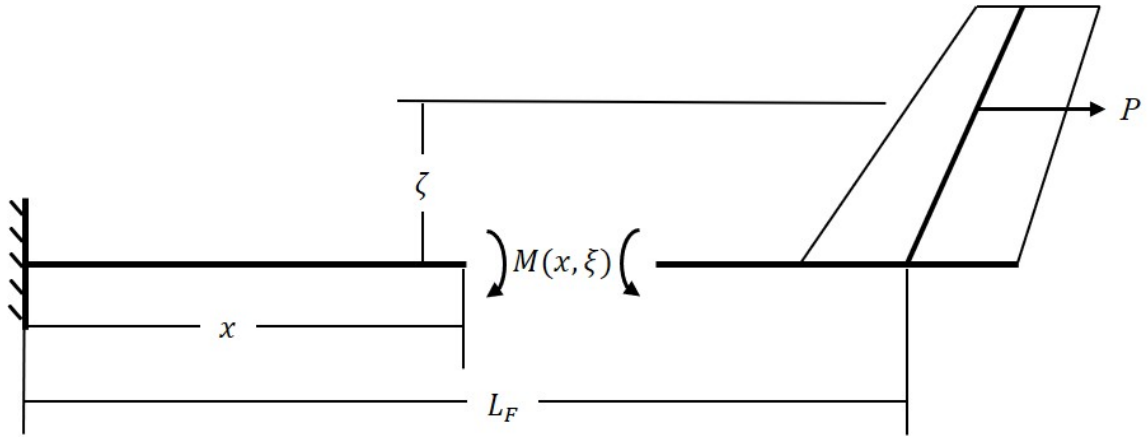
Figure 4.7 Bending Moment at x Due to an Applied P_x on a Vertical Tail Segment

The load is applied to the centroid of the vertical tail segment. Using Equation (4.36), the fuselage influence coefficients due to a load applied in the X direction on a vertical tail segment are:

$$C_{F_3,V_1}(x,z,\xi,\zeta) = -\frac{1}{EI_{yy}(x)}\left(\tfrac{1}{2}\zeta x^2 + C_1 x + C_2\right) \tag{4.65}$$

and the slope is:

$$C_{F_5,V_1}(x,z,\xi,\zeta) = \frac{1}{EI_{yy}(x)}\left(\zeta x + C_1\right) \tag{4.66}$$

Applying a unit load to the vertical tail in the Y direction (side force) results in a bending moment and torque at fuselage station x. The bending moment is equal to the difference in X between the location of the segment's applied load and where the displacement is to be measured; the torque is equal to the difference in Z between the location of the load and the center of rotation. Figure 4.8 shows the internal moment M_z and torque T that results from the applied load P. Then, from Equation (4.36) the bending influence coefficients are:

$$C_{F_2,V_2}(x,\xi) = \frac{1}{EI_{zz}(x)}\left(\tfrac{1}{2}\xi x^2 - \tfrac{1}{6}x^3 + C_1 x + C_2\right) \qquad (0 \le \xi \le L_f) \tag{4.67}$$
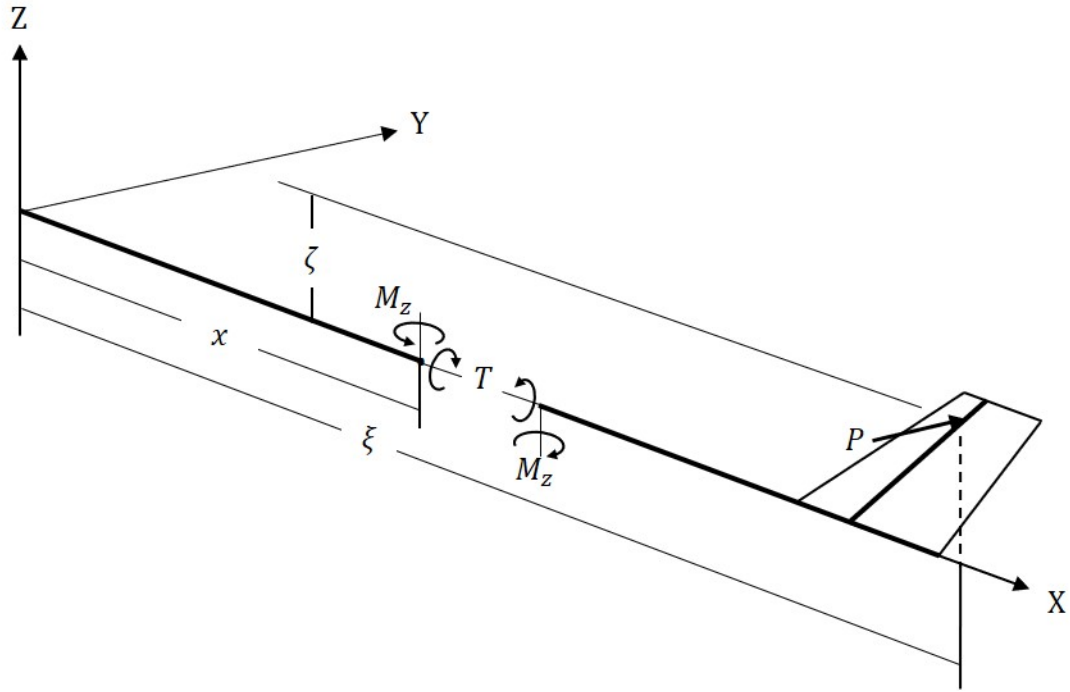
Figure 4.8 Bending Moment and Torque at x Due to an Applied P_y on a Vertical Tail Segment

and the rotational influence coefficients are:

$$C_{F_6,V_2}(x,\xi) = \frac{1}{EI_{zz}(x)}\left(\xi x - \tfrac{1}{2}x^2 + C_1\right) \qquad (0 \le \xi \le L_f) \qquad (4.68)$$

From Equation (4.37), the torsional influence coefficients are:

$$C_{F_4,V_2}(x,z,\xi,\zeta) = -\frac{1}{GJ(x)}(x+C_1)\zeta \qquad (0 \le \xi \le L_f) \qquad (4.69)$$

where ζ is the distance from the EA of the fuselage to the mid-chord of the vertical tail

segment. Applying a unit load to a vertical tail segment in the Z direction results in a

moment at fuselage station x that is equal to the difference in X between the location

where the load is applied and where the internal moment is to be determined. Figure 4.9

shows the internal moment that results from this applied load P.
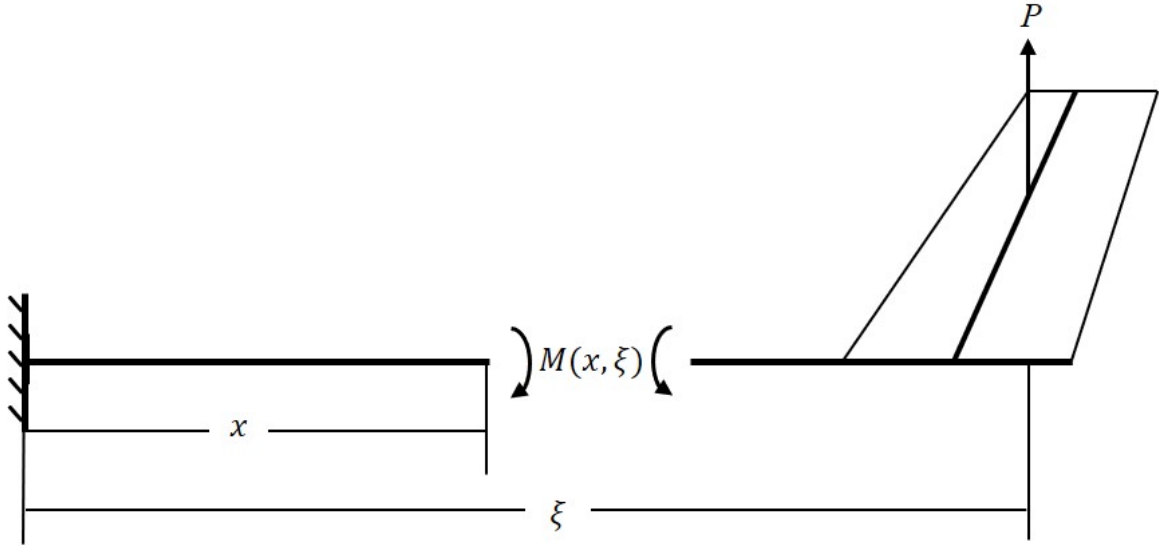
Figure 4.9 Bending Moment at x Due to an Applied P_z on a Vertical Tail Segment

Then, from Equation (4.36) the bending influence coefficients are:

$$C_{F_3,V_3}(x,\xi) = \frac{1}{EI_{yy}(x)}\left(\tfrac{1}{2}\xi x^2 - \tfrac{1}{6}x^3 + C_1 x + C_2\right) \tag{4.70}$$

and from Equation (4.40), the rotational influence coefficients are:

$$C_{F_5,V_3}(x,\xi) = -\frac{1}{EI_{yy}(x)}\left(\xi x - \tfrac{1}{2}x^3 + C_1\right) \tag{4.71}$$

Now, a torsional moment on the vertical tail is considered. Since the strips of the vertical

tail are aligned in the streamwise direction and not aligned with the swept axis, a VT

torsional moment is simply a moment about the Z axis. This means that the deflections

that result from a VT torsional moment are equivalent to the deflections from a moment

about the Z axis applied to the end of the fuselage. Therefore, the bending influence
coefficients are:

$$C_{F_2,V_6}(x,\xi) = C_{F_2,F_6}(x,L_F) \tag{4.72}$$

and the rotational influence coefficients are:

$$C_{F_6,V_6}(x,\xi) = C_{F_6,F_6}(x,L_F) \tag{4.73}$$

For the moment, it will be assumed that the vertical tail is rigid and the loads from the
horizontal tail are directly transported to the fuselage. Therefore, a load applied on a
starboard horizontal tail segment will influence the internal bending and torsional
moments at fuselage station x.

Applying a unit load in the X (drag) direction on the starboard side of a horizontal tail
segment results in a bending moment about the Y and Z axes of the fuselage. The internal
forces in the X direction are neglected since the fuselage is assumed to be rigid in the X
direction. Figure 4.10 shows the internal moments that result from this applied load P_x.
The resulting moment about the Z axis is:

$$M_z = -\eta(1) \tag{4.74}$$

where η is the Y location of the applied load. Then using Equation (4.36), the bending
influence coefficients are:

$$C_{F_2,HS_1} = -\frac{1}{EI_{zz}(x)}\left(\tfrac{1}{2}\eta x^2 + C_1 x + C_2\right) \tag{4.75}$$
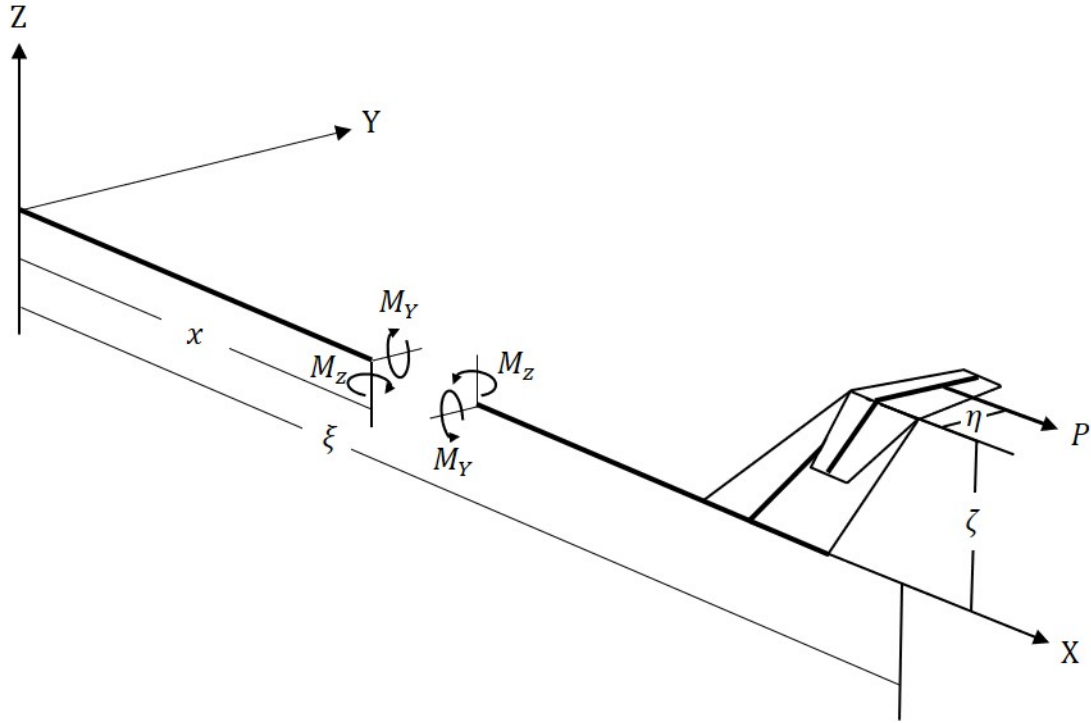
Figure 4.10 Fuselage Bending Moments at x Due to an Applied P_x on a Horizontal Tail Segment

and from Equation (4.40), the rotational influence coefficients are:

$$C_{F6,HS_1} = -\frac{1}{EI_{zz}(x)}(\eta x + C_1) \tag{4.76}$$

The resulting moment about the Y axis is:

$$M_Y = \zeta(1) \tag{4.77}$$

Using Equation (4.36), the bending influence coefficients are:

$$C_{F3,HS_1} = -\frac{1}{EI_{yy}(x)}\left(\tfrac{1}{2}\zeta x^2 + C_1 x + C_2\right) \tag{4.78}$$

and from Equation (4.40), the rotational influence coefficients are:

$$C_{F_5,HS_1} = \frac{1}{EI_{zz}(x)}(\zeta x + C_1) \tag{4.79}$$

Applying a unit load in the Y direction on the starboard side of a horizontal tail segment results in a bending moment about the Z axis and a torque about the X axis at fuselage station x. The consideration of this DOF is necessary to capture the kinetic energy of the HT when the tail is oscillating in the $X - Y$ plane. Figure 4.11 shows the internal moments that result from the applied load P_y.
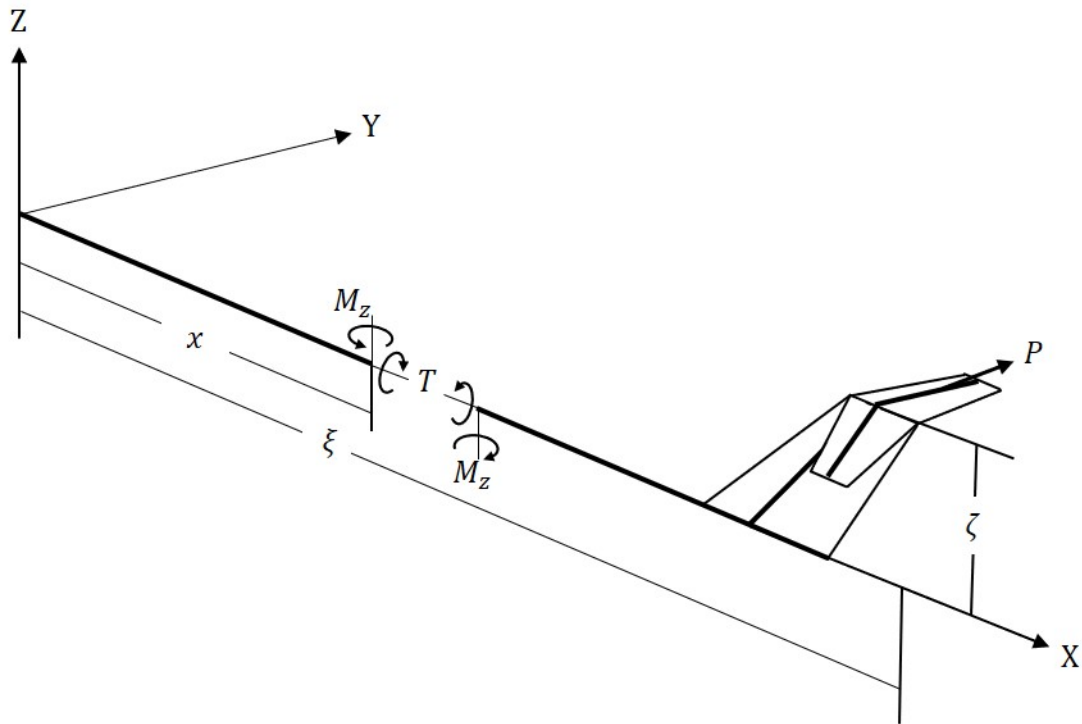
Figure 4.11 Fuselage Bending Moment and Torque at x Due to an Applied P_y on a Starboard Horizontal Tail Segment

The resulting moment about the Z axis is:

$$M_z = (1)(\xi - x) \qquad (0 \le \xi \ L_f) \tag{4.80}$$

Using Equation (4.36), the bending influence coefficients are:

$$C_{F2,HS_2}(x,\xi) = \frac{1}{EI_{zz}(x)} \left(\tfrac{1}{2}\xi x^2 - \tfrac{1}{6}x^3 + C_1 x + C_2 \right) \qquad (0 \le \xi \ L_f) \qquad (4.81)$$

and using Equation (4.40), the rotational influence coefficients are:

$$C_{F6,HS_2}(x,\xi) = \frac{1}{EI_{zz}(x)} \left(\xi x - \tfrac{1}{2}x^2 + C_1 \right) \qquad (0 \le \xi \ L_f) \qquad (4.82)$$

The resulting torque is:

$$T = -\zeta(1) \qquad (4.83)$$

Using Equation (4.37), the torsional influence coefficients are:

$$C_{F4,HS_2}(x,\xi) = -\frac{1}{GJ(x)} (x + C_1) \, \zeta \qquad (4.84)$$

Applying a unit load in the Z direction on the starboard side of a horizontal tail segment results in a bending moment about the Y axis and a torque about the X axis. Figure 4.12 shows the internal moment and torque that result from the applied load P_z. The moment about the Y axis is:

$$M_Y = (\xi - x)(1) \qquad (4.85)$$

Using Equation (4.36), the bending influence coefficients are:

$$C_{F3,HS_3}(x,\xi) = \frac{1}{EI_{yy}(x)} \left(\tfrac{1}{2}\xi x^2 - \tfrac{1}{6}x^3 + C_1 x + C_2 \right) \qquad (4.86)$$
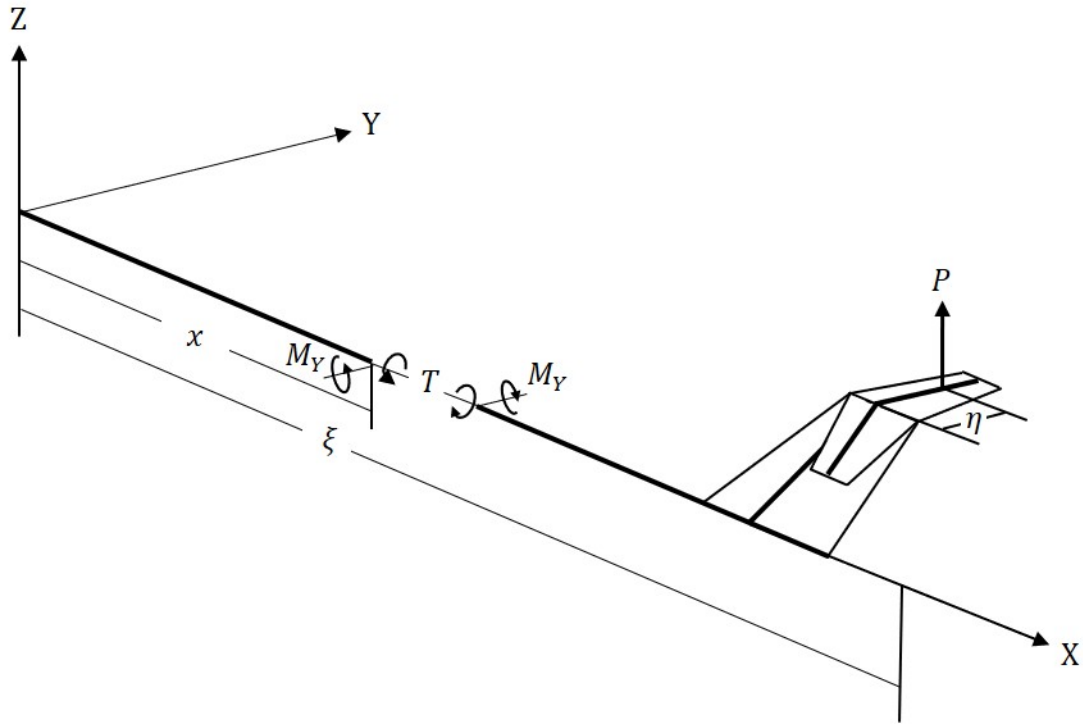
Figure 4.12 Fuselage Bending Moment and Torque at x Due to an Applied P_z on a Starboard Horizontal Tail Segment

and using Equation (4.40), the rotational influence coefficients are:

$$C_{F_5,HS_3}(x,\xi) = \frac{1}{EI_{yy}(x)}\left(\xi x - \tfrac{1}{2}x^2 + C_1\right)$$

(4.87)

The resulting torque is:

$$T = \eta(1)$$

(4.88)

and using Equation (4.37), the torsional influence coefficients are:

$$C_{F_4,HS_3}(x,\xi) = \frac{1}{GJ(x)}(x+C_1)\eta$$

(4.89)

Now a torsional moment on the starboard horizontal tail is considered. Similar to the vertical tail, the strips of the horizontal tail are aligned in the streamwise direction and not the swept axis, so a moment on the horizontal tail is equivalent to applying a moment on the end of the fuselage. Therefore, the bending influence coefficients are:

$$C_{F_3,HTS5_5}(x,\xi) = C_{F_3,F_5}(x,L_F) \tag{4.90}$$

and the rotational influence coefficients are:

$$C_{F_5,HTS_5}(x,\xi) = C_{F_5,F_5}(x,L_F) \tag{4.91}$$

The same equations used to find the fuselage flexibility influence coefficients for the starboard horizontal tail apply to the port side as well. However, as η is defined as positive in the Y direction, the value of y and η for all points on the port horizontal tail will be a negative number. The process to calculate the influence felt by the fuselage when a load is applied to any other part of the tail was laid out in this section. The same process and governing equations are used to determine how applied loads influence the vertical and horizontal tails. The full derivation of these influence coefficients is given in Appendix A. Now that the influence coefficients for each of the structural components have been determined, the global influence coefficient matrix can be formed.

4.3.   Matrix Iteration Method

Matrix iteration is a method used to determine the frequencies and mode shapes of a dynamical system that is of the form:

$$[M]\ddot{\bar{x}} + [K]\bar{x} = \bar{0} \tag{4.92}$$

Under the assumption of simple harmonic motion where $\bar{x} = \bar{x}_0 e^{i\omega t}$, Equation (4.92) becomes:

$$\left([K] - \omega^2 [M]\right)\bar{x}_0 = \bar{0} \tag{4.93}$$

According to Flomenhoft (1950), the problem of determining vibrational mode shapes and frequencies of a dynamic system is to reduce Equation (4.93) to an eigenvalue problem of the form,

$$[D]\{A\} = \lambda\{A\} \tag{4.94}$$

where $\{A\}$ is a column matrix of mode shapes and $[D]$ is known as the dynamic matrix, given by:

$$[D] = [K]^{-1}[M] \tag{4.95}$$

where $[K]$ is the matrix of stiffness influence coefficients, and $[M]$ is the mass matrix. Substituting Equation (4.31) into Equation (4.95) allows for direct computation of the dynamic matrix once the flexibility influence coefficients are known:

$$[D] = [C][M] \tag{4.96}$$

The dynamic matrix is useful in the matrix iteration process to determine the first fundamental frequency and mode shape of the dynamic system. When calculating the uncoupled modes, Bisplinghoff et. al. (1996) show that the characteristic equation of the system is:

$$\frac{1}{\omega_r^2}\phi^{(r)} = [D]\phi^{(r)}$$

(4.97)

where ω_r is the frequency of vibration of the rth mode and $\phi^{(r)}$ is its corresponding mode shape. The fundamental mode, $r = 1$, is determined by making an initial guess of the mode shape $\phi_1^{(1)}$ such that one of the elements $\phi_{1n}^{(1)}$ is equal to 1. The subscript indicates the iteration number. The simplest approach is to take a trial mode shape, $\phi_1^{(1)}$, to be a vector of ones. Substituting the trial mode shape into the right hand side of Equation (4.97) gives,

$$[D]\phi_1^{(1)} = \{N_1\}$$

(4.98)

The resulting vector, the left hand side of Equation (4.98), is then normalized with the nth element,

$$\{N_1\} = N_{1n}\left\{\frac{N_1}{N_{1n}}\right\} = N_{1n}\phi_2^{(1)}$$

(4.99)

The process is then repeated using $\phi_2^{(1)}$ as the trial mode shape. After m iterations, this resulting vector will converge to the following:

$$[D]\phi_m^{(1)} = N_{mn}\phi_m^{(1)}$$

(4.100)

where $\phi_m^{(1)}$ is the converged fundamental mode shape and $1/N_{mn}$ is equal to the fundamental frequency ω_1^2. To determine the higher mode shapes, the orthogonality condition,

$$\sum_i B_i^{(r)} A_i^{(r+1)} = 0 \qquad (4.101)$$

between mode shapes must be enforced, where $A_i^{(r+1)}$ are unknown values of the relative displacement of the $(r+1)$th mode and $B_i^{(r)}$ is a constant. For the case of no dynamic coupling,

$$B_i^{(r)} = m_i \phi_i^{(r)} \qquad (4.102)$$

where for the case with dynamic coupling,

$$B_i^{(r)} = \sum_j m_{ij} \phi_j^{(r)} \qquad (4.103)$$

where $\phi^{(r)}$ is a vector of the converged values of the rth mode of a fixed system. NASA Technical Note D-1247 describes the process to include rigid body degrees of freedom in the matrix iteration process. The individual elements of the $\{A^{(r+1)}\}$ vector for the $(r+1)$th mode can be written as:

$$\left. \begin{aligned} A_1^{(r+1)} &= -\frac{B_2^{(r)}}{B_1^{(r)}} A_2^{(r+1)} - \frac{B_3^{(r)}}{B_1^{(r)}} A_3^{(r+1)} \ldots - \frac{B_n^{(r)}}{B_1^{(r)}} A_n^{(r+1)} \\ A_2^{(r+1)} &= A_2^{(r+1)} \\ &\vdots \\ A_n^{(r+1)} &= A_n^{(r+1)} \end{aligned} \right\} \qquad (4.104)$$

Then, for simplicity, the ratio of weighting factors is defined:

$$K_{1i}^{(r)} = -\frac{B_i^{(r)}}{B_1^{(r)}}$$

such that Equation (4.104) can be written in matrix notation as in terms of the coefficients $K_{1i}^{(r)}$.

$$\begin{Bmatrix} A_1^{(r+1)} \\ A_2^{(r+1)} \\ \cdot \\ \cdot \\ \cdot \\ A_n^{(r+1)} \end{Bmatrix} = \begin{bmatrix} 0 & K_{12}^{(r)} & K_{13}^{(r)} & \cdots & K_{1n}^{(r)} \\ 0 & 1 & 0 & \cdots & 0 \\ \cdot & 0 & 1 & \cdots & \cdot \\ \cdot & \cdot & \cdot & \cdots & \cdot \\ 0 & 0 & 0 & \cdots & 1 \end{bmatrix} \begin{Bmatrix} A_1^{(r+1)} \\ A_2^{(r+1)} \\ \cdot \\ \cdot \\ \cdot \\ A_n^{(r+1)} \end{Bmatrix} \qquad (4.105)$$

or in more compact form,

$$\left\{A^{(r+1)}\right\} = \left[S^{(r)}\right]\left\{A^{(r+1)}\right\} \qquad (4.106)$$

where the square matrix $\left[S^{(r)}\right]$ is known as the "sweeping" matrix. Substituting Equation (4.106) into Equation (4.94) yields:

$$\left[D^{(r)}\right]\left[S^{(r)}\right]\left\{A^{(r+1)}\right\} = \lambda\left\{A^{(r+1)}\right\} \qquad (4.107)$$

Flomenhoft notes that since the first column of $\left[S^{(r)}\right]$ is composed of all zeros, the order of the matrix is effectively reduced by one. In the case of determining the second mode,

A_1 is multiplied by zero and has no effect on the iteration process. For each subsequent

mode that is solved, another column of the sweeping matrix will become all zeros and

another row will be comprised of the coefficients K_{ij}, thus the name "sweeping matrix"

(Flomenhoft, 1950). Essentially, the first mode is removed to determine the second mode.

Clough and Penzien (2010) explain that iterating a trial mode shape that contains no

component of the fundamental mode will converge to the second mode. Expressed

mathematically,

$$\left[D^{(1)} \right] \left[S^{(1)} \right] \left\{ A^{(2)} \right\} = \left[D^{(2)} \right] \left\{ A^{(2)} \right\}$$

(4.108)

Therefore, the dynamic matrix for higher modes can be found using the following:

$$\left[D^{(r+1)} \right] = \left[D^{(r)} \right] \left[S^{(r)} \right]$$

(4.109)

With this new dynamic matrix, the higher modes are calculated using the iteration process

discussed above. However, the computation of higher modes must be approached

cautiously. The lower modes must be calculated with great precision as each higher mode

reduces by an order of magnitude. Therefore, this sweeping process is generally used to

compute no more than the first four or five modes (Clough & Penzien, 2010). The

uncoupled mode shapes can now be used to compute the system equations of motion.

Now that the normal modes of the structure are known, the generalized displacement

of the tail can be written as a superposition of the normal modes, where $\xi_i(t)$ is the

generalized coordinate corresponding to the ith mode (Scanlan & Rosenbaum, 1968).

That is, for the fuselage:

$$h_{F_2}(x,t) = \sum_{i=1}^{N} h_{F_{2_i}}(x)\,\xi_i(t) \tag{4.110}$$

$$h_{F_3}(x,t) = \sum_{i=1}^{N} h_{F_{3_i}}(x)\,\xi_i(t) \tag{4.111}$$

where $h_{F_{2_i}}(x)$ is the relative displacement of the fuselage in the Y direction when

oscillating at the ith normal mode, $h_{F_{3_i}}(x)$ is the relative displacement of the fuselage in

the Z direction when oscillating at the ith normal mode, and $\xi_i(t)$ is the ith normal mode.

Similarly, the displacements of the vertical tail are:

$$h_{VT_1}(z,t) = \sum_{i=1}^{N} h_{VT_{1_i}}(z)\,\xi_i(t) \tag{4.112}$$

$$h_{VT_2}(z,t) = \sum_{i=1}^{N} h_{VT_{2_i}}(z)\,\xi_i(t) \tag{4.113}$$

$$h_{VT_3}(z,t) = \sum_{i=1}^{N} h_{VT_{3_i}}(z)\,\xi_i(t) \tag{4.114}$$

$$\alpha_{VT}(z,t) = \sum_{i=1}^{N} \alpha_{VT_i}(z)\,\xi_i(t) \tag{4.115}$$

$$\beta_{VT}(z,t) = \sum_{i=1}^{N} \beta_{VT_i}(z)\,\xi_i(t) \tag{4.116}$$

where $h_{VT_{1_i}}(z)$ is the relative displacement of the vertical tail in the X direction when

oscillating at the ith normal mode, $h_{VT_{2_i}}(z)$ is the relative displacement in the Y direction,

$h_{VT_{1_3}}(z)$ is the relative displacement in the Z direction, $\alpha_{VT_i}(z)$ is the relative rotation

about the Z axis, and $\beta_{VT_i}(z)$ is the relative rudder deflection. The displacements of the

starboard horizontal tail are:

$$h_{HTS_1}(y,t) = \sum_{i=1}^{N} h_{HTS_{1_i}}(y)\,\xi_i(t) \tag{4.117}$$

$$h_{HTS_2}(y,t) = \sum_{i=1}^{N} h_{HTS_{2_i}}(y)\,\xi_i(t) \tag{4.118}$$

$$h_{HTS_3}(y,t) = \sum_{i=1}^{N} h_{HTS_{3_i}}(y)\,\xi_i(t) \tag{4.119}$$

$$\alpha_{HTS}(y,t) = \sum_{i=1}^{N} \alpha_{HTS_i}(y)\,\xi_i(t) \tag{4.120}$$

$$\beta_{HTS}(y,t) = \sum_{i=1}^{N} \beta_{HTS_i}(y)\,\xi_i(t) \tag{4.121}$$

where $h_{HTS_{1_i}}(y)$ is the relative displacement of the starboard horizontal tail in the X

direction when oscillating at the ith normal mode, $h_{HTS_{2_i}}(y)$ is the relative displacement in

the Y direction, $h_{HTS_{1_3}}(y)$ is the relative displacement in the Z direction, $\alpha_{HTS_i}(y)$ is the

relative rotation about the Y axis, and $\beta_{HTS_i}(z)$ is the relative elevator deflection. The

displacements of the port horizontal tail are:

$$h_{HTP_1}(y,t) = \sum_{i=1}^{N} h_{HTP_{1_i}}(y)\,\xi_i(t) \tag{4.122}$$

$$h_{HTP_2}(y,t) = \sum_{i=1}^{N} h_{HTP_{2_i}}(y)\,\xi_i(t) \tag{4.123}$$

$$h_{HTP_3}(y,t) = \sum_{i=1}^{N} h_{HTP_{3_i}}(y)\,\xi_i(t) \tag{4.124}$$

$$\alpha_{HTP}(y,t) = \sum_{i=1}^{N} \alpha_{HTP_i}(y)\xi_i(t) \tag{4.125}$$

$$\beta_{HTP}(y,t) = \sum_{i=1}^{N} \beta_{HTP_i}(y)\xi_i(t) \tag{4.126}$$

where $h_{HTP_{1_i}}(y)$ is the relative displacement of the port horizontal tail in the X direction when oscillating at the ith normal mode, $h_{HTP_{2_i}}(y)$ is the relative displacement in the Y direction, $h_{HTP_{3_i}}(y)$ is the relative displacement in the Z direction, $\alpha_{HTP_i}(y)$ is the relative rotation about the Y axis, and $\beta_{HTP_i}(z)$ is the relative elevator deflection.

4.4. Kinetic Energy

Determining the kinetic energy of the system is the next step in deriving the equations of motion. The total kinetic energy of system is the sum of the kinetic energies of each of the structural components,

$$T = T_F + T_{VT} + T_{HTS} + T_{HTP} \tag{4.127}$$

where T is the total kinetic energy of the system, T_F is the kinetic energy of the fuselage due to elastic deformations, T_{VT} is the kinetic energy of the vertical tail, and T_{HTS} and T_{HTP} are the kinetic energies of the starboard and port horizontal tail respectively. The total kinetic energy of the fuselage is calculated by finding the kinetic energy of an infinitesimally thin section and then integrating along the length of the fuselage. The kinetic energy per unit length of the fuselage is:

$$\frac{dT_F}{dx} = \tfrac{1}{2}m_F(x)\dot{\vec{P}}_F(x,t) \cdot \dot{\vec{P}}_F(x,t) \tag{4.128}$$

where $\bar{P}_F(x,t)$ is a vector of fuselage displacements due to elastic deformation at station x and time t that is given by:

$$\bar{P}_F(x,t) = 0\hat{\mathbf{i}} + h_{F_2}(x,t)\hat{\mathbf{j}} + h_{F_3}(x,t)\hat{\mathbf{k}} \tag{4.129}$$

Using Equation (4.110) and Equation (4.111), the KE per unit length of the fuselage is:

$$\frac{dT_F}{dx} = \tfrac{1}{2}m_F(x)\sum_{i=1}^{N}h_{F_{2_i}}(x)^2\dot{\xi}_i(t)^2 + \tfrac{1}{2}m_F(x)\sum_{i=1}^{N}h_{F_{3_i}}(x)^2\dot{\xi}_i(t)^2 \tag{4.130}$$

Then, by integrating Equation (4.130), the total kinetic energy of the fuselage becomes:

$$T_F = \tfrac{1}{2}\sum_{i=1}^{N}\left(\int_0^{L_F}m_F(x)h_{F_{2_i}}(x)^2\,dx\right)\dot{\xi}_i(t)^2$$

$$+ \tfrac{1}{2}\sum_{i=1}^{N}\left(\int_0^{L_F}m_F(x)h_{F_{3_i}}(x)^2\,dx\right)\dot{\xi}_i(t)^2 \tag{4.131}$$

which can be written as:

$$T_F = \tfrac{1}{2}\sum_{i=1}^{N}\left(M_{F_{2_i}} + M_{F_{3_i}}\right)\dot{\xi}_i(t)^2 \tag{4.132}$$

where,

$$M_{F_{2_i}} = \int_0^{L_F}m_F(x)h_{F_{2_i}}(x)^2\,dx \tag{4.133}$$

and,

$$M_{F_{3_i}} = \int_0^{L_F}m_F(x)h_{F_{3_i}}(x)^2\,dx \tag{4.134}$$

Finally, for simplicity, Equation (4.132) is written as,

$$T_F = \tfrac{1}{2} \sum_{i=1}^{N} A_{F_i} \dot{\xi}_i(t)^2 \tag{4.135}$$

The total kinetic energy of the vertical tail due to elastic deformation is determined by finding the kinetic energy per unit span then integrating over the total span. Recall the process for deriving the kinetic energy of the typical section. The airfoil is split into two sections in the chordwise direction, the wing section (subscript w) and the flap section (subscript f). Similarly, the KE per unit span of a strip of the VT is split into the KE per unit span of the wing section and the KE per unit span of the flap section. These are treated as two separate regions of integration. Then, the kinetic energy per unit span of a strip of the vertical tail is given by:

$$\frac{dT_{VT}}{dz} = \frac{1}{2} \int_{-b}^{b} \rho_{VT}(x') \, \dot{\bar{P}}_{VT}(x',z,t) \cdot \dot{\bar{P}}_{VT}(x',z,t) \, dx' \tag{4.136}$$

which can be expanded to:

$$\frac{dT_{VT}}{dz} = \frac{1}{2} \int_{-b}^{be} \rho_{VT_w}(x) \, \dot{\bar{P}}_{VT_w}(x',z,t) \cdot \dot{\bar{P}}_{VT_w}(x',z,t) \, dx'$$
$$+ \frac{1}{2} \int_{be}^{b} \rho_{VT_f}(x) \, \dot{\bar{P}}_{VT_f}(x',z,t) \cdot \dot{\bar{P}}_{VT_f}(x',z,t) \, dx' \tag{4.137}$$

where $\bar{P}_{VT_w}(x',z,t)$ is a vector of vertical tail wing section displacements at chordwise location x' of the wing section, station z on the vertical tail, and time t. $\bar{P}_{VT_f}(x',z,t)$ is a vector of vertical tail flap displacements at chordwise location x' of the flap, station z on

the vertical tail, and time t. Using what is known about the typical section, the elastic displacement vectors are:

$$\bar{P}_{VT_w}(x',z,t) = h_{VT_1}(z,t)\hat{\mathbf{i}} + \left\{-h_{VT_2}(z,t) - b(x'-a)\alpha_{VT}(z,t)\right\}\hat{\mathbf{j}} + h_{VT_3}(z,t)\hat{\mathbf{k}} \qquad (4.138)$$

and,

$$\bar{P}_{VT_f}(x',z,t) = h_{VT_1}(z,t)\hat{\mathbf{i}}$$

$$+ \left\{-h_{VT_2}(z,t) - b(c-a)\alpha_{VT}(z,t) - b(x'-c)(\alpha_{VT}(z,t) + \beta_{VT}(z,t))\right\}\hat{\mathbf{j}}$$

$$+ h_{VT_3}(z,t)\hat{\mathbf{k}} \quad (4.139)$$

Following the same procedure as that of the typical section derivation, the kinetic energy per unit span of the vertical tail is:

$$\frac{dT_{VT}}{dz} = \tfrac{1}{2}m_{VT}(z)\dot{h}_{VT_1}(z,t)^2 + \tfrac{1}{2}m_{VT}(z)\dot{h}_{VT_2}(z,t)^2 + \tfrac{1}{2}m_{VT}(z)\dot{h}_{VT_3}(z,t)^2$$

$$+ \tfrac{1}{2}I_{\alpha_{VT}}(z)\dot{\alpha}_{VT}(z,t)^2 + \tfrac{1}{2}I_{\beta_{VT}}(z)\dot{\beta}(z,t)^2 + S_{\beta_{VT}}(z)\dot{h}_{VT_2}(z,t)\dot{\beta}_{VT}(z,t) \qquad (4.140)$$

$$+ S_{\alpha_{VT}}(z)\dot{h}_{VT_2}(z,t)\dot{\alpha}_{VT}(z,t) + P_{\alpha\beta_{VT}}(z)\dot{\alpha}_{VT}(z,t)\dot{\beta}_{VT}(z,t)$$

where:

$m(z)$ = mass per unit span of the airfoil-flap at station z

$I_\alpha(z)$ = mass moment of inertia per unit span of the airfoil-flap about the elastic axis at station z

$I_\beta(z)$ = mass moment of inertia per unit span of the flap about the hinge line at station z

$S_\alpha(z)$ = static moment per unit span of the airfoil-flap about the elastic axis at station z

$S_\beta(z)$ = static moment per unit span of the flap about the hinge line at station z

$P_{\alpha\beta(z)}$ = product of inertia per unit span of the airfoil-flap about the elastic axis and hinge line at station z. This is shown in Equation (4.11) and Equation (4.12) as: $P_{\alpha\beta} = I_\beta + S_\beta b(c-a)$

After substituting Equation (4.112) through Equation (4.116), Equation (4.140) becomes:

$$
\begin{aligned}
\frac{dT_{VT}}{dz} =\, & \tfrac{1}{2}m_{VT}(z)\sum_{i=1}^{N} h_{VT_{1_i}}(z)^2\dot\xi_i(t)^2 + \tfrac{1}{2}m_{VT}(z)\sum_{i=1}^{N} h_{VT_{2_i}}(z)^2\dot\xi_i(t)^2 \\
& + \tfrac{1}{2}m_{VT}(z)\sum_{i=1}^{N} h_{VT_{3_i}}(z)^2\dot\xi_i(t)^2 + \tfrac{1}{2}I_\alpha(z)\sum_{i=1}^{N} \alpha_{VT_i}(z)^2\dot\xi_i(t)^2 \\
& + \tfrac{1}{2}I_\beta(z)\sum_{i=1}^{N} \beta_{VT_i}(z)^2\dot\xi_i(t)^2 + S_\beta(z)\sum_{i=1}^{N} h_{VT_{2_i}}(z)\dot\xi_i \sum_{j=1}^{N}\beta_{VT_j}(z)\dot\xi_j(t)^2 \\
& + S_\alpha(z)\sum_{i=1}^{N} h_{VT_{2_i}}(z)\dot\xi_i(t) \sum_{j=1}^{N}\alpha_{VT_j}(z)\dot\xi_j(t) \\
& + P_{\alpha\beta}(z)\sum_{i=1}^{N} \alpha_{VT_i}(z)\dot\xi_i(t) \sum_{j=1}^{N}\beta_{VT_j}(z)\dot\xi_j(t)
\end{aligned}
\tag{4.141}
$$

Recall, $\xi(t)$ is a vector containing the normal mode shapes of the structure and are subjected to the orthogonality condition:

$$
\sum_{i=1}^{N}\xi_i(t)\sum_{j=1}^{N}\xi_j(t) = 0 \qquad (i \neq j)
\tag{4.142}
$$

Now, Equation (4.141) reduces to:

$$
\begin{aligned}
\frac{dT_{VT}}{dz} =\; & \tfrac{1}{2}m_{VT}(z)\sum_{i=1}^{N}h_{VT_{1_i}}(z)^2\dot{\xi}_i(t)^2 + \tfrac{1}{2}m_{VT}(z)\sum_{i=1}^{N}h_{VT_{2_i}}(z)^2\dot{\xi}_i(t)^2 \\
& + \tfrac{1}{2}m_{VT}(z)\sum_{i=1}^{N}h_{VT_{3_i}}(z)^2\dot{\xi}_i(t)^2 + \tfrac{1}{2}I_\alpha(z)\sum_{i=1}^{N}\alpha_{VT_i}(z)^2\dot{\xi}_i(t)^2 \\
& + \tfrac{1}{2}I_\beta(z)\sum_{i=1}^{N}\beta_{VT_i}(z)^2\dot{\xi}_i(t)^2 + S_\beta(z)\sum_{i=1}^{N}h_{VT_{2_i}}(z)\beta_{VT_i}(z)\dot{\xi}_i(t)^2 \\
& + S_\alpha(z)\sum_{i=1}^{N}h_{VT_{2_i}}(z)\,\alpha_{VT_i}(z)\dot{\xi}_i(t)^2 + P_{\alpha\beta}(z)\sum_{i=1}^{N}\alpha_{VT_i}(z)\beta_{VT_i}(z)\dot{\xi}_i(t)^2
\end{aligned}
\tag{4.143}
$$

Then, the total kinetic energy of the vertical tail is:

$$
\begin{aligned}
T_{VT} =\; & \tfrac{1}{2}\sum_{i=1}^{N}\left(\int_0^{L_{VT}}m_{VT}(z)\,h_{VT_{1_i}}(z)^2\,dz\right)\dot{\xi}_i(t)^2 + \tfrac{1}{2}\sum_{i=1}^{N}\left(\int_0^{L_{VT}}m_{VT}(z)\,h_{VT_{2_i}}(z)^2\,dz\right)\dot{\xi}_i(t)^2 \\
& + \tfrac{1}{2}\sum_{i=1}^{N}\left(\int_0^{L_{VT}}m_{VT}(z)\,h_{VT_{3_i}}(z)^2\,dz\right)\dot{\xi}_i(t)^2 + \tfrac{1}{2}\sum_{i=1}^{N}\left(\int_0^{L_{VT}}I_\alpha(z)\,\alpha_{VT_i}(z)^2\,dz\right)\dot{\xi}_i(t)^2 \\
& + \tfrac{1}{2}\sum_{i=1}^{N}\left(\int_0^{L_{VT}}I_\beta(z)\,\beta_{VT_i}(z)^2\,dz\right)\dot{\xi}_i(t)^2 + \tfrac{1}{2}\sum_{i=1}^{N}\left(\int_0^{L_{VT}}S_\beta(z)\,h_{VT_{2_i}}(z)\,\beta_{VT_i}(z)\,dz\right)\dot{\xi}_i(t)^2 \\
& + \tfrac{1}{2}\sum_{i=1}^{N}\left(\int_0^{L_{VT}}S_\alpha(z)\,h_{VT_{2_i}}(z)\,\alpha_{VT_i}(z)\,dz\right)\dot{\xi}_i(t)^2 \\
& + \tfrac{1}{2}\sum_{i=1}^{N}\left(\int_0^{L_{VT}}P_{\alpha\beta}(z)\alpha_{VT_i}(z)\beta_{VT_i}(z)\right)\dot{\xi}_i(t)^2 \quad (4.144)
\end{aligned}
$$

which can be written as:

$$
T_{VT} = \tfrac{1}{2}\sum_{i=1}^{N}\left(M_{VT_{1_i}} + M_{VT_{2_i}} + M_{VT_{3_i}} + I_{\alpha VT_i} + I_{\beta VT_i} \right.
$$
$$
\left. + 2\left[S_{\alpha VT_i} + S_{\beta VT_i} + P_{\alpha\beta VT_i} \right] \right)\dot{\xi}(t)^2 \quad (4.145)
$$

where:

$$M_{VT_{1_i}} = \int_0^{L_{VT}} m_{VT}(z)\, h_{VT_{1_i}}(z)^2 \, dz \tag{4.146}$$

$$M_{VT_{2_i}} = \int_0^{L_{VT}} m_{VT}(z)\, h_{VT_{2_i}}(z)^2 \, dz \tag{4.147}$$

$$M_{VT_{3_i}} = \int_0^{L_{VT}} m_{VT}(z)\, h_{VT_{3_i}}(z)^2 \, dz \tag{4.148}$$

$$I_{\alpha VT_i} = \int_0^{L_{VT}} I_\alpha(z)\, \alpha_{VT_i}(z)^2 \, dz \tag{4.149}$$

$$I_{\beta VT_i} = \int_0^{L_{VT}} I_\beta(z)\, \alpha_{VT_i}(z)^2 \, dz \tag{4.150}$$

$$S_{\alpha VT_i} = \int_0^{L_{VT}} S_\alpha(z)\, h_{VT_{2_i}}(z) \alpha_{VT_i}(z) \, dz \tag{4.151}$$

$$S_{\beta VT_i} = \int_0^{L_{VT}} S_\beta(z)\, h_{VT_{2_i}}(z) \beta_{VT_i}(z) \, dz \tag{4.152}$$

For simplicity, Equation (4.145) is written as:

$$T_{VT} = \tfrac{1}{2} \sum_{i=1}^N A_{VT_i} \dot{\xi}_i(t)^2 \tag{4.153}$$

The kinetic energy of the horizontal tail is determined by splitting the tail into the port (left) side and starboard (right) side to determine the energy of each section individually and then adding them together. The kinetic energy of one side of the horizontal tail is determined by finding the kinetic energy per unit span of that side of the HT and then integrating over the semi-span in either the port or starboard direction. Similarly to the vertical tail, a strip on the horizontal tail is split up into the wing section and flap section. The kinetic energy per unit span of a strip on the horizontal tail is given by:

$$\frac{dT_{HTS}}{dy} = \frac{1}{2} \int_{-b}^{b} \rho_{HT}(x') \, \dot{\bar{P}}_{HT}(x',y,t) \cdot \dot{\bar{P}}_{HT}(x',y,t) \, dx' \tag{4.154}$$

which can be expanded to:

$$\frac{dT_{HTS}}{dy} = \frac{1}{2} \int_{-b}^{be} \rho_{HT_w}(x') \, \dot{\bar{P}}_{HT_w}(x',y,t) \cdot \dot{\bar{P}}_{HT_w}(x',y,t) \, dx'$$

$$+ \frac{1}{2} \int_{be}^{b} \rho_{HT_f}(x') \, \dot{\bar{P}}_{HT_f}(x',y,t) \cdot \dot{\bar{P}}_{HT_f}(x',y,t) \, dx' \tag{4.155}$$

where $\bar{P}_{HT_w}(x',y,t)$ is a vector of horizontal tail wing section displacements at chordwise

location x' of the wing section, station y of the horizontal tail, and time t. $\bar{P}_{HT_f}(x',y,t)$ is

a vector of horizontal tail flap displacements at chordwise location x' of the flap, station y

of the horizontal tail, and time t. Using what is known about the typical section, the elastic

displacement vectors are:

$$\bar{P}_{HTS_w}(x',y,t) = h_{HTS_1}(y,t)\hat{\mathbf{i}} + h_{HTS_2}(y,t)\hat{\mathbf{j}} + \left\{ -h_{HTS_3}(y,t) - b(x'-a)\,\alpha_{HTS}(y,t) \right\} \hat{\mathbf{k}}$$

$$\tag{4.156}$$

and,

$$\bar{P}_{HTS_f}(x',y,t) = h_{HTS_1}(y,t)\hat{\mathbf{i}} + h_{HTS_2}(y,t)\hat{\mathbf{j}}$$

$$+ \left\{ -h_{HTS_3}(y,t) - b(c-a)\,\alpha_{HTS}(y,t) - b(x'-c)(\alpha_{HTS}(y,t) + \beta_{HTS}(y,t)) \right\} \hat{\mathbf{k}}$$

$$\tag{4.157}$$

Then, following the procedure from Section 4.1., the kinetic energy per unit span of the starboard horizontal tail is:

$$\frac{dT_{HTS}}{dy} = \tfrac{1}{2}m_{HTS}(y)\dot{h}_{HTS_1}(y,t)^2 + \tfrac{1}{2}m_{HTS}(y)\dot{h}_{HTS_2}(y,t)^2 + \tfrac{1}{2}m_{HTS}(y)\dot{h}_{HTS_3}(y,t)^2$$

$$+ \tfrac{1}{2}I_{\alpha HTS}(y)\alpha_{\dot{H}TS}(y,t)^2 + \tfrac{1}{2}I_{\beta HTS}(y)\dot{\beta}(y,t)^2 + S_{\beta HTS}(y)\dot{h}_{HTS_3}(y,t)\dot{\beta}_{HTS}(y,t)$$

$$+ S_{\alpha HTS}(y)\dot{h}_{HTS_3}(y,t)\dot{\alpha}_{HTS}(y,t) + P_{\alpha\beta HTS}(y)\dot{\alpha}_{HTS}(y,t)\dot{\beta}_{HTS}(y,t) \quad (4.158)$$

where: After substituting Equation (4.117) and Equation (4.121) into Equation (4.158)

$m(y)$	=	mass per unit span of the airfoil-flap at station y
$I_\alpha(y)$	=	mass moment of inertia per unit span of the airfoil-flap about the elastic axis at station y
$I_\beta(y)$	=	mass moment of inertia per unit span of the flap about the hinge line at station y
$S_\alpha(y)$	=	static moment per unit span of the airfoil-flap about the elastic axis at station y
$S_\beta(y)$	=	static moment per unit span of the flap about the hinge line at station y
$P_{\alpha\beta(z)}$	=	product of inertia per unit span of the airfoil-flap about the elastic axis and hinge line at station y. This is shown in Equation (4.11) and Equation (4.12) as: $P_{\alpha\beta} = I_\beta + S_\beta b(c-a)$

and applying the orthogonality condition, the kinetic energy per unit span of the starboard

horizontal tail becomes:

$$
\frac{dT_{HTS}}{dy} = \tfrac{1}{2} m_{HTS}(y) \sum_{i=1}^{N} h_{HTS_{1_i}}(y)^2 \dot{\xi}_i(t)^2 + \tfrac{1}{2} m_{HTS}(y) \sum_{i=1}^{N} h_{HTS_{2_i}}(y)^2 \dot{\xi}_i(t)^2
$$

$$
+ \tfrac{1}{2} m_{HTS}(y) \sum_{i=1}^{N} h_{HTS_{3_i}}(y)^2 \dot{\xi}_i(t)^2 + \tfrac{1}{2} I_\alpha(y) \sum_{i=1}^{N} \alpha_{HTS_i}(y)^2 \dot{\xi}_i(t)^2
$$

$$
+ \tfrac{1}{2} I_\beta(y) \sum_{i=1}^{N} \beta_{HTS_i}(y)^2 \dot{\xi}_i(t)^2 + S_\beta(y) \sum_{i=1}^{N} h_{HTS_{3_i}}(y) \beta_{HTS_i}(y) \dot{\xi}_i(t)^2
$$

$$
+ S_\alpha(y) \sum_{i=1}^{N} h_{HTS_{3_i}}(y) \alpha_{HTS_i}(y) \dot{\xi}_i(t)^2 + P_{\alpha\beta}(y) \sum_{i=1}^{N} \alpha_{HTS_i}(y) \beta_{HTS_i}(y) \dot{\xi}(t)^2 \quad (4.159)
$$

Then, integrating this over the starboard horizontal tail, the tail's total kinetic energy is:

$$
T_{HTS} = \tfrac{1}{2} \sum_{i=1}^{N} \left(\int_0^{L_{HTS}} m_{HTS}(y) h_{HTS_{1_i}}(y)^2 \, dy \right) \dot{\xi}_i(t)^2
$$

$$
+ \tfrac{1}{2} \sum_{i=1}^{N} \left(\int_0^{L_{HTS}} m_{HTS}(y) h_{HTS_{2_i}}(y)^2 \, dy \right) \dot{\xi}_i(t)^2
$$

$$
+ \tfrac{1}{2} \sum_{i=1}^{N} \left(\int_0^{L_{HTS}} m_{HTS}(y) h_{HTS_{3_i}}(y)^2 \, dy \right) \dot{\xi}_i(t)^2 + \tfrac{1}{2} \sum_{i=1}^{N} \left(\int_0^{L_{HTS}} I_\alpha(y) \alpha_{HTS_i}(y)^2 \, dy \right) \dot{\xi}_i(t)^2
$$

$$
+ \tfrac{1}{2} \sum_{i=1}^{N} \left(\int_0^{L_{HTS}} I_\beta(y) \beta_{HTS_i}(y)^2 \, dy \right) \dot{\xi}_i(t)^2 + \tfrac{1}{2} \sum_{i=1}^{N} \left(\int_0^{L_{HTS}} S_\beta(y) h_{HTS_{2_i}}(y) \beta_{HTS_i}(y) \, dy \right) \dot{\xi}_i(t)^2
$$

$$
+ \tfrac{1}{2} \sum_{i=1}^{N} \left(\int_0^{L_{HTS}} S_\alpha(y) h_{HTS_{2_i}}(y) \alpha_{HTS_i}(y) \, dy \right) \dot{\xi}_i(t)^2
$$

$$
+ \tfrac{1}{2} \sum_{i=1}^{N} \left(\int_0^{L_{HTS}} P_{\alpha\beta}(y) \alpha_{HTS_i}(y) \beta_{HTS_i}(y) \right) \dot{\xi}_i(t)^2 \quad (4.160)
$$

which can be written as:

$$T_{HTS} = \frac{1}{2} \sum_{i=1}^{N} \left(M_{HTS_{1_i}} + M_{HTS_{2_i}} + M_{HTS_{3_i}} + I_{\alpha HTS_i} + I_{\beta HTS_i} \right.$$

$$\left. + 2 \left[S_{\alpha HTS_i} + S_{\beta HTS_i} + P_{\alpha \beta HTS_i} \right] \right) \dot{\xi}(t)^2 \quad (4.161)$$

where:

$$M_{HTS_{1_i}} = \int_0^{L_{HTS}} m_{HTS}(y) \, h_{HTS_{1_i}}(y)^2 \, dy \qquad (4.162)$$

$$M_{HTS_{2_i}} = \int_0^{L_{HTS}} m_{HTS}(y) \, h_{HTS_{2_i}}(y)^2 \, dy \qquad (4.163)$$

$$M_{HTS_{3_i}} = \int_0^{L_{HTS}} m_{HTS}(y) \, h_{HTS_{3_i}}(y)^2 \, dy \qquad (4.164)$$

$$I_{\alpha HTS_i} = \int_0^{L_{HTS}} I_\alpha(y) \, \alpha_{HTS_i}(y)^2 \, dy \qquad (4.165)$$

$$I_{\beta HTS_i} = \int_0^{L_{HTS}} I_\beta(y) \, \alpha_{HTS_i}(y)^2 \, dy \qquad (4.166)$$

$$S_{\alpha HTS_i} = \int_0^{L_{HTS}} S_\alpha(y) \, h_{HTS_{2_i}}(y) \alpha_{HTS_i}(y) \, dy \qquad (4.167)$$

$$S_{\beta HTS_i} = \int_0^{L_{HTS}} S_\beta(y) \, h_{HTS_{2_i}}(y) \beta_{HTS_i}(y) \, dy \qquad (4.168)$$

For simplicity, Equation (4.161) is written as:

$$T_{HTS} = \frac{1}{2} \sum_{i=1}^{N} A_{HTS_i} \dot{\xi}_i(t)^2 \qquad (4.169)$$

The kinetic energy of the port horizontal tail is calculated using the same process as that for the starboard horizontal tail. This results in the expression:

$$T_{HTP} = \frac{1}{2} \sum_{i=1}^{N} \left(M_{HTP_{1_i}} + M_{HTP_{2_i}} + M_{HTP_{3_i}} + I_{\alpha HTP_i} + I_{\beta HTP_i} \right.$$

$$\left. + 2 \left[S_{\alpha HTP_i} + S_{\beta HTP_i} + P_{\alpha \beta HTP_i} \right] \right) \dot{\xi}(t)^2 \quad (4.170)$$

where:

$$M_{HTP_{1_i}} = \int_0^{L_{HTP}} m_{HTP}(y) \, h_{HTP_{1_i}}(y)^2 \, dy \quad (4.171)$$

$$M_{HTP_{2_i}} = \int_0^{L_{HTP}} m_{HTP}(y) \, h_{HTP_{2_i}}(y)^2 \, dy \quad (4.172)$$

$$M_{HTP_{3_i}} = \int_0^{L_{HTP}} m_{HTP}(y) \, h_{HTP_{3_i}}(y)^2 \, dy \quad (4.173)$$

$$I_{\alpha HTP_i} = \int_0^{L_{HTP}} I_\alpha(y) \, \alpha_{HTP_i}(y)^2 \, dy \quad (4.174)$$

$$I_{\beta HTP_i} = \int_0^{L_{HTP}} I_\beta(y) \, \alpha_{HTP_i}(y)^2 \, dy \quad (4.175)$$

$$S_{\alpha HTP_i} = \int_0^{L_{HTP}} S_\alpha(y) \, h_{HTP_{2_i}}(y) \alpha_{HTP_i}(y) \, dy \quad (4.176)$$

$$S_{\beta HTP_i} = \int_0^{L_{HTP}} S_\beta(y) \, h_{HTP_{2_i}}(y) \beta_{HTP_i}(y) \, dy \quad (4.177)$$

For simplicity, Equation (4.170) is written as:

$$T_{HTP} = \frac{1}{2} \sum_{i=1}^{N} A_{HTP_i} \dot{\xi}_i(t)^2 \quad (4.178)$$

and Equation (4.170) can be condensed to:

$$T_{HTP} = \tfrac{1}{2} \sum_{i=1}^{N} A_{HTP_i} \dot{\xi}_i(t)^2 \tag{4.179}$$

Finally, the kinetic energy due to elastic deformation of the entire structure is:

$$T = \tfrac{1}{2} \sum_{i=1}^{N} \left(A_{F_i} + A_{VT_i} + A_{HTS_i} + A_{HTP_i} \right) \dot{\xi}_i(t)^2 \tag{4.180}$$

It should be noted that in the expressions for kinetic energy above, if the control surfaces do not span the entire length of the lifting surface, the control surface terms are determined by integrating over that portion of the span where the control surface exists. In other words, $\beta = 0$ for the portions of the vertical tail or horizontal tail that do not contain a control surface (Scanlan & Rosenbaum, 1968).

4.5. Potential Energy

According to Scanlan and Rosenbaum (1967), the potential energy of the system can be expressed as a quadratic function that contains the squares of the generalized coordinates ξ_i. This leads to the following expression for the potential energy of the system:

$$V = \tfrac{1}{2} \sum_{i=1}^{N} B_i \xi_i(t)^2 \tag{4.181}$$

The coefficients B_i are found by using Lagrange's Equation with no forcing function,

$$\frac{d}{dt} \left(\frac{\partial T}{\partial \dot{\xi}_i} \right) + \left(\frac{\partial V}{\partial \xi_i} \right) = 0 \qquad (i = 1, 2, \cdots, N) \tag{4.182}$$

which gives N equations of the form:

$$\left(A_{F_i} + A_{VT_i} + A_{HTS_i} + A_{HTP_i}\right)\ddot{\xi}_i + B_i\xi_i = 0 \qquad (i = 1, 2, \cdots, N) \tag{4.183}$$

Applying the assumption of simple harmonic motion,

$$\left(A_{F_i} + A_{VT_i} + A_{HTS_i} + A_{HTP_i}\right)(-\omega_i^2)\xi_i + B_i\xi_i = 0 \tag{4.184}$$

Solving for B_i,

$$B_i = \omega_i^2\left(A_{F_i} + A_{VT_i} + A_{HTS_i} + A_{HTP_i}\right) \tag{4.185}$$

defines the potential energy as:

$$V = \frac{1}{2}\sum_{i=1}^{N}\omega_i^2\left(A_{F_i} + A_{VT_i} + A_{HTS_i} + A_{HTP_i}\right)\xi_i(t)^2 \tag{4.186}$$

4.6. Structural Damping Dissipation Factor

In two-dimensional flutter theory, the structural damping of a vibrating system is represented by a function of the amplitude of elastic deformation, not the frequency of oscillation. Experimentally, it was found that the damping force is proportional to the elastic restoring force and in phase with the velocity of oscillation. It is common practice to replace each generalized coordinate ξ_i with $\xi_i(1 + ig_i)$. where the damping force is proportional to the generalized displacement ξ_i by the damping constant g and in phase with the velocity $\dot{\xi}_i$. To represent the damping force in the equations of motion using Lagrange's equation, a structural damping dissipation factor is developed. This structural

damping dissipation factor D is represented as a function of the mass, natural frequency, and velocity of a given normal mode. For T-tail flutter analysis with N normal modes considered, D is given by:

$$D = \tfrac{1}{2} \sum_{i=1}^{N} \left(A_{F_i} + A_{VT_i} + A_{HTS_i} + A_{HTP_i} \right) g_i \tfrac{\omega_i^2}{\omega} \dot{\xi}_i(t) \tag{4.187}$$

where ω_i is the frequency of the ith normal mode, g_i is the damping constant of the ith normal mode, and ω is the flutter frequency. Furthermore, the damping constant can be approximated as a constant such that:

$$g_1 = g_2 = \cdots = g \tag{4.188}$$

With the inclusion of a structural damping dissipation factor, Equation (4.3) becomes:

$$\frac{d}{dt}\left(\frac{\partial T}{\partial \dot{\xi}_i} \right) + \left(\frac{\partial D}{\partial \dot{\xi}_i} \right) + \left(\frac{\partial V}{\partial \xi_i} \right) = Q_i \tag{4.189}$$

Evaluating Equation (4.189) will yield the equations of motion for an N degree-of-freedom vibrational system.

4.7. Restrained Matrix Equations of Motion

Now that the kinetic and potential energies of the system are known including the structural damping dissipation factor, applying Equation (4.189) will produce a set of N

linear differential equations in $\xi(t)$. To write the equations in a more compact form, the following substitution is made:

$$A_i = \left(A_{F_i} + A_{VT_i} + A_{HTS_i} + A_{HTP_i} \right) \tag{4.190}$$

for which the equations of motion become:

$$
\begin{aligned}
&\left\{ A_1 \left[1 - \left(\tfrac{\omega_1}{\omega} \right)^2 (1 + ig) \right] \right\} \xi_1(t) + 0\xi_2(t) + \cdots + 0\xi_N(t) = Q_1 \\
&0\xi_1(t) + \left\{ A_2 \left[1 - \left(\tfrac{\omega_2}{\omega} \right)^2 (1 + ig) \right] \right\} \xi_2(t) + \cdots + 0\xi_N(t) = Q_2 \\
&\qquad\qquad\qquad\qquad\qquad\qquad\qquad\qquad\qquad\vdots \\
&0\xi_1(t) + 0\xi_2(t) + \cdots + \left\{ A_N \left[1 - \left(\tfrac{\omega_1}{\omega} \right)^2 (1 + ig) \right] \right\} \xi_N(t) = Q_N
\end{aligned}
\tag{4.191}
$$

where the eigenvalues of the system given in Equation (4.191) produce the normal modes of vibration. The next step in the modeling process is an expression for the generalized forces, Q, that define the unsteady aerodynamic forcing.

5. Unsteady Aerodynamic Modeling

The unsteady aerodynamic forces for incompressible subsonic flow, compressible

subsonic flow, and supersonic flow are developed in the following section. Figure 4.1

shows a pitch-plunge-flap typical section as presented by Theodorsen. The plunging

degree of freedom, represented by h, is defined as positive when the airfoil is displaced

downward. The pitching degree of freedom, represented by α, is defined as positive when

the airfoil leading edge is deflected upwards. The flap degree of freedom, represented by

β, is defined as positive when the trailing edge is deflected downward. For the purpose of

aeroelastic analysis, it is common to treat the plunge DOF as a nondimensional quantity.

The dimensional plunge is related to the nondimensional by the semispan such that:

$$h^* = hb \tag{5.1}$$

where h^* is the plunge with dimensions of length, h is nondimensional plunge, and b is the

semichord of the typical section under consideration. The typical section is used to derive

the unsteady aerodynamic forces for incompressible, compressible subsonic, and

supersonic flow.

5.1. Incompressible Subsonic Flow

The aerodynamic forcing functions for incompressible flow are developed using the

methods laid out by Theodorsen in NACA TR-496 and Theodorsen and Garrick in NACA

TR-685 and NACA TR-736. Theodorsen's original derivation for the unsteady

aerodynamic forces was for a flat plate with a flap that rotated about the leading edge (LE)

of the flap.

The unsteady lift, pitching moment, and hinge moment are given in terms of T-functions and Küssner functions, which are functions of the location of the hinge line. These functions are defined in Appendix B. Bisplinghoff et al. (1996) discusses that compressibility effects for Mach numbers less than 0.50 are negligibly small for flutter analysis. Therefore, incompressible unsteady aerodynamic theories are used to calculate the aerodynamic forces and moment for Mach numbers less than 0.5. However for steady flow, incompressible aerodynamics are utilized for a Mach number less than 0.30 (Bisplinghoff et al., 1996).

Smilg and Wasserman (1942) re-derived the lift, pitching moment, and hinge moment for a typical section to include an unsealed gap, with an arbitrary hinge line location, in AF TR-4798. The T-functions, T_i, and Küssner functions, Φ_i, are geometric functions that were used to reduce the integrals originally derived by Theodorsen. The lift per unit span for a pitch-plunge-flap airfoil oscillating in incompressible flow is given by:

$$
\begin{aligned}
L' = \pi \rho b^3 \Bigg\{ &-\ddot{h} - \frac{2U}{b}C(k)\dot{h} + a\ddot{\alpha} + \left[2\left(a - \frac{1}{2}\right)C(k) - 1 \right]\frac{U}{b}\dot{\alpha} - \frac{2U^2}{b^2}C(k)\alpha \\
&+ \left[\frac{T_1}{\pi} + (c - e)\frac{\Phi_3}{\pi} \right]\ddot{\beta} + \left[\frac{T_4}{\pi} + 2(c - e)\frac{\Phi_1}{\pi}C(k) - \frac{T_{11}}{\pi}C(k) \right]\frac{U}{b}\dot{\beta} \\
&- \frac{2T_{10}}{\pi}C(k)\frac{U^2}{b^2}\beta \Bigg\}
\end{aligned}
\tag{5.2}
$$

The pitching moment about the elastic axis per unit span is given by:

$$M' = \pi \rho b^4 \left\{ a\ddot{h} + 2\left(\tfrac{1}{2}+a\right)C(k)\frac{U}{b}\dot{h} - \left(\frac{1}{8}+a^2\right)\ddot{\alpha} \right.$$

$$+ \left[a - \frac{1}{2} + 2\left(\frac{1}{4}-a^2\right)C(k) \right]\frac{U}{b}\dot{\alpha} + 2\left(\frac{1}{2}+a\right)C(k)\frac{U^2}{b^2}\alpha$$

$$+ \left[\frac{T_7}{\pi} + (e-a)\frac{T_1}{\pi} + (c-e)\frac{\Phi_6}{4\pi} - (c-e)\left(\frac{1}{2}+a\right)\frac{\Phi_3}{\pi} \right]\ddot{\beta}$$

$$+ \left[\frac{2p}{\pi} - \left(a-\frac{1}{2}\right)\frac{T_4}{\pi} + (c-e)\frac{\Phi_5}{\pi} + \right.$$

$$\left\{ \left(\frac{1}{2}+a\right)\frac{T_{11}}{\pi} - 2(c-e)\left(\frac{1}{2}+a\right)\frac{\Phi_1}{\pi}\right\}C(k) \right]\frac{U}{b}\dot{\beta}$$

$$\left. + \left[2\left(\frac{1}{2}+a\right)\frac{T_{10}}{\pi}C(k) - \frac{T_4+T_{10}}{\pi} \right]\frac{U^2}{b^2}\beta \right\}$$

(5.3)

The hinge moment per unit span is given by:

$$T' = \pi \rho b^4 \left\{ \left[\frac{T_1}{\pi} + (c-e)\frac{\Phi_3}{\pi} \right]\ddot{h} + \left[2(c-e)\frac{\Phi_{31}}{\pi} - \frac{T_{12}}{\pi} \right]C(k)\frac{U}{b}\dot{h} \right.$$

$$+ \left[\frac{T_7}{\pi} + (e-a)\frac{T_1}{\pi} + (c-e)\frac{\Phi_6}{4\pi} - (c-e)\left(\frac{1}{2}+a\right)\frac{\Phi_3}{\pi} \right]\ddot{\alpha}$$

$$+ \left[(c-e)\frac{\Phi_{32}}{\pi} - \frac{2p-2T_1-T_4}{2\pi} + \left(a-\frac{1}{2}\right)\frac{T_{12}}{\pi}C(k) \right.$$

$$\left. -2(c-e)\left(a-\frac{1}{2}\right)\frac{\Phi_{31}}{\pi}C(k) \right]\frac{U}{b}\dot{\alpha} + \left[2(c-e)\frac{\Phi_{31}}{\pi} - \frac{T_{12}}{\pi} \right]C(k)\frac{U^2}{b^2}\alpha$$

$$+ \left[\frac{T_3}{\pi^2} + (c-e)\frac{\Phi_{37}}{\pi^2} - (c-e)^2\frac{\Phi_{17}}{\pi^2} \right]\ddot{\beta} + \left[\frac{T_4 T_{11}}{2\pi^2} + (c-e)\frac{\Phi_{36}+\Phi_{10}}{\pi^2} \right.$$

$$- (c-e)^2\frac{\Phi_{35}}{\pi^2} + \left(-\frac{T_{11}T_{12}}{2\pi^2} + (c-e)\frac{\Phi_2\Phi_{31}+\Phi_1\Phi_8}{\pi^2} \right)$$

$$\left. -2(c-e)^2\frac{\Phi_1\Phi_{31}}{\pi^2} \right)C(k) \right]\frac{U}{b}\ddot{\beta} + \left[-\frac{T_5-T_4 T_{10}}{\pi^2} + (c-e)\frac{\Phi_{35}}{\pi^2} \right.$$

$$\left. + \left(-\frac{T_{10}T_{12}}{\pi^2} + 2(c-e)\frac{\Phi_1\Phi_{31}}{\pi^2} \right)C(k) \right]\frac{U^2}{b^2}\beta \right\}$$

(5.4)

In the case of the flutter problem, it is common practice to assume the airfoil is oscillating with simple harmonic motion of frequency ω at a constant airspeed and altitude. Under this assumption, the following substitutions can be made:

$$h = \bar{h}e^{i\omega t} \qquad\qquad \alpha = \bar{\alpha}e^{i\omega t} \qquad\qquad \beta = \bar{\beta}e^{i\omega t}$$

where ω is the frequency of oscillation and the quantities with the bar are the magnitude of the oscillation. After substituting the simple harmonic motion relationships, the lift, pitching moment, and hinge moment equations can be rewritten in terms of complex coefficients. Equation (5.2) reduces to:

$$\bar{L}' = \pi\rho b^3 \omega^2 \left\{ L_h\bar{h} + \left[L_\alpha - \left(\tfrac{1}{2} + a\right) L_h \right]\bar{\alpha} + \left[L_\beta - (c - e)L_z \right]\bar{\beta} \right\} \tag{5.5}$$

where L_h, L_α, L_β, and L_z are complex coefficients in terms of reduced frequency, k, that are given in Appendix B. Next, Equation (5.3) reduces to:

$$\bar{M}' = \pi\rho b^4 \omega^2 \left\{ \left[M_h - \left(\tfrac{1}{2} + a\right) L_h \right]\bar{h} + \left[M_\alpha - \left(\tfrac{1}{2} + a\right)(L_\alpha + M_h) + \left(\tfrac{1}{2} + a\right)^2 L_h \right]\bar{\alpha} \right.$$
$$\left. + \left[M_\beta - \left(\tfrac{1}{2} + a\right) L_\beta - (c - e)M_z + (c - e)\left(\tfrac{1}{2} + a\right) L_z \right]\bar{\beta} \right\} \tag{5.6}$$

where M_h, M_α, M_β, and M_z are complex coefficients in terms of reduced frequency, k, that are given in Appendix B. Finally, Equation (5.4) that reduces to:

$$\bar{T}' = \pi \rho b^4 \omega^2 \left\{ [T_h - (c-e)P_h]\,\bar{h} + \left[T_\alpha - (c-e)P_\alpha - \left(\tfrac{1}{2} + a \right)T_h + \left(\tfrac{1}{2} + a \right)(c-e)P_h \right] \bar{\alpha} \right.$$
$$\left. + \left[T_\beta - (c-e)\left(P_\beta + T_z \right) + (c-e)^2 P_z \right] \bar{\beta} \right\} \quad (5.7)$$

where T_h, T_α, T_β, T_z, P_h, P_α, P_β, P_z are complex coefficients in terms of reduced frequency, k, that are listed in Appendix B. It is important to note that, in the equations above, $\bar{h}$ is the amplitude of plunge, non-dimensionalized with respect to the airfoil semichord. In other words, $\bar{h}$ is analogous to h in Equation (5.1), where α and β are also amplitudes, given in radians, which do not require being non-dimensionalized. Each of the complex coefficients can then be written as a polynomial terms of (b_r/b) where b_r is the reference semichord of the lifting surface (75% of the semispan) and b is the semichord at a given spanwise location. This is done to make integrating over the span of a lifting surface easier. For example:

$$L_\alpha = K_1(L_\alpha) + \left(\frac{b_r}{b} \right) K_2(L_\alpha) + \left(\frac{b_r}{b} \right)^2 K_3(L_\alpha) \quad (5.8)$$

where $K_1(L_\alpha)$ is the constant part of L_α, $K_2(L_\alpha)$ is the coefficient in front of the first order term (b_r/b), and $K_3(L_\alpha)$ is the coefficient in front of the second order term $(b_r/b)^2$. A comprehensive list of these coefficients and their polynomial expansions are identified in Appendix B.

5.2. Compressible Subsonic Flow

As the Mach number increases, it is important to consider the effects of compressibility on the aerodynamic forces. When analyzing unsteady compressible flows, the change in magnitude and the change in phase must be accounted for. Therefore, accounting for compressibility effects in unsteady flows extends beyond a simple scale factor such as the Prandtl-Glauert correction factor. Possio first proposed a method to determine the unsteady aerodynamic forces on an oscillating airfoil in compressible flow by replacing the airfoil's camber line with a distribution of acceleration doublets to represent the unsteady pressure distribution. Possio's integral equation is used to describe the magnitude of downwash at a given point on the airfoil due to contributions of the doublet distribution.

$$\bar{w}_a(x) = -\frac{\omega}{\rho_\infty U^2} \int_{-b}^{b} \Delta \bar{p}_a(\xi) K\left(M, \frac{k(x-\xi)}{b}\right) d\xi \qquad (-b \le x \le b) \qquad (5.9)$$

where $\bar{w}_a(x)$ is the downwash magnitude at point x on the airfoil, ω is the frequency of oscillation, $\Delta \bar{p}_a(\xi)$ is the disturbance pressure caused by the doublet at point ξ, and K is the kernel function. The kernel function, which is a function of Mach number, reduced frequency, semichord, position x, and the coordinate ξ is defined by:

$$K\left(M, \frac{k(x-\xi)}{b}\right) = \frac{1}{4\sqrt{(1-M^2)}} \left\{ e^{i\frac{kM^2(x-\xi)}{(1-M^2)b}} \left[iM\frac{|x-\xi|}{(x-\xi)} H_1^{(2)}\left(\frac{kM|x-\xi|}{(1-M^2)b}\right) \right. \right.$$
$$\left. - H_0^{(1)}\left(\frac{kM|x-\xi|}{(1-M^2)b}\right) \right] + i(1-M^2)e^{-i\frac{k(x-\xi)}{b}} \left[\frac{2}{\pi\sqrt{1-M^2}} \ln\frac{1+\sqrt{(1-M^2)}}{M} \right.$$
$$\left. \left. + \int_0^{\frac{k(x-\xi)}{(1-M^2)b}} e^{iu} H_0^{(2)}(M|u|) du \right] \right\} \qquad (5.10)$$

where u is a dummy variable of integration defined by:

$$u = \frac{k(\xi' - \xi)}{(1 - M^2)b} \qquad (5.11)$$

Possio then used an approach similar to that used in thin airfoil theory, in an attempt to solve for the disturbance pressure by transforming the ξ variable into θ by the following relationship:

$$\xi = b\cos\theta \qquad (5.12)$$

Here, θ is measured from the LE where $\theta = \pi$ and decreases to the TE where $\theta = 0$. In addition, Possio defined the disturbance pressure as a Fourier series such that:

$$\Delta \bar{p}_a(\theta) = A_0 \cot\tfrac{\theta}{2} + \sum_{n=1}^{\infty} A_n \sin(n\theta) \qquad (5.13)$$

Upon substituting Equation (5.13) and Equation (5.10) into Equation (5.2.), the Fourier coefficients are found by evaluating $\bar{w}_a(x)$ at a finite number of collocation points along the airfoil chord (Bisplinghoff et al., 1996). A Matlab adaptation of the Fortran code Lin2D developed by Samuel R. Bland of NASA's Langley Research Center was used to calculate the unsteady aerodynamic coefficients for a range of Mach numbers (M) and reduced frequencies (k) in the compressible flow regime. The unsteady lift coefficient is given by:

$$C_l(M, k) = C_{l_h}(M, k)h + C_{l_\alpha}(M, k)\alpha + C_{l_\beta}(M, k)\beta \qquad (5.14)$$

where $C_l(M,k)$ is the total unsteady complex lift coefficient, $C_{l_h}(M,k)$ is the lift

coefficient due to simple harmonic plunging, $C_{l_\alpha}(M,k)$ is the lift coefficient due to simple

harmonic pitching, and $C_{l_\beta}(M,k)$ is the lift coefficient due to simple harmonic flapping.

Similarly, the unsteady pitching moment coefficient is given by:

$$C_M(M,k) = C_{M_h}(M,k)h + C_{M_\alpha}(M,k)\alpha + C_{M_\beta}(M,k)\beta \qquad (5.15)$$

where $C_M(M,k)$ is the total unsteady complex pitching moment coefficient about the EA,

$C_{M_h}(M,k)$ is the pitching moment coefficient due to simple harmonic plunging,

$C_{M_\alpha}(M,k)$ is the pitching moment coefficient due to simple harmonic pitching, and

$C_{M_\beta}(M,k)$ is the pitching moment due to simple harmonic flapping. Finally, the unsteady

hinge moment coefficient is given by:

$$C_H(M,k) = C_{H_h}(M,k)h + C_{H_\alpha}(M,k)\alpha + C_{H_\beta}(M,k)\beta \qquad (5.16)$$

where $C_H(M,k)$ is the total unsteady complex hinge moment coefficient, $C_{H_h}(M,k)$ is the

hinge moment coefficient due to simple harmonic plunging, $C_{H_\alpha}(M,k)$ is the hinge

moment coefficient due to simple harmonic pitching, and $C_{H_\beta}(M,k)$ is the hinge moment

coefficient due to simple harmonic flapping. It is important to note that in classical

aeroelastic formulations, aerodynamic coefficients are non-dimensionalized with

semichord such that the lift coefficient is:

$$C_l^b = \frac{L'}{\frac{1}{2}\rho U_\infty^2 b} \qquad (5.17)$$

The pitching moment coefficient is:

$$C_M^b = \frac{M'}{\frac{1}{2}\rho U_\infty^2 b^2} \qquad (5.18)$$

and the hinge moment coefficient is:

$$C_H^b = \frac{T'}{\frac{1}{2}\rho U_\infty^2 b^2} \qquad (5.19)$$

However, Lin2D outputs are non-dimensionalized with chord length such that the lift

coefficient is:

$$C_l^c = \frac{L'}{\frac{1}{2}\rho U_\infty^2 c} \qquad (5.20)$$

The pitching moment coefficient is:

$$C_M^c = \frac{M'}{\frac{1}{2}\rho U_\infty^2 c^2} \qquad (5.21)$$

and the hinge moment is:

$$C_H^c = \frac{T'}{\frac{1}{2}\rho U_\infty^2 c^2} \qquad (5.22)$$

By inspection, the following are determined:

$$C_l^b = 2C_l^c \qquad (5.23)$$

$$C_M^b = 4C_M^c \qquad (5.24)$$

$$C_H^b = 4C_H^c \qquad (5.25)$$

Therefore, the complex force and moment coefficients are written in terms of semichord (b) to remain consistent with Theodorsen's derivation. The total lift force acting on an airfoil oscillating in compressible subsonic flow is:

$$L' = \rho U_\infty^2 b \left\{ C_{l_h^b}(M,k)h + C_{l_\alpha^b}(M,k)\alpha + C_{l_\beta^b}(M,k)\beta \right\} \tag{5.26}$$

The pitching moment about the elastic axis is:

$$M' = 2\rho U_\infty^2 b^2 \left\{ C_{M_h}(M,k)h + C_{M_\alpha}(M,k)\alpha + C_{M_\beta}(M,k)\beta \right\} \tag{5.27}$$

The hinge moment is:

$$T' = 2\rho U_\infty^2 b^2 \left\{ C_{H_h}(M,k)h + C_{H_\alpha}(M,k)\alpha + C_{H_\beta}(M,k)\beta \right\} \tag{5.28}$$

Finally, Scanlan and Rosenbaum (1968) state that Possio's integral equation is valid up to a Mach number of 0.70. This is because typical airfoils have a critical Mach number near Mach 0.70 where a normal shock will form on the airfoil surface and the underlying assumptions in Possio's derivation will no longer be valid. However, supersonic aircraft use much thinner airfoils that have critical Mach numbers near Mach 0.90; thus the limit described by Scanlan and Rosenbaum (1968) can be extended without substantial error.

5.3. Supersonic Flow

The supersonic airloads for a typical section were developed using First-Order Piston Theory. Piston Theory was first presented by Ashley and Zartarian in the Journal of the Aeronautical Sciences in 1956. Piston Theory refers to the method for calculating the

aerodynamic loads on a body in which the local pressure is generated by the body's motion normal to the flow direction. For piston motion that generates only simple,
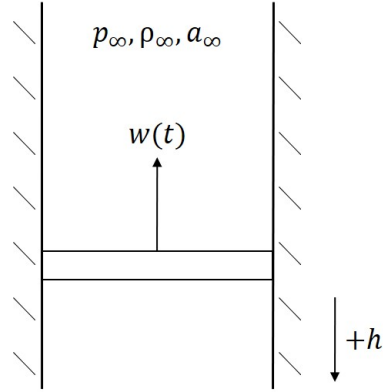
Figure 5.1 Pressure on a Piston in a One-Dimensional Channel

isentropic waves, the instantaneous pressure of the piston surface was estimated to be:

$$p = p_\infty \left\{ 1 + \left[\frac{(\gamma - 1)}{2} \right] \left(\frac{w}{a_\infty} \right) \right\}^{2\gamma/(\gamma-1)} \tag{5.29}$$

where w is the velocity of the piston normal to the flow. For appropriate magnitudes of the ratio of w/a_∞, Equation (5.29) may be reduced to its linear approximation:

$$p - p_\infty = \rho_\infty a_\infty w \tag{5.30}$$

where p is the local static pressure, p_∞ is the freestream static pressure, ρ_∞ is the freestream density, a_∞ is the freestream speed of sound, and w is the velocity of the piston surface. The local pressure on the upper and lower surfaces of an airfoil oscillating normal to the direction of flow are given by:

$$p_u - p_\infty = \rho_\infty a_\infty^2 \left(\frac{-w}{a_\infty} \right) \tag{5.31}$$

$$p_l - p_\infty = \rho_\infty a_\infty^2 \left(\frac{w}{a_\infty} \right) \tag{5.32}$$

where p_u is the local pressure on the upper surface and p_l is the local pressure on the lower surface. Then, utilizing Equation (5.30), the difference in pressure between the upper and lower surfaces is given by:

$$\Delta p = p_u - p_l = -2\rho_\infty a_\infty w \tag{5.33}$$

and the pressure coefficient for the piston surface is:

$$\Delta C_p = \frac{p_u - p_l}{\frac{1}{2}\rho_\infty U_\infty^2} = \frac{-2}{\rho_\infty U_\infty^2} (2\rho_\infty a_\infty w) \tag{5.34}$$

Next, substituting the definition of Mach number simplifies Equation (5.34),

$$\Delta C_p = -\frac{4}{M} \left(\frac{w}{U_\infty} \right) \tag{5.35}$$

Utilizing Equation (5.35), the piston surface now represents an oscillating airfoil. The downwash velocity of the typical section can be written in terms of the pitch and plunge degrees of freedom as:

$$w = - \left[\dot{h}b + (x^* - ab)\dot{\alpha} + U_\infty \alpha \right] \qquad (-b \le x^* \le be) \tag{5.36}$$

Similarly, the downwash velocity of the flap section can be written as:

$$w = -\left[\dot{h}b + (x^* - ab)\dot{\alpha} + (x^* - be)\dot{\beta} + U_\infty\alpha + U_\infty\beta\right] \qquad (be \leq x^* \leq b) \qquad (5.37)$$

Recall, Equation (5.36) and Equation (5.37) can be obtained from Figure 4.1. Since lift on the lifting surface is found by integrating the pressure coefficient over its chord length, it is expressed as:

$$L'_w = \int_{-b}^{be} \Delta p \, dx^* = \int_{-b}^{be} \Delta C_p q \, dx^* \qquad (5.38)$$

Then, substituting Equation (5.35) and Equation (5.36) into Equation (5.38) yields:

$$L'_w = \frac{4q}{MU_\infty} \int_{-b}^{be} \left[\dot{h}b + (x^* - ab)\dot{\alpha} + U_\infty\alpha\right] dx^* \qquad (5.39)$$

After evaluating the integral and simplifying, Equation (5.39) becomes:

$$L'_w = \frac{4bq}{MU_\infty} \left\{\dot{h}b(1+e) - \tfrac{1}{2}b(1-e^2)\dot{\alpha} - ab(1+e)\dot{\alpha} + U_\infty(1+e)\alpha\right\} \qquad (5.40)$$

The lift on the flap section can also be found by following the above procedure.

$$L'_f = \int_{be}^{b} \Delta p \, dx^* = \int_{be}^{b} \Delta C_p q \, dx^* \qquad (5.41)$$

whereby substituting Equation (5.35) and Equation (5.37) into Equation (5.41) yields:

$$L'_f = \frac{4q}{MU_\infty} \int_{be}^{b} \left[\dot{h}b + (x^* - ab)\dot{\alpha} + (x^* - be)\dot{\beta} + U_\infty\alpha + U_\infty\beta\right] dx^* \qquad (5.42)$$

Evaluating the integral and simplifying, Equation (5.42) becomes:

$$L'_f = \frac{4bq}{MU_\infty}\left\{\dot{h}b(1-e)+\tfrac{1}{2}b(1-e^2)\dot{\alpha}-ab(1-e)\dot{\alpha}+\tfrac{1}{2}b(1-e^2)\dot{\beta}-\right.$$

$$\left. be(1-e)\dot{\beta}+U_\infty(1-e)\alpha+U_\infty(1-e)\beta\right\} \quad (5.43)$$

The total lift on the airfoil section is a combination of the wing section lift and flap section lift,

$$L' = L'_w + L'_f \quad (5.44)$$

Substituting Equation (5.40) and Equation (5.43) into Equation (5.44) and simplifying defines the total lift force per unit span for a pitch-plunge-flap typical section oscillating in supersonic flow.

$$L' = \frac{4bq}{MU_\infty}\left\{2b\dot{h}-2ab\dot{\alpha}+2U_\infty\alpha+\left(\frac{1}{2}b(1-e)-be(1-e)\right)\dot{\beta}+U_\infty(1-e)\beta\right\} \quad (5.45)$$

To reduce this equation for the two degree of freedom pitch-plunge case, e, which is the location of the flap break, is set to 1. Next, the airfoil pitching moment about its elastic axis is found using the same process. The pitching moment contribution from the wing section is:

$$M'_w = -\int_{-b}^{be} \Delta p\,(x^*-ab)\,dx^* = -\int_{-b}^{be} \Delta C_p q\,(x^*-ab)\,dx^* \quad (5.46)$$

whereby substituting Equation (5.35) into Equation (5.46) produces:

$$M'_w = \frac{4q}{MU_\infty}\int_{-b}^{be} \left[\dot{h}b+(x^*-ab)\,\dot{\alpha}+U_\infty\alpha\right](x^*-ab)\,dx^* \quad (5.47)$$

Evaluating this integral and simplifying defines the pitching moment contribution of the wing section:

$$M'_w = \frac{4ab^3q}{MU_\infty}\left\{\left[\dot{h} - a\dot{\alpha}\left(\frac{U_\infty}{b}\right)\alpha\right](1+e) - \frac{1}{3a}\left(e^3+1\right)\dot{\alpha} - \frac{1}{2}\left(1-e^2\right)\dot{\alpha}\right.$$
$$\left. - \frac{1}{2a}\left[\dot{h} - \frac{1}{2}\dot{\alpha} + \left(\frac{U_\infty}{b}\right)\alpha\right]\left(e^2-1\right)\right\} \quad (5.48)$$

Next, the contribution of the flap is determined by:

$$M'_f = \int_{be}^{b} \Delta p(x^* - ab)\,dx^* = \int_{be}^{b} \Delta p x^*\,dx^* - ab\int_{be}^{b} \Delta p\,dx^* \quad (5.49)$$

which becomes:

$$M'_f = \int_{be}^{b} \Delta p x^*\,dx^* - abL_f = \int_{be}^{e} \Delta C_p q x^*\,dx^* - abL_f \quad (5.50)$$

Evaluating the integral and simplifying yields:

$$M'_f = \frac{4ab^3q}{MU_\infty}\left\{\left(\dot{h} - a\alpha + \left(\frac{U_\infty}{b}\right)\alpha\right)(1+e) - \frac{1}{3a}\left(e^3+1\right)\dot{\alpha} - \frac{1}{2}\left(1-e^2\right)\dot{\alpha}\right.$$
$$- \frac{1}{2a}\left(\dot{h} - \frac{1}{2}\dot{\alpha} + \frac{U_\infty}{b}\alpha\right)\left(e^2-1\right)$$
$$- \frac{1}{2a}\left(\dot{h} - a\dot{\alpha} - e\dot{\beta} + \left(\frac{U_\infty}{b}\right)(\alpha+\beta)\right)\left(e^2-1\right) - \frac{1}{3a}\left(\dot{\alpha}+\dot{\beta}\right)\left(e^3-1\right)$$
$$\left. - \left(\dot{h} - a\dot{\alpha} + \left(\frac{1}{2}-e\right)\dot{\beta} + \left(\frac{U_\infty}{b}(\alpha+\beta)\right)\right)(1-e) - \frac{1}{2}\left(1-e^2\right)\dot{\alpha}\right\} \quad (5.51)$$

Combining the wing section contribution and flap contribution produces the total pitching

moment about the elastic axis,

$$
\begin{aligned}
M' = \frac{4ab^3 q}{MU_\infty} \Bigg\{ & \left[\dot{h} - a\dot{\alpha} \left(\frac{U_\infty}{b} \right) \alpha \right] (1+e) - \frac{2e^3}{3a} \dot{\alpha} - \frac{1}{3b} \dot{\beta} \left(e^3 - 1 \right) \\
& - \left(1 - e^2 \right) \dot{\alpha} - \frac{1}{2a} \left[2\dot{h} - \left(a + \frac{1}{2} \right) \dot{\alpha} + 2 \left(\frac{U_\infty}{b} \right) \alpha - e\dot{\beta} + \left(\frac{U_\infty}{b} \right) \beta \right] \left(e^2 - 1 \right) \\
& - \left[\dot{h} - a\dot{\alpha} + \left(\frac{1}{2} - e \right) \dot{\beta} + \left(\frac{U_\infty}{b} \right) (\alpha + \beta) \right] (1 - e) \Bigg\}
\end{aligned}
\tag{5.52}
$$

where a, b, and e are geometric parameters defined in Figure 4.1, q is the dynamic

pressure, M is the Mach number, and U_∞ is the freestream velocity. The above process is

repeated once again for the pitching moment and the hinge moment is found using the

same process, starting with :

$$
T' = \int_{be}^{b} \Delta p \, (x^* - eb) \, dx^* = \int_{be}^{b} \Delta C_p q \, (x^* - eb) \, dx^*
\tag{5.53}
$$

or:

$$
T' = \int_{be}^{b} \Delta C_p q \, x^* \, dx^* - eb \int_{be}^{b} \Delta C_p q \, dx^*
\tag{5.54}
$$

which reduces to:

$$
T' = \int_{be}^{b} \Delta C_p q \, x^* \, dx^* - eb L_f
\tag{5.55}
$$

Substituting Equation (5.37) into Equation (5.55), the hinge moment becomes:

$$
T' = \frac{4q}{MU_\infty} \int_{be}^{b} \left[\dot{h} b + (x^* - ab) \dot{\alpha} + (x^* - be) \dot{\beta} + U_\infty \alpha + U_\infty \alpha \right] x^* \, dx^* - eb L_f
\tag{5.56}
$$

Evaluating the integral and simplifying yields the total hinge moment:

$$T' = \frac{4eb^3 q}{MU_\infty}\left\{\left[\frac{1}{2e}\left(1-e^2-(1-e)\right)\right]\left[\dot{h}-a\dot{\alpha}-e\dot{\beta}+\left(\frac{U_\infty}{b}(\alpha+\beta)\right)\right]\right.$$
$$\left.+\left[\frac{1}{3e}\left(1-e^3\right)+\frac{1}{2}\left(1-e^2\right)\right]\left[\dot{\alpha}+\dot{\beta}\right]\right\} \quad (5.57)$$

For the loads to be useful in flutter analysis, simple harmonic motion is once again

assumed. This assumption modifies the lift equation to:

$$\bar{L}' = \frac{4\omega b^2 q}{MU_\infty}\left\{2i\bar{h}+2\left[\left(\frac{1}{k}\right)-ai\right]\bar{\alpha}+\left[\left(\frac{1}{k}\right)+\left(\frac{1}{2}-e\right)i\right](1-e)\bar{\beta}\right\} \quad (5.58)$$

where ω is the circular frequency of oscillation and k is the reduced frequency. The

pitching moment reduces to:

$$\bar{M}' = \frac{4a\omega b^3 q}{MU_\infty}\left\{\left[2ei-\frac{1}{a}\left(e^2-1\right)\right]\bar{h}\right.$$
$$+\left[2e\left[-ai+\left(\frac{1}{k}\right)\right]+\left[i+\frac{1}{2a}\left(a+\frac{1}{2}\right)-\frac{1}{a}\left(\frac{1}{k}\right)\right]\left(e^2-1\right)-\frac{2}{3}\frac{e^3}{a}i\right]\bar{\alpha} \quad (5.59)$$
$$\left[-\frac{1}{3a}\left(e^3-1\right)i+\frac{1}{2a}\left[i+\left(\frac{1}{k}\right)\right]\left(e^2-1\right)-\left[\left(\frac{1}{2}-a\right)i+\left(\frac{1}{k}\right)\right](1-e)\right]\bar{\beta}\right\}$$

and the hinge moment reduces to:

$$\bar{T}' = \frac{4e\omega b^3 q}{MU_\infty}\left\{[pi]\bar{h}+\left[(-pa+r)i+p\left(\frac{1}{k}\right)\right]\bar{\alpha}+\left[(-pe+r)i+p\left(\frac{1}{k}\right)\right]\bar{\beta}\right\} \quad (5.60)$$

where,

$$p = \frac{1}{2e}\left(1-e^2\right)-(1-e)$$

and,

$$r = \frac{1}{3e}\left(1 - e^3\right) + \frac{1}{2}\left(1 - e^2\right)$$

Finally, the loads can be algebraically manipulated to simplify the calculation of the generalized forces. The lift equation in terms of the semichord, b, is simplified to:

$$L' = \frac{2\rho\, b_r}{M\, k_r} b^2 \omega^2 \left\{ L_h \bar{h} + L_\alpha \bar{\alpha} + L_\beta \bar{\beta} \right\} \tag{5.61}$$

where L_h is the lift due to plunging, L_α is the lift due to pitching, and L_β is the lift due to flap deflection. Similar to the incompressible loads, each of these coefficients is written as a polynomial of (b_r/b), where b_r is the reference semichord and b is the semichord at a given spanwise location. For example:

$$L_\alpha = K_1(L_\alpha) + \left(\frac{b_r}{b}\right) K_2(L_\alpha) \tag{5.62}$$

The pitching moment about the EA becomes:

$$M' = \frac{2a\rho\, b_r}{M\, k_r} b^3 \omega^2 \left\{ M_h \bar{h} + M_\alpha \bar{\alpha} + M_\beta \bar{\beta} \right\} \tag{5.63}$$

where M_h is the moment due to plunging, M_α is the moment due to pitching, and M_β is the moment due to flap deflection. Since these coefficients are complex they can be written as a polynomial in terms of (b_r/b). The hinge moment reduces to:

$$T' = \frac{2e\rho\, b_r}{M\, k_r} b^3 \omega^2 \left\{ T_h \bar{h} + T_\alpha \bar{\alpha} + T_\beta \bar{\beta} \right\} \tag{5.64}$$

where T_h is the hinge moment due to plunging, T_α is the hinge moment due to pitching, and T_β is the hinge moment due to flap deflection. All of the above coefficients associated with L', M', and T', and their polynomial expansions are identified in Appendix B.

5.4. Aerodynamic Forcing Functions

The aerodynamic forcing functions used in this flutter analysis are calculated using the principle of virtual work. The total virtual work done by the aerodynamic forces is the amount of work required to deform the structure from ξ_i to $(\xi_i + \delta\xi_i)$ while all of other degrees of freedom are constant (Scanlan & Rosenbaum, 1968). Since the fuselage is not treated as lifting surface, the virtual work done by the fuselage is:

$$\delta W_{F_i} = 0 \tag{5.65}$$

The virtual work done by the vertical tail when it is oscillating at the ith normal mode is:

$$\delta W_{VT_i} = \delta\xi_i \int_0^{L_{VT}} (L'h_{VT_{2_i}} + M'\alpha_{VT_i} + T'\beta_{VT_i})\, dz \tag{5.66}$$

Equation (5.66) shows that the virtual work done by the vertical tail is the combination of the work done per unit span of each of the DOFs, integrated along the span. The first term under the integral represents the work done by vertical tail plunging, where the aerodynamic load associated with the plunge DOF is lift on the vertical tail (side force). The second term under the integral represents the work done by vertical tail pitching, where the aerodynamic load associated with the pitch DOF is the pitching moment about the EA of the VT. The last term under the integral represents the work done by flap

deflection, where the aerodynamic load associated with the flap DOF is the hinge moment, or the rudder hinge moment. The virtual work done by the starboard horizontal tail when it is oscillating at the *i*th normal mode is:

$$\delta W_{HTS_i} = \delta \xi_i \int_0^{L_{HTS}} (L' h_{HTS_{3_i}} + M' \alpha_{HTS_i} + T' \beta_{HTS_i}) \, dy \qquad (5.67)$$

where the first term under the integral represents the work done by starboard horizontal tail plunging, where the aerodynamic load associated with the plunge DOF is lift on the starboard horizontal tail. The second term under the integral represents the work done by starboard horizontal tail pitching, where the aerodynamic load associated with the pitch DOF is the pitching moment about the EA of the starboard HT. The last term under the integral represents the work done by flap deflection, where the aerodynamic load associated with the flap DOF is the hinge moment, or the starboard elevator hinge moment. The virtual work done by the port horizontal tail when it is oscillating at the *i*th normal mode is:

$$\delta W_{HTP_i} = \delta \xi_i \int_0^{L_{HTP}} (L' h_{HTS_{3_i}} + M' \alpha_{HTP_i} + T' \beta_{HTP_i}) \, dy \qquad (5.68)$$

where the first term under the integral represents the work done by port horizontal tail plunging, where the aerodynamic load associated with the plunge DOF is lift on the port horizontal tail. The second term under the integral represents the work done by port horizontal tail pitching, where the aerodynamic load associated with the pitch DOF is the pitching moment about the EA of the port HT. The last term under the integral represents

the work done by flap deflection, where the aerodynamic load associated with the flap

DOF is the hinge moment, or the port elevator hinge moment. The total virtual work done

by the aerodynamic forces for the ith normal mode is:

$$\delta W_i = \left(\delta W_{F_i} + \delta W_{VT_i} + \delta W_{HTS_i} + \delta W_{HTP_i} \right) \tag{5.69}$$

To determine the generalized aerodynamic forcing function, the following expression can

be utilized:

$$Q_i = \frac{\delta W_i}{\delta \xi_i} \tag{5.70}$$

The generalized aerodynamic forcing function for the ith mode is the superposition of the

various components,

$$Q_i = Q_{F_i} + Q_{VT_i} + Q_{HTS_i} + Q_{HTP_i} \tag{5.71}$$

where generalized force contribution of the fuselage is:

$$Q_{F_i} = 0 \tag{5.72}$$

The generalized force contribution of the vertical tail is:

$$Q_{VT_i} = \int_0^{L_{VT}} (L' h_{VT_{2_i}} + M' \alpha_{VT_i} + T' \beta_{VT_i}) \, dz \tag{5.73}$$

the generalized force contribution of the starboard horizontal tail is:

$$Q_{HTS_i} = \int_0^{L_{HTS}} (L' h_{HTS_{3_i}} + M' \alpha_{HTS_i} + T' \beta_{HTS_i}) \, dy \tag{5.74}$$

the generalized force contribution of the port horizontal tail is:

$$Q_{HTP_i} = \int_0^{L_{HTP}} (L'h_{HTS_{3_i}} + M'\alpha_{HTP_i} + T'\beta_{HTP_i})\,dy \qquad (5.75)$$

where L' is the two-dimensional unsteady lift, M' is the two-dimensional unsteady pitching moment about the EA, and T' is the two-dimensional unsteady hinge moment. The expressions for L', M', and T' developed in Section 5.1 for subsonic incompressible, 5.2 for subsonic compressible, and 5.3 for supersonic can be substituted into Equations (5.73) through (5.75) to define the generalized aerodynamics of each lifting surface. The difficulty resides in evaluating the integrals as lift and moment, and hinge moment are calculated for a constant single value of reduced frequency. For a tapered wing, the semichord varies along the span and thus the reduced frequency varies with it. However, the reduced frequency can be defined as:

$$k = \left(\frac{b\omega}{U_\infty}\right) = \frac{b}{b_r}\left(\frac{b_r\omega}{U_\infty}\right) \qquad (5.76)$$

or,

$$k = \frac{b}{b_r}k_r \qquad (5.77)$$

where b_r is the reference semichord, defined at 75% of the semispan, and k_r is the reduced frequency at 75% of the semispan. Then the generalized forces can be evaluated at the reference reduced frequency (k_r) and the integration becomes a function of geometry only. Furthermore, Scanlan and Rosenbaum state that Theodorsen's function does not vary rapidly with $1/k$ and the following substitution can be made:

$$C(k) = C(k_r) \tag{5.78}$$

These assumptions hold true for conventional taper ratios (Scanlan & Rosenbaum, 1968).

Once the aerodynamic influence coefficients for each mode are known, Equation (5.71)

can be rewritten such that the generalized force on the ith mode is:

$$Q_i = \omega^2 \sum_{j=1}^{N} C_{ij} \xi_j \tag{5.79}$$

where C_{ij} is the aerodynamic influence of the jth mode on the ith mode.

To determine the three-dimensional aerodynamic loads, that is the loads acting on the

entire lifting surface, the two-dimensional loads are integrated over the span of each lifting

surface. For the system described in Chapter 3, whose semichord is known at discrete

positions along its span, the lift, pitching moment, and hinge moment are calculated at

these locations. These represent the aerodynamic loads for each segment. The summation

of the loads on each segment gives the aerodynamic loads on the whole lifting surface.

Recall the typical section in Figure 4.1. The x' axis is aligned in the direction of flow

and the z' axis is normal to the flow such that lift acts in the positive z' direction. The

lifting surfaces are all treated as three-dimensional extensions of the typical section. For

the vertical tail, the x' axis is aligned with the X axis and the z' points in the positive Y

direction. For both the port and starboard sides of the horizontal tail, the x' axis is parallel

to the X axis and the z' axis points in the positive Z direction. Since the section properties

are known at discrete locations along the span, the properties are assumed to vary linearly

between stations.

For the vertical tail, the integral is evaluated from zero to L_{VT} in the Z direction.

Figure 5.2 shows the lengths used in integrating along the span of the vertical tail. The
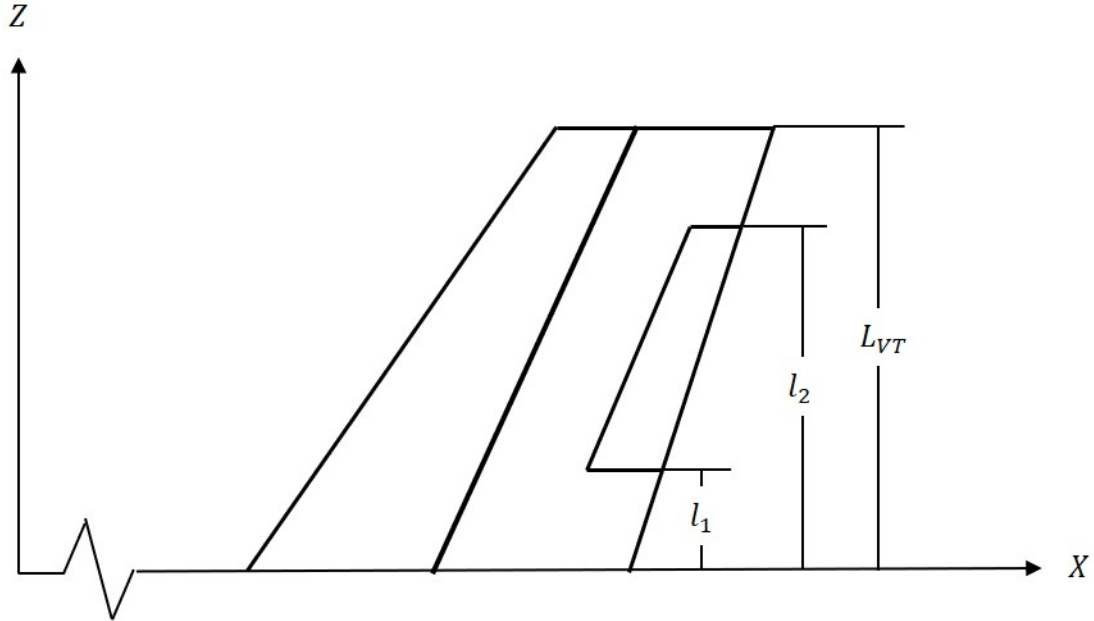
Figure 5.2 Vertical Tail Lengths

length l_1 is the distance from the root of the VT to the lower break point of the rudder, l_2 is

the distance from the root of the VT to the upper break point of the rudder, and L_{VT} is the

distance from the root of the VT to the tip of the VT. For the vertical tail, the plunging

(bending) degree of freedom is the bending in the Y direction. The pitching (torsion)

degree of freedom is the rotation about the Z axis. The flap degree of freedom corresponds

to rudder deflection. In other words, the ith bending mode of the vertical tail is:

$$h_i = h_{VT_{2_i}}(z) \qquad\qquad (5.80)$$

the ith torsional mode of the vertical tail is:

$$\alpha_i = \alpha_{VT_i}(z) \tag{5.81}$$

the ith flapping mode of the vertical tail is:

$$\beta_i = \beta_{VT_i}(z) \tag{5.82}$$

To determine the three-dimensional airloads for the starboard horizontal tail, the integral is evaluated from zero to L_{HTS} in the positive Y direction. Figure 5.3 shows the lengths used in integrating along the span of the starboard side of the horizontal tail. The length l_3 is
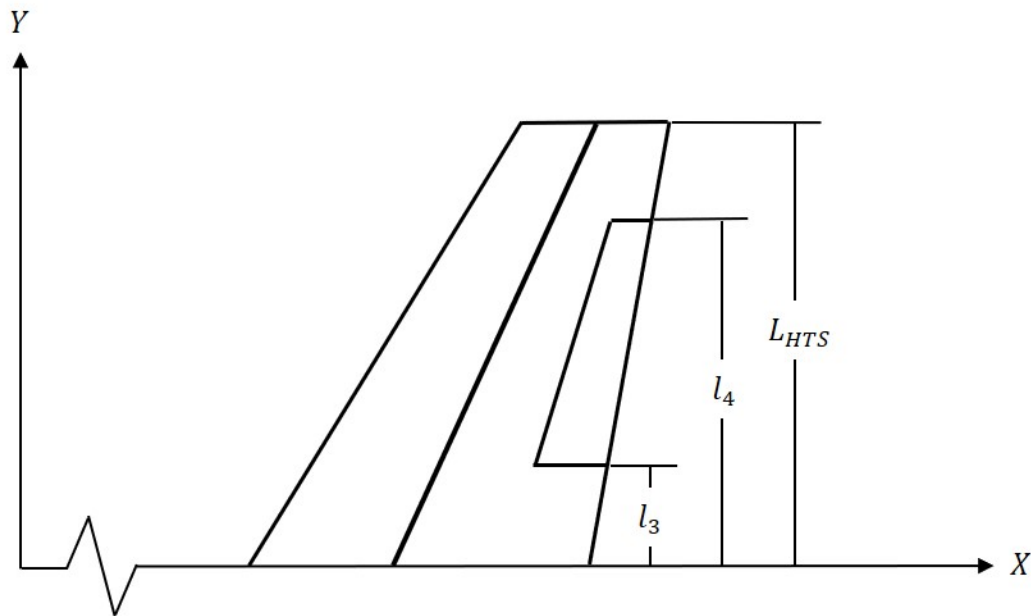
Figure 5.3 Starboard Horizontal Tail Lengths

the distance from the root of the HT to the inboard break point of the starboard elevator, l_4 is the distance from the root of the HT to the outboard break point of the starboard elevator, and L_{HTS} is the distance from the root of the HT to the tip of the starboard HT.

For the starboard horizontal tail, the bending degree of freedom is the bending in the Z direction. The torsional degree of freedom is the rotation about the Y axis. The flap degree of freedom corresponds to elevator deflection. The ith bending mode of the starboard horizontal tail is:

$$h_i = h_{HTS_{3_i}}(y) \tag{5.83}$$

The ith torsional mode of the starboard horizontal tail is:

$$\alpha_i = \alpha_{HTS_i}(y) \tag{5.84}$$

The ith flap mode of the starboard HT is:

$$\beta_i = \beta_{HTS_i}(y) \tag{5.85}$$

For the port horizontal tail, the bending degree of freedom is the bending in the Z direction. The torsional degree of freedom is the rotation about the Y axis. The flap degree of freedom corresponds to elevator deflection. The ith bending mode of the port horizontal tail is:

$$h_i = h_{HTP_{3_i}}(y) \tag{5.86}$$

the ith torsional mode of the port HT is:

$$\alpha_i = \alpha_{HTP_i}(y) \tag{5.87}$$

the ith flap mode of the port HT is:

$$\beta_i = \beta_{HTP_i}(y) \tag{5.88}$$

To determine the three-dimensional airloads for the port horizontal tail, the integral is evaluated from zero to L_{HTP} in the negative Y direction. Figure 5.4 shows the lengths used in integrating along the span of the port side of the horizontal tail.
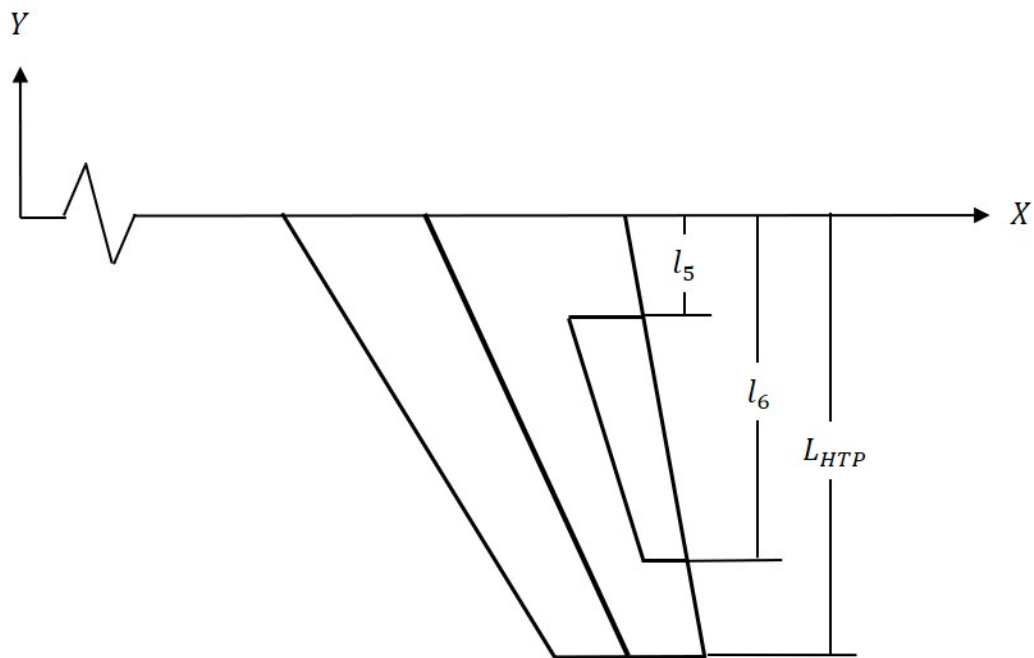
Figure 5.4 Port Horizontal Tail Lengths

These equations are used to determine the aerodynamic influence coefficients for each of the lifting surfaces. Now the process for determining the generalized aerodynamic forces for use in flutter analysis has been shown, the process for calculating the aerodynamic influence coefficients for incompressible flow, compressible subsonic flow, and supersonic flow will be discussed.

5.4.1. Incompressible Flow

The following section discusses the procedure for determining the aerodynamic influence coefficients of a three dimensional lifting surface oscillating in incompressible flow. The methods discussed by Scanlan and Rosenbaum have been adapted from a cantileverd wing to a T-tail structure. For incompressible flow, the aerodynamic influence of the jth normal mode on the ith generalized force is:

$$
\begin{aligned}
C_{ij} = \pi\rho \int_0^L & b^2 h_i h_j L_h + b^3 h_i \alpha_j \left[L_\alpha - \left(\tfrac{1}{2}+a\right) L_h \right] + b^3 h_i \beta_j \left[L_\beta - (c-e) L_z \right] \\
& + b^3 \alpha_i h_j \left[M_h - \left(\tfrac{1}{2}+a\right) L_h \right] + b^4 \alpha_i \alpha_j \left[M_\alpha - \left(\tfrac{1}{2}+a\right)(L_\alpha + M_h) + \left(\tfrac{1}{2}+a\right)^2 L_h \right] \\
& + b^4 \alpha_i \beta_j \left[M_\beta - \left(\tfrac{1}{2}+a\right) L_\beta - (c-e) M_z + (c-e)\left(\tfrac{1}{2}+a\right) L_z \right] + b^3 \beta_i h_j \left[T_h - (c-e) P_h \right] \\
& + b^4 \beta_i \alpha_j \left[T_\alpha - (c-e) P_\alpha - \left(\tfrac{1}{2}+a\right) T_h + \left(\tfrac{1}{2}+a\right)(c-e) P_h \right] \\
& + b^4 \beta_i \beta_j \left[T_\beta - (c-e)(P_\beta + T_z) + (c-e)^2 P_z \right] \quad (5.89)
\end{aligned}
$$

where L, M, T, and P are complex coefficients that are functions of geometry. These constants were previously defined in Section 5.1. For simplicity, Equation (5.89) can be written as:

$$
C_{ij} = C_{h_i h_j} + C_{h_i \alpha_j} + C_{h_i \beta_j} + C_{\alpha_i h_j} + C_{\alpha_i \alpha_j} + C_{\alpha_i \beta_j} + C_{\beta_i h_j} + C_{\beta_i \alpha_j} + C_{\beta_i \beta_j} \tag{5.90}
$$

The aerodynamic influence of the jth bending mode on the ith bending mode is:

$$
C_{h_i h_j} = \pi\rho \int_0^L b^2 h_i h_j L_h \tag{5.91}
$$

which can be expanded to :

$$C_{h_i h_j} = \pi \rho \, K_1(L_h) \int_0^L b^2 h_i h_j + \pi \rho \, b_r K_2(L_h) \int_0^L b \, h_i h_j \qquad (5.92)$$

where $K_1(L_h)$ and $K_2(L_h)$ are constant and first order in L_h, respectively, when they are is written as polynomials in terms of b_r/b. These coefficients were previously discussed in Section 5.1. The influence of the jth torsional mode on the ith bending mode is:

$$C_{h_i \alpha_j} = \pi \rho \int_0^L b^3 h_i \alpha_j \left[L_\alpha - \left(\tfrac{1}{2} + a \right) L_h \right] \qquad (5.93)$$

which can be expanded to:

$$
\begin{aligned}
C_{h_i \alpha_j} = \pi \rho \left[K_1(L_\alpha) - \left(\tfrac{1}{2} + a \right) K_1(L_h) \right] \int_0^L b^3 h_i \alpha_j \\
+ \pi \rho \, b_r \left[K_2(L_\alpha) - \left(\tfrac{1}{2} + a \right) K_2(L_h) \right] \int_0^L b^2 h_i \alpha_j \\
+ \pi \rho \, b_r^2 K_3(L_\alpha) \int_0^L b \, h_i \alpha_j \quad (5.94)
\end{aligned}
$$

The influence of the jth flapping mode on the ith bending mode is:

$$C_{h_i \beta_j} = \pi \rho \int_0^L b^3 h_i \beta_j \left[L_\beta - (c - e) L_z \right] \qquad (5.95)$$

which can be expanded to:

$$C_{h_i\beta_j} = \pi\rho \left[K_1(L_\beta) - (c-e) K_1(L_z) \right] \int_0^L b^3 h_i \beta_j$$

$$+ \pi\rho b_r \left[K_2(L_\beta) - (c-e) K_2(L_z) \right] \int_0^L b^2 h_i \beta_j$$

$$+ \pi\rho b_r^2 K_3(L_\beta) \int_0^L b\, h_i \beta_j \quad (5.96)$$

The influence of the jth bending mode on the ith torsional mode is:

$$C_{\alpha_i h_j} = \pi\rho \int_0^L b^3 \alpha_i h_j \left[M_h - \left(\tfrac{1}{2} + a \right) L_h \right] \quad (5.97)$$

which can be expanded to:

$$C_{\alpha_i h_j} = \pi\rho \left[K_1(M_h) - \left(\tfrac{1}{2} + a \right) K_1(L_h) \right] \int_0^L b^3 \alpha_i h_j$$

$$- \pi\rho b_r \left(\tfrac{1}{2} + a \right) K_2(L_h) \int_0^L b^2 \alpha_i h_j \quad (5.98)$$

The influence of the jth torsional mode on the ith torsional mode is:

$$C_{\alpha_i \alpha_j} = \pi\rho \int_0^L b^4 \alpha_i \alpha_j \left[M_\alpha - \left(\tfrac{1}{2} + a \right)(L_\alpha + M_h) + \left(\tfrac{1}{2} + a \right)^2 L_h \right] \quad (5.99)$$

which can be expanded to:

$$C_{\alpha_i\alpha_j} = \pi\rho \left[K_1(M_\alpha) - \left(\tfrac{1}{2}+a\right)(K_1(L_\alpha)+K_1(M_h)) + \left(\tfrac{1}{2}+a\right)^2 K_1(L_h) \right] \int_0^L b^4\alpha_i\alpha_j$$

$$+ \pi\rho\, b_r \left[K_2(M_\alpha) - \left(\tfrac{1}{2}+a\right) K_2(L_\alpha) + \left(\tfrac{1}{2}+a\right)^2 K_2(L_h) \right] \int_0^L b^3\alpha_i\alpha_j$$

$$+ \pi\rho\, b_r^2 K_3(L_\alpha) \int_0^L b^2\alpha_i\alpha_j \quad (5.100)$$

The influence of the jth flapping mode on the ith torsional mode is:

$$C_{\alpha_i\beta_j} = \pi\rho \int_0^L b^4\alpha_i\beta_j \left[M_\beta - \left(\tfrac{1}{2}+a\right) L_\beta - (c-e)M_z + (c-e)\left(\tfrac{1}{2}+a\right) L_z \right] \quad (5.101)$$

which can be expanded to:

$$C_{\alpha_i\beta_j} = \pi\rho \left[K_1(M_\beta) - \left(\tfrac{1}{2}+a\right) K_1(L_\beta) - (c-e)K_1(M_z) \right.$$

$$\left. + (c-e)\left(\tfrac{1}{2}+a\right) K_1(L_z) \right] \int_0^L b^4\alpha_i\beta_j + \pi\rho\, b_r \left[K_2(M_\beta) - \left(\tfrac{1}{2}+a\right) K_2(L_\beta) \right.$$

$$\left. - (c-e)K_2(M_z) + (c-e)\left(\tfrac{1}{2}+a\right) K_2(L_z) \right] \int_0^L b^3\alpha_i\beta_j$$

$$\pi\rho\, b_r^2 \left[K_3(M_\beta) - \left(\tfrac{1}{2}+a\right) K_3(L_\beta) \right] \int_0^L b^2\alpha_i\beta_j \quad (5.102)$$

The influence of the jth bending mode on the ith flapping mode is:

$$C_{\beta_i h_j} = \pi\rho \int_0^L b^3\beta_i h_j \left[T_h - (c-e)P_h \right] \quad (5.103)$$

which can be expanded to:

$$C_{\beta_i h_j} = \pi\rho \left[K_1(T_h) - (c-e)K_1(P_h) \right] \int_0^L b^3 \beta_i h_j$$

$$+ \pi\rho \, b_r \left[K_2(T_h) - (c-e)K_2(P_h) \right] \int_0^L b^2 \beta_i h_j \quad (5.104)$$

The influence of the jth torsional mode on the ith flapping mode is:

$$C_{\beta_i \alpha_j} = \pi\rho \int_0^L b^4 \beta_i \alpha_j \left[T_\alpha - (c-e)P_\alpha - \left(\tfrac{1}{2} + a \right) T_h + \left(\tfrac{1}{2} + a \right)(c-e)P_h \right] \quad (5.105)$$

which can be expanded to:

$$C_{\beta_i \alpha_j} = \pi\rho \left[K_1(T_\alpha) - (c-e)K_1(P_\alpha) - \left(\tfrac{1}{2} + a \right) K_1(T_h) \right.$$

$$+ \left(\tfrac{1}{2} + a \right)(c-e)K_1(P_h) \right] \int_0^L b^4 \beta_i \alpha_j + \pi\rho \, b_r \left[K_2(T_\alpha) - (c-e)K_2(P_\alpha) \right.$$

$$- \left(\tfrac{1}{2} + a \right) K_2(T_h) + \left(\tfrac{1}{2} + a \right)(c-e)K_2(P_h) \right] \int_0^L b^3 \beta_i \alpha_j + \pi\rho \, b_r^2 \left[K_3(T_\alpha) \right.$$

$$- (c-e)K_3(P_\alpha) \right] \int_0^L b^2 \beta_i \alpha_j \quad (5.106)$$

Finally, the influence of the jth flapping mode on the ith flapping mode is:

$$C_{\beta_i \beta_j} = \pi\rho \int_0^L b^4 \beta_i \beta_j \left[T_\beta - (c-e)\left(P_\beta + T_z \right) + (c-e)^2 P_z \right] \quad (5.107)$$

which can be expanded to:

$$C_{\beta_i\beta_j} = \pi\rho \left[K_1(T_\beta) - (c-e)(K_1(P_\beta) + K_1(T_z)) + (c-e)^2 K_1(P_z) \right] \int_0^L b^4 \beta_i \beta_j$$

$$+ \pi\rho \, b_r \left[K_2(T_\beta) - (c-e)(K_2(P_\beta) + K_2(T_z)) + (c-e)^2 K_2(P_z) \right] \int_0^L b^3 \beta_i \beta_j$$

$$\pi\rho \, b_r^2 \left[K_3(T_\beta) - (c-e)K_3(P_\beta) \right] \int_0^L b^2 \beta_i \beta_j \quad (5.108)$$

5.4.2. Compressible Subsonic Flow

Some difficulty exists when determining the airloads for a three dimensional lifting surface in compressible flow. While the formulation of the incompressible and supersonic airloads both lend themselves to straightforward integration, the outputs from the Lin2D code are for a single reduced frequency. As discussed previously, for a constant frequency of oscillation, the reduced frequency varies with the span. For compressible flow, the aerodynamic influence of the jth normal mode on the ith generalized force is:

$$C_{ij} = \rho \frac{b_r^2}{k^2} \int_0^L b h_i h_j C_{l_h}(M,k) + b h_i \alpha_j C_{l_\alpha}(M,k) + b h_i \beta_j C_{l_\beta}(M,k)$$

$$+ 2\rho \frac{b_r^2}{k^2} \int_0^L b^2 \alpha_i h_j C_{M_h}(M,k) + b^2 \alpha_i \alpha_j C_{M_\alpha}(M,k) + b^2 \alpha_i \beta_j C_{M_\beta}(M,k)$$

$$+ 2\rho \frac{b_r^2}{k^2} \int_0^L b^2 \beta_i h_j C_{H_h}(M,k) + b^2 \beta_i \alpha_j C_{H_\alpha}(M,k) + b^2 \beta_i \beta_j C_{H_\beta}(M,k) \quad (5.109)$$

where C_l, C_m, and C_h are the unsteady lift, pitching moment, and hinge moment respectively. These coefficients are functions of Mach number (M) and reduced frequency (k) as were previously described in section 5.2. Equation (5.109) can be written as:

$$C_{ij} = C_{h_i h_j} + C_{h_i \alpha_j} + C_{h_i \beta_j} + C_{\alpha_i h_j} + C_{\alpha_i \alpha_j} + C_{\alpha_i \beta_j} + C_{\beta_i h_j} + C_{\beta_i \alpha_j} + C_{\beta_i \beta_j} \tag{5.110}$$

The aerodynamic influence of the jth bending mode on the ith bending mode is:

$$C_{h_i h_j} = \rho \frac{b_r^2}{k^2} \int_0^L b h_i h_j C_{l_h}(M,k) \tag{5.111}$$

The aerodynamic influence of the jth torsional mode on the ith bending mode is:

$$C_{h_i \alpha_j} = \rho \frac{b_r^2}{k^2} \int_0^L b h_i \alpha_j C_{l_\alpha}(M,k) \tag{5.112}$$

The aerodynamic influence of the jth flapping mode on the ith bending mode is:

$$C_{h_i \beta_j} = \rho \frac{b_r^2}{k^2} \int_0^L b h_i \beta_j C_{l_\beta}(M,k) \tag{5.113}$$

The aerodynamic influence of the jth bending mode on the ith torsional mode is:

$$C_{\alpha_i h_j} = 2\rho \frac{b_r^2}{k^2} \int_0^L b^2 \alpha_i h_j C_{M_h}(M,k) \tag{5.114}$$

The aerodynamic influence of the *jth* torsional mode on the *i*th torsional mode is:

$$C_{\alpha_i \alpha_j} = 2\rho \, \frac{b_r^2}{k^2} \int_0^L b^2 \alpha_i \alpha_j C_{M_\alpha}(M,k) \tag{5.115}$$

The aerodynamic influence of the *jth* flapping mode on the *i*th torsional mode is:

$$C_{\alpha_i \beta_j} = 2\rho \, \frac{b_r^2}{k^2} \int_0^L b^2 \alpha_i \beta_j C_{M_\beta}(M,k) \tag{5.116}$$

The aerodynamic influence of the *jth* bending mode on the *i*th flapping mode is:

$$C_{\beta i h_j} = 2\rho \, \frac{b_r^2}{k^2} \int_0^L b^2 \beta_i h_j C_{H_h}(M,k) \tag{5.117}$$

The aerodynamic influence of the *jth* torsional mode on the *i*th flapping mode is:

$$C_{\beta i \alpha_j} = 2\rho \, \frac{b_r^2}{k^2} \int_0^L b^2 \beta_i \alpha_j C_{H_\alpha}(M,k) \tag{5.118}$$

The aerodynamic influence of the *jth* flapping mode on the *i*th flapping mode is:

$$C_{\beta i \beta_j} = 2\rho \, \frac{b_r^2}{k^2} \int_0^L b^2 \beta_i \beta_j C_{H_\beta}(M,k) \tag{5.119}$$

Since the coefficients contained within Equation (5.109) are a given for a single reduced frequency, integrating the loads to determine the aerodynamic influence coefficient has its difficulties. However, two options present themselves. First, take the value for the reduced frequency used to calculate the force coefficients as the reference

reduced frequency k_r. That is, the reduced frequency at 75% of the span of the lifting surface. The other option is for a given mode, which has a constant value of ω, find the correct reduced frequency at each strip based on its semichord and then perform a numerical integration to find C_{ij}. For this thesis, the coefficients were calculated at the reference reduced frequency and treated as constant over the span.

5.4.3. Supersonic Flow

For supersonic flow, the aerodynamic influence of the jth normal mode on the ith generalized force is:

$$
\begin{aligned}
C_{ij} = \frac{2\rho\, b_r}{M\, k_r} \int_0^L \left[b^2 h_i j_j L_h + b^2 h_i \alpha_j L_\alpha + b^2 h_i \beta_j L_\beta \right] \\
\frac{2a\rho\, b_r}{M\, k_r} \int_0^L \left[b^3 \alpha_i j_j M_h + b^3 \alpha_i \alpha_j M_\alpha + b^3 \alpha_i \beta_j M_\beta \right] \\
\frac{2e\rho\, b_r}{M\, k_r} \int_0^L \left[b^3 \beta i j_j T_h + b^3 \beta_i \alpha_j T_\alpha + b^3 \beta_i \beta_j M_\beta \right] \quad (5.120)
\end{aligned}
$$

which can be reduced to a summation of all of the individual aerodynamic influence coefficients,

$$
C_{ij} = C_{h_i h_j} + C_{h_i \alpha_j} + C_{h_i \beta_j} + C_{\alpha_i h_j} + C_{\alpha_i \alpha_j} + C_{\alpha_i \beta_j} + C_{\beta_i h_j} + C_{\beta_i \alpha_j} + C_{\beta_i \beta_j} \quad (5.121)
$$

The aerodynamic influence of the jth bending mode on the ith bending mode is:

$$
C_{h_i h_j} = \frac{2\rho\, b_r}{M\, k_r} \int_0^L b^2 h_i h_j L_h \quad (5.122)
$$

which can be expanded to:

$$C_{h_i h_j} = \frac{2\rho\, b_r}{M\, k_r} K_1(L_h) \int_0^L b^2 h_i h_j \tag{5.123}$$

The aerodynamic influence of the jth torsional mode on the ith bending mode is:

$$C_{h_i \alpha_j} = \frac{2\rho\, b_r}{M\, k_r} \int_0^L b^2 h_i \alpha_j L_\alpha \tag{5.124}$$

which can be expanded to:

$$C_{h_i \alpha_j} = \frac{2\rho\, b_r}{M\, k_r} K_1(L_\alpha) \int_0^L b^2 h_i \alpha_j + \frac{2\rho\, b_r^2}{M\, k_r} K_2(L_\alpha) \int_0^L b\, h_i \alpha_j \tag{5.125}$$

The aerodynamic influence of the jth flapping mode on the ith bending mode is:

$$C_{h_i \beta j} = \frac{2\rho\, b_r}{M\, k_r} \int_0^L b^2 h_i \beta j L_\beta \tag{5.126}$$

which can be expanded to:

$$C_{h_i \beta j} = \frac{2\rho\, b_r}{M\, k_r} K_1(L_\beta) \int_0^L b^2 h_i \beta j + \frac{2\rho\, b_r^2}{M\, k_r} K_2(L_\beta) \int_0^L b\, h_i \beta j \tag{5.127}$$

The aerodynamic influence of the jth bending mode on the ith torsional mode is:

$$C_{\alpha_i h_j} = \frac{2a\rho\, b_r}{M\, k_r} \int_0^L b^3 \alpha_i h_j M_h \tag{5.128}$$

which can be expanded to:

$$C_{\alpha_i h_j} = \frac{2a\rho\,b_r}{M\,k_r} K_1(M_h) \int_0^L b^3 \alpha_i h_j \tag{5.129}$$

The aerodynamic influence of the jth torsional mode on the ith torsional mode is:

$$C_{\alpha_i \alpha_j} = \frac{2a\rho\,b_r}{M\,k_r} \int_0^L b^3 \alpha_i \alpha_j M_\alpha \tag{5.130}$$

which can be expanded to:

$$C_{\alpha_i \alpha_j} = \frac{2a\rho\,b_r}{M\,k_r} K_1(M_\alpha) \int_0^L b^3 \alpha_i \alpha_j + \frac{2a\rho\,b_r^2}{M\,k_r} K_2(M_\alpha) \int_0^L b^2 \alpha_i \alpha_j \tag{5.131}$$

The aerodynamic influence of the jth flapping mode on the ith torsional mode is:

$$C_{\alpha_i \beta j} = \frac{2a\rho\,b_r}{M\,k_r} \int_0^L b^3 \alpha_i \beta_j M_\beta \tag{5.132}$$

which can be expanded to:

$$C_{\alpha_i \beta j} = \frac{2a\rho\,b_r}{M\,k_r} K_1(M_\beta) \int_0^L b^3 \alpha_i \beta_j + \frac{2a\rho\,b_r^2}{M\,k_r} K_2(M_\beta) \int_0^L b^2 \alpha_i \beta_j \tag{5.133}$$

The aerodynamic influence of the jth bending mode on the ith flapping mode is:

$$C_{\beta_i h j} = \frac{2e\rho\,b_r}{M\,k_r} \int_0^L b^3 \beta_i h_j T_h \tag{5.134}$$

which can be expanded to:

$$C_{\beta_i h_j} = \frac{2e\rho\, b_r}{M\, k_r} K_1(T_h) \int_0^L b^3 \beta_i h_j \tag{5.135}$$

The aerodynamic influence of the jth torsional mode on the ith flapping mode is:

$$C_{\beta_i \alpha_j} = \frac{2e\rho\, b_r}{M\, k_r} \int_0^L b^3 \beta_i \alpha_j T_\alpha \tag{5.136}$$

which can be expanded to:

$$C_{\beta_i \alpha_j} = \frac{2e\rho\, b_r}{M\, k_r} K_1(T_\alpha) \int_0^L b^3 \beta_i \alpha_j + \frac{2e\rho\, b_r^2}{M\, k_r} K_2(T_\alpha) \int_0^L b^2 \beta_i \alpha_j \tag{5.137}$$

The aerodynamic influence of the jth flapping mode on the ith flapping mode is:

$$C_{\beta_i \beta_j} = \frac{2e\rho\, b_r}{M\, k_r} \int_0^L b^3 \beta_i \beta_j T_\beta \tag{5.138}$$

which can be expanded to:

$$C_{\beta_i \beta_j} = \frac{2e\rho\, b_r}{M\, k_r} K_1(T_\beta) \int_0^L b^3 \beta_i \beta_j + \frac{2e\rho\, b_r^2}{M\, k_r} K_2(T_\beta) \int_0^L b^2 \beta_i \beta_j \tag{5.139}$$

In the section above, the procedure for defining the influence coefficients in terms of their generalized forces and moments for each speed regime has been defined. Now, the option is how to describe these generalized functions. Several options exist, such as direct

computation, the minimum state approximation, matrix Padé approximations, and Roger's

Approximation.

5.5. Rational Function Approximations

One of the difficulties in aeroelastic modeling is the representation of unsteady

aerodynamic loads. The loads contain time-lag components due to phenomena such as

vortex shedding. When formulating an analytical expression, these time-lag effects

manifest as non-rational terms. Roger first proposed the use of common denominator

coefficients to reduce the number of required augmented states. Roger's Approximation

takes the form:

$$\hat{Q} = A_0 + A_1(ik) + A_2(ik)^2 + \sum_{m=3}^{6} \frac{A_m(ik)}{ik + \beta_{m-2}} \tag{5.140}$$

In matrix form, Roger's Approximation in terms of the Laplace variable (s) becomes:

$$[\hat{Q}] = [A_0] + [A_1]\left(\frac{b}{U}\right)s + [A_2]\left(\frac{b}{U}\right)^2 s^2 + \sum_{m=3}^{6} \frac{[A_m]s}{\left(s + \frac{U}{b}\beta_{m-2}\right)} \tag{5.141}$$

The matrices $[A_0]$, $[A_1]$, $[A_2]$, etc. are determined using a least squares approximation of

tabular data. The augmented aerodynamic states are written as:

$$X_{a_i}(s) = \frac{s}{s + \frac{U}{b}\beta_{i-2}} X(s) \tag{5.142}$$

Then, the system's equation of motion can be written as:

$$\left[[M]s^2 + [2\zeta M\omega_n]s + [K] - q[\hat{Q}]\right]\bar{x} = 0 \tag{5.143}$$

Substituting Equation (5.140) into Equation (5.143) gives:

$$
\begin{Bmatrix} \dot{x} \\ \ddot{x} \\ \dot{x}_{a_1} \\ \dot{x}_{a_2} \\ \dot{x}_{a_3} \\ \dot{x}_{a_4} \end{Bmatrix} = \begin{bmatrix} 0 & [I] & 0 & 0 & 0 & 0 \\ -[M]^{-1}[K] & -[M]^{-1}[B] & [M]^{-1}[A_3] & [M]^{-1}[A_4] & [M]^{-1}[A_5] & [M]^{-1}[A_6] \\ 0 & [I] & -\left(\frac{U}{b}\right)\gamma_1[I] & 0 & 0 & 0 \\ 0 & [I] & 0 & -\left(\frac{U}{b}\right)\gamma_2[I] & 0 & 0 \\ 0 & [I] & 0 & 0 & -\left(\frac{U}{b}\right)\gamma_3[I] & 0 \\ 0 & [I] & 0 & 0 & 0 & -\left(\frac{U}{b}\right)\gamma_4[I] \end{bmatrix} \begin{Bmatrix} x \\ \dot{x} \\ x_{a_1} \\ x_{a_2} \\ x_{a_3} \\ x_{a_4} \end{Bmatrix} = \bar{0} \quad (5.144)
$$

which is of the form $\dot{X} = [A]X$. Then, the eigenvalues of the A matrix correspond to

frequency and mode shapes of system for a given airspeed. As can be identified in the $[A]$

matrix above, the upper-left 2×2 is the $[A]$ matrix of a typical dynamic system. The

additional terms in the second row capture the contributions of the lag states on the system

dynamics. The remaining rows represent the Roger's Approximation lag states as

appended aerodynamic states.

6. Flutter Solutions

This section discusses the typical methods used to solve the flutter stability determinant. Scanlan and Rosenbaum discuss some of the methods used to solve the flutter determinant before computers were widely available. These include Theodorsen's Method and Arnold's Graphical Method. Theodorsen's Method is a guess and check that involves finding the value of $1/k$ and ω at which the real and imaginary parts of the flutter stability determinant simultaneously vanish. Arnold's graphical method represents the elements of the determinant and uses conformal mapping to map vectors from the real-imaginary plane onto a circle (Scanlan & Rosenbaum, 1968). With the use of improved computational power in the mid to late 1900s, many iterative matrix techniques were introduced.

6.1. P-Method Flutter Solution

The p-method solves the aeroelastic equations of the form

$$\left\{ [M]p^2 + [K] - Q(p) \right\} \bar{X} = 0 \tag{6.1}$$

where p is a complex eigenvalue $p = \gamma + ik$. For a given reduced frequency k, the above equation is solved for p. Then, referring this back to the original substitution, γ is simply the real part of p. The damping is then found based on the decay rate of $e^{(\gamma+ik)t}$. Once the damping term, g, is known, this can be plotted against airspeed. The flutter speed is then the speed at which the damping switches from positive to negative.

6.2. K-Method Flutter Solution (U-g method)

The k-method solves the aeroelastic equations of the form

$$\left\{ [M] - \tfrac{1}{\omega^2}[K] - \tfrac{1}{\omega^2}Q(ik) \right\} \bar{X} = 0 \tag{6.2}$$

where ω is the flutter frequency. For a given value of reduced frequency k, the

aerodynamic forcing, $Q(ik)$, is determined and the above equation is solved for

$$Z = \tfrac{1}{\omega^2}(1 + ig) \tag{6.3}$$

where Z are the complex roots of the matrix equation. Once the roots are known, the

damping can be determined and plotted against airspeed to determine the flutter speed.

6.3. PK-Method Flutter Solution

The pk-method solves the aeroelastic equations of the form

$$\left\{ [M]p^2 + [K] - Q(ik) \right\} \bar{X} = 0 \tag{6.4}$$

It is referred to as the pk-method as it draws from the the p-method and k-method

solutions. The solution is similar to that of the p-method where for a given value of

reduced frequency, the system is solved for $p = \gamma + ik$. However, the aerodynamic forcing

is determined in the same manner as the k-method.

7. Results

This section provides the results from the Nastran simulations, Matlab simulations, and compares the two. First, the normal modes as determined by the matrix iteration method are compared to the output from Nastran's Solution 103 (normal modes).

7.1.   Normal Modes

The normal modes were found using a Matlab implementation of the matrix iteration method as discussed in the Chapters above. To gauge the correctness of the Matlab solution, both the frequencies and mode shapes are compared to the Nastran solution. While the frequencies can easily be compared, the accuracy of the mode shape given by Matlab is computed by taking the two-norm of the error. In other words the error metric is:

$$e = ||\phi_M - \phi_N|| \tag{7.1}$$

where ϕ_M is the mode shape found using Matlab and ϕ_N is the mode shape found using Nastran. Table 7.1 shows the shape error, calculated using Equation (7.1). The mode shapes can also be compared graphically. While the torsional deformations are not evident on a stick model, the overall shape due to bending can be compared. According to the FAA, compliance with the aeroelastic stability requirements given in 14 CFR §25.629, "must be shown by analyses, wind tunnel tests, ground vibration tests, flight tests, or other means" (FAA, 1992). Since Nastran is widely used in the aerospace industry for aeroelastic analysis, the Nastran results are taken as the true solution.

Figure 7.1 shows the comparison of the mode shapes from Matlab and Nastran. Recall, the normal modes are a result of solving the homogeneous system, given by Equation

(4.191). The undeformed structure is shown in black, the Matlab mode shape is shown in blue, and the Nastran mode shape is shown in red. The predominant mode of motion is bending in the $X - Y$ plane. However, there is some torsion of the fuselage due to the mass of the vertical tail and horizontal tail being above the center of rotation. This shows that
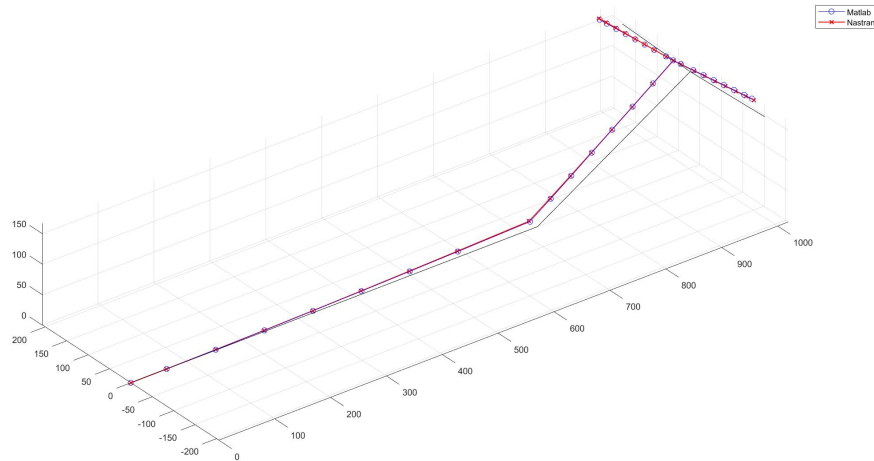
Figure 7.1 Comparison of Normal Mode 1

for the fundamental mode, the matrix iteration method can very accurately predict the frequency and mode shape. Figure 7.2 shows the second mode shape, which corresponds to the first bending mode in the $X - Z$ plane.

Since the structure is symmetric about the $X - Z$ plane, all of the motion lies in that plane. The second mode calculated using Matlab is a very close match to the Nastran output. From Table 7.1, the error for the second mode is the lowest of the five. While the shape matches very closely, Table 7.1 also shows that the error in the frequency is the greatest of the five modes.

The third mode gave way to one of the flaws of the matrix iteration method. While the shape of the fuselage has good accuracy, the differences in the rotation of the horizontal
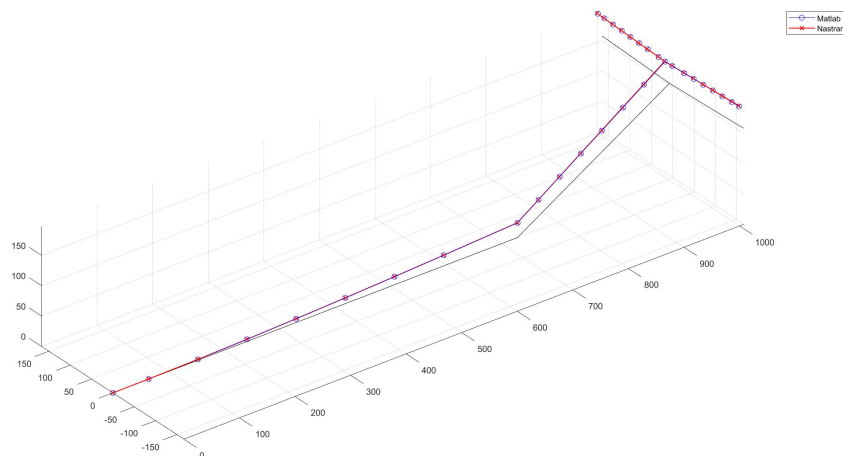
Figure 7.2 Comparison of Normal Mode 2

tail between the Matlab solution and the Nastran solution are evident. Figure 7.3 shows the

third normal mode, an antisymmetric mode that incorporates some of the characteristics of

the second bending mode in the $X - Y$ plane. The third mode output from Nastran shows

that the Matrix iteration code underpredicts the rotation of the vertical tail, which is

apparent in the fourth mode as well.
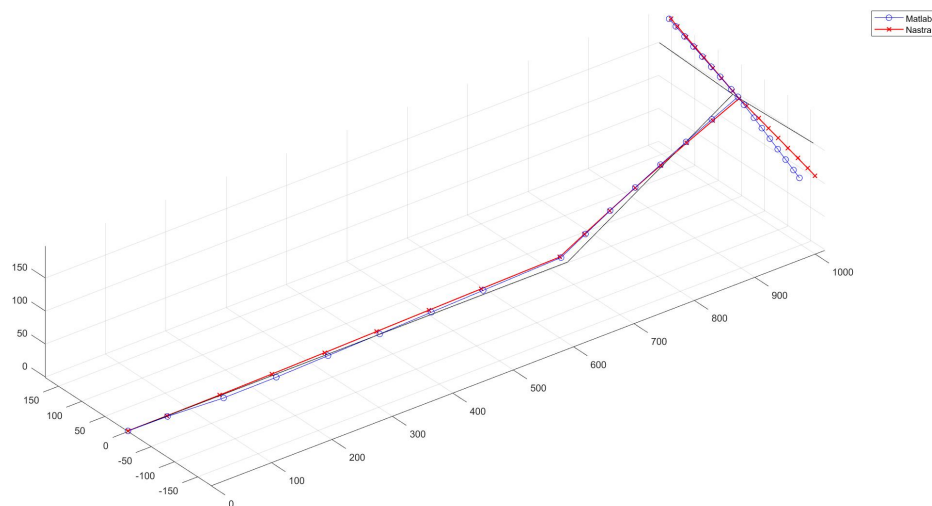
Figure 7.3 Comparison of Normal Mode 3

Figure 7.4 shows the fourth normal mode, the second antisymmetric mode, and incorporates the same fuselage bending characteristics as the third mode. Similar to the third mode, the fuselage shape predicted by matrix iteration is quite accurate but the horizontal tail is noticeably different. Further examination shows that vertical tail in the Nastran solution experiences much more rotation about its swept axis than that of the Matlab output.
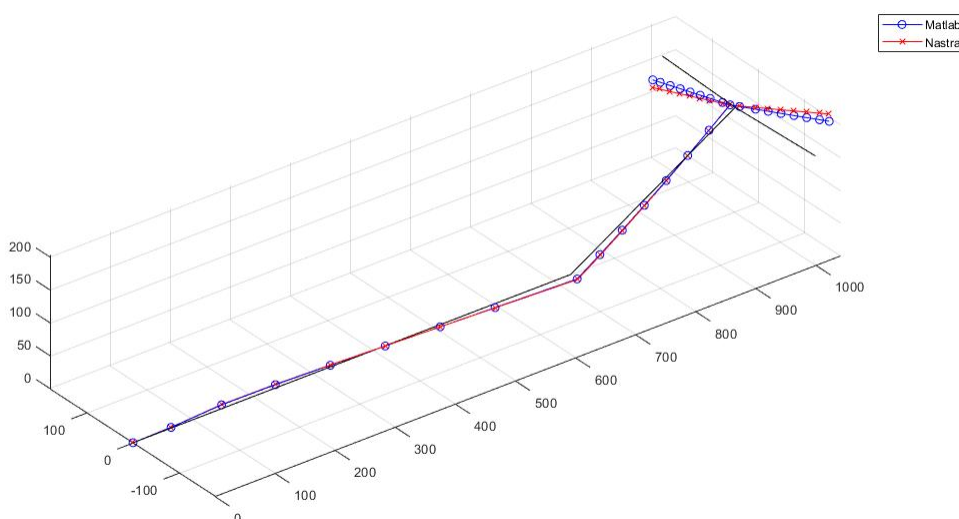
Figure 7.4 Comparison of Normal Mode 4

Figure 7.5 shows the fifth normal mode, which corresponds to the second fuselage bending mode in the $X - Z$ plane. The fuselage shape matches the Nastran output well but the horizontal tail is deforming much more in the Nastran output than that of the matrix iteration solution.

After comparing the first five normal modes, the matrix iteration method shows it can accurately predict the normal modes of vibration for the aft fuselage and empennage of a T-tail configuration. While the mode shapes calculated by matrix iteration have some
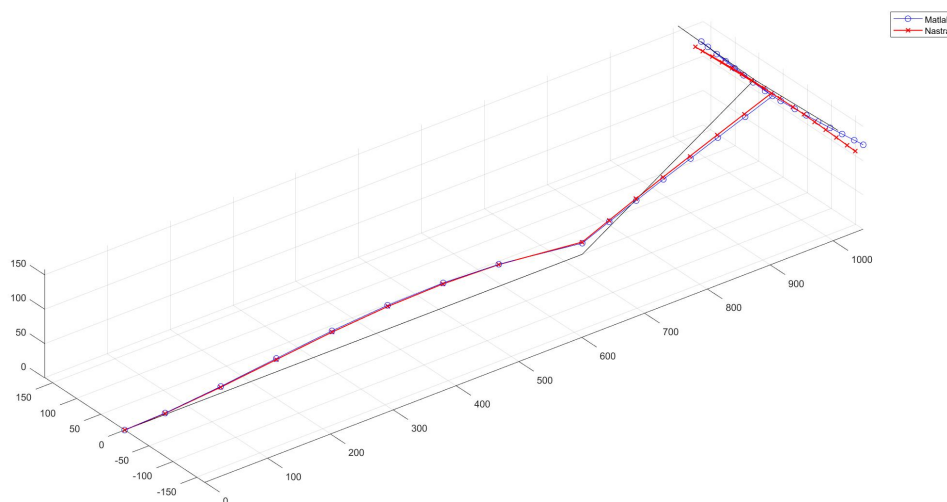
Figure 7.5 Comparison of Normal Mode 5

visible differences from the Nastran solution, the frequencies were all calculated within ten

percent error. Table 7.1 shows the natural frequency of each of the first five normal modes

as determined by Matlab and Nastran. It has been shown that the matrix iteration method

Table 7.1

Normal Mode Frequency Comparison

Mode	Matlab Frequency [Hz]	Nastran Frequency [Hz]	% Difference	Mode Error
1	1.692	1.718	1.53	0.3150
2	1.954	1.835	6.30	0.1331
3	4.814	4.782	0.66	1.2670
4	8.920	9.310	4.27	0.8120
5	10.156	9.717	4.42	0.8439

using flexibility influence coefficients can predict a reasonable number of normal modes.

Now, these normal modes are used in the flutter calculations by first finding the three

dimensional generalized aerodynamic forcing functions.

7.2. Aerodynamic Forcing Functions

This section discusses the results of Roger's Approximation to fit the three-dimensional aerodynamic forcing functions for all speed regimes. Roger's Approximation with four lag states was used to estimate the aerodynamics for the incompressible airloads (Theodorsen's method), subsonic compressible (Possio's acceleration potential), and supersonic (first-order Piston Theory). Roger's Approximation worked very well for low subsonic and supersonic flight regimes. Figure 7.6 provides an example of the approximation for the influence of mode 3 on mode 1 at Mach = 0.00 at sea level conditions to illustrate the fit. Each red mark corresponds to the real and imaginary part of the aerodynamic load for a given value of reduced frequency.
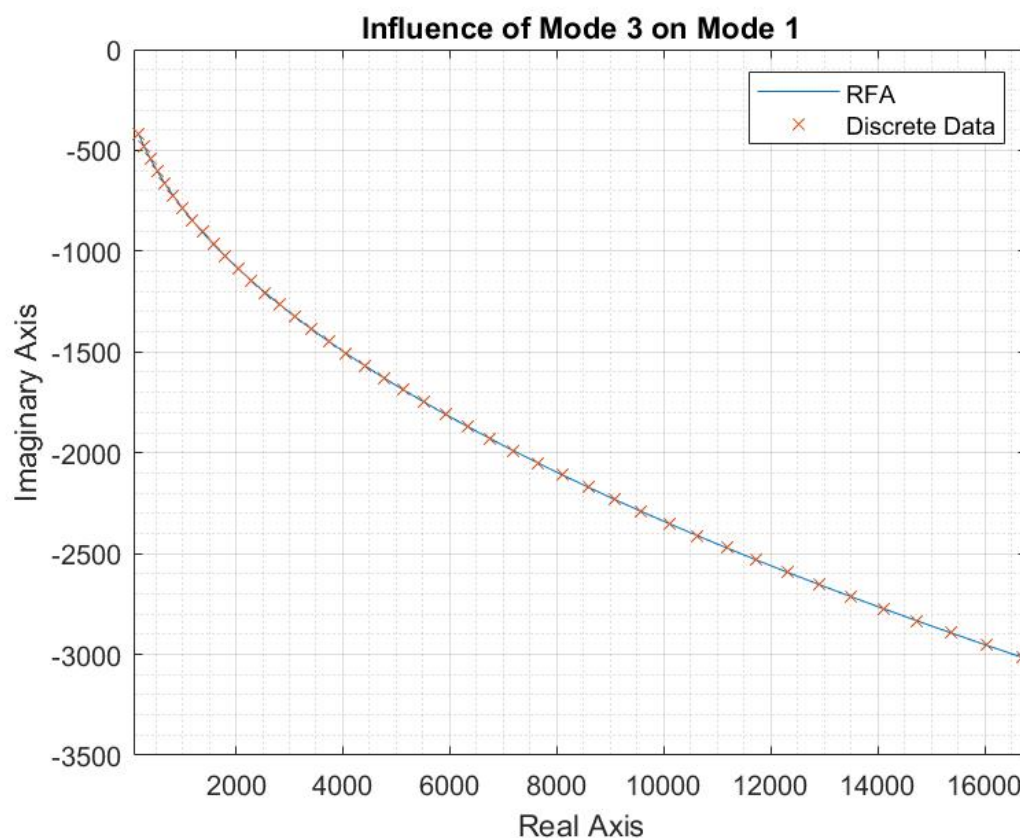
Figure 7.6 Aerodynamic Influence of Mode 3 on Mode 1 at Mach = 0.00 at Sea Level

Figure 7.7 shows the approximation for the influence of mode 3 on mode 1 at Mach =
0.80 at sea level conditions. At high subsonic Mach numbers, the approximation begins to
break down as the Possio kernel varied less smoothly with reduced frequency. The fit was
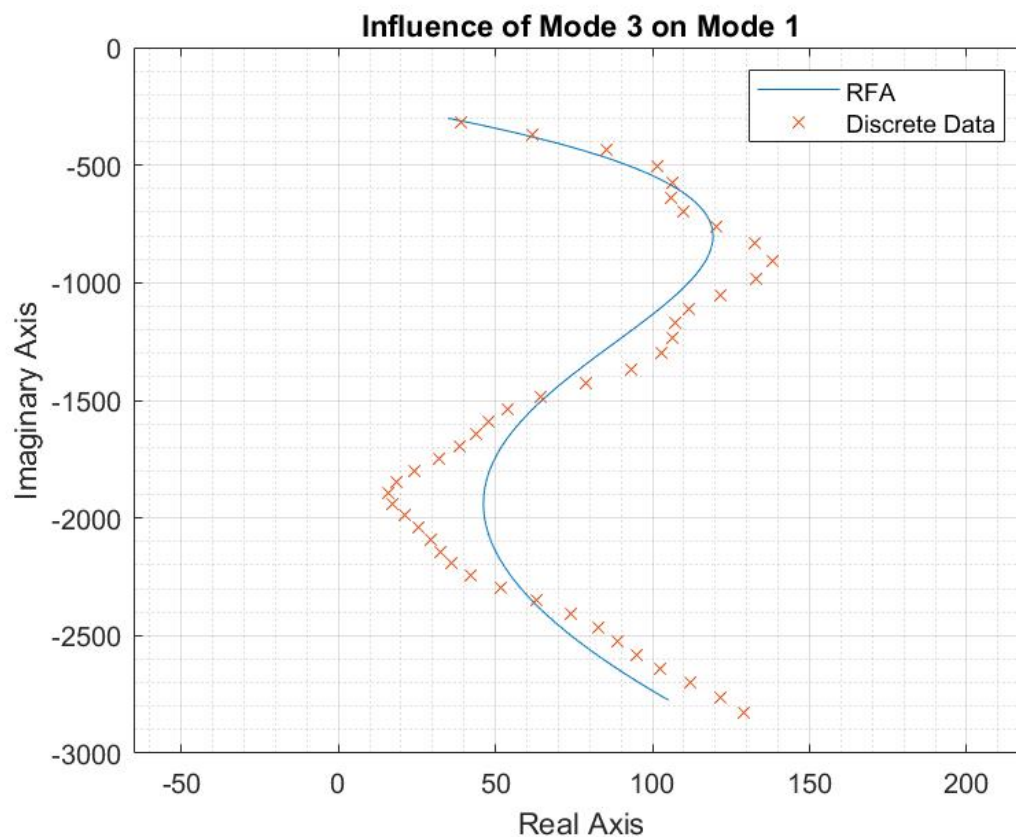
Figure 7.7 Aerodynamic Influence of Mode 3 on Mode 1 at Mach = 0.80 at Sea Level

tuned by modifying the minimum and maximum values of reduced frequency in the
approximation while monitoring the flutter results. In some cases, the range of reduced
frequency used in Roger's Approximation can be greatly reduced with no loss of fidelity in
the flutter solution.

Figure 7.8 shows the approximation for the influence of mode 3 on mode 1 at Mach =
1.20 at sea level conditions. Roger's Approximation was able to find a much better fit as
the supersonic airloads all vary linearly with reduced frequency.
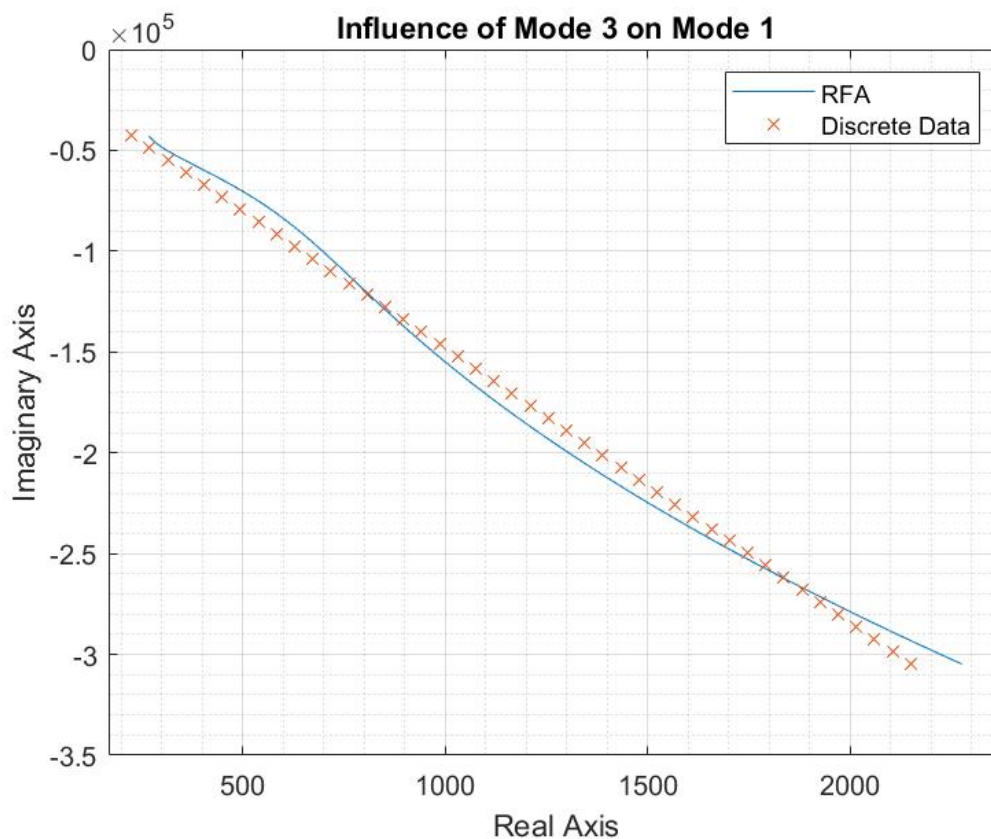
Figure 7.8 Aerodynamic Influence of Mode 3 on Mode 1 at Mach = 1.20 at Sea Level

While for this analysis, the number of lag states used in Roger's Approximation was four, the number can be varied to obtain a best fit. Figure 7.6 appears to have the appropriate number of lag states, Figure 7.7 may be improved by including more lag states, and Figure 7.8 may not need any lag states. The remainder of the RFA plots for all Mach numbers tested are found in Appendix C.

7.3. Flutter

This section discusses the results gathered by finding the eigenvalues of Equation (5.144). The solution was calculated for a range of reduced frequencies, dynamic pressures, and Mach numbers. Figure 7.9 shows the eigenvalues, in the real-imaginary plane, as a function of airspeed for Mach = 0.00 using incompressible aerodynamics. Each branch corresponds to a mode of vibration. These branches start on the imaginary axis, where the system is oscillating with simple harmonic motion at its natural frequency. Figure 7.9 shows that for incompressible aerodynamic forcing flutter does not occur since no eigenvalues exist on the right hand side of the real-imaginary plane. As the dynamic pressure increases, the frequency and damping of each of the modes change due to aerodynamic effects. Increasing dynamic pressure corresponds to a point further along, or further to the left, on each of the branches. Figure 7.9 shows that the damping ratio for all modes reduces with the damping ratio of mode 2 becoming critically damped.
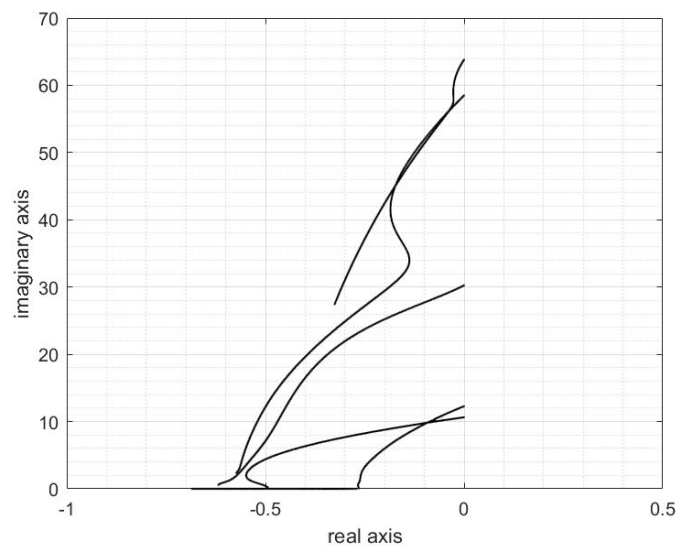
Figure 7.9 Flutter Eigenvalues for Mach = 0.00, Theodorsen Solution

Figure 7.10 shows the eigenvalues as a function of airspeed for Mach = 0.00 using compressible aerodynamics.
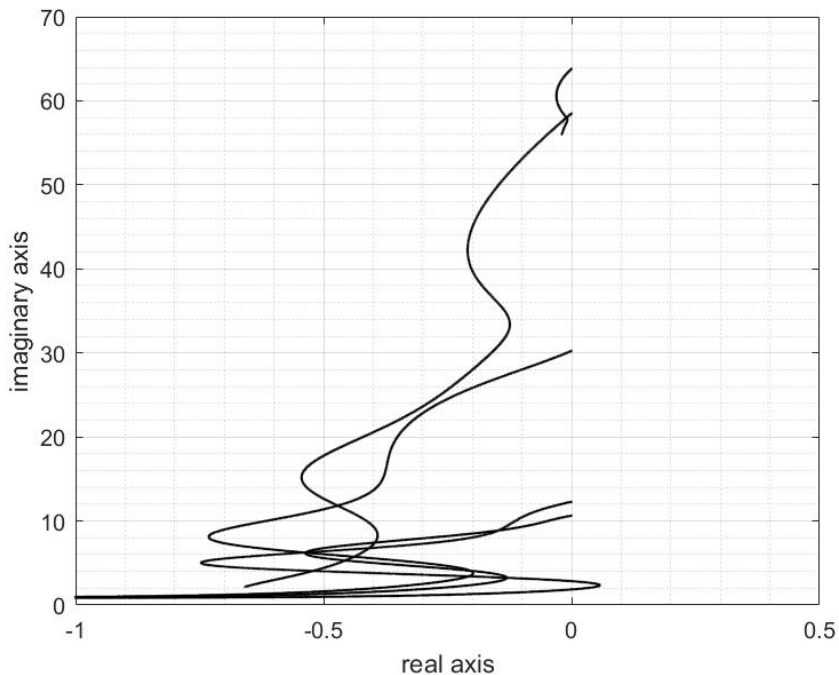
Figure 7.10 Flutter Eigenvalues for Mach = 0.00, Possio Solution

For this case, mode 2 begins to flutter at a dynamic pressure of $37.92psi$ before later returning to the stable half of the real-imaginary plane. At the same time, modes 1 and 3 approach a damping ratio of $\zeta = 1$ while the frequency increases. For this case, Nastran's pk-method solution shows the fourth mode beginning to flutter at a dynamic pressure of $45.60psi$.

Figure 7.11 shows the eigenvalues as a function of airspeed for Mach = 0.50. For the case of Mach = 0.50 using the compressible aerodynamic solution, both modes 2 and 3 go unstable. Mode 2 becomes unstable at a dynamic pressure of $36.92psi$ while mode 3 becomes unstable at a dynamic pressure of $35.47psi$. This means that flutter will onset at a dynamic pressure of $35.47psi$ and the flutter mode is mode 3. For this case, Nastran's
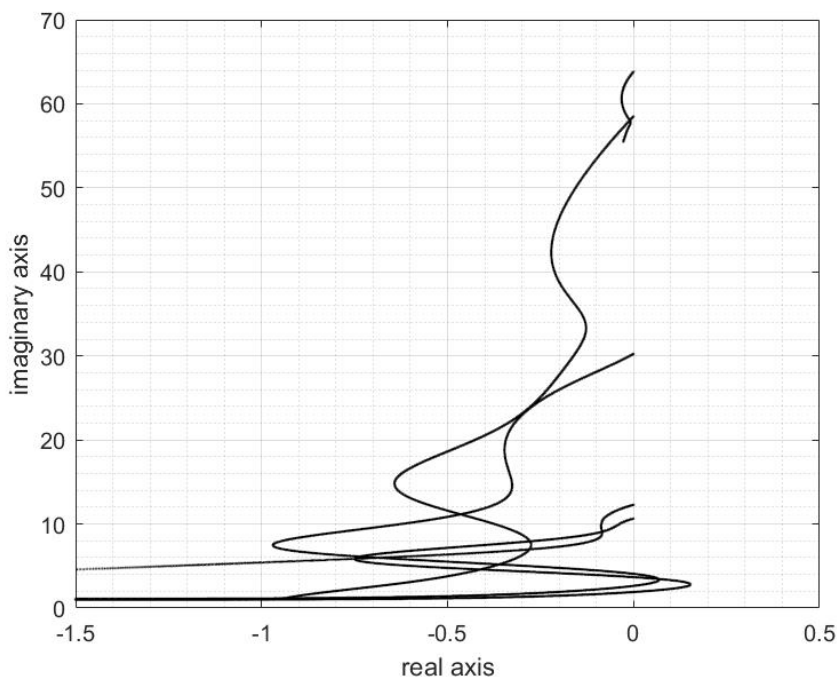
Figure 7.11 Flutter Eigenvalues for Mach = 0.50

pk-method solution shows the fourth mode becoming unstable with a dynamic pressure of

41.80psi. When comparing Figure 7.3 and Figure 7.4, the shape and frequency are similar

such that they would develop similar aerodynamic loading as the dynamic pressure

increases. This may be a cause for the differences between the Matlab solution and the

Nastran Solution.

Figure 7.12 shows the eigenvalues as a function of airspeed for Mach = 0.85. For the

case of Mach = 0.85 using the compressible aerodynamic solution, both modes 2 and 3

become unstable, in a similar fashion to the case of Mach = 0.50. Mode 2 becomes

unstable at a dynamic pressure of 37.28psi while mode 3 becomes unstable at a dynamic

pressure of 31.34psi. This means that flutter will onset at a dynamic pressure of 31.34psi

and the flutter mode is mode 3. For this case, Nastran's pk-method solution shows the

fourth mode going unstable with a dynamic pressure of 36.41psi. When studying the
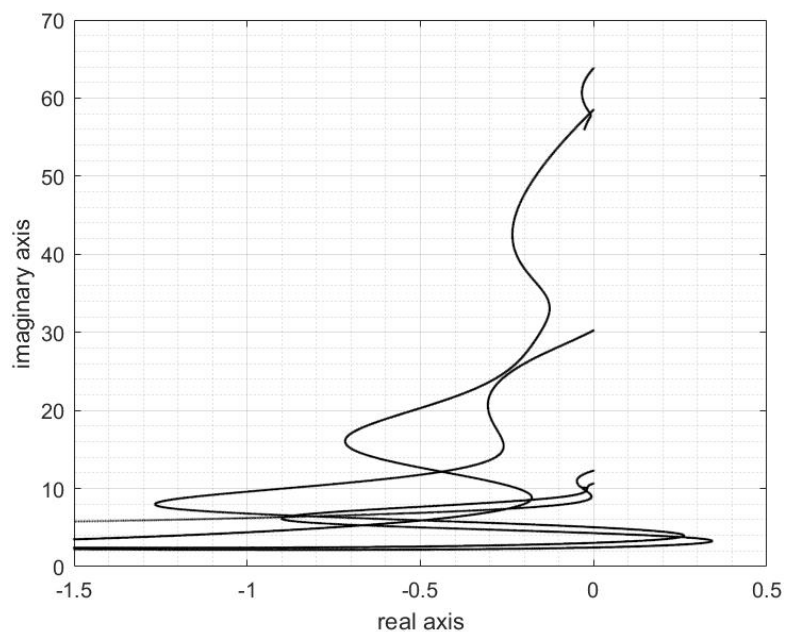
Figure 7.12 Flutter Eigenvalues for Mach = 0.85

validity of Possio's solution for flat plate aerodynamics, after Mach 0.80 the solution

beings to break down.

Figure 7.13 shows the eigenvalues as a function of airspeed for Mach = 0.95. For the
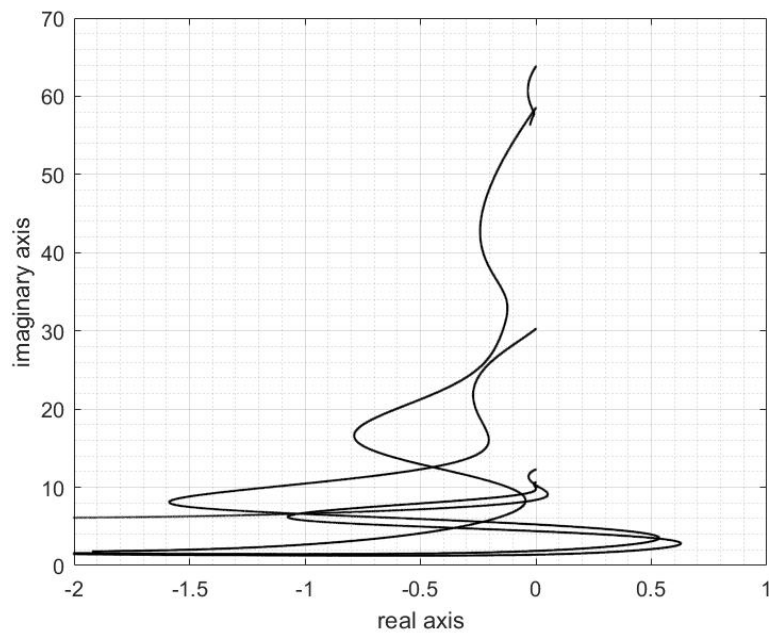
Figure 7.13 Flutter Eigenvalues for Mach = 0.95

case of Mach = 0.95 using the compressible aerodynamic solution, mode 1 becomes

unstable at a very low dynamic pressure. This is likely a result of the compressible

aerodynamic solution breaking down at Mach numbers close to the speed of sound. Since

this is believed to be a non-physical result the other modes are examined. In addition to

mode 1, modes 2 and 3 also become unstable. Mode 2 becomes unstable at a dynamic

pressure of $36.24psi$ and mode 3 becomes unstable at a dynamic pressure of $26.52psi$.

This means that flutter will onset at a dynamic pressure of $26.52psi$ and the flutter mode is

mode 3.

For the cases of Mach = 1.05, Mach = 1.10, and Mach = 1.20 using the piston theory

aerodynamic solution, the system does not flutter. Modes 3 through 5 exhibit nearly

identical behavior for all three supersonic cases, where the first two modes differ slightly.

Figure 7.14 shows the eigenvalues as function of airspeed for Mach = 1.05.
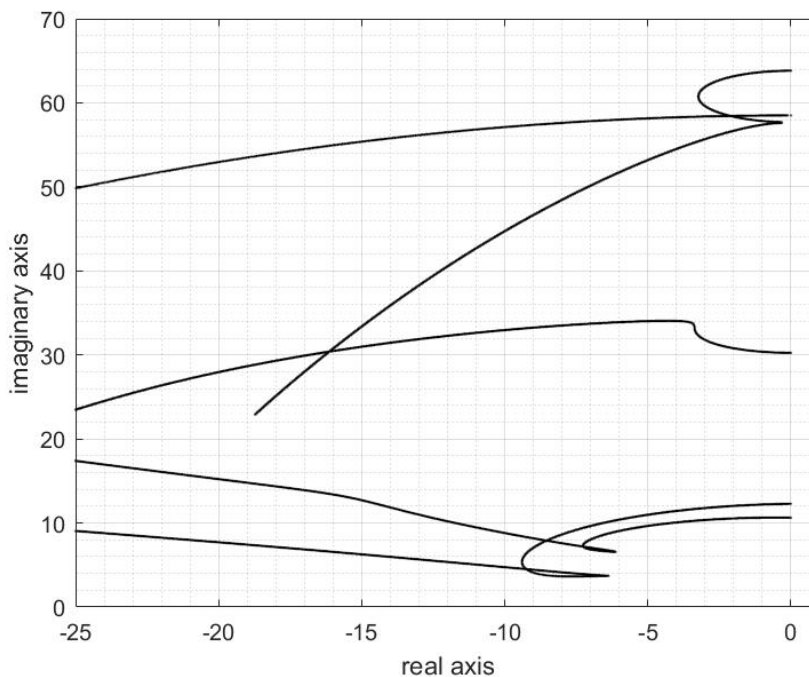
Figure 7.14 Flutter Eigenvalues for Mach = 1.05

The eigenvalues of the two lowest frequency modes initially move to the left on the real axis while their damping ratios approach $\zeta = 1$. However, they each turn back towards back towards the imaginary axis before abruptly reversing direction and become increasingly stable with the increase in dynamic pressure. Modes 3 and 4 both move left, becoming increasingly stable with dynamic pressure, while their damping ratios slowly increase. Figure 7.15 shows the eigenvalues as a function of airspeed for Mach = 1.10.
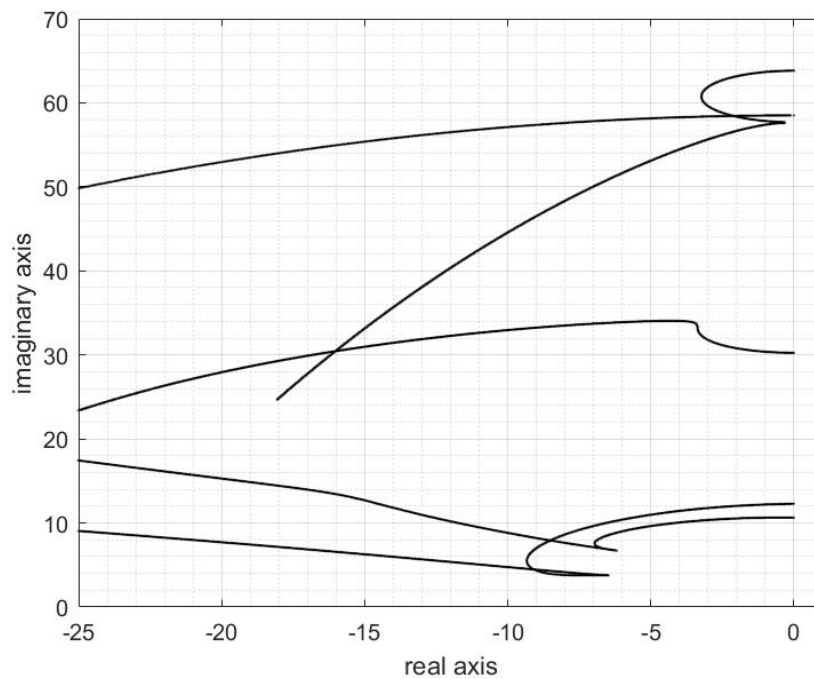
Figure 7.15 Flutter Eigenvalues for Mach = 1.10

Mode 5 appears as if it will become unstable, however as the damping ration approaches zero, the trajectory suddenly reverses direction and moves to the left in the real-imaginary plane while the damping ratio approaches $\zeta = 1$. The eigenvalue flutter solution for piston theory aerodynamics was the least sensitive to changes in range of reduced frequency when compared to the two other methods.

Figure 7.16 shows the eigenvalues as a function of airspeed for Mach = 1.20.
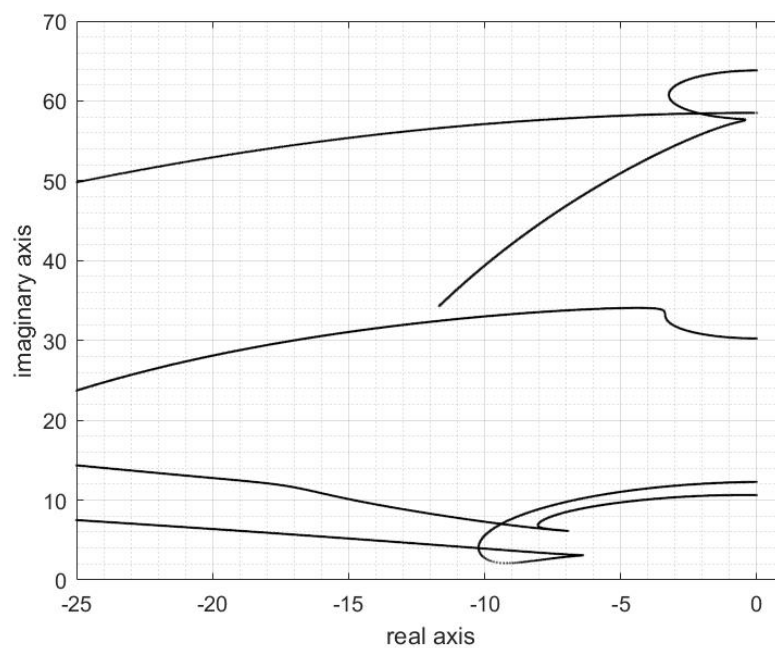
Figure 7.16 Flutter Eigenvalues for Mach = 1.20

Figure 7.17 shows a comparison of the flutter dynamic pressure vs. Mach number of the Matlab results with the Nastran results.
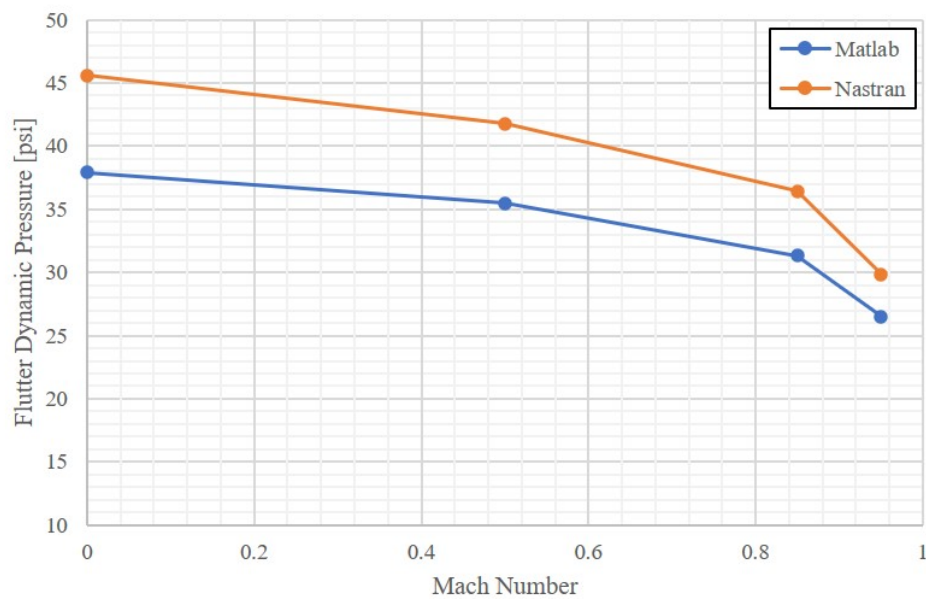
Figure 7.17 Flutter Dynamic Pressure vs. Mach Number

This shows that the analytical solution yields more conservative results for the flutter

dynamic pressure than the Nastran solution. The analytical solution also accurately

predicts the reduction in flutter dynamic pressure at the Mach number approaches Mach 1.

8. Conclusions and Recommendations

This thesis lays out the process for determining the flutter characteristics for the aft fuselage of a T-tail aircraft through the development of an analytical model. A T-tail aircraft is presented and modeled in MSC Nastran and Matlab is used to determine the flutter speeds for Mach numbers ranging from 0.00 to 1.20. The method of influence coefficients is used to calculate the normal modes of vibration of the structure. The influence coefficients are derived using the Euler-Bernoulli beam bending equations, neglecting the contribution of shear deformations. The influence coefficients also include an elastic fitting between the fuselage and vertical tail as well as the vertical tail and the horizontal tail. Once the flexibility influence coefficients are known, the normal modes are determined using the matrix iteration process presented by Flomenthoft.

The incompressible aerodynamic forcing functions are developed using the equations originally presented by Theodorsen and Küssner and reduced using the simple harmonic motion assumption. The compressible subsonic aerodynamic forcing functions are determined using a Matlab adaptation of Lin2D, a Fortran code developed by Samuel Bland. This code uses a Kernel function approximation of Possio's acceleration potential solution for a sheet of pulsing doublets in compressible flow. The equations for an airfoil oscillating in supersonic flow are derived for the case of a pitch-plunge-flap airfoil section using First-Order Piston Theory. The forcing functions are extended to three-dimensions by weighting the two-dimensional forcing functions with the mode shape and integrating over the span of a lifting surface.

Roger's approximation with four lag states is used to curve fit discrete values of the three-dimensional aerodynamic data for a range of reduced frequencies. Roger's

approximation makes way for a straightforward eigenvalue method for determining the flutter characteristics of the system with changing dynamic pressure. The dynamic pressure that corresponds to the first eigenvalue with a positive real part is the flutter dynamic pressure.

The results from the matrix iteration process showed that this method is able to estimate at least the first five normal modes of the system with the frequency having a very low error when compared to Nastran and the shape for symmetric modes having a very low variance from the Nastran solution. The asymmetric and antisymmetric modes show a good match with the frequency but do not estimate the mode shape as accurately. While this method works well, it must be approached with caution. When forming the global influence matrix, the degrees of freedom considered in the analysis impact the convergence of the iteration process. It may take multiple attempts to estimate the full set of normal modes as one attempt may skip over modes that exist and predict erroneous ones instead.

The flutter solution using the eigenvalue method is able to rapidly approximate the flutter dynamic pressure and provides a more conservative estimate when compared to the results from Nastran. However, the the solution is very sensitive to different ranges of reduced frequency at each Mach number which must be investigated further.

This process combined existing knowledge of structural dynamics, unsteady aerodynamics, and wing flutter to develop an approach to analyzing tail flutter. In addition, this will allow for reductions in the time required to model and analyze the flutter of new aircraft configurations. This approach also has the potential to be used for real time, online flutter prediction in all types of aircraft.

The following are recommendations to improve and expand upon the work presented in this thesis:

1. Modify the flexibility influence coefficients for the fuselage such that they are applicable to a more generic shape, not one that lies purely on one axis.

2. Implement the mean axis theorem such that the eigenvalue solution returns the rigid body aircraft dynamics as well as the elastic characteristics.

3. Study the accuracy of Possio's acceleration potential solution for compressible flow for a wider range of reduced frequencies at each Mach number to understand where the solution begins to break down.

4. Study the Roger's Approximation fit for different numbers of lag states to determine their effect on the flutter dynamic pressure to determine the trade off between accuracy and computational requirements.

5. Implement a pk-method solution as a secondary check which also allows for a one-to-one comparison with the Nastran results.

6. Use the process laid out in this thesis to model the forward fuselage of the aircraft to develop a simulation of an elastic aircraft.

7. Implement close-loop control algorithms to test the ability of different control laws to suppress the onset of flutter.

REFERENCES

Ashley, H., & Zartarian, G. (1956, December). Piston theory - a new aerodynamic tool for the aeroelastician. *Journal of the Aeronautical Sciences*.

Bisplinghoff, R. L., Ashley, H., & Halfman, R. L. (1996). *Aeroelasticity*. Dover.

Bland, S. R. (1982, May). *Development of low-frequency kernel-function aerodynamics for comparison with time-dependent finite-difference methods* (Technical Memorandum No. 83283). NASA.

Clough, R., & Penzien, J. (2010). *Dynamics of structures*. Computers and Structures Inc.

Collar, A. R. (1978, February). The first fifty years of aeroelasticity. *Aerospace*, 12-20.

Edwards, J. W. (1977). *Unsteady aerodynamic modeling and active aeroelastic control* (Unpublished doctoral dissertation). Stanford University.

FAA. (1992, June). *Title 14, code of federal regulations part 25 - airworthiness standards: Transport category airplanes* (Tech. Rep.). Federal Aviation Administration.

Flomenhoft, H. I. (1950, September). A method for determining mode shapes and frequencies above the fundamental by matrix iteration. *Journal of Applied Mechanics*, *Vol. 17*(No. 3), pp. 249-256.

Fung, Y. C. (2008). *An introduction to the theory of aeroelasticity*. Dover.

Karpel, M. (1981, November). *Design for active and passive flutter suppression and gust alleviation* (Contractor Report No. 3482). NASA.

Karpel, M. (1982, March). Design for active flutter suppression and gust alleviation using state-space aeroelastic modeling. *Journal of Aircraft*, *Vol. 19*(No. 3).

Kussner, H. G., & Schwarz, I. (1941). *The oscillating wing with aerodynamically balanced elevator* (Tech. Rep.). NACA.

Livne, E. (2018). Aircraft active flutter suppression: State of the art and technology maturation needs. *Journal of Aircraft*.

Mykytow, W. J. (1977, October). A brief overview of transonic flutter problems..

Palazzo, F. (2017). *Multiple-input active aeroelastic control using the receptance method on a flexible wing* (Unpublished master's thesis). Politecnico Di Torino.

Ramsey, J. K. (2006, November). *Nasa aeroelasticity handbook volume 2: Design guides* (Tech. Rep. No. TP 2006/212490). NASA Glenn Research Center.

Roger, K. L., & Hodges, G. E. (1975, June). Active flutter suppression - a flight test demonstration. *Journal of Aircraft*, *Vol. 12*(No. 6).

Scanlan, R. H., & Rosenbaum, R. (1968). *Aircraft vibration and flutter*. Dover.

Smilg, B., & Wasserman, L. S. (1942). *Application of three-dimensioal flutter theory to aircraft structures (with corrections for the effects of control surface aerodynamic balance and geared tab)* (Tech. Rep.). Air Corps War Department.

Theodorsen, T. (1936). *General theory of aerodynamic instability and the mechanism of flutter* (Tech. Rep.). NACA.

Theodorsen, T., & Garrick, I. E. (1942). *Nonstational flow about a wing-aileron-tab combination including aerodynamic balance* (Technical Report No. 736). NACA.

APPENDIX A - Flexibility Influence Coefficient Derivation

This Appendix shows the process to develop the flexibility influence coefficients for

the vertical tail and horizontal tail.

Vertical Tail Influence Coefficients

The vertical tail influence coefficients are determined by finding the deflections of the

vertical tail due to loads and moments applied to the fuselage, vertical tail, starboard

horizontal tail, and port horizontal tail independently of one another. To do this, a new

swept coordinate frame is defined with its origin at the intersections between the fuselage

and vertical tail. The x_s axis is aligned with the elastic axis of the VT and the z_s axis is

perpendicular in the $X - Z$ plane. Figure A.1 shows the swept axis in relation to the global

axis system.
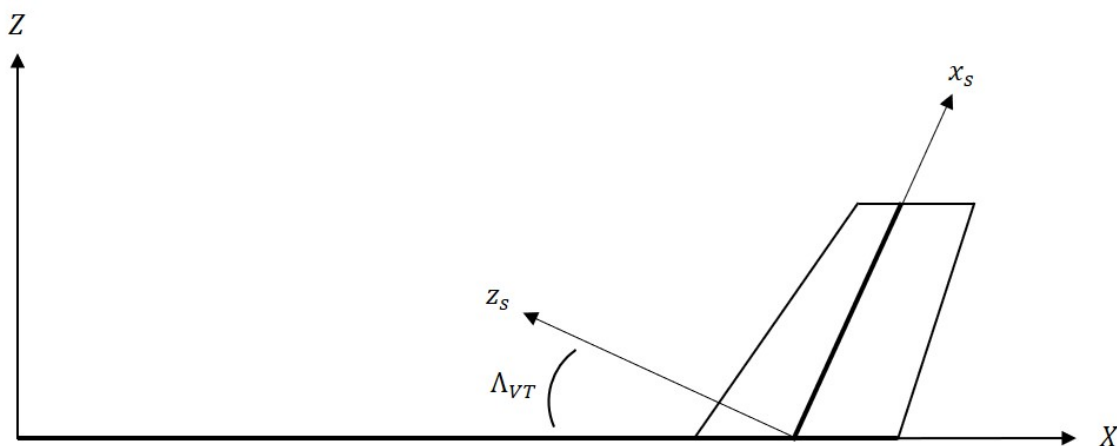
Figure A.1 Vertical Tail Swept Axis

The angle the z_s axis makes with the X axis is Λ_{VT}, or the sweep angle of the elastic axis

of the VT. It is assumed that the fuselage cannot deform in the X direction; therefore a

force applied in X on the fuselage does not result in any deflections of the vertical tail and

there exists no influence coefficient in that direction. A load applied on the fuselage in the

Y direction results in a deflection of the vertical tail in *Y* and a rotation about *Z*. Figure

A.3 shows the displacement and rotation of the vertical tail due to a load on the fuselage in

the *Y* direction. The rigid displacement of the vertical tail in the *Y* direction δ_y is
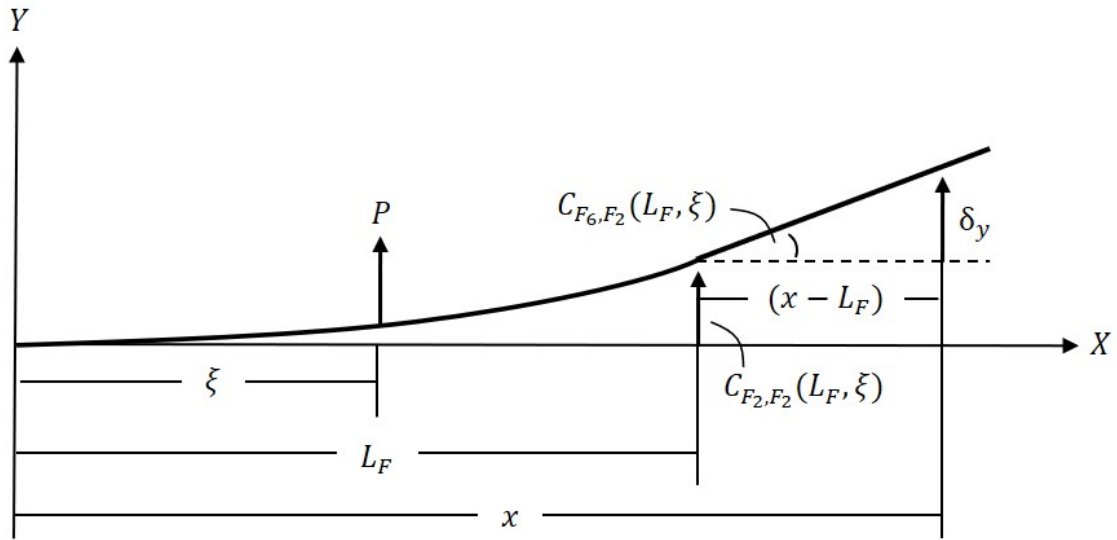
Figure A.2 Vertical Tail Displacement and Rotation Due to P_y on the Fuselage

determined using a small angle approximation of C_{F_6,F_2}:

$$\delta_{V_2,F_2}(x,\xi) = C_{F_6,F_2}(L_F,\xi)(x - L_F) \tag{A.1}$$

Then, the bending influence coefficient is determined by the total displacement:

$$C_{V_2,F_2}(x,\xi) = C_{F_2,F_2}(L_F,\xi) + \delta_{VT_2,F_2}(x,\xi) \tag{A.2}$$

Since there is no elastic deformation of the vertical tail due to a load on the fuselage, the

rotation of the vertical tail about *Z* is constant over the span and is equal to:

$$C_{V_6,F_2}(x,\xi) = C_{F_6,F_2}(L_F,\xi) \tag{A.3}$$

Now a unit load in the Z direction results in displacement in the Z direction as well as a rotation about the Y axis. Figure A.3 shows the undeformed shape in grey and the deformations due to a load applied on the fuselage in black. Closer examination of the tail
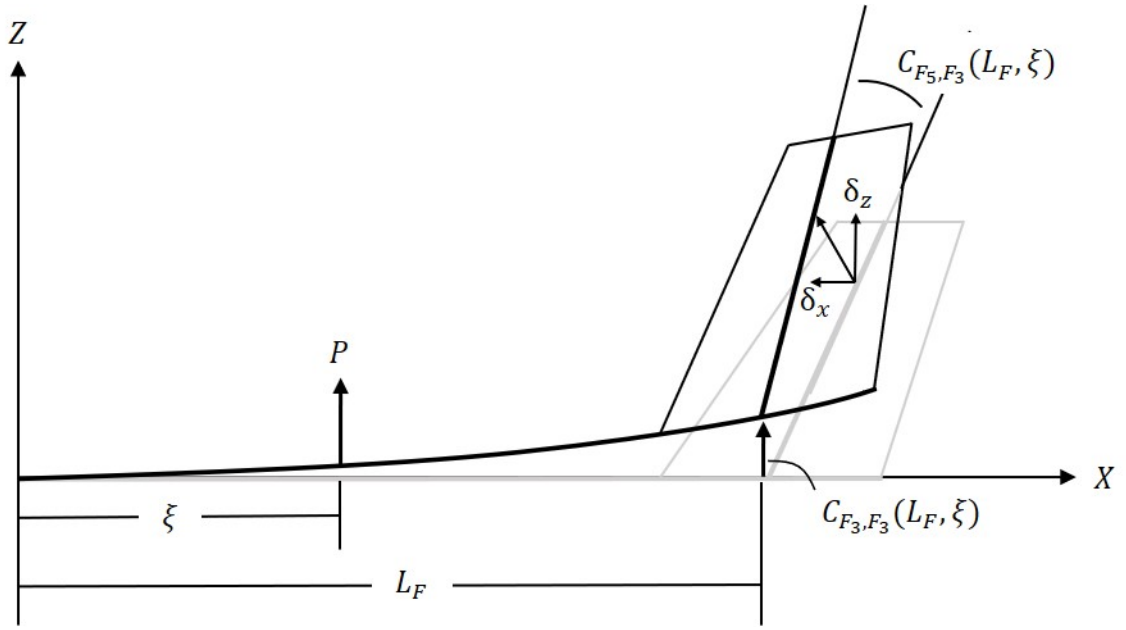
Figure A.3 Vertical Tail Displacement and Rotation Due to P_z on the Fuselage

allows the calculation of δ_y and δ_z. Figure A.4 shows the vertical tail in more detail. Since the vertical tail is assumed to be swept, small angle approximations for the displacements due to rotation cannot be used. The displacement in X due to a rotation about the Y axis is:

$$\delta_{V_1,F_3}(\xi,\xi_s,\Lambda_{VT}) = -\left(sin(\Lambda_{VT}) - sin(\Lambda_{VT} + C_{F_5,F_3}(L_F,\xi))\right)\xi_s \qquad (A.4)$$

where ξ_s is the distance along the EA of the vertical tail to the point of interest, measured from the fuselage intersection point, and ξ is the distance from the origin to the point on
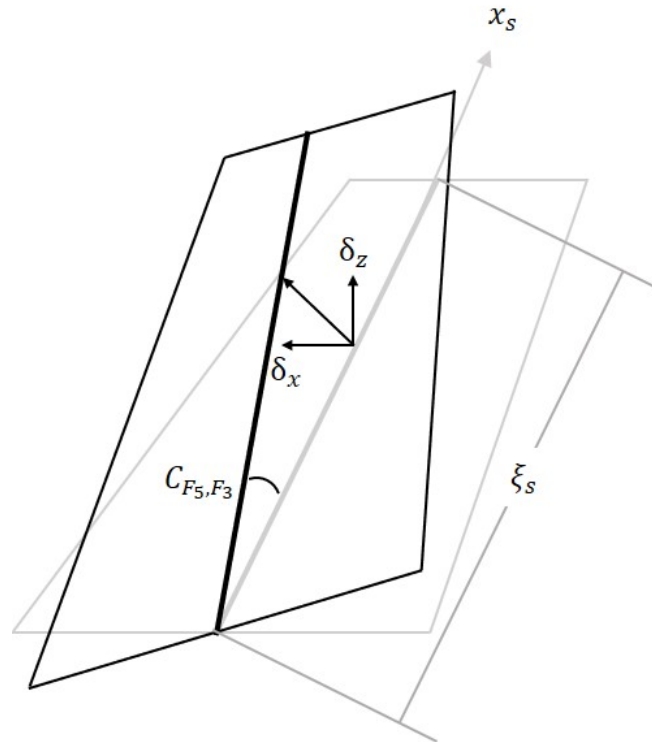
Figure A.4 Vertical Tail Rotations Due to P_z on the Fuselage

the fuselage where the load is being applied. The deflection in Z due to the rotation of the vertical tail is:

$$\delta_{V_3,F_3}(\xi,\xi_s,\Lambda_{VT}) = -\left(cos(\Lambda_{VT}) - cos(\Lambda_{VT} + C_{F_5,F_3}(L_F,\xi))\right)\xi_s \tag{A.5}$$

Since it is assumed the fuselage cannot deform in the X direction, the bending influence coefficient in the X direction is:

$$C_{V_1,F_3} = \delta_{V_1,F_3}(\xi,\xi_s,\Lambda_{VT}) \tag{A.6}$$

Then, the bending influence coefficient in the Z direction is a combination of the deflection due to fuselage bending and the deflection due to rotation,

$$C_{V_3,F_3}(\xi,\xi_s,\Lambda_{VT}) = C_{F_3,F_3}(L_F,\xi) + \delta_{VT_3,F_3}(\xi,\xi_s,\Lambda_{VT}) \tag{A.7}$$

And the rotational influence coefficient is:

$$C_{V_5,F_3}(\xi,\xi_s,\Lambda_{VT}) = C_{F_5,F_3}(L_F,\xi)(\xi,\xi_s,\Lambda_{VT}) \tag{A.8}$$

Next, loads applied in X, Y, and Z on the vertical tail are considered. A load applied on the vertical tail in the X direction must be broken down into its normal and axial components. Figure A.5 shows the relationship between the force normal to the VT, force in the axial direction of the VT, and the sweep angle of the elastic axis. The internal
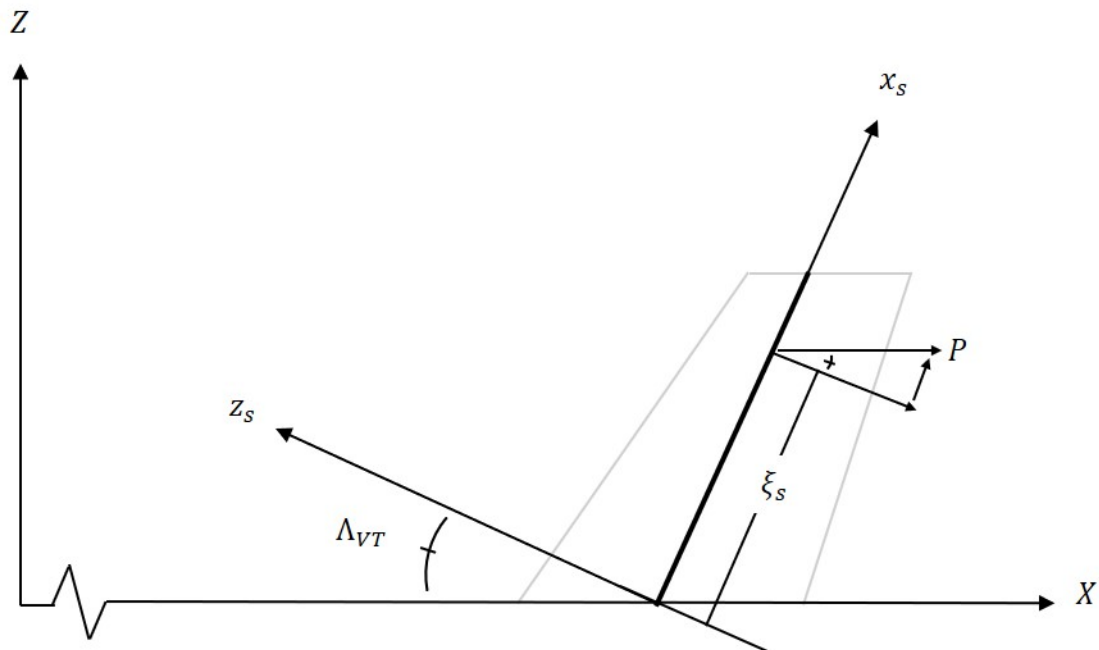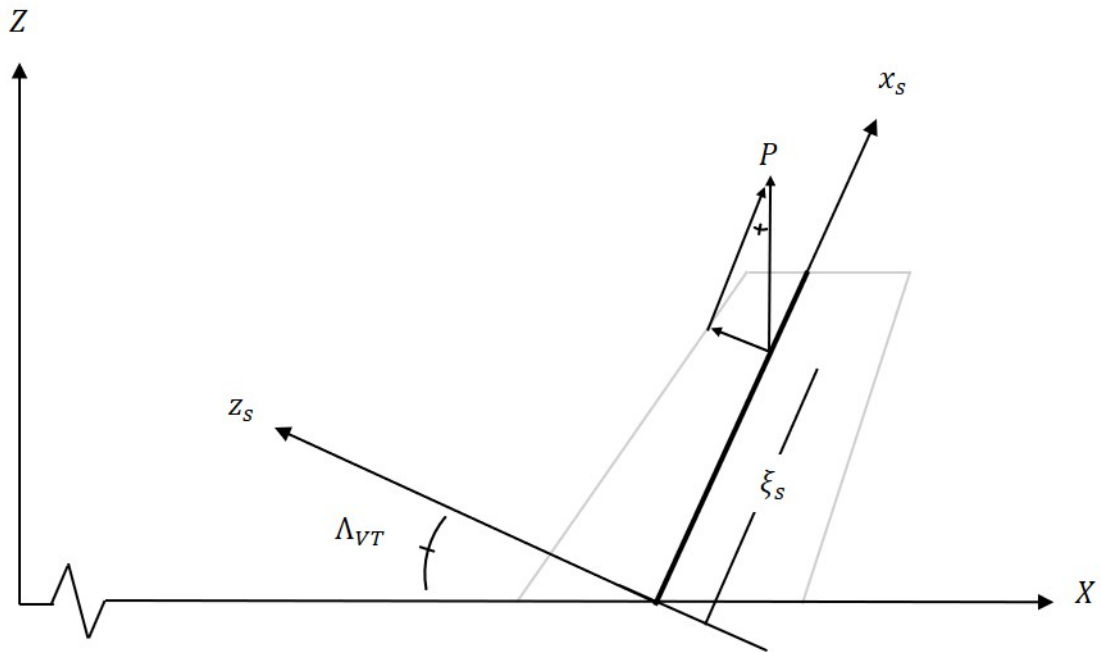

Figure A.5 Vertical Tail P_x Components in Swept Coordinate Frame

bending moment on the vertical tail is:

$$M = (1)(\xi_s - x_s)cos(\Lambda_{VT}) \tag{A.9}$$

where ξ_s is the location of the applied load, normal to the vertical tail, along the x_s axis and x_s is the location of measurement. Using Equation (4.36), the bending deflections in the swept coordinates are:

$$w(x_s, \xi_s, \Lambda_{VT}) = \frac{cos(\Lambda_{VT})}{EI_{yy}(x_s)} \left(\tfrac{1}{2}\xi x_s^2 - \tfrac{1}{6}x_s^3 + C_1 x_s + C_2 \right) \tag{A.10}$$

and the rotations are:

$$w'(x_s, \xi_s, \Lambda_{VT}) = \frac{cos(\Lambda_{VT})}{EI_{yy}(x_s)} \left(\tfrac{1}{2}\xi x_s - \tfrac{1}{2}x_s^2 + C_1 \right) \tag{A.11}$$

Since a load in the z_s direction will result in a deflection in the z_s direction, the deflections of the vertical tail due to bending must be converted back to the global coordinate frame. Figure A.6 show the components of the deflection in the global coordinate frame. Then, the fuselage deflections, displacement due to a rigid rotation of the vertical tail, and bending of the vertical tail are combined. The bending influence coefficients are:

$$C_{V_1,V_1}(x_s, \xi_s, \Lambda_{VT}) = w(x_s, \xi_s, \Lambda_{VT}) \, cos(\Lambda_{VT}) \tag{A.12}$$
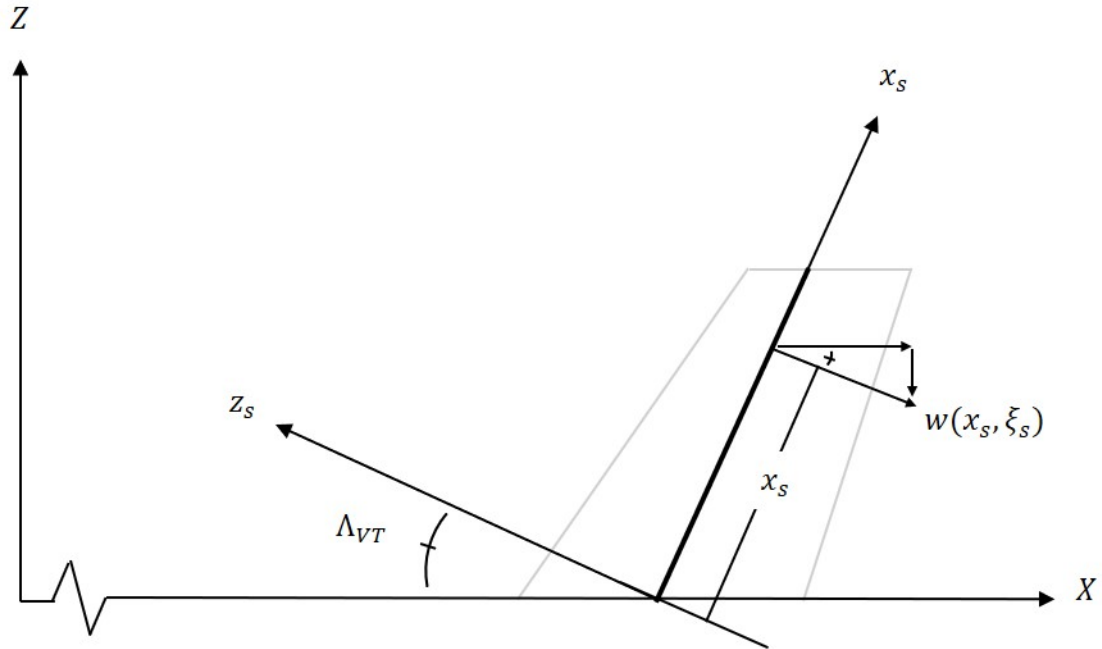
Figure A.6 Vertical Tail Bending due to P_x Components in the Global Coordinate Frame

and the bending in the Z direction is:

$$C_{V_3,V_1} = C_{F_3,V_1}(L_F,\xi) - w(x_s,\xi_s,\Lambda_{VT})\sin(\Lambda_{VT}) \tag{A.13}$$

Using Equation (4.40), the rotation about the Y axis is:

$$C_{V_5,V_1} = C_{F_5,V_1}(L_F,\xi) + w'(x_s,\xi_s,\Lambda_{VT}) \tag{A.14}$$

Next, a force in the Y direction on the vertical tail is considered. Figure A.7 shows the

deflections of the vertical tail in the Y direction due to a unit load in the Y direction. Just as

with a load applied to the fuselage, a rigid rotation of the vertical tail about the Z axis

causes a displacement. However, in this case there is also a rigid rotation about the X axis
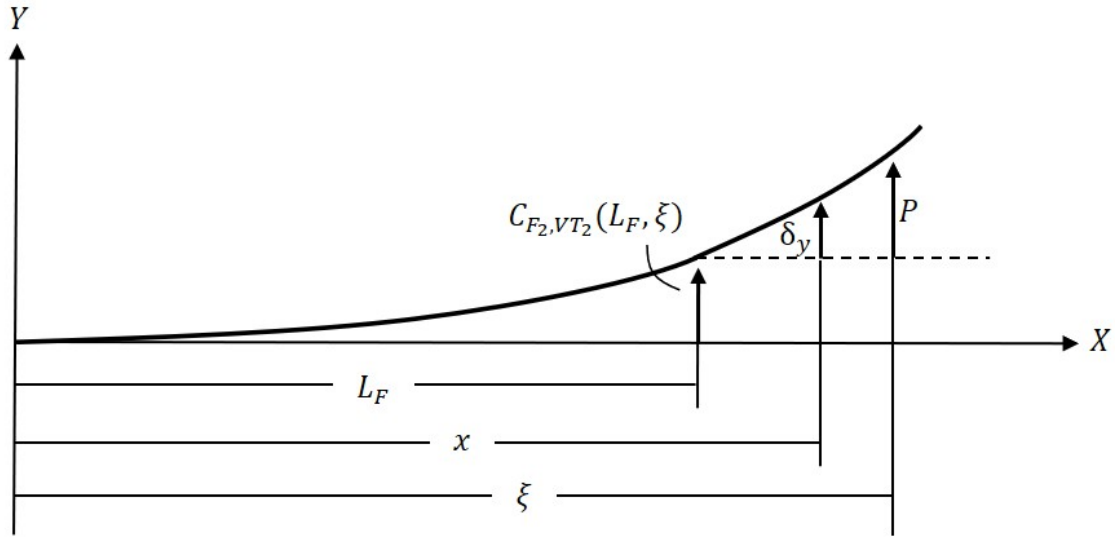
Figure A.7 Vertical Tail Bending due to P_y

that causes a displacement in the Y direction. This displacement about the Z axis is given

in Equation (A.1). The displacement due to rigid rotation about the X axis is:

$$\delta_{V_2,F_4}(x,z,\xi) = C_{F_4,VT_2}(L_F,\xi)\,z \qquad\qquad \text{(A.15)}$$

where z is the height of the point where displacement is being measured. In this case, the

vertical tail bending is purely in the Y direction, but the rotation is about the x_z axis.

Therefore, the rotation must be resolved into the global coordinate system. Figure A.8

shows the rotation about the z_s axis and its components in the X and Z direction. From

Figure A.7, the displacement due to rigid rotation about the Z axis is:

$$\delta_y(x,\xi) = C_{F_6,V_2}(L_F,\xi)(x-L_F) \qquad\qquad \text{(A.16)}$$

The vertical tail is connected to the fuselage with a spring fitting which can deform

independently of the other degrees of freedom. This deformation causes a rigid rotation
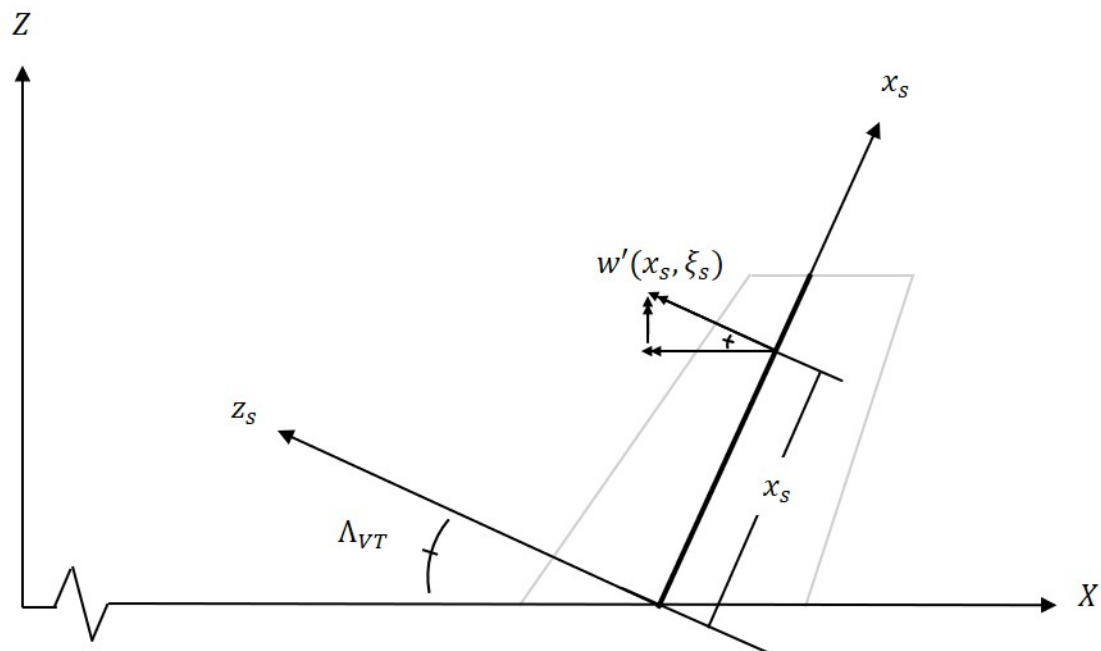
Figure A.8 Vertical Tail Bending due to P_y

about the X axis and thus a displacement in the Y direction. Figure A.9 shows the rotation

of the vertical tail and horizontal tail due to bending of the spring fitting. It is assumed that
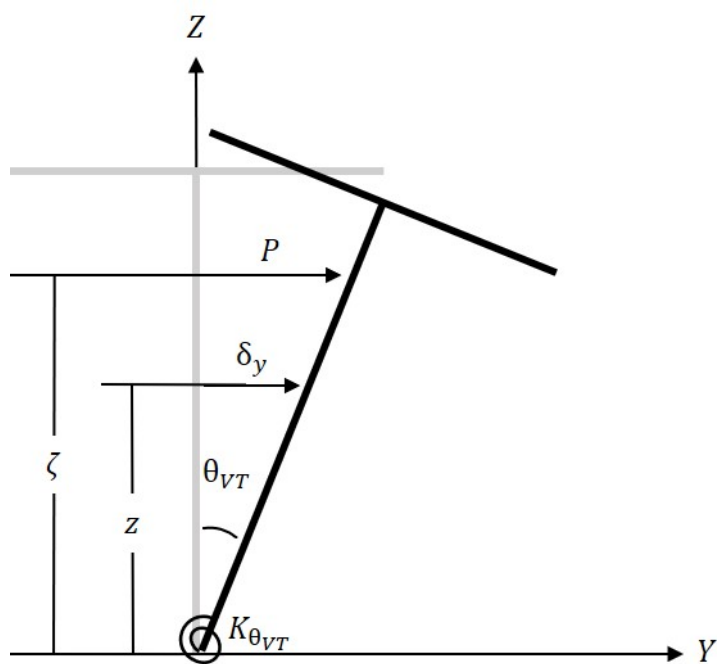
Figure A.9 Vertical Tail Due to Spring Fitting Rotation

the spring $K_{\theta_{VT}}$ is sufficiently stiff such that the resulting angle θ_{VT} is a small angle. Then, using a moment balance, the rotation of spring fitting is:

$$\theta_{VT}(\zeta) = \frac{\zeta}{K_{\theta_{VT}}} \tag{A.17}$$

where ζ is the height of the applied load, measured from the base of the vertical tail in the Z direction. Then, the displacement due to spring fitting rotations is:

$$\delta_{VT_s}(z,\zeta) = \frac{z\zeta}{K_{\theta_{VT}}} \tag{A.18}$$

The bending influence coefficients are a superposition of the displacements due to fuselage deformation, rigid rotations about X and Z, bending of the spring fitting, and vertical tail bending. For the case of $(\xi_s \geq x_s)$, the bending is:

$$w(x_s,\xi_s) = \frac{1}{EI_{zz}(x_s)} \left(\tfrac{1}{2}\xi x_s^2 - \tfrac{1}{6}x_s^3 + C_1 x_s + C_2 \right) \tag{A.19}$$

and the slope is:

$$w'(x_s,\xi_s) = \frac{1}{EI_{zz}(x_s)} \left(\tfrac{1}{2}\xi x_s - \tfrac{1}{2}x_s^2 + C_1 \right) \tag{A.20}$$

Then, the bending influence coefficients are:

$$C_{V_2,V_2} = C_{F_2,V_2}(L_F,\xi) + \delta_{V_2,F_4}(x,z,\xi) + \delta_y(x,\xi) + \delta_{VT_s}(z,\zeta) + w(x_s,\xi_s) \tag{A.21}$$

The rotational influence coefficients are:

$$C_{V_4,V_2} = C_{F_4,V_2}(L_F,\xi) - w'(x_s,\xi_s)\,cos(\Lambda_{VT}) \tag{A.22}$$

and:

$$C_{V_4,V_2} = C_{F_6,V_2}(L_F,\xi) + w'(x_s,\xi_s)\,sin(\Lambda_{VT}) \tag{A.23}$$

Next, a load in the Z direction on the vertical tail is considered. Figure A.10 shows the components of the applied load in the swept axis system.

Figure A.10 Vertical Tail P_z Components in Swept Coordinate Frame

The internal moment on the vertical tail is:

$$M = (1)(\xi_s - x_s)sin(\Lambda_{VT}) \tag{A.24}$$

Using Equation (4.36), the deflection of the vertical tail in the z_s direction is:

$$w(x_s, \xi_s) = \frac{sin(\Lambda_{VT})}{EI_{yy}(x_s)} \left(\tfrac{1}{2}\xi x_s^2 - \tfrac{1}{6}x_s^3 + C_1 x_s + C_2 \right) \qquad (A.25)$$

and the slope is:

$$w'(x_s, \xi_s) = \frac{sin(\Lambda_{VT})}{EI_{yy}(x_s)} \left(\tfrac{1}{2}\xi x_s - \tfrac{1}{2}x_s^2 + C_1 \right) \qquad (A.26)$$

Just as in the case of an applied load in the X direction on the vertical tail, a load applied in the Z direction causes a rigid rotation of the vertical tail about the Y axis. The displacement in X due to this rigid body rotation is:

$$\delta_{V_1, V_3}(x, \xi) = - \left(sin(\Lambda_{VT}) - sin(\Lambda_{VT} + C_{F_5, V_3}(L_F, \xi)) \right) \xi_s \qquad (A.27)$$

and the displacement in Z is:

$$\delta_{V_3, V_3}(x, \xi) = \left(cos(\Lambda_{VT}) - cos(\Lambda_{VT} + C_{F_5, V_3}(L_F, \xi)) \right) \xi_s \qquad (A.28)$$

Now the displacements in the z_s direction are resolved into their components in X and Z. Figure A.11 shows the components of the displacement due to bending. Combining the displacements in the X direction due to rigid rotation of the VT and elastic deformation gives:

$$C_{V_1, V_3} = \delta_{V_1, V_3}(x, \xi) - w(x_s, \xi_s) cos(\Lambda_{VT}) \qquad (A.29)$$
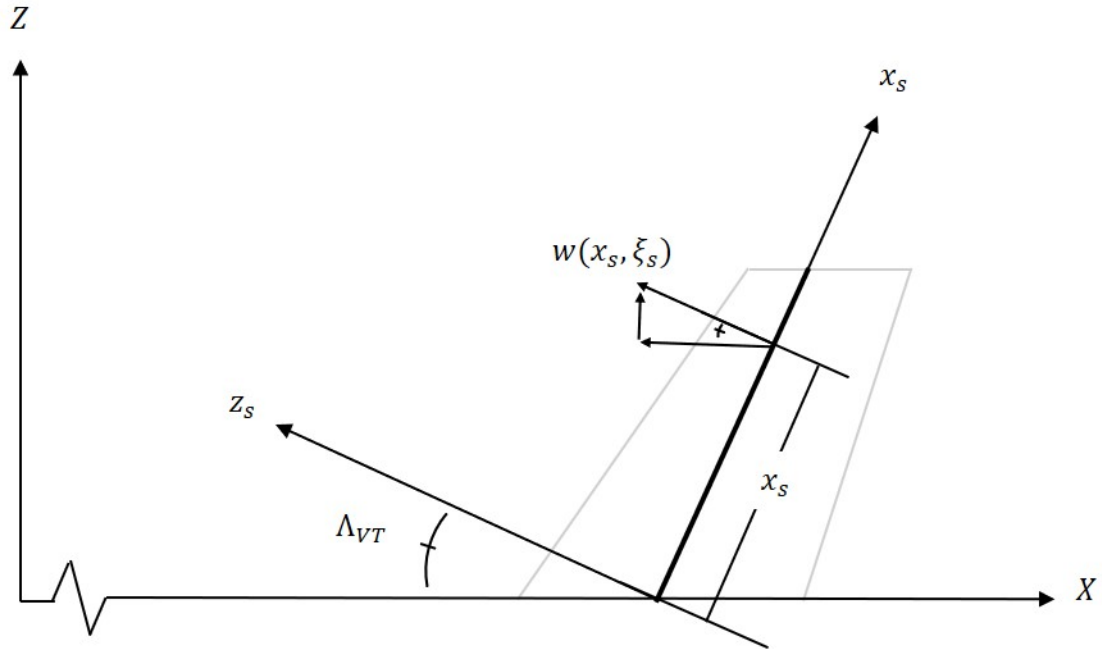
Figure A.11 Vertical Tail Bending due to P_z Components in the Global Coordinate Frame

Combining the displacements in the X direction due to fuselage displacement, rigid rotation of the VT, and elastic deformation gives:

$$C_{V_3,V_3} = C_{F_3,V_3}(L_f,\xi) + \delta_{V_3,V_3}(x,\xi) + w(x_s,\xi_s)\sin(\Lambda_{VT}) \tag{A.30}$$

and combining the rotations from the fuselage, rigid rotation of the VT, and elastic deformation gives:

$$C_{V_5,V_3} = C_{F_5,V_3}(L_f\xi) - w'(x_s,\xi_s)\sin(\Lambda_{VT}) \tag{A.31}$$

Next, a torsional moment on the vertical tail is considered. Since the strips of the VT are assumed to be aligned with the direction of flow, a torsional moment is simply a moment about the Z Axis. Since the vertical tail is swept, a torsion about Z will result in a displacement in the Y direction, a rotation about the Z axis, and a rotation about the X

axis. To determine the deflections of the vertical tail, the applied moment is broken down

into its x_s and z_s components. Figure A.12 shows the components of the applied moment

in the swept axis system.
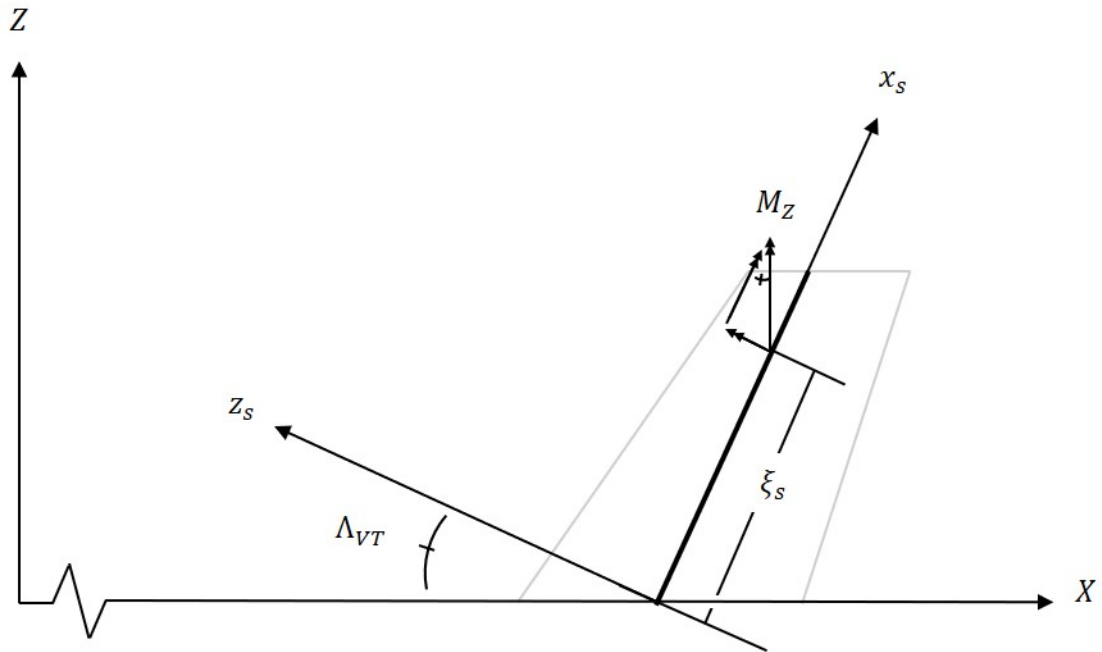
Figure A.12 Vertical Tail Moment Components in Swept Axis

The component of the moment that produces a bending deflection is:

$$M = (1)sin(\Lambda_{VT}) \tag{A.32}$$

Then, using Equation (4.36) the displacements due to bending in the Y direction are:

$$w(x_s, \xi_s) = \frac{sin(\Lambda_{VT})}{EI_{zz}(x_s)} \left(\tfrac{1}{2}x_s^2 + C_1 x_s + C_2 \right) \tag{A.33}$$

and using Equation (4.40), the slope is:

$$w'(x_s, \xi_s) = \frac{sin(\Lambda_{VT})}{EI_{zz}(x_s)}(x_s + C_1) \tag{A.34}$$

The total bending influence coefficient is a combination of the fuselage contribution and the vertical tail contribution:

$$C_{V_2,V_6} = C_{F_2,V_6}(L_f, \xi) + C_{F_6,V_6}(L_F, \xi)(x - L_F) + w(x_s, \xi_s) \tag{A.35}$$

The torsional moment is:

$$T = (1)cos(\Lambda_{VT}) \tag{A.36}$$

Then, using Equation (4.37) the rotation of the vertical tail about the x_s axis is:

$$\theta(x_s, \xi_s) = \frac{cos(\Lambda_{VT})}{GJ(x_s)}(x_s + C_1) \tag{A.37}$$

To determine the rotational influence coefficients, the rotations due to bending and torsion must be resolved into their components in the global coordinates. Figure A.13 shows the components of the rotations in global coordinates.

Then, the rotation about the X axis is a combination of bending and torsion rotations:

$$C_{V_4,V_6} = -w'(x_s, \xi_s)cos(\Lambda_{VT}) + \theta(x_s, \xi_s)sin(\Lambda_{VT}) \tag{A.38}$$
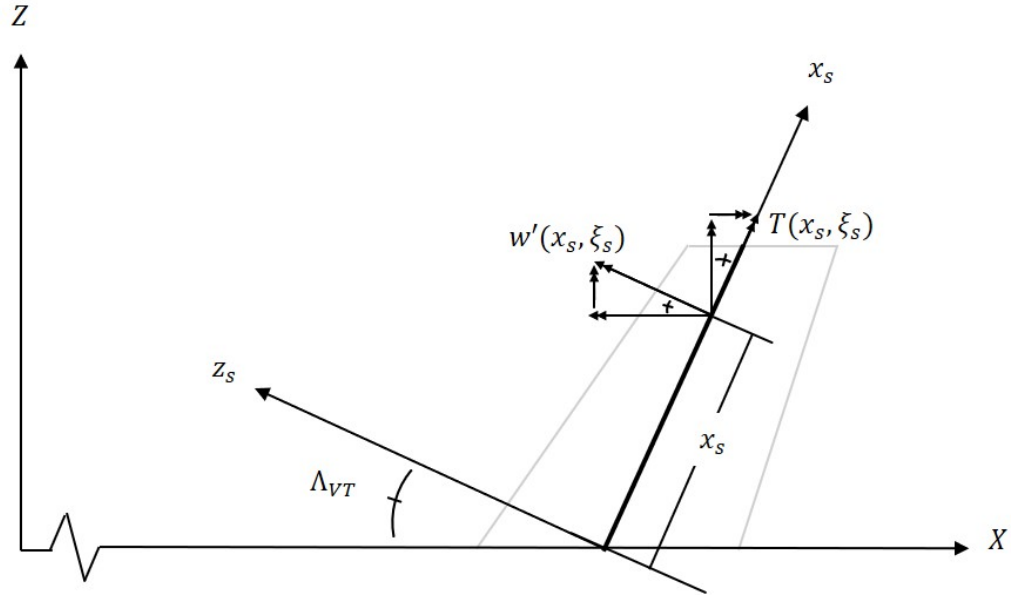
Figure A.13 Bending and Torsion Components in the Global Coordinates

and the rotation about the Z axis is a combination of fuselage rotation, rotation due to bending, and rotation due to torsion,

$$C_{V_6,V_6} = C_{F_6,V_6}(L_F,\xi) + w'(x_s,\xi_s)\,sin(\Lambda_{VT}) + \theta(x_s,\xi_s)\,cos(\Lambda_{VT}) \qquad (A.39)$$

Finally, an applied moment about the X axis at the tip of the vertical tail is considered. This case is useful in determining the flexibility influence coefficients of the horizontal tail. By following the same process used for the applied M_z, the bending influence coefficients are:

$$C_{V_2,V_4} = -C_{F_2,V_4}(L_f,\xi) + C_{F_6,V_6}(L_F,\xi)(x-L_F) + w(x_s,\xi_s)\,sin(\Lambda_{VT}) \qquad (A.40)$$

Then, the rotational influence coefficients about the X axis are:

$$C_{V_4,V_4} = C_{F_4,V_4}(L_F,\xi) + w'(x_s,\xi_s)\,cos(\Lambda_{VT}) + \theta(x_s,\xi_s)\,sin(\Lambda_{VT}) + \theta_{VT}(z) \qquad (A.41)$$
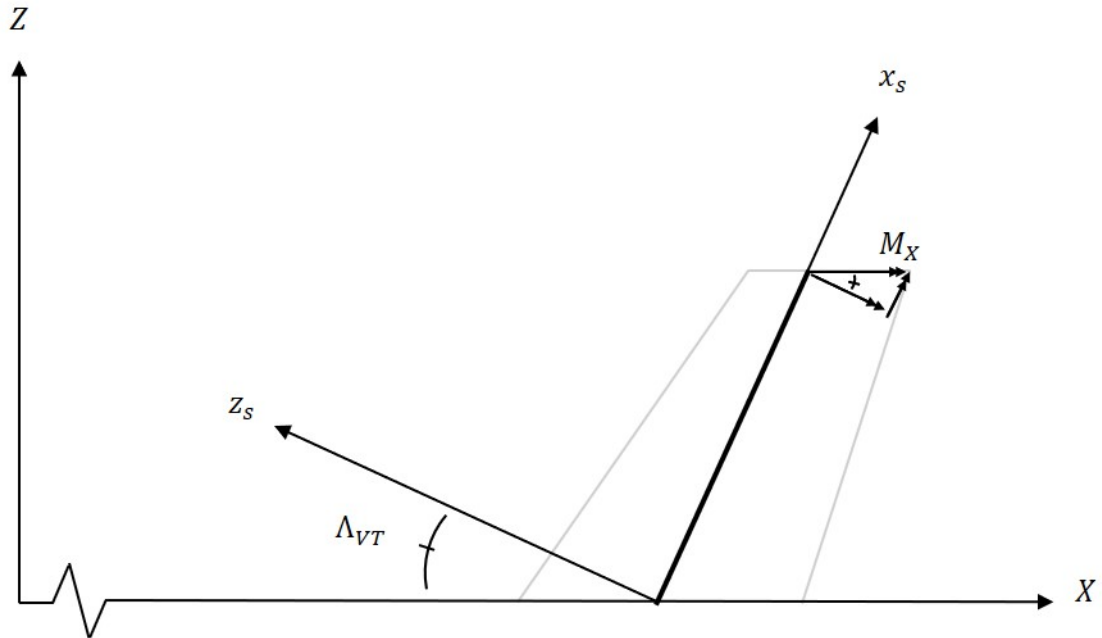
Figure A.14 M_x components in Vertical Tail Swept Axis System

and the rotational influence coefficients about the Z axis are:

$$C_{V_6,V_4} = -w'(x_s,\xi_s)\,sin(\Lambda_{VT}) + \theta(x_s,\xi_s)\,cos(\Lambda_{VT}) \tag{A.42}$$

Next, a load in the X direction on the starboard horizontal tail is considered. A load in the X direction results in displacement in X, Y, and Z as well as rotations about the X, Y, and Z axes. Figure A.15 shows the internal moments on the vertical tail that result from a load applied in the X direction on the starboard horizontal tail. From Figure A.15, the moment about the Y axis is:

$$M_y = (1)(\zeta - z) \tag{A.43}$$
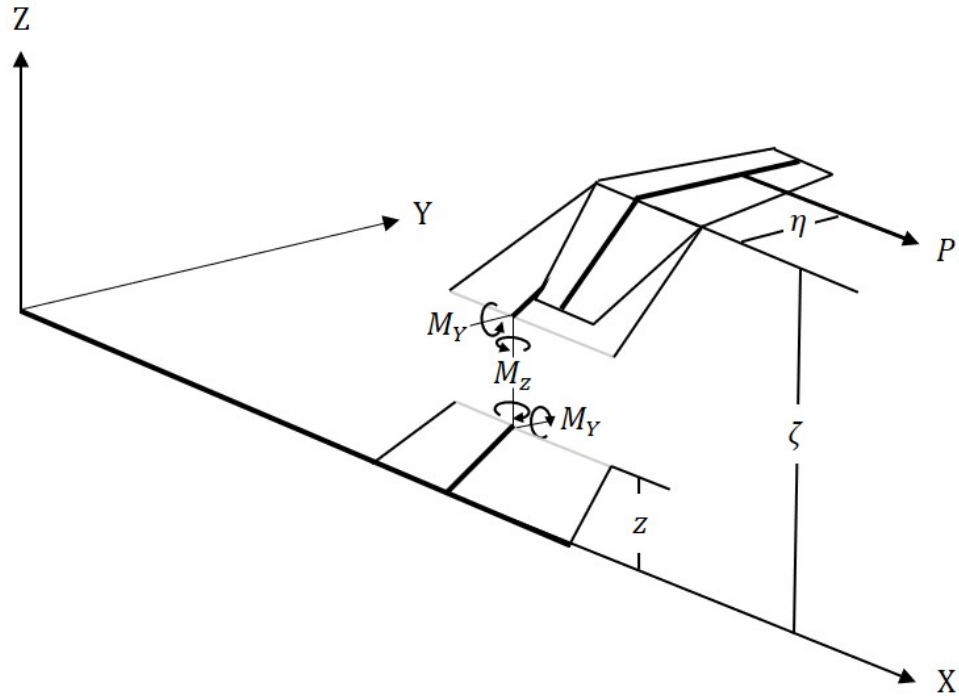
Figure A.15 Vertical Tail Internal Moments Due to P_x on the Starboard Horizontal Tail

Since the horizontal is assumed to have no dihedral angle, M_y is a constant. Therefore, the deflection of the vertical tail in the X due to a load on the horizontal tail is equivalent to that of a load applied on the tip of the vertical tail. In other words:

$$C_{V_1,HS_1} = C_{V_1,V_1}(x_s, L_{VT}) \tag{A.44}$$

The same can be said for the displacement in the Z direction. Thus, the bending influence coefficients are given by:

$$C_{V_3,HS_1} = C_{V_3,V_1}(x_s, L_{VT}) \tag{A.45}$$

and the rotational influence coefficients are:

$$C_{V_5,HS_1} = C_{V_5,V_1}(x_s, L_{VT}) \tag{A.46}$$

From Figure A.15, the moment about the Z axis is:

$$M_z = -(1)\eta \tag{A.47}$$

and the bending moment in the swept axis system is:

$$M_{z_s} = -(1)\eta \, sin(\Lambda_{VT}) \tag{A.48}$$

and the torsional moment is:

$$M_{x_s} = -(1)\eta \, cos(\Lambda_{VT}) \tag{A.49}$$

Then, using Equation (4.36) the displacement is:

$$w(x_s, \eta, \Lambda_{VT}) = -\frac{\eta \, sin(\Lambda_{VT})}{EI_{zz}(x_s)} \left(\tfrac{1}{2}x_s^2 + C_1 x_s + C_2 \right) \tag{A.50}$$

using Equation (4.40) the slope is:

$$w'(x_s, \eta, \Lambda_{VT}) = -\frac{\eta \, sin(\Lambda_{VT})}{EI_{zz}(x_s)} \left(\tfrac{1}{2}x_s + C_1 \right) \tag{A.51}$$

and using Equation (4.37) the angular rotation of the beam about its swept axis is:

$$\theta(x_s, \xi_s, \Lambda_{VT}) = -\frac{cos(\Lambda_{VT})}{GJ(x_s)} (x_s + C_1) \tag{A.52}$$

Now the total displacement in the Y direction is a combination of fuselage displacement, vertical tail rotation about the Z axis, and vertical tail bending. The deformation due to

bending is determined by plugging Equation (A.47) into Equation (A.33). Then the total

bending influence coefficient is a combination of fuselage bending, displacement due to

rigid rotation, and bending of the vertical tail,

$$C_{V_2,HS_1} = C_{F_2,HS_1}(L_F,\xi) + C_{F_6,HS_1}(L_F,\xi)(x - L_F) + w(x_s,\eta,\Lambda_{VT}) \tag{A.53}$$

The rotational influence coefficients about the X axis are:

$$C_{V_4,HS_1} = -w'(x_s,\eta,\Lambda_{VT})\cos(\Lambda_{VT}) + \theta(x_s,\xi_s,\Lambda_{VT})\sin(\Lambda_{VT}) \tag{A.54}$$

The rotational influence coefficients about the Z axis are:

$$C_{V_6,HS_1} = C_{F_6,HS_1}(L_F,\xi) + w'(x_s,\eta,\Lambda_{VT})\sin(\Lambda_{VT}) + \theta(x_s,\xi_s,\Lambda_{VT})\cos(\Lambda_{VT}) \tag{A.55}$$

Next, a load in the Y direction on the starboard horizontal tail is considered. A load in

the Y direction results in displacement in Y as well as rotations about the X and Z axes.

Figure A.16 shows the internal moments on the vertical tail that result from the applied

load. From Figure A.16, the moment about the Z axis is:

$$M_z = (1)(\xi - x) \tag{A.56}$$

Then the moment about the z_s axis is:

$$M_{z_s} = (1)(\xi - x)\sin(\Lambda_{VT}) \tag{A.57}$$
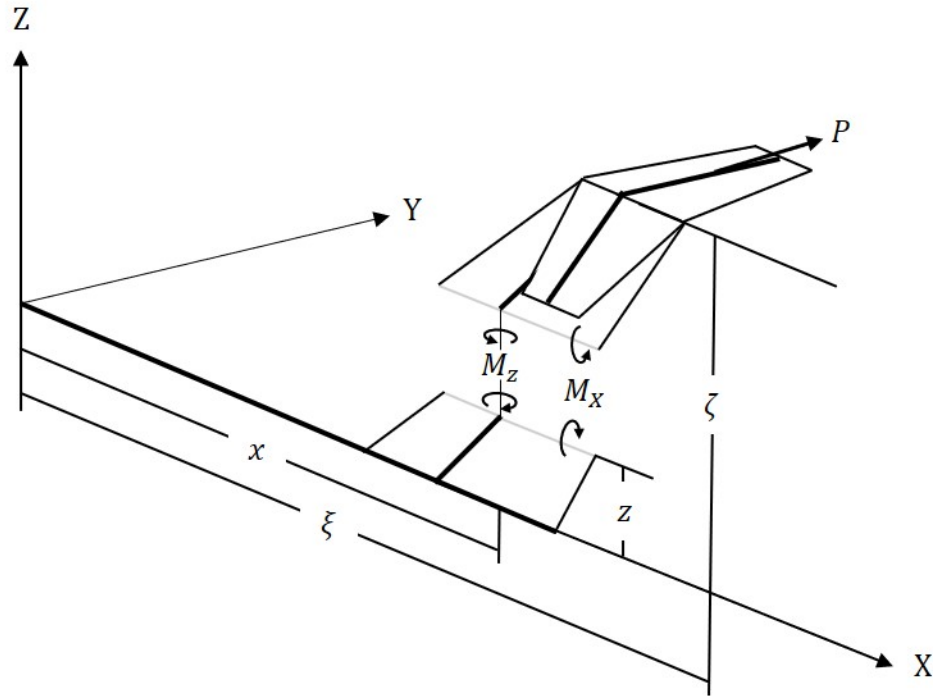
Figure A.16 Vertical Tail Internal Moments Due to P_y on the Starboard Horizontal Tail

and the moment about the x_s axis is:

$$M_{x_s} = (1)(\xi - x)cos(\Lambda_{VT}) \tag{A.58}$$

Then, for simplicity the vertical tail bending was split into the contribution from the applied force and the contribution from the resulting moment. Using Equation (4.36), the contribution from the applied force is:

$$w_P(x_s) = \frac{1}{EI_{zz}(x_s)} \left(\tfrac{1}{2} L_{VT} x_s^2 - \tfrac{1}{6} x_s^3 + C_1 x_s + C_2 \right) \tag{A.59}$$

The contribution from the moment is:

$$w_M(x, x_s, \xi) = \frac{(\xi - x)sin(\Lambda_{VT})}{EI_{zz}(x_s)} \left(\tfrac{1}{2} x_s^2 + C_1 x_s + C_2 \right) \tag{A.60}$$

Using Equation (4.37), the torsion about the x_s axis is:

$$\theta(x,x_s,\xi) = \frac{(\xi-x)cos(\Lambda_{VT})}{GJ(x_s)}(x_s+C_1) \tag{A.61}$$

The total displacement of the vertical tail in the Y direction is a combination of fuselage bending, rigid rotations about the X and Z axis, and bending of the spring fitting. The displacement due to rigid rotation about the X axis is:

$$\delta_{rx}(x,z,\xi) = C_{F4,HS_2}(L_f,\xi)\,z \tag{A.62}$$

The displacement due to rigid rotation about the Z axis is:

$$\delta_{rz}(x,z,\xi) = C_{F6,HS_2}(L_F,\xi)(x-L_F) \tag{A.63}$$

the rotation due to the spring fitting is:

$$\theta_s = -\frac{L_{VT}}{K_{\theta_{VT}}} \tag{A.64}$$

and the displacement due to the spring fitting is:

$$\delta_{VT_s}(z,\zeta) = \frac{z\,L_{VT}}{K_{\theta_{VT}}} \tag{A.65}$$

Then, the total bending influence coefficient is:

$$C_{V_2,HS_2}(x,x_s,z,\xi,\zeta) = C_{V_F,HS_2}(L_F,\xi) + \delta_{rx}(x,z,\xi) + \delta_{rz}(x,z,\xi) + w_P(x_s)$$

$$+ w_M(x,x_s,\xi) + \delta_{VT_s}(z,\zeta) \quad \text{(A.66)}$$

where x and z give the location of the point of interest in the global coordinate frame, x_s is the location of the point of interest in the swept axis system, and ξ and ζ give the location of the applied force in the global coordinate frame. It follows that the rotations about the X axis are:

$$C_{V_4,HS_2} = C_{F_4,HS_2}(L_F,\xi) + (w_p(x_s) + w_M(x,x_s,\xi))cos(\Lambda_{VT}) + \theta\,sin(\Lambda_{VT}) + \theta_s \quad \text{(A.67)}$$

and the rotations about the Z axis are:

$$C_{V_6,HS_2} = C_{F_6,HS_2}(L_F,\xi) - (w_p(x_s) + w_M(x,x_s,\xi))sin(\Lambda_{VT}) + \theta\,cos(\Lambda_{VT}) \quad \text{(A.68)}$$

Next, a load in the Z direction on the starboard horizontal tail is considered. A load in the Z direction results in displacement in X, Y, and Z as well as rotations about the X, Y, and Z axes. Figure A.17 shows hte internal moments on the vertical tail that result from a load applied in the Z direction on the starboard HT.

From Figure A.17, the moment about the Y axis is:

$$M_y = -(1)(\xi - x) \quad \text{(A.69)}$$
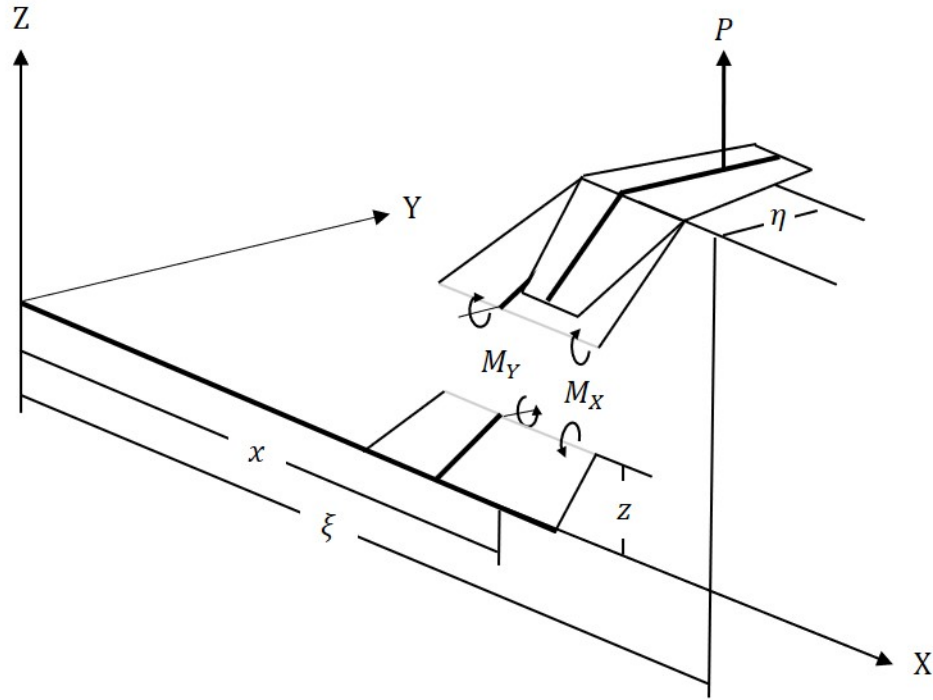
Figure A.17 Vertical Tail Internal Moments Due to P_z on the Starboard Horizontal Tail

For simplicity, the bending in the z_s direction was split up into the contribution from the applied load and the contribution from the resulting moment. Using Equation (4.36), the bending due to the applied force is:

$$w_P(x_s, \Lambda_{VT}) = \frac{sin(\Lambda_{VT})}{EI_{yy}(x_s)} \left(\tfrac{1}{2} L_{VT} x_s^2 - \tfrac{1}{6} x_s^3 + C_1 x_s + C_2 \right) \tag{A.70}$$

The contribution of the moment is:

$$w_M(x, x_s, \xi, \Lambda_{VT}) = -\frac{(\xi - x)}{EI_{yy}(x_s)} \left(\tfrac{1}{2} x_s^2 + C_1 x_s + C_2 \right) \tag{A.71}$$

Using Equation (4.40), the rotation due to a point load is:

$$w'_P(x_s, \Lambda_{VT}) = -\frac{sin(\Lambda_{VT})}{EI_{yy}(x_s)} \left(L_{VT} x_s - \tfrac{1}{2} x_s^2 + C_1 \right) \tag{A.72}$$

and the rotation due a moment is:

$$w'_M(x, x_s, \xi, \Lambda_{VT}) = -\frac{(\xi - x)}{EI_{yy}(x_s)} (x_s + C_1) \tag{A.73}$$

Just as the case with a load applied to the vertical tail or the fuselage, there is a rigid rotation of the VT about the Y axis due to the fuselage bending. The displacements in the X direction are:

$$\delta_x(\xi, \xi_s, \Lambda_{VT}) = -\left(sin(\Lambda_{VT}) - sin(\Lambda_{VT} + C_{F_5, HS_3}(L_F, \xi))\right) \xi_s \tag{A.74}$$

and the displacements in the Z direction are:

$$\delta_z(\xi, \xi_s, \Lambda_{VT}) = -\left(cos(\Lambda_{VT}) - cos(\Lambda_{VT} + C_{F_5, HS_3}(L_F, \xi))\right) \xi_s \tag{A.75}$$

The total bending influence coefficient in the X direction is the combination of displacement due to rigid rotation and the bending,

$$C_{V_1, HS_3} = \delta_x(\xi, \xi_s, \Lambda_{VT}) + (-w_P + w_M)cos(\Lambda_{VT}) \tag{A.76}$$

Similarly, the bending influence coefficient in the Z direction is:

$$C_{V_3, HS_3} = C_{F_3, HS_3}(L_F, \xi) + \delta_z(\xi, \xi_s, \Lambda_{VT})$$

$$+ (w_P(x_s, \Lambda_{VT}) - w_M(x, x_s, \xi, \Lambda_{VT}))cos(\Lambda_{VT}) \tag{A.77}$$

And the rotational influence coefficients are:

$$C_{V_5,HS_3} = C_{F_5,HS_3}(L_F,\xi) - w'_P(x_s,\Lambda_{VT}) + w'_M(x,x_s,\xi,\Lambda_{VT}) \qquad \text{(A.78)}$$

From Figure A.17, the moment about the X axis is:

$$M_X = (1)\eta \qquad \text{(A.79)}$$

and the moment about the z_s axis is:

$$M_{z_s} = -\eta\cos(\Lambda_{VT}) \qquad \text{(A.80)}$$

and the moment about the x_s axis is:

$$M_{x_s} = \eta\sin(\Lambda_{VT}) \qquad \text{(A.81)}$$

Then, using Equation (4.36) the displacement due to bending is:

$$w(x_s,\eta,\Lambda_{VT}) = -\frac{\eta\cos(\Lambda_{VT})}{EI_{yy}(x_s)}\left(\tfrac{1}{2}x_s^2 + C_1 x_s + C_2\right) \qquad \text{(A.82)}$$

using Equation (4.40), the slope is:

$$w'(x_s,\Lambda_{VT}) = -\frac{\eta\cos(\Lambda_{VT})}{EI_{yy}(x_s)}(x_s + C_1) \qquad \text{(A.83)}$$

and using Equation (4.37), the angular rotation about the swept axis is:

$$\theta(x_s, \Lambda_{VT}) = \frac{\eta \sin(\Lambda_{VT})}{GJ(x_s)}(x_s + C_1) \tag{A.84}$$

The displacement of the vertical tail in the Y direction due to the fuselage rotating about the X axis is:

$$\delta_{rx}(\xi, z) = -C_{F4,HS_3}(L_F, \xi)\, z \tag{A.85}$$

Finally, the spring fitting must be considered. The rotation of the vertical tail due to the spring is:

$$\theta_{VT_s}(\eta) = \frac{\eta}{K_{\theta_{VT}}} \tag{A.86}$$

and the displacement of the vertical tail in the Y direction due to the spring fitting is:

$$\delta_{VT_s}(z, \eta) = -\frac{\eta}{K_{\theta_{VT}}}\, z \tag{A.87}$$

The bending influence coefficients in the Y direction are:

$$C_{V_2,HS_3} = \delta_{rx}(\xi, z) + w(x_s, \eta, \Lambda_{VT}) + \delta_{VT_s}(z, \eta) \tag{A.88}$$

The rotational influence coefficient about the X axis is:

$$C_{V_4,HS_3} = C_{F4,HS_3}(L_F, \xi) + w'(x_s, \Lambda_{VT})\cos(\Lambda_{VT}) + \theta(x_s, \Lambda_{VT})\sin(\Lambda_{VT}) + \theta_{VT_s}(\eta) \tag{A.89}$$

and the rotational influence coefficient about the Z axis is:

$$C_{V_6,HS_3} = -w'(x_s, \Lambda_{VT}) \sin(\Lambda_{VT}) + \theta(x_s, \Lambda_{VT}) \cos(\Lambda_{VT}) \qquad (A.90)$$

Next a torsional moment on the starboard horizontal tail is considered. Since the strips

of the horizontal tail are assumed to be aligned in the streamwise direction, a torsional

moment about a strip on the HT is equivalent to applying a moment about the Y axis at the

tip of the vertical tail. Using Equation (4.36), the displacements in the z' direction are:

$$w(x_s) = \frac{1}{EI_{yy}(x_s)} \left(\tfrac{1}{2} x_s^2 + C_1 x_s + C_2 \right) \qquad (A.91)$$

and the slope is:

$$w'(x_s) = \frac{1}{EI_{yy}(x_s)} (x_s + C_1) \qquad (A.92)$$

The displacement of the VT in the X direction due to fuselage bending is:

$$\delta_x = (\sin(\Lambda_{VT} + C_{F_5,HS_5}) - \sin(\Lambda_{VT})) x_s \qquad (A.93)$$

and the displacement of the VT in the Z direction due to fuselage bending is:

$$\delta_z = (\cos(\Lambda_{VT} + C_{F_5,HS_5}) - \cos(\Lambda_{VT})) x_s \qquad (A.94)$$

Then bending influence coefficient in the X direction due to a torsional moment on the

starboard HT is:

$$C_{V_1,HS_5} = \delta_x + w(x_s) \cos(\Lambda_{VT}) \qquad (A.95)$$

the bending influence coefficient in the Z direction is:

$$C_{V_3,HS_5} = C_{V_3,HS_5}(L_f,\xi) + \delta_z - w(x_s)\,sin(\Lambda_{VT}) \qquad (A.96)$$

and the rotational influence coefficient about the Y axis is:

$$C_{V_5,HS_5} = C_{V_5,HS_5}(L_f,\xi) + w'(x_s) \qquad (A.97)$$

Finally, a hinge moment on the starboard horizontal tail is considered. Since the applied moment is a free vector, a unit moment about the hinge line is equivalent to a unit moment about the elastic axis. Therefore, the same deformations will result from a hinge moment as those from a pitching moment at some location z on the vertical tail.

The same equations used to find the vertical tail flexibility influence coefficients for the starboard horizontal tail apply to the port side as well. However, due to the sign convention defined in Chapter 3, all values of y and η will be a negative number.

Horizontal Tail Influence Coefficients

The flexibility influence coefficients from the port horizontal tail can be found primarily using the same equations for the flexibility influence coefficients of the starboard side. The one exception is the influence of forces and moments on the port HT to the starboard HT. First, a load applied in the Y direction on the fuselage is considered. Figure A.18 shows the displacement and rotation of the horizontal tail due to a load applied on the fuselage.
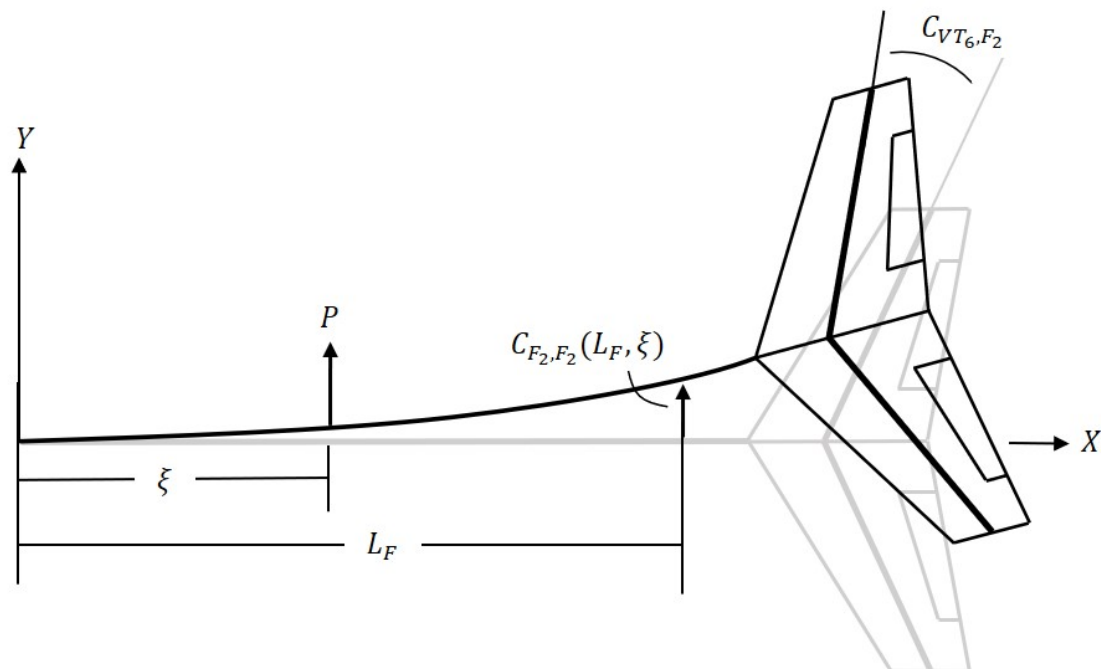
Figure A.18 Horizontal Tail Displacement due to P_y on the Fuselage

Figure A.19 shows the displacement of a point on the starboard HT due to the rigid

rotation.
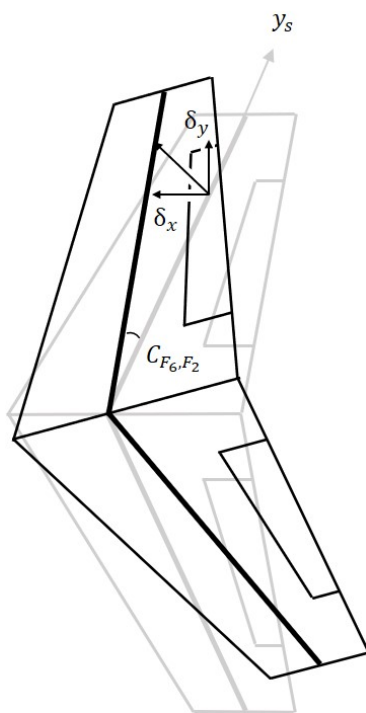
Figure A.19 Horizontal Tail Displacement due to Rotation

Since the HT is assumed to be swept, small angle approximations cannot be used to find the displacements due to the rigid rotation of the tail. By inspecting Figure A.19, the displacement in the X direction is:

$$\delta_x(\xi, \Lambda_{VT}) = (sin(\Lambda_{VT} - C_{V_6,F_2}(L_{VT}, \xi)) - sin(\Lambda_{VT})) \qquad (A.98)$$

and the displacement in the Y direction is:

$$\delta_y(\xi, \Lambda_{VT}) = (cos(\Lambda_{VT} - C_{V_6,F_2}(L_{VT}, \xi)) - cos(\Lambda_{VT})) \qquad (A.99)$$

Since the fuselage cannot deform in the X direction, the bending influence coefficients are:

$$C_{HS_1,F_2} = \delta_x(\xi, \Lambda_{VT}) \qquad (A.100)$$

The bending in the Y direction is a combination of vertical tail displacements and the rigid rotation of the HT. Thus, the bending influence coefficients in the Y direction are:

$$C_{HS_2,F_2} = C_{V_2,F_2}(L_F, \xi) + \delta_y(\xi, \Lambda_{VT}) \qquad (A.101)$$

and the rotational influence coefficients are:

$$C_{HS_6,F_2} = C_{V_6,F_2}(L_F, \xi) \qquad (A.102)$$

Next, a load in the Z direction is considered. This results in a displacement due to the fuselage bending and a rigid rotation about the Y axis.Figure A.20 shows the displacement of the horizontal tail in the Z direction due to a force applied in the Z direction on the fuselage.
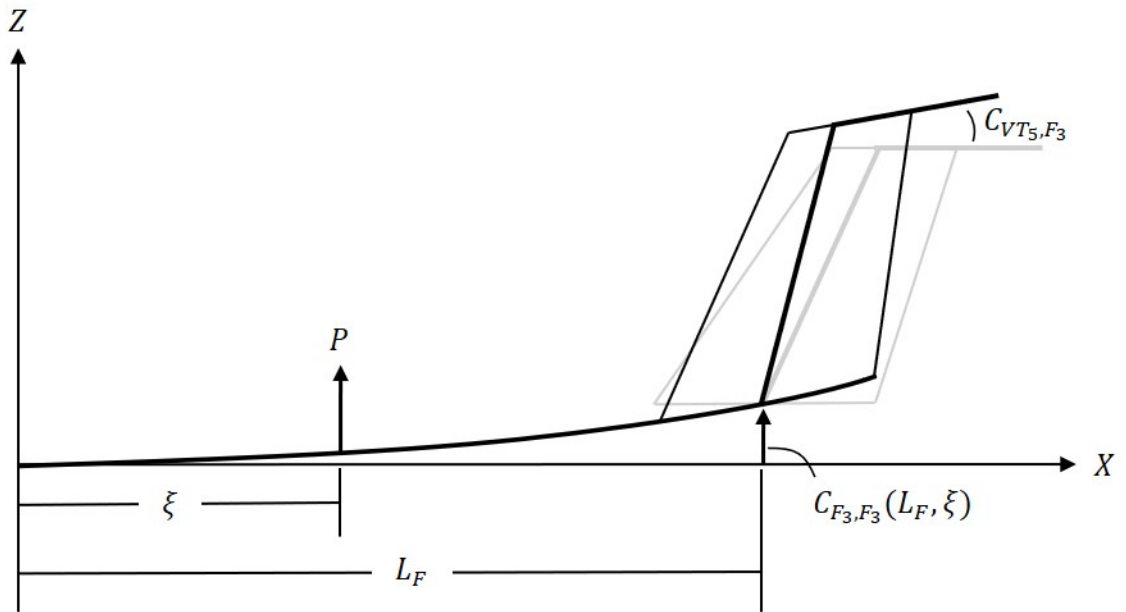
Figure A.20 Horizontal Tail Displacement due to P_z on the Fuselage

The displacements of the HT in the X direction,

$$C_{HS_1,F_3} = C_{V_1,F_3}(L_{VT},\xi) \tag{A.103}$$

The displacement in Z due to the rigid rotation about the Y axis is:

$$\delta_z = -C_{V_5,F_3}(L_{VT},\xi)(x - L_F - L_{VT}tan(\Lambda_{VT})) \tag{A.104}$$

Then, the bending influence coefficients in the Z direction are:

$$C_{HS3,F_3} = C_{V3,F_3}(L_{VT}, \xi) + \delta_z \tag{A.105}$$

and the rotations about the Y axis are:

$$C_{HS5,F_3} = C_{V5,F_3}(L_{VT}, \xi) \tag{A.106}$$

Next, a load applied in the X direction on the vertical tail is considered. This results in displacements in the X and Z direction due to the fusealge and vertical tail bending. This also results in a displacement in the Z direction due a a rigid rotation of the HT about the Y axis. Figure A.21 shows the displacements of the HT due to a load applied in the X direction on the vertical tail.
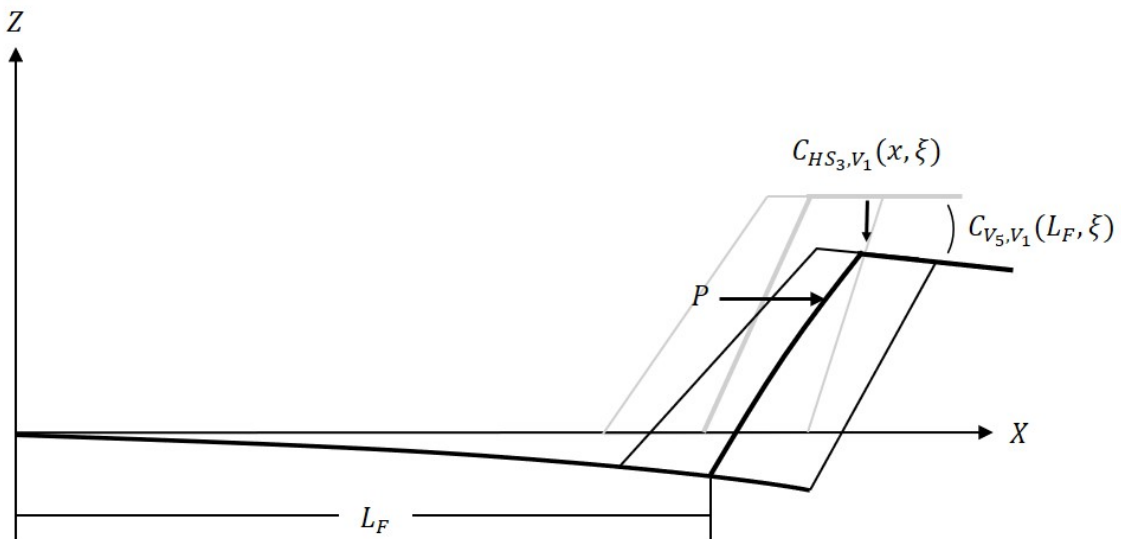
Figure A.21 Horizontal Tail Displacement due to P_x on the Vertical Tail

The displacements in the X direction are given by:

$$C_{HS_1,V_1} = C_{VT_1,V_1}(L_{VT},\zeta) \tag{A.107}$$

The displacements in the Z direction due to the rigid rotation of the HT are:

$$\delta_z = -C_{V_5,V_1}(L_{VT},\xi)(x - L_F - L_{VT}tan(\Lambda_{VT})) \tag{A.108}$$

Then, the total displacements of the HT in Z due to a force applied to the VT in the X direction are given by:

$$C_{HS_3,VT_1} = C_{V_3,V_1}(L_{VT},\zeta) + \delta_z \tag{A.109}$$

and the rotations about the Y axis are:

$$C_{HS_5,VT_1} = C_{V_5,V_1}(L_{VT},\zeta) \tag{A.110}$$

Next, a load applied in the Y direction on the vertical tail is considered. This results in displacements of the horizontal tail in the Y direction due to the fuselage and vertical tail bending. This also results in a displacement in the X, Y, and Z directions due to a rigid rotation of the HT about the X axis and the Z axis. Figure A.22 shows the displacements of the HT due to a load applied in the Y direction on the VT. The displacement in the X direction due to the rigid rotation about the Z axis is:

$$\delta_x = (sin(\Lambda_{VT} - C_{V_6,V_2}(L_{VT},\zeta)) - sin(\Lambda_{VT}))\, y_s \tag{A.111}$$
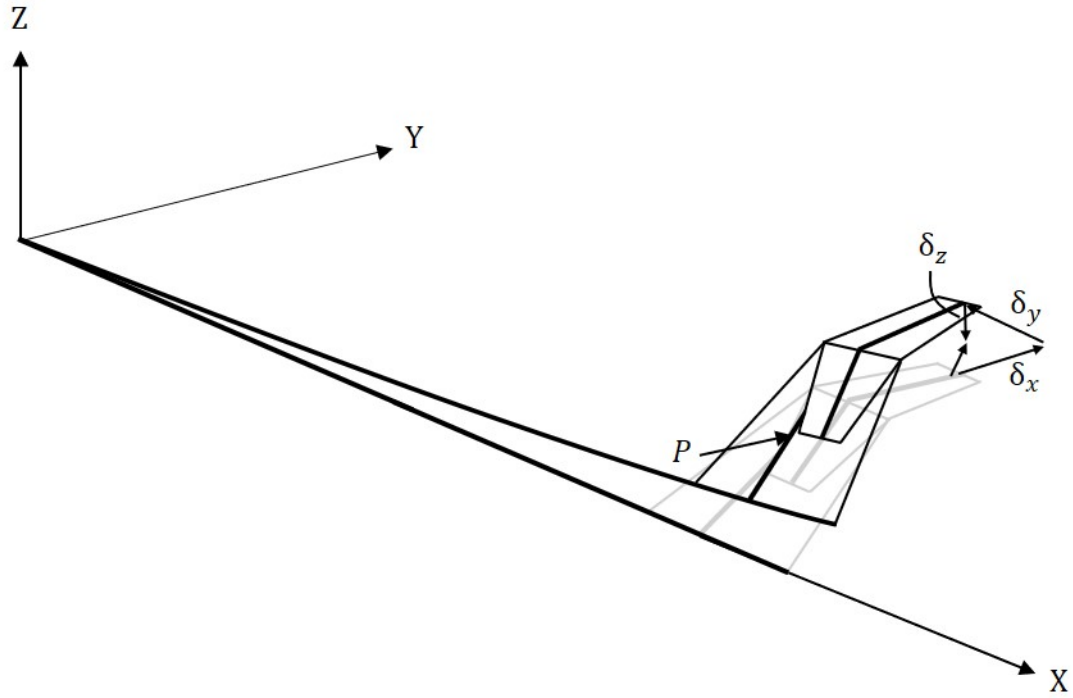
Figure A.22 Horizontal Tail Displacement due to P_y on the Vertical Tail

The displacement in the Y direction due to the rigid rotation about the Z axis is:

$$\delta_y = (cos(\Lambda_{VT} - C_{V_6,V_2}(L_{VT}, \zeta)) - cos(\Lambda_{VT})) y_s \qquad \text{(A.112)}$$

The displacement in the Z direction due to the rigid rotation about the X axis is:

$$\delta_z = C_{V_4,V_2}(L_{VT}, \zeta) y \qquad \text{(A.113)}$$

Since a load applied in the Y direction does not result in a any deformations of the fuselage or VT in the X direction, the displacement of the VT in the X direction is only due to rigid rotation. In other words, the bending influence coefficients in the X direction are:

$$C_{HS_1,VT_2} = \delta_x \qquad \text{(A.114)}$$

The bending influence coefficients in the Y direction are:

$$C_{HS_2,VT_2} = C_{V_2,V_2}(L_{VT},\zeta) + \delta_y \qquad (A.115)$$

and the bending influence coefficients in the Z direction are:

$$C_{HS_3,VT_2} = \delta_z \qquad (A.116)$$

The rotations of the horizontal tail due to a load applied on the vertical tail, are equal to the vertical tail rotational infleunce coefficients, evaluated at the tip of the VT. This means that the horizontal tail rotational influence coefficients about the X axis are:

$$C_{HS_4,VT_2} = C_{V_4,V_2}(L_{VT},\zeta) \qquad (A.117)$$

and the rotational influence coefficients about the Z axis are:

$$C_{HS_6,VT_2} = C_{V_6,V_2}(L_{VT},\zeta) \qquad (A.118)$$

Next, a load applied in the Z direction on the vertical tail is considered. This results in displacement in the X and Z direction due to the fuselage and vertical tail bending. This also results in a displacement in the Z direction due to a rigid rotation of the HT about the Y axis. Figure A.23 shows the displacements of the horizontal tail due to a load applied to the vertical tail in the Z direction. The displacements of the horizontal tail due to a load
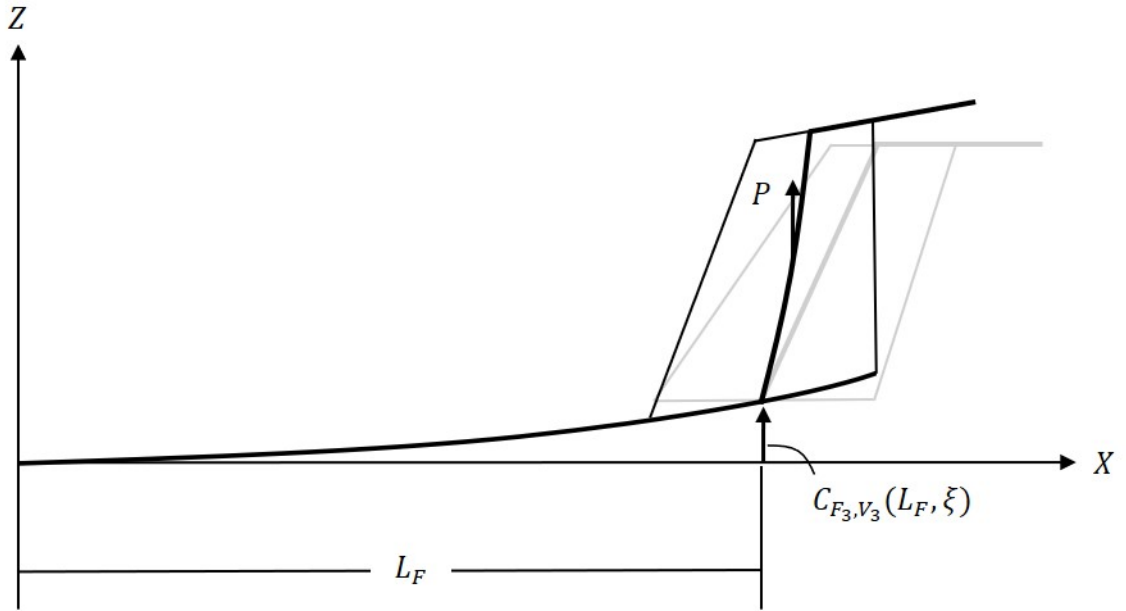
Figure A.23 Horizontal Tail Displacement due to P_z on the Vertical Tail

applied in the Z direction on the vertical tail are equal to the vertical tail bending influence

coefficients, evaluated at the tip,

$$C_{HS_1,VT_3} = C_{V_1,V_3}(L_{VT},\zeta) \tag{A.119}$$

The displacement due to a rigid rotation of the HT about the Y axis is:

$$\delta_z = -C_{V_5,V_3}(L_{VT},\zeta)(x - L_F - L_{VT}tan(\Lambda_{VT})) \tag{A.120}$$

Then, the bending influence coefficients in the Z direction are:

$$C_{HS_3,VT_3} = C_{V_3,V_3}(L_{VT},\zeta) + \delta_z \tag{A.121}$$

and the rotational influence coefficients about the Y axis are:

$$C_{HS_5,VT_3} = C_{V_5,V_3}(L_{VT}, \zeta) \tag{A.122}$$

Now, vertical tail torsion is considered. In other words, a moment about the Z axis on the the vertical tail is considered. Since the horizontal tail is assumed to be swept, small angle approximations cannot be used. Then, the displacement in the X direction due to vertical tail torsion is:

$$\delta_x = -(sin(\Lambda_{HT}) - sin(\Lambda - C_{V_6,V_6}(L_{VT}, \zeta))) y_s \tag{A.123}$$

and the displacement in the y direction in the is:

$$\delta_y = -(cos(\Lambda_{HT}) - cos(\Lambda - C_{V_6,V_6}(L_{VT}, \zeta))) y_s \tag{A.124}$$

Due to the sweep of the vertical tail, torsion about the Z axis results in a rotation about the X axis and thus the displacement of the horizontal tail in the in the Z direction due to vertical tail torsion is:

$$\delta_z = C_{v_4,V_6}(L_{VT}, \zeta) y \tag{A.125}$$

Then, the influence of vertical torsion on horizontal displacement in the X direction is:

$$C_{HS_1,VT_6} = \delta_x \tag{A.126}$$

for horizontal tail displacement in the Y direction:

$$C_{HS_2,VT_6} = C_{V_2,V_6}(L_{VT},\zeta) + \delta_y \qquad (A.127)$$

and horizontal displacement in Z direction,

$$C_{HS_3,VT_6} = \delta_z \qquad (A.128)$$

The rotational influence about the X axis is:

$$C_{HS_4,VT_6} = C_{V_4,V_6}(L_{VT},\zeta) \qquad (A.129)$$

and the rotational influence about the Z axis is:

$$C_{HS_6,VT_6} = C_{V_6,V_6}(L_{VT},\zeta) \qquad (A.130)$$

Next, a load applied in the X direction in on the starboard horizontal tail is considered. The total displacements are the result of a combination of fuselage bending, vertical tail bending, vertical tail torsion, and bending of the horizontal tail. Just as the case with the vertical tail, a swept axis system is defined with its y axis aligned with the elastic axis of the starboard horizontal tail. Figure A.24 shows the swept axis definition of the starboard horizontal tail. Just as the case with the vertical tail, the applied load must be expressed in terms of its normal component and axial component in the swept axis frame. Since the horizontal tail is assumed to be rigid along its swept axis, the axial component of the
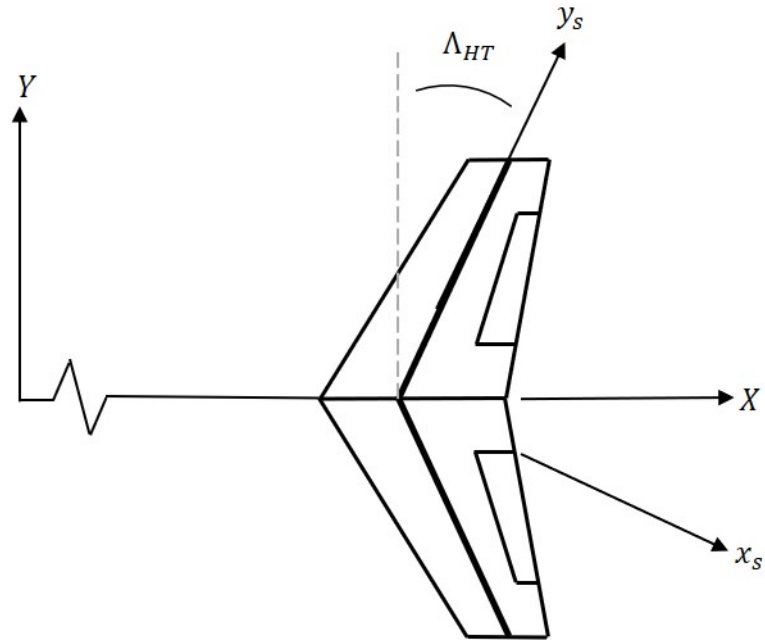
Figure A.24 Horizontal Tail Swept Axis System

applied load has no impact. Figure A.25 shows the load applied to the vertical tail and its

components in the swept axis system. Then, the deflection of the horizontal tail in the x_s
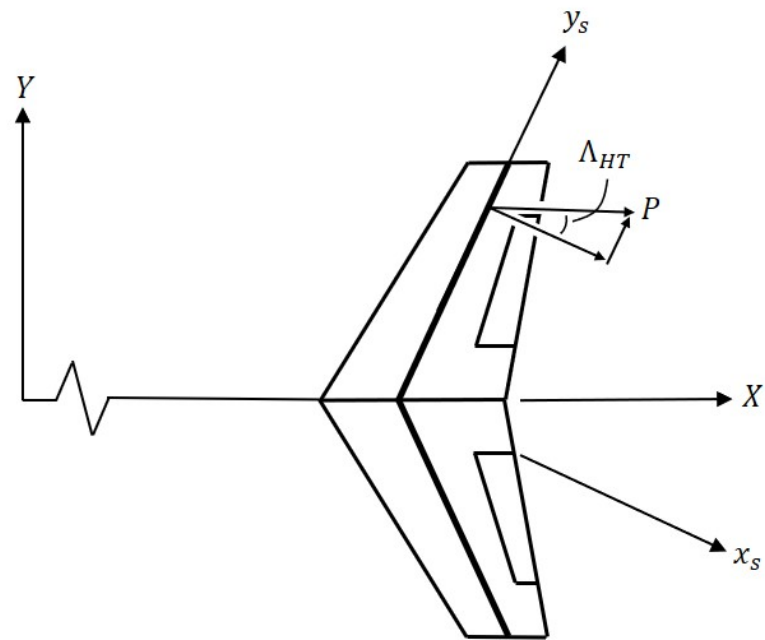
Figure A.25 P_x components in the Horizontal Tail Swept Axis System

direction is:

$$w(y_s, \eta_s) = \frac{cos(\Lambda_{VT})}{EI_{zz}(y_s)} \left(\tfrac{1}{2}\eta_s y_s^2 - \tfrac{1}{6}y_s^3 + C_1 y_s + C_2 \right) \qquad \text{(A.131)}$$

And the slope is:

$$w'(y_s, \eta_s) = \frac{cos(\Lambda_{VT})}{EI_{zz}(y_s)} \left(\tfrac{1}{2}\eta_s x_s - \tfrac{1}{2}y_s^2 + C_1 \right) \qquad \text{(A.132)}$$

Once the displacement in the swept axis system is known it must be transformed back into the global coordinates. Figure A.26 shows the X and Y components of the displacement in the x_s direction. Then the total displacement of a point on the starboard horizontal tail is
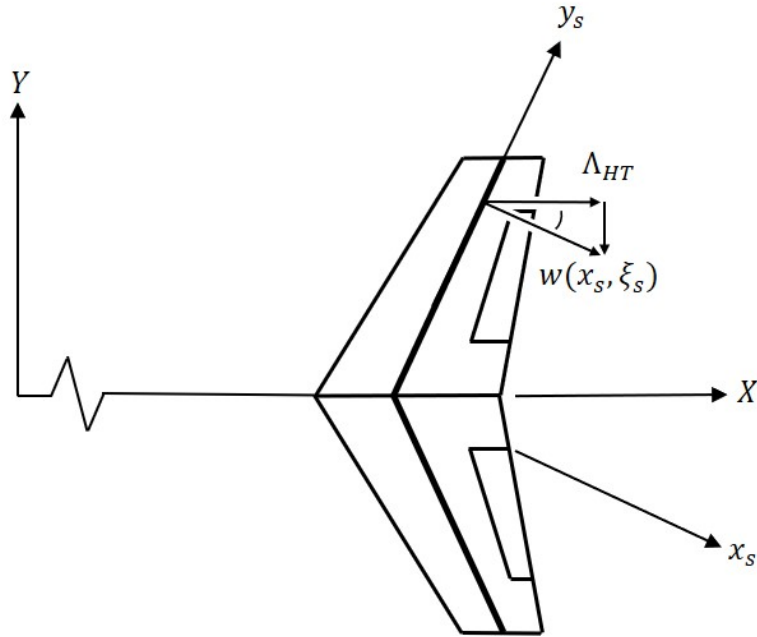
Figure A.26 Horizontal Tail Displacements due to P_x in Global Coordinates

the combination of vertical tail bending, rigid rotation of the HT due to vertical tail torsion, and bending of the horizontal tail structure. The displacement in X direction due to rigid rotation is:

$$\delta_x = -(sin(\Lambda_{VT} - C_{V_6,HS_1}(L_{VT}, \xi)) - sin(\Lambda_{VT})) y_s \qquad \text{(A.133)}$$

and the displacement in the Y direction due to rigid rotation is:

$$\delta_y = (cos(\Lambda_{VT} - C_{V_6,HS_1}(L_{VT},\xi)) - cos(\Lambda_{VT})) \, y_s \tag{A.134}$$

Then the total displacement in the X direction is:

$$C_{HS_1,HS_1} = C_{V_1,HS_1}(L_{VT},\xi) + \delta_x + w(x_s,\xi_s) \, cos(\Lambda_{VT}) \tag{A.135}$$

and the displacement in the Y direction is:

$$C_{HS_2,HS_1} = C_{V_2,HS_1}(L_{VT},\xi) + \delta_y - w(x_s,\xi_s) \, sin(\Lambda_{VT}) \tag{A.136}$$

Then, the displacement in the Z direction is due to the vertical tail bending under load. Thus, the bending influence coefficients are given by:

$$C_{HS_3,HS_1} = C_{V_3,HS_1}(L_{VT},\xi) + C_{V_4,HS_1}(L_{VT},\xi) \, y$$
$$- C_{V_5,HS_1}(L_{VT},\xi)(x - L_{VT}tan(\Lambda_{VT}) - L_f) \tag{A.137}$$

Since the bending only occurs in the $x_s - y_s$ plane which is parallel to the $X - Y$ plane, the rotations about the X axis are:

$$C_{HS_4,HS_1} = C_{V_4,HS_1}(L_{VT},\xi) \tag{A.138}$$

the rotations about the Y axis are:

$$C_{HS_5,HS_1} = C_{V_5,HS_1}(L_{VT},\xi) \qquad (A.139)$$

and the rotations about the Z axis are:

$$C_{HS_6,HS_1} = C_{V_6,HS_1}(L_{VT},\xi) - w'(x_s,\xi_s) \qquad (A.140)$$

Next a load in the Y direction on the starboard horizontal tail is considered. Figure A.27 shows the applied load to the vertical tail and its components in the swept axis system. Using Equation (4.36), the displacement in the x_s direction due to a load applied
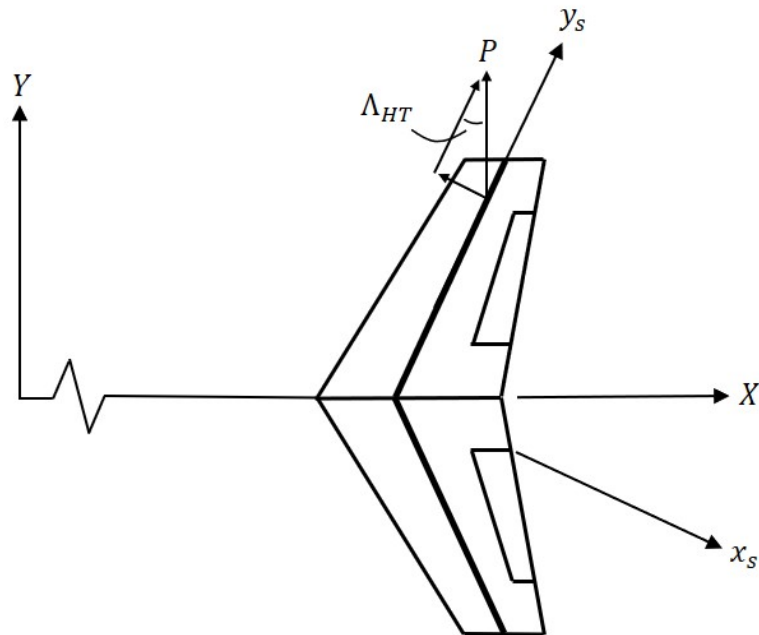
Figure A.27 P_y components in the Horizontal Tail Swept Axis System

in the Y direction is:

$$w(y_s, \eta_s) = -\frac{sin(\Lambda_{VT})}{EI_{zz}(y_s)} \left(\tfrac{1}{2}\eta_s y_s^2 - \tfrac{1}{6}y_s^3 + C_1 y_s + C_2 \right) \qquad \text{(A.141)}$$

and using Equation (4.40), the slope is:

$$w'(y_s, \eta_s) = \frac{sin(\Lambda_{VT})}{EI_{zz}(y_s)} \left(\tfrac{1}{2}\eta_s x_s - \tfrac{1}{2}y_s^2 + C_1 \right) \qquad \text{(A.142)}$$

Once the displacement in the x_s direction is determined it must be transformed back into the global coordinate frame. Figure A.28 shows the X and Y components of the displacement in the x_s direction. The total displacement in the Y direction is due to
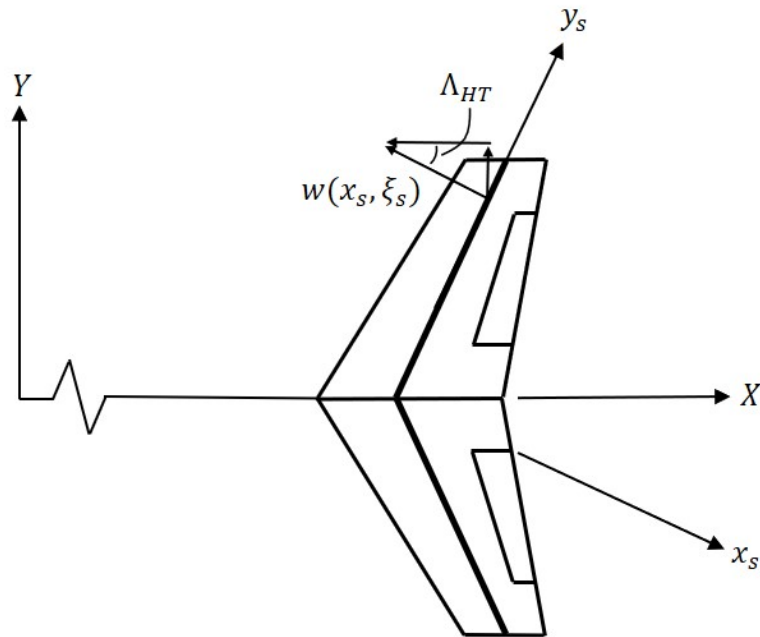
Figure A.28 Horizontal Tail Displacements due to P_y in Global Coordinates

fuselage bending, fuselage torsion, vertical tail bending, vertical tail torsion, rotation of the

vertical tail spring fitting, and bending of the horizontal tail structure. The displacement in the Y direction due to rigid rotation of the HT about the Z axis is:

$$\delta_x = (sin(\Lambda_{VT} - C_{V_6,HS_2}(L_{VT},\xi)) - sin(\Lambda_{VT}))\, y_s \tag{A.143}$$

and the displacement in the Y direction is:

$$\delta_y = (cos(\Lambda_{VT} - C_{V_6,HS_2}(L_{VT},\xi)) - cos(\Lambda_{VT}))\, y_s \tag{A.144}$$

The total displacement in the X direction is:

$$C_{HS_1,HS_2} = \delta_y + w(x_s,\xi_s)\, cos(\Lambda_{VT}) \tag{A.145}$$

The total displacement in the Y direction is:

$$C_{HS_2,HS_2} = C_{V_2,HS_2}(L_{VT},\xi) + delta_y - w(x_s,\xi_s)\, sin(\Lambda_{VT}) \tag{A.146}$$

The total displacement in the Z direction is:

$$C_{HS_3,HS_2} = C_{V_4,HS_2}(L_{VT},\xi)\, y \tag{A.147}$$

$$C_{HS_4,HS_2} = C_{V_4,HS_2}(L_{VT},\xi) \tag{A.148}$$

$$C_{HS_6,HS_2} = C_{V_6,HS_2}(L_{VT},\xi) + w'(x_s,\xi_s) \tag{A.149}$$

Next, a load applied in the Z direction on the starboard horizontal tail is considered. For a load in the Z direction the spring fitting of the horizontal tail must be considered. Using Equation (4.36), the displacement in the Z direction due to a load applied in the Z direction is:

$$w(y_s,\eta_s) = \frac{1}{EI_{xx}(y_s)}\left(\tfrac{1}{2}\eta_s y_s^2 - \tfrac{1}{6}y_s^3 + C_1 y_s + C_2\right) \tag{A.150}$$

and using Equation (4.40), the slope is:

$$w'(y_s,\eta_s) = \frac{1}{EI_{xx}(y_s)}\left(\tfrac{1}{2}\eta_s y_s - \tfrac{1}{2}y_s^2 + C_1\right) \tag{A.151}$$

Figure A.29 shows the rotation of the horizontal tail due to the spring fitting when a load is applied in the Z direction. The rotation of the spring fitting due to a load applied in the Z direction on the starboard HT is determined by taking a moment balance about the axis of rotation, Thus the rotation of the spring fitting is given by:

$$\theta_{HT_s}(\eta) = \frac{\eta}{K_{\theta_{HT}}} \tag{A.152}$$

and the displacement of a point on the horizontal tail in the Z direction due to the rotation is:

$$\delta_{HT_s}(y,\eta) = \frac{\eta\, y}{K_{\theta_{HT}}} \tag{A.153}$$
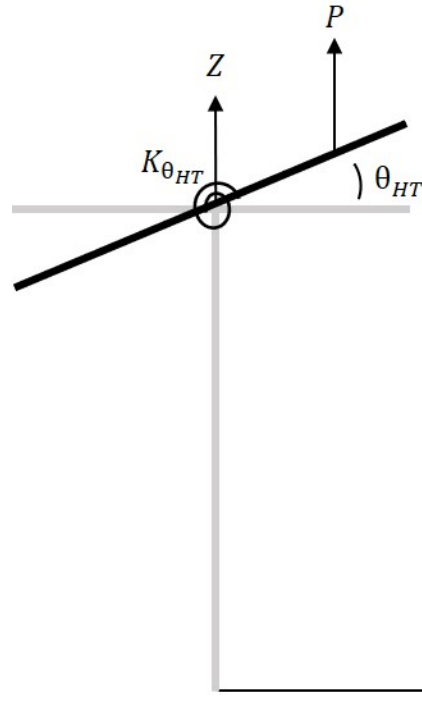
Figure A.29 Horizontal Tail Spring Fitting Rotation Due to P_z

where η is the distance in the Y direction where the load is applied and y is the location of the point being measured. The displacement in the X direction,

$$\delta_x = (sin(\Lambda_{VT} - C_{V_6,HS_2}(L_{VT},\xi)) - sin(\Lambda_{VT})) \, y_s \qquad \text{(A.154)}$$

and the displacement in the Y direction is:

$$\delta_y = (cos(\Lambda_{VT} - C_{V_6,HS_2}(L_{VT},\xi)) - cos(\Lambda_{VT})) \, y_s \qquad \text{(A.155)}$$

The total displacement in the X direction is given by:

$$C_{HS_1,HS_3} = C_{V_1,HS_3}(L_{VT},\xi) + \delta_x \qquad \text{(A.156)}$$

the total displacement in the Y direction is given by:

$$C_{HS_2,HS_3} = C_{V_2,HS_3}(L_{VT},\xi) + \delta_y \tag{A.157}$$

and the total displacement in the Z direction is given by:

$$C_{HS_3,HS_3} = C_{V_3,HS_3}(L_{VT},\xi) + C_{V_4,HS_3}(L_{VT},\xi)\,y$$

$$- C_{V_5,HS_3}(L_{VT},\xi)(x - L_x - L_{VT}tan(\Lambda_{VT})) + w() + \delta_{HT_s} \tag{A.158}$$

Then, the rotation about the X axis due to the combination of bending of the vertical tail, the slope of the HT due to bending, and rotation of the spring fitting. The rotational influence coefficients about the X are given by:

$$C_{HS_4,HS_3} = C_{V_4,HS_3}(L_{VT},\xi) + w'(y_s,\eta_s)\cos(\Lambda_{HT}) + \theta_{HT_s} \tag{A.159}$$

The rotation about the Y axis is:

$$C_{HS_5,HS_3} = C_{V_5,HS_3}(L_{VT},\xi) - w'(y_s,\eta_s)\sin(\Lambda_{HT}) \tag{A.160}$$

and the rotation about the Z axis is:

$$C_{HS_6,HS_3} = C_{V_6,HS_3}(L_{VT},\xi) \tag{A.161}$$

APPENDIX B - Unsteady Aerodynamic Coefficients

Theodorsen Funtions

The T-Functions, as defined by Theodorsen in NACA TR-736:

$$T_1 = -\tfrac{1}{3}\left(2+c^2\right)\sqrt{1-c^2}+c\,cos^{-1}c \tag{B.1}$$

$$T_2 = c\left(1-c^2\right)-\left(1+c^2\right)\sqrt{1-c^2}\,cos^{-1}c+c\left(cos^{-1}c\right)^2 \tag{B.2}$$

$$T_3 = -\tfrac{1}{8}\left(1-c^2\right)\left(5c^2+4\right)+\tfrac{1}{4}c\left(7+2c^2\right)\sqrt{1-c^2}\,cos^{-1}c-\left(\tfrac{1}{8}+c^2\right)\left(cos^{-1}c\right)^2 \tag{B.3}$$

$$T_4 = c\sqrt{1-c^2}-cos^{-1}c \tag{B.4}$$

$$T_5 = -\left(1-c^2\right)+2c\sqrt{1-c^2}\,cos^{-1}c-\left(cos^{-1}c\right)^2 \tag{B.5}$$

$$T_6 = T_2 \tag{B.6}$$

$$T_7 = -\tfrac{1}{8}c\left(7+2c^2\right)\sqrt{1-c^2}-\left(\tfrac{1}{8}+c^2\right)cos^{-1}c \tag{B.7}$$

$$T_8 = -\tfrac{1}{3}\left(1+2c^2\right)\sqrt{1-c^2}+c\,cos^{-1}c \tag{B.8}$$

$$T_9 = \tfrac{1}{2}\left[\tfrac{1}{3}\left(1-c^2\right)^{3/2}+aT_4\right] \tag{B.9}$$

$$T_{10} = \sqrt{1-c^2}+cos^{-1}c \tag{B.10}$$

$$T_{11} = (2-c)\sqrt{1-c^2}+(1-2c)\,cos^{-1}c \tag{B.11}$$

$$T_{12} = (2+c)\sqrt{1-c^2}-(1+2c)\,cos^{-1}c \tag{B.12}$$

$$T_{13} = -\tfrac{1}{2}\left[T_7+(c-a)T_1\right] \tag{B.13}$$

$$T_{14} = \tfrac{1}{16} + \tfrac{1}{2}ac \tag{B.14}$$

Küssner Functions

The Küssner functions as defined in NACA TM-991:

$$\Phi_1(\varphi) = \pi - \varphi + sin\varphi \tag{B.15}$$

$$\Phi_2(\varphi) = (\pi - \varphi)(1 + 2\,cos\varphi) + sin\varphi\,(2 + cos\varphi) \tag{B.16}$$

$$\Phi_3(\varphi) = \pi - \varphi + sin\varphi\,cos\varphi \tag{B.17}$$

$$\Phi_4(\varphi) = (\pi - \varphi)\cdot 2\,cos\varphi + sin\varphi \cdot \tfrac{2}{3}\left(2 + cos^2\varphi\right) \tag{B.18}$$

$$\Phi_5(\varphi) = sin\varphi\,(1 - cos\varphi) \tag{B.19}$$

$$\Phi_6(\varphi) = 2(\pi - \varphi) + sin\varphi \cdot \tfrac{2}{3}(2 - cos\varphi)(1 + 2\,cos\varphi) \tag{B.20}$$

$$\Phi_7(\varphi) = (\pi - \varphi)\left(\tfrac{1}{2} + 2\,cos\varphi\right) + sin\varphi \cdot \tfrac{1}{6}\left(8 + 5\,cos\varphi + 4\,cos^2\varphi - 2\,cos^3\varphi\right) \tag{B.21}$$

$$\Phi_8(\varphi) = (\pi - \varphi)(-1 + 2\,cos\varphi) + sin\varphi\,(2 - cos\varphi) \tag{B.22}$$

$$\Phi_9(\varphi) = (\pi - \varphi)(1 + 2\,cos\varphi) + sin\varphi \cdot \tfrac{1}{3}\left(2 + 3\,cos\varphi + 4\,cos^2\varphi\right) \tag{B.23}$$

$$\Phi_{10}(\varphi) = \Phi_{31}(\varphi) \cdot \Phi_5(\varphi) \tag{B.24}$$

$$\Phi_{11}(\varphi) = \Phi_2(\varphi) \cdot \Phi_3(\varphi) \tag{B.25}$$

$$\Phi_{12}(\varphi) = (\pi - \varphi)^2 \left(\tfrac{1}{2} + 4\cos^2\varphi\right) + (\pi - \varphi)\sin\varphi\cos\varphi \cdot \left(7 + 2\cos^2\varphi\right)$$

$$+ \sin^2\varphi \left(2 + \tfrac{5}{2}\cos^2\varphi\right) \quad \text{(B.26)}$$

$$\Phi_{13}(\varphi) = \tan\left(\tfrac{\varphi}{2}\right) \tag{B.27}$$

$$\Phi_{14}(\varphi) = 2\sin\varphi \tag{B.28}$$

$$\Phi_{15}(\varphi) = \Phi_{13}(\varphi) - \Phi_{14}(\varphi) \tag{B.29}$$

$$\Phi_{16}(\varphi) = 2\,\Phi_1(\varphi) \cdot \sin\varphi \tag{B.30}$$

$$\Phi_{17}(\varphi) = [\Phi_3(\varphi)]^2 + \sin^4\varphi \tag{B.31}$$

$$\Phi_{18}(\varphi) = -\Phi_{13}(\varphi) \cdot [(\pi - \varphi)(1 + 2\cos\varphi) - \sin\varphi \cdot \cos\varphi] \tag{B.32}$$

$$\Phi_{19}(\varphi) = \Phi_3(\varphi) \cdot \sin\varphi \tag{B.33}$$

$$\Phi_{20}(\varphi) = \sin\varphi\,(1 + \cos\varphi) \tag{B.34}$$

$$\Phi_{21}(\varphi) = -2\left(\cos\varphi + \ln\sin^2\varphi\right) \tag{B.35}$$

$$\Phi_{31}(\varphi) = (\pi - \varphi) - \sin\varphi \tag{B.36}$$

$$\Phi_{32}(\varphi) = (\pi - \varphi) + \sin\varphi\,(1 + 2\cos\varphi) \tag{B.37}$$

$$\Phi_{35}(\varphi) = 2\sin^2\varphi \tag{B.38}$$

$$\Phi_{36}(\varphi) = \Phi_{32}(\varphi) \cdot \Phi_3(\varphi) + 2\sin^4\varphi \tag{B.39}$$

$$\Phi_{37}(\varphi) = \Phi_3(\varphi) \cdot [\Phi_2(\varphi) - \Phi_3(\varphi)] \tag{B.40}$$

Scanalan and Resonbaum discuss how the Küssner functions can be re-written in terms of the variable c by mapping the airfoil onto the unit circle and applying the following substitutions (Scanlan & Rosenbaum, 1968): $x = -cos\theta$ defines any point on the airfoil

$c = -cos\varphi$ is the leading edge of the flap

$\theta = 0$ is the leading edge of the wing section

$\theta = \pi$ is the trailing edge of the wing or flap

After applying the above substitutions and simplifying, the Küssner functions become

$$\Phi_1 = \sqrt{1-c^2} + cos^{-1}c = T_{10} \tag{B.41}$$

$$\Phi_2 = (2-c)\sqrt{1-c^2} + (1-2c)\,cos^{-1}c = T_{11} \tag{B.42}$$

$$\Phi_3 = -c\,\sqrt{1-c^2} + cos^{-1}c = -T_4 \tag{B.43}$$

$$\Phi_4 = \tfrac{2}{3}\left(2+c^2\right)\sqrt{1-c^2} - 2c\,cos^{-1}c = -2T_1 \tag{B.44}$$

$$\Phi_5 = (1+c)\sqrt{1-c^2} = T_4 + T_{10} \tag{B.45}$$

$$\Phi_6 = \tfrac{2}{3}(2+c)(1-2c)\sqrt{1-c^2} + 2\,cos^{-1}c \tag{B.46}$$

$$\Phi_7 = \tfrac{1}{6}\left(8 - 10c + 4c^2 + 2c^3\right)\sqrt{1-c^2} + \left(\tfrac{1}{2} - 2c\right)cos^{-1}c = 8T_{13} \tag{B.47}$$

$$\Phi_8 = (2+c)\sqrt{1-c^2} - (1+2c)\,cos^{-1}c = T_{12} \tag{B.48}$$

$$\Phi_9 = \tfrac{1}{3}\left(2 - 3c + 4c^2\right)\sqrt{1-c^2} + (1-2c)\,cos^{-1}c = -2\left[2T_9 + T_1 - \left(a - \tfrac{1}{2}\right)T_4\right] \tag{B.49}$$

$$\Phi_{10} = \Phi_{31} \cdot \Phi_5 = \left(-\sqrt{1-c^2} + \cos^{-1}c\right)(1+c)\sqrt{1-c^2} \tag{B.50}$$

$$\Phi_{11} = \Phi_2 \cdot \Phi_3 = -T_4 T_{11} = \left[(2-c)\sqrt{1-c^2} + (1-2c)\cos^{-1}c\right]\left[-c\sqrt{1-c^2} + \cos^{-1}c\right] \tag{B.51}$$

$$\Phi_{12} = -4\left\{-\tfrac{1}{8}\left(1-c^2\right)\left(5c^2+4\right) + \tfrac{1}{4}c\left(7+2c^2\right)\sqrt{1-c^2}\,\cos^{-1}c\right.$$
$$\left.-\left(\tfrac{1}{8}+c^2\right)\left(\cos^{-1}c\right)^2 = -4T_3 \right. \tag{B.52}$$

$$\Phi_{13} = \frac{\sqrt{1-c^2}}{1-c} \tag{B.53}$$

$$\Phi_{14} = 2\sqrt{1-c^2} \tag{B.54}$$

$$\Phi_{15} = \Phi_{13} - \Phi_{14} = \frac{2c-1}{1-c}\sqrt{1-c^2} \tag{B.55}$$

$$\Phi_{16} = 2\left(1-c^2\right) + 2\sqrt{1-c^2}\cos^{-1}c \tag{B.56}$$

$$\Phi_{17} = [\Phi_3]^2 + \left(1-c^2\right)^2 = \left[-c\sqrt{1-c^2} + \cos^{-1}c\right]^2 + \left(1-c^2\right)^2 \tag{B.57}$$

$$\Phi_{18} = \frac{\sqrt{1-c^2}}{1-c}\left[c\sqrt{1-c^2} + (1-2c)\cos^{-1}c\right] \tag{B.58}$$

$$\Phi_{19} = \left[-c\sqrt{1-c^2} + \cos^{-1}c\right]\sqrt{1-c^2} \tag{B.59}$$

$$\Phi_{20} = (1-c)\sqrt{1-c^2} \tag{B.60}$$

$$\Phi_{21} = 2\left[c - \ln\left(1-c^2\right)\right] \tag{B.61}$$

$$\Phi_{31} = -\sqrt{1-c^2} + \cos^{-1}c \tag{B.62}$$

$$\Phi_{32} = (1-2c)\sqrt{1-c^2} + \cos^{-1}c \tag{B.63}$$

$$\Phi_{35} = 2\left(1 - c^2\right) \tag{B.64}$$

$$\Phi_{36} = \Phi_{32} \cdot \Phi_3 + 2\left(1 - c^2\right)^2 = \left[(1 - 2c)\sqrt{1 - c^2} + \cos^{-1}c\right]\left[-c\sqrt{1 - c^2} + \cos^{-1}c\right]$$
$$+ 2\left(1 - c^2\right)^2 \tag{B.65}$$

$$\Phi_{37} = \Phi_3 \cdot [\Phi_2 - \Phi_3] = 2\left(-c\sqrt{1 - c^2} + \cos^{-1}c\right)\left(\sqrt{1 - c^2} - c\cos^{-1}c\right) \tag{B.66}$$

Incompressible Aerodynamic Complex Coefficients

Complex coefficients for two-dimensional incompressible unsteady aerodynamic loads

$$L_h = 1 - 2i\left(\frac{U}{b\omega}\right)(F + iG) \tag{B.67}$$

$$L_\alpha = \frac{1}{2} - i\left(\frac{U}{b\omega}\right)[1 + 2(F + iG)] - 2\left(\frac{U}{b\omega}\right)^2(F + iG) \tag{B.68}$$

$$L_\beta = -\frac{T_1}{\pi} + i\left(\frac{U}{b\omega}\right)\left(\frac{T_4}{\pi}\right) - i\left(\frac{U}{b\omega}\right)\frac{T_{11}}{\pi}(F + iG) - 2\left(\frac{U}{b\omega}\right)^2\frac{T_{10}}{\pi}(F + iG) \tag{B.69}$$

$$L_z = -2i\left(\frac{U}{b\omega}\right)\frac{\Phi_1}{\pi}(F + iG) + \frac{\Phi_3}{\pi} \tag{B.70}$$

$$M_h = \frac{1}{2} \tag{B.71}$$

$$M_\alpha = \frac{3}{8} - i\left(\frac{U}{b\omega}\right) \tag{B.72}$$

$$M_\beta = -\frac{T_1}{\pi} - \left(e + \frac{1}{2}\right)\frac{T_1}{\pi} + i\left(\frac{U}{b\omega}\right)\left(\frac{-\frac{2}{3}\left(1 - c^2\right)^{3/2} + T_4}{\pi}\right) - \left(\frac{U}{b\omega}\right)^2\left(\frac{T_4 + T_{10}}{\pi}\right) \tag{B.73}$$

$$M_z = -i\left(\frac{U}{b\omega}\right)\frac{\Phi_5}{\pi} + \frac{1}{4}\frac{\Phi_6}{\pi} \tag{B.74}$$

$$T_h = -\frac{T_1}{\pi} - i\left(\frac{U}{b\omega}\right)\frac{T_{12}}{\pi}(F+iG) \tag{B.75}$$

$$T_\alpha = -\frac{1}{\pi}\left[T_7 + \left(e+\frac{1}{2}\right)T_1\right] - i\left(\frac{U}{b\omega}\right)\left(\frac{-\frac{2}{3}(1-c^2)^{3/2} - 2T_1 - T_4}{2\pi}\right) - i\left(\frac{U}{b\omega}\right)\frac{T_{12}}{\pi}(F+iG)$$

$$-\left(\frac{U}{b\omega}\right)^2 \frac{T_{12}}{\pi}(F+iG) \tag{B.76}$$

$$T_\beta = -\left(\frac{T_3}{\pi^2}\right) + i\left(\frac{U}{b\omega}\right)\frac{T_4 T_{11}}{2\pi^2} - i\left(\frac{U}{b\omega}\right)\left(\frac{T_{11}T_{12}}{2\pi^2}\right)(F+ig) - \left(\frac{U}{b\omega}\right)^2\left(\frac{T_5 - T_4 T_{10}}{\pi^2}\right)$$

$$-\left(\frac{U}{b\omega}\right)^2 \frac{T_{10}T_{12}}{\pi^2}(F+ig) \tag{B.77}$$

$$T_z = -i\left(\frac{U}{b\omega}\right)\frac{\Phi_1\Phi_8}{\pi^2}(F+ig) - i\left(\frac{U}{b\omega}\right)\left(\frac{\Phi_{10}}{\pi^2}\right) + \frac{1}{2}\left(\frac{\Phi_{37}}{\pi^2}\right) \tag{B.78}$$

$$P_h = -2i\left(\frac{U}{b\omega}\right)\frac{\Phi_{31}}{\pi}(F+iG) + \frac{\Phi_3}{\pi} \tag{B.79}$$

$$P_\alpha = -2\left[\left(\frac{U}{b\omega}\right)^2 + i\left(\frac{U}{b\omega}\right)\right]\frac{\Phi_{31}}{\pi}(F+iG) - i\left(\frac{U}{b\omega}\right)\frac{\Phi_{32}}{\pi} + \frac{1}{4}\frac{\Phi_6}{\pi} \tag{B.80}$$

$$P_\beta = -\frac{2}{\pi}\left[\left(\frac{U}{b\omega}\right)^2\Phi_1 + \frac{1}{2}i\left(\frac{U}{b\omega}\right)\Phi_2\right]\frac{\Phi_{31}}{\pi}(F+iG) - \left(\frac{U}{b\omega}\right)^2\frac{\Phi_{35}}{\pi^2}$$

$$-i\left(\frac{U}{b\omega}\right)\left(\frac{\Phi_{36}}{\pi^2}\right) + \frac{1}{2}\frac{\Phi_{37}}{\pi^2} \tag{B.81}$$

$$P_z = -2i\left(\frac{U}{b\omega}\right)\frac{\Phi_1\Phi_{31}}{\pi^2}(F+iG) - i\left(\frac{U}{b\omega}\right)\frac{\Phi_{35}}{\pi^2} + \frac{\Phi_{17}}{\pi^2} \tag{B.82}$$

Incompressible Flow Force Coefficients

Define k_r as the reference reduced frequency which is the reduced frequency at $\frac{3}{4}b$ and b_r is the semichord at $\frac{3}{4}b$.

$$L_h = K_1(L_h) + \left(\frac{b_r}{b}\right) K_2(L_h) \tag{B.83}$$

$$K_1(L_h) = 1 \tag{B.84}$$

$$K_2(L_h) = -2i\left(\frac{U}{b_r\omega}\right) C(k_r) \tag{B.85}$$

$$L_\alpha = K_1(L_\alpha) + \left(\frac{b_r}{b}\right) K_2(L_\alpha) + \left(\frac{b_r}{b}\right)^2 K_3(L_\alpha) \tag{B.86}$$

$$K_1(L_\alpha) = \frac{1}{2} \tag{B.87}$$

$$K_2(L_\alpha) = -i\left(\frac{U}{b_r\omega}\right)[1 + 2C(k_r)] \tag{B.88}$$

$$K_3(L_\alpha) = -2\left(\frac{U}{b_r\omega}\right)^2 C(k_r) \tag{B.89}$$

$$L_\beta = K_1(L_\beta) + \left(\frac{b_r}{b}\right) K_2(L_\beta) + \left(\frac{b_r}{b}\right)^2 K_3(L_\beta) \tag{B.90}$$

$$K_1(L_\beta) = -\frac{T_1}{\pi} \tag{B.91}$$

$$K_2(L_\beta) = i\left(\frac{U}{b_r\omega}\right)\left(\frac{T_4}{\pi}\right) - i\left(\frac{U}{b_r\omega}\right)\frac{T_{11}}{\pi} C(k_r) \tag{B.92}$$

$$K_3(L_\beta) = -2i \left(\frac{U}{b_r \omega}\right)^2 \frac{T_{10}}{\pi} C(k_r) \tag{B.93}$$

$$L_z = K_1(L_z) + \left(\frac{b_r}{b}\right) K_2(L_z) \tag{B.94}$$

$$K_1(L_z) = \frac{\Phi_3}{\pi} \tag{B.95}$$

$$K_2(L_z) = -2i \left(\frac{U}{b_r \omega}\right) \frac{\Phi_1}{\pi} C(k_r) \tag{B.96}$$

$$M_h = K_1(M_h) \tag{B.97}$$

$$K_1(M_h) = \frac{1}{2} \tag{B.98}$$

$$M_\alpha = K_1(M_\alpha) + \left(\frac{b_r}{b}\right) K_2(M_\alpha) \tag{B.99}$$

$$K_1(M_\alpha) = \frac{3}{8} \tag{B.100}$$

$$K_2(M_\alpha) = -i \left(\frac{U}{b_r \omega}\right) \tag{B.101}$$

$$M_\beta = K_1(M_\beta) + \left(\frac{b_r}{b}\right) K_2(M_\beta) + \left(\frac{b_r}{b}\right)^2 K_3(M_\beta) \tag{B.102}$$

$$K_1(M_\beta) = -\frac{T_1}{\pi} - \left(e + \frac{1}{2}\right) \frac{T_1}{\pi} \tag{B.103}$$

$$K_2(M_\beta) = i\left(\frac{U}{b_r\omega}\right)\left(\frac{-\frac{2}{3}\left(1-c^2\right)^{3/2}+T_4}{\pi}\right) \tag{B.104}$$

$$K_3(M_\beta) = -\left(\frac{U}{b_r\omega}\right)^2\left(\frac{T_4+T_{10}}{\pi}\right) \tag{B.105}$$

$$M_z = K_1(M_z) + \left(\frac{b_r}{b}\right)K_2(M_z) \tag{B.106}$$

$$K_1(M_z) = \frac{1}{2}\frac{\Phi_6}{\pi} \tag{B.107}$$

$$K_2(M_z) = -i\left(\frac{U}{b_r\omega}\right)\frac{T_{12}}{\pi}C(k_r) \tag{B.108}$$

$$T_h = K_1(T_h) + \left(\frac{b_r}{b}\right)K_2(T_h) \tag{B.109}$$

$$K_1(T_h) = -\frac{T_1}{\pi} \tag{B.110}$$

$$K_2(T_h) = -i\left(\frac{U}{b_r\omega}\right)\frac{T_{12}}{\pi}C(k_r) \tag{B.111}$$

$$T_\alpha = K_1(T_\alpha) + \left(\frac{b_r}{b}\right)K_2(T_\alpha) + \left(\frac{b_r}{b}\right)^2 K_3(T_\alpha) \tag{B.112}$$

$$K_1(T_\alpha) = -\frac{1}{\pi}\left[T_7 + \left(e+\frac{1}{2}\right)T_1\right] \tag{B.113}$$

$$K_2(T_\alpha) = -i\left(\frac{U}{b_r\omega}\right)\left(\frac{-\frac{2}{3}\left(1-c^2\right)^{3/2}-2T_1-T_4}{2\pi}\right) - i\left(\frac{U}{b_r\omega}\right)\frac{T_{12}}{\pi}C(k_r) \tag{B.114}$$

$$K_3(T_\alpha) = -\left(\frac{U}{b_r\omega}\right)^2 \frac{T_{12}}{\pi} C(k_r) \tag{B.115}$$

$$T_\beta = K_1(T_\beta) + \left(\frac{b_r}{b}\right) K_2(T_\beta) + \left(\frac{b_r}{b}\right)^2 K_3(T_\beta) \tag{B.116}$$

$$K_1(T_\beta) = -\left(\frac{T_3}{\pi^2}\right) \tag{B.117}$$

$$K_2(T_\beta) = i\left(\frac{U}{b_r\omega}\right)\frac{T_4 T_{11}}{2\pi^2} - i\left(\frac{U}{b_r\omega}\right)\left(\frac{T_{11}T_{12}}{2\pi^2}\right)C(k_r) \tag{B.118}$$

$$K_3(T_\beta) = \left(\frac{U}{b_r\omega}\right)^2\left(\frac{T_5 - T_4 T_{10}}{\pi^2}\right) - i\left(\frac{U}{b_r\omega}\right)^2 \frac{T_{10}T_{12}}{\pi^2} C(k_r) \tag{B.119}$$

$$T_z = K_1(T_z) + \left(\frac{b_r}{b}\right) K_2(T_z) \tag{B.120}$$

$$K_1(T_z) = \frac{1}{2}\left(\frac{\Phi_{37}}{\pi^2}\right) \tag{B.121}$$

$$K_2(T_z) = -i\left(\frac{U}{b_r\omega}\right)\frac{\Phi_1\Phi_8}{\pi^2}C(k_r) - i\left(\frac{U}{b_r\omega}\right)\left(\frac{\Phi_{10}}{\pi^2}\right) \tag{B.122}$$

$$P_h = K_1(P_h) + \left(\frac{b_r}{b}\right) K_2(P_h) \tag{B.123}$$

$$K_1(P_h) = \frac{\Phi_3}{\pi} \tag{B.124}$$

$$K_2(P_h) = -2i\left(\frac{U}{b_r\omega}\right)\frac{\Phi_{31}}{\pi}C(k_r) \tag{B.125}$$

$$P_\alpha = K_1(P_\alpha) + \left(\frac{b_r}{b}\right) K_2(P_\alpha) + \left(\frac{b_r}{b}\right)^2 K_3(P_\alpha) \tag{B.126}$$

$$K_1(P_\alpha) = \frac{1}{4}\frac{\Phi_6}{\pi} \tag{B.127}$$

$$K_2(P_\alpha) = -2i\left(\frac{U}{br}\omega\right)\frac{\Phi_{31}}{\pi}C(k_r) - i\left(\frac{U}{b_r\omega}\right)\frac{\Phi_{32}}{\pi} \tag{B.128}$$

$$K_3(P_\alpha) = -2\left(\frac{U}{b_r]\omega}\right)^2 \frac{\Phi_{31}}{\pi}C(k_r) \tag{B.129}$$

$$P_\beta = K_1(P_\beta) + \left(\frac{b_r}{b}\right) K_2(P_\beta) + \left(\frac{b_r}{b}\right)^2 K_3(P_\beta) \tag{B.130}$$

$$K_1(P_\beta) = \frac{1}{2}\frac{\Phi_{37}}{\pi^2} \tag{B.131}$$

$$K_2(P_\beta) = -\frac{1}{\pi}i\left(\frac{U}{b_r\omega}\right)\frac{\Phi_2\Phi_{31}}{\pi}C(k_r) - i\left(\frac{U}{b_r\omega}\right)\left(\frac{\Phi_{36}}{\pi^2}\right) \tag{B.132}$$

$$K_3(P_\beta) = -\frac{2}{\pi}\left(\frac{U}{b_r\omega}\right)^2 \frac{\Phi_1\Phi_{31}}{\pi}C(k_r) - \left(\frac{U}{b_r\omega}\right)^2 \frac{\Phi_{35}}{\pi^2} \tag{B.133}$$

$$P_z = K_1(P_z) + \left(\frac{b_r}{b}\right) K_2(P_z) \tag{B.134}$$

$$K_1(P_z) = \frac{\Phi_{17}}{\pi^2} \tag{B.135}$$

$$K_2(P_z) = -2i\left(\frac{U}{b_r\omega}\right)\frac{\Phi_1\Phi_{31}}{\pi^2}C(k_r) - \left(\frac{U}{b_r\omega}\right)\frac{\Phi_{35}}{\pi^2} \tag{B.136}$$

Supersonic Flow Force Coefficients

$$L_h = K_1(L_h) \tag{B.137}$$

$$K_1(L_h) = 2i \tag{B.138}$$

$$L_\alpha = K_1(L_\alpha) + \left(\frac{b_r}{b}\right) K_2(L_\alpha) \tag{B.139}$$

$$K_1(L_\alpha) = -2ai \tag{B.140}$$

$$K_2(L_\alpha) = 2\left(\frac{1}{k_r}\right) \tag{B.141}$$

$$L_\beta = K_1(L_\beta) + \left(\frac{b_r}{b}\right) K_2(L_\beta) \tag{B.142}$$

$$K_1(L_\beta) = (1 - e)\left(\tfrac{1}{2} - e\right) i \tag{B.143}$$

$$K_2(L_\beta) = (1 - e)\left(\frac{1}{k_r}\right) \tag{B.144}$$

$$M_h = K_1(M_h) \tag{B.145}$$

$$K_1(M_h) = 2ei - \left(\tfrac{1}{a}\left(e^2 - 1\right)\right) \tag{B.146}$$

$$M_\alpha = K_1(M_\alpha) + \left(\frac{b_r}{b}\right) K_2(M_\alpha) \tag{B.147}$$

$$K_1(M_\alpha) = -2eai + \left(e^2 - 1\right)\left(i + \tfrac{1}{2a}\left(\tfrac{1}{2} + a\right)\right) - \tfrac{2}{3}\tfrac{e^3}{a} i \tag{B.148}$$

$$K_2(M_\alpha) = \left(2e - \left(e^2 - 1\right)\left(\tfrac{1}{a}\right)\right)\left(\tfrac{1}{k_r}\right) \tag{B.149}$$

$$M_\beta = K_1(M_\beta) + \left(\frac{b_r}{b}\right)K_2(M_\beta) \tag{B.150}$$

$$K_1(M_\beta) = \tfrac{1}{3a}\left(e^3 - 1\right)i + \tfrac{1}{2a}\left[\left(e^2 - 1\right)i - (1 - e)\left(\tfrac{1}{2} - a\right)i\right] \tag{B.151}$$

$$K_2(M_\beta) = \tfrac{1}{2a}\left[\left(e^2 - 1 + (e - 1)\right)\right]\left(\tfrac{1}{k_r}\right) \tag{B.152}$$

$$T_h = K_1(T_h) \tag{B.153}$$

$$K_1(T_h) = pi \tag{B.154}$$

$$T_\alpha = K_1(T_\alpha) + \left(\frac{b_r}{b}\right)K_2(T_\alpha) \tag{B.155}$$

$$K_1(T_\alpha) = (-pa + r)i \tag{B.156}$$

$$K_2(T_\alpha) = p\left(\tfrac{1}{k_r}\right) \tag{B.157}$$

$$T_\beta = K_1(T_\beta) + \left(\frac{b_r}{b}\right)K_2(T_\beta) \tag{B.158}$$

$$K_1(T_\beta) = (-pe + r)i \tag{B.159}$$

$$K_2(T_\beta) = p\left(\tfrac{1}{k_r}\right) \tag{B.160}$$

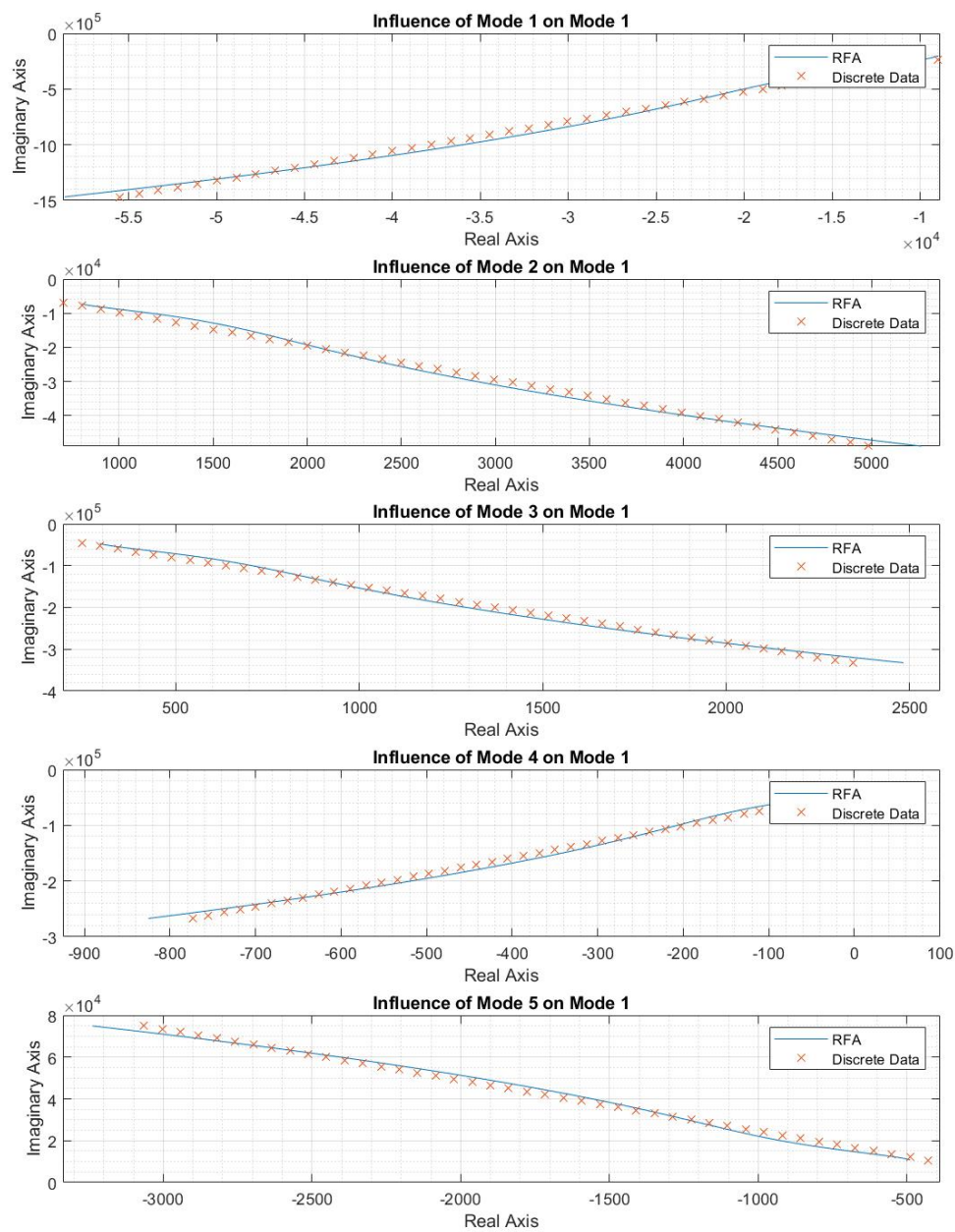# APPENDIX C - Roger's Approximation Results Summary
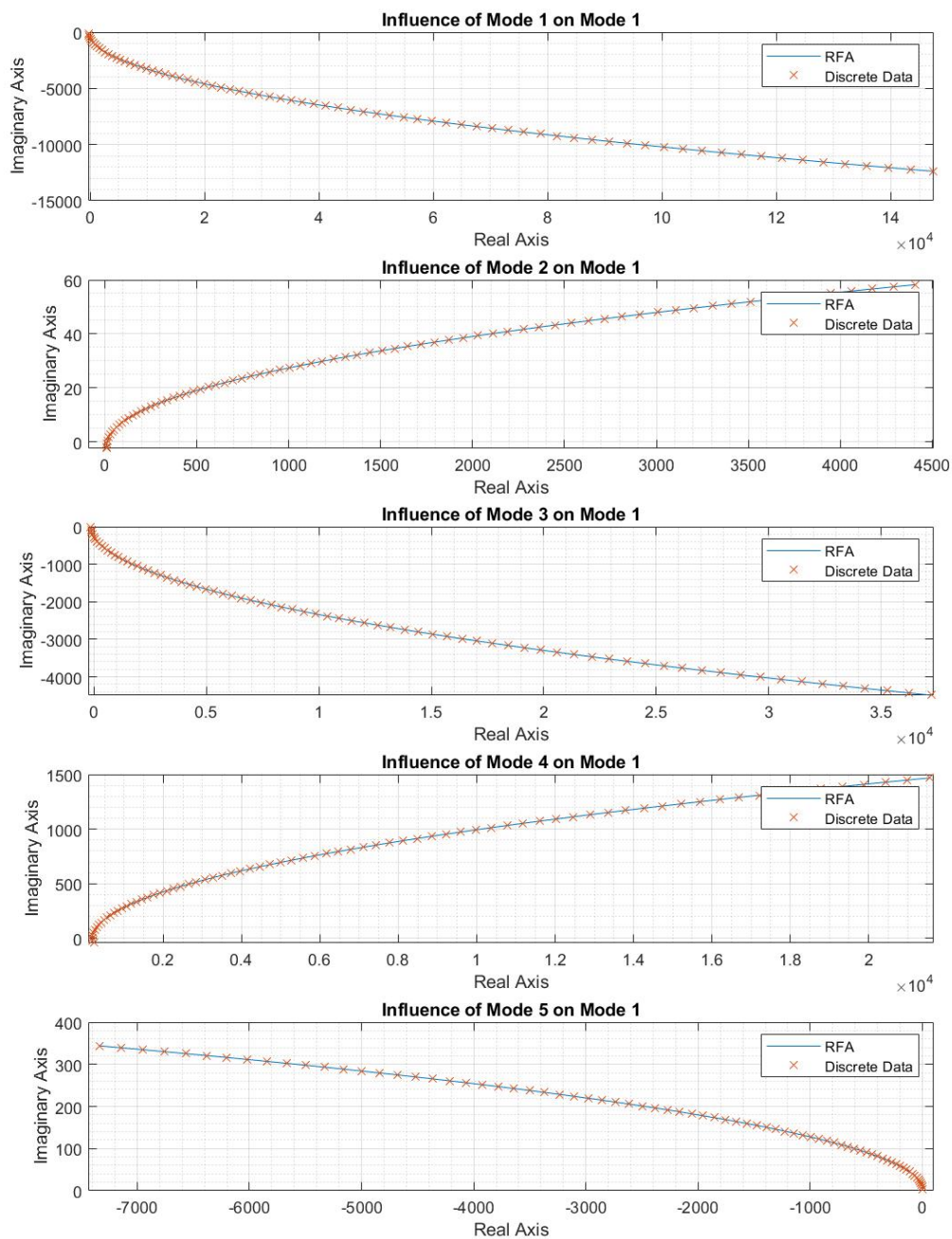
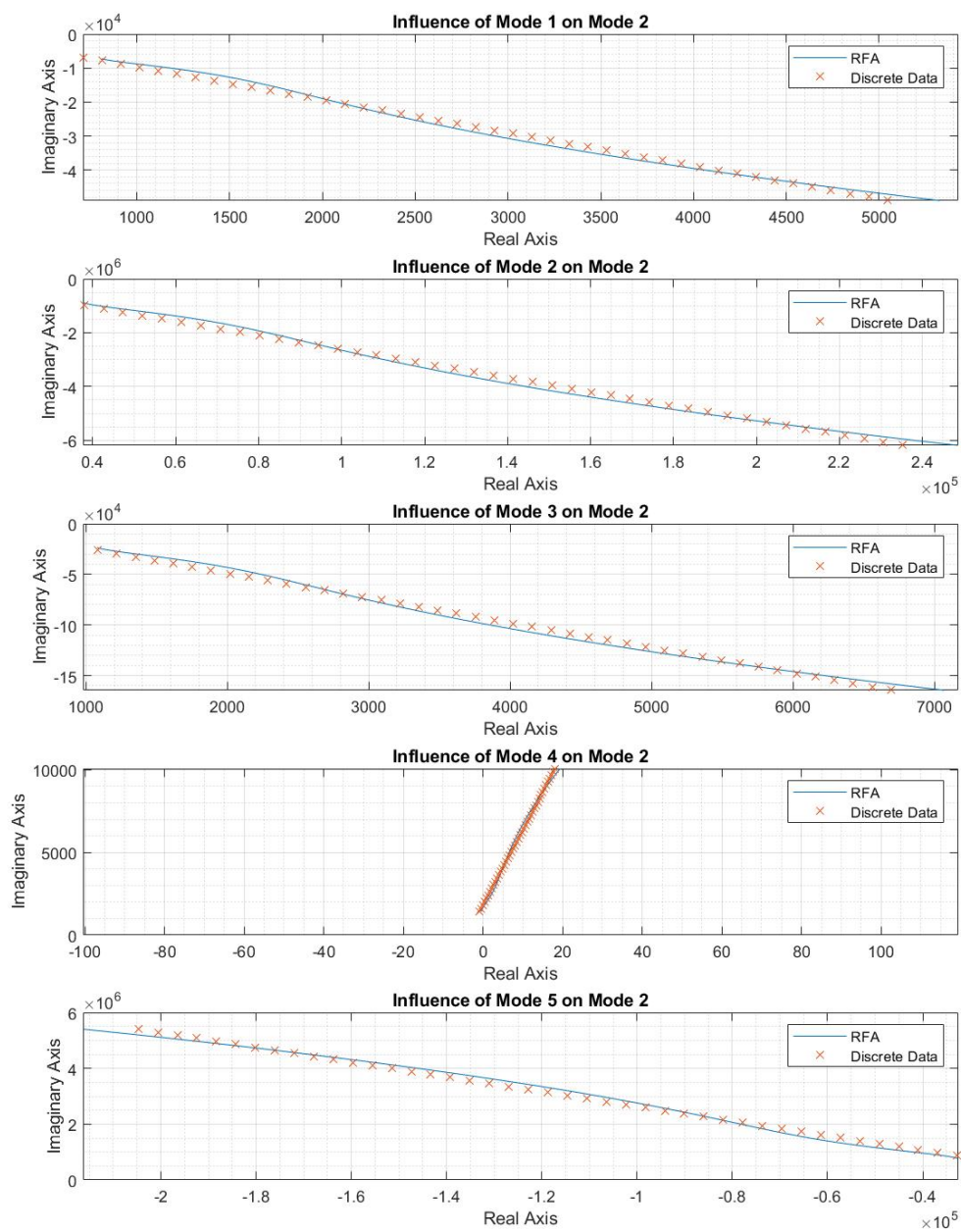*Figure C.1* Roger's Approximation for Mode 1 at Mach = 0.00
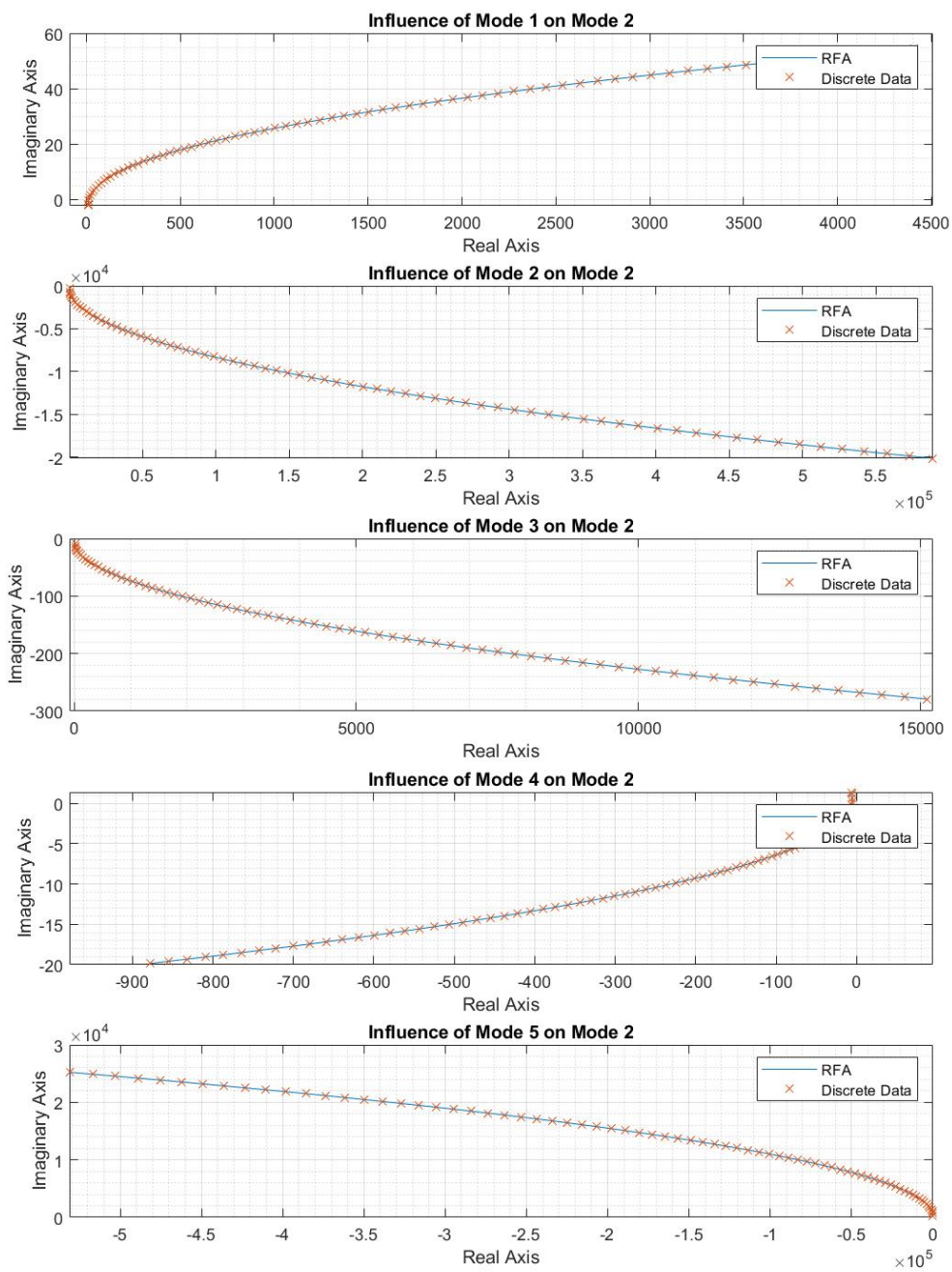
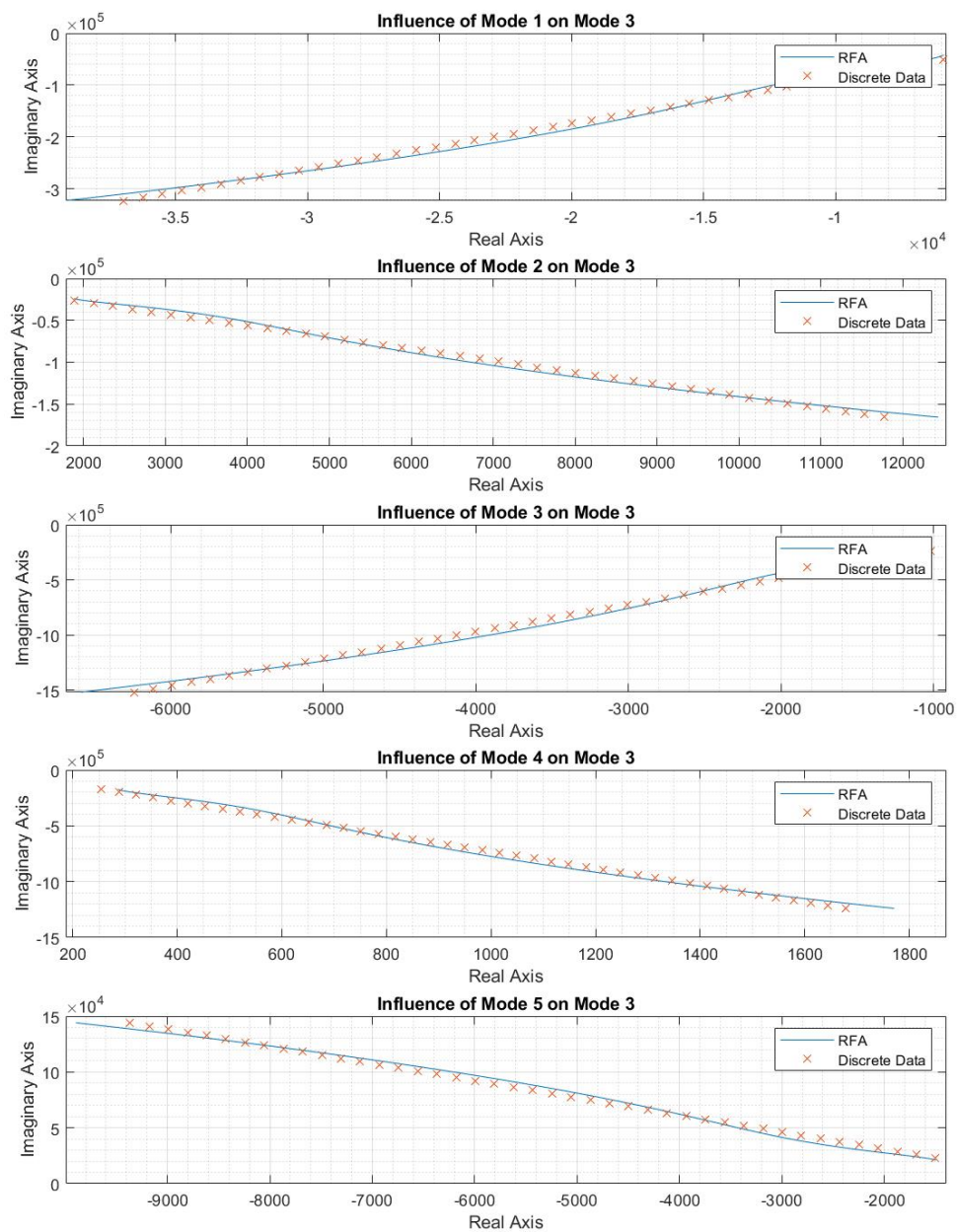*Figure C.2* Roger's Approximation for Mode 2 at Mach = 0.00
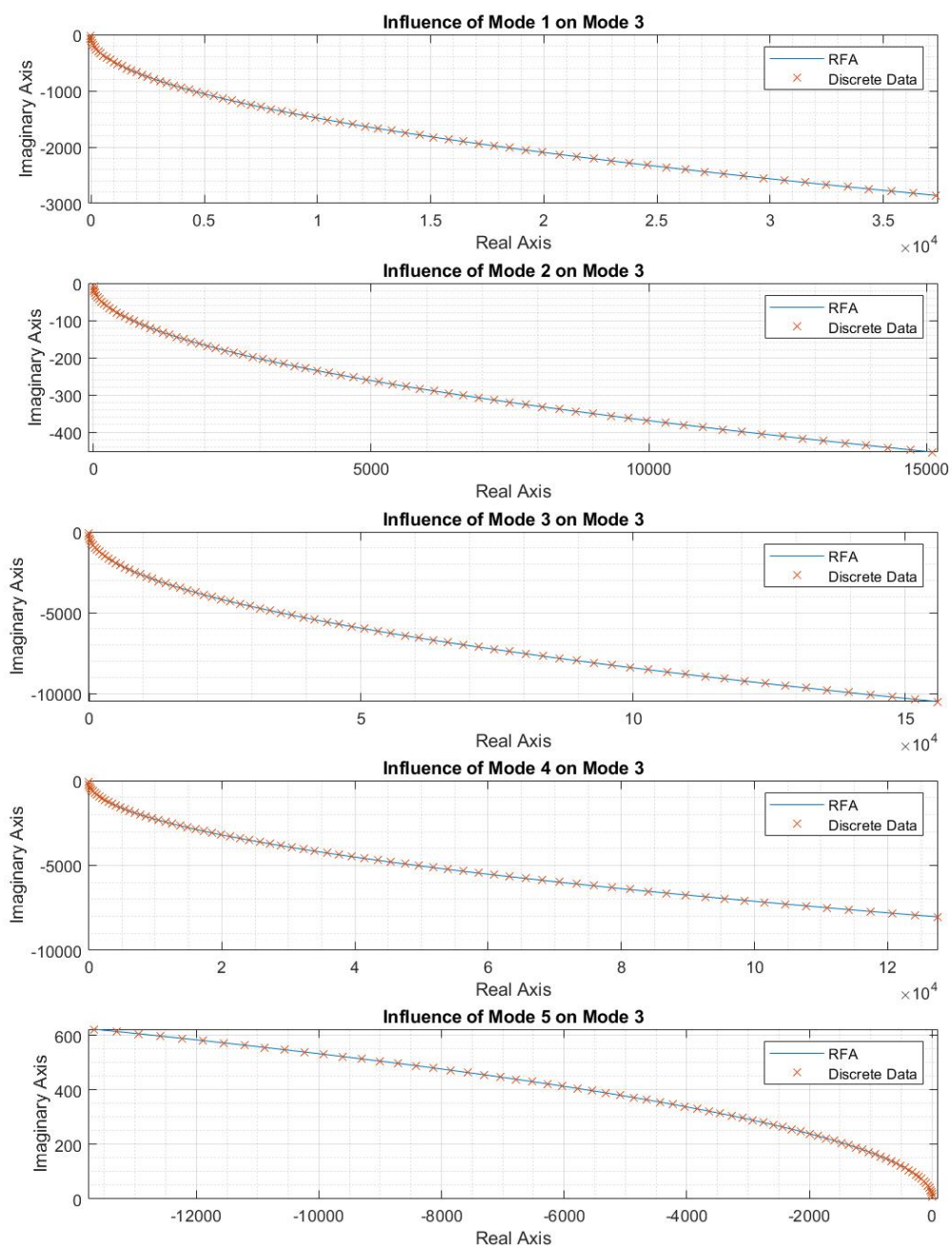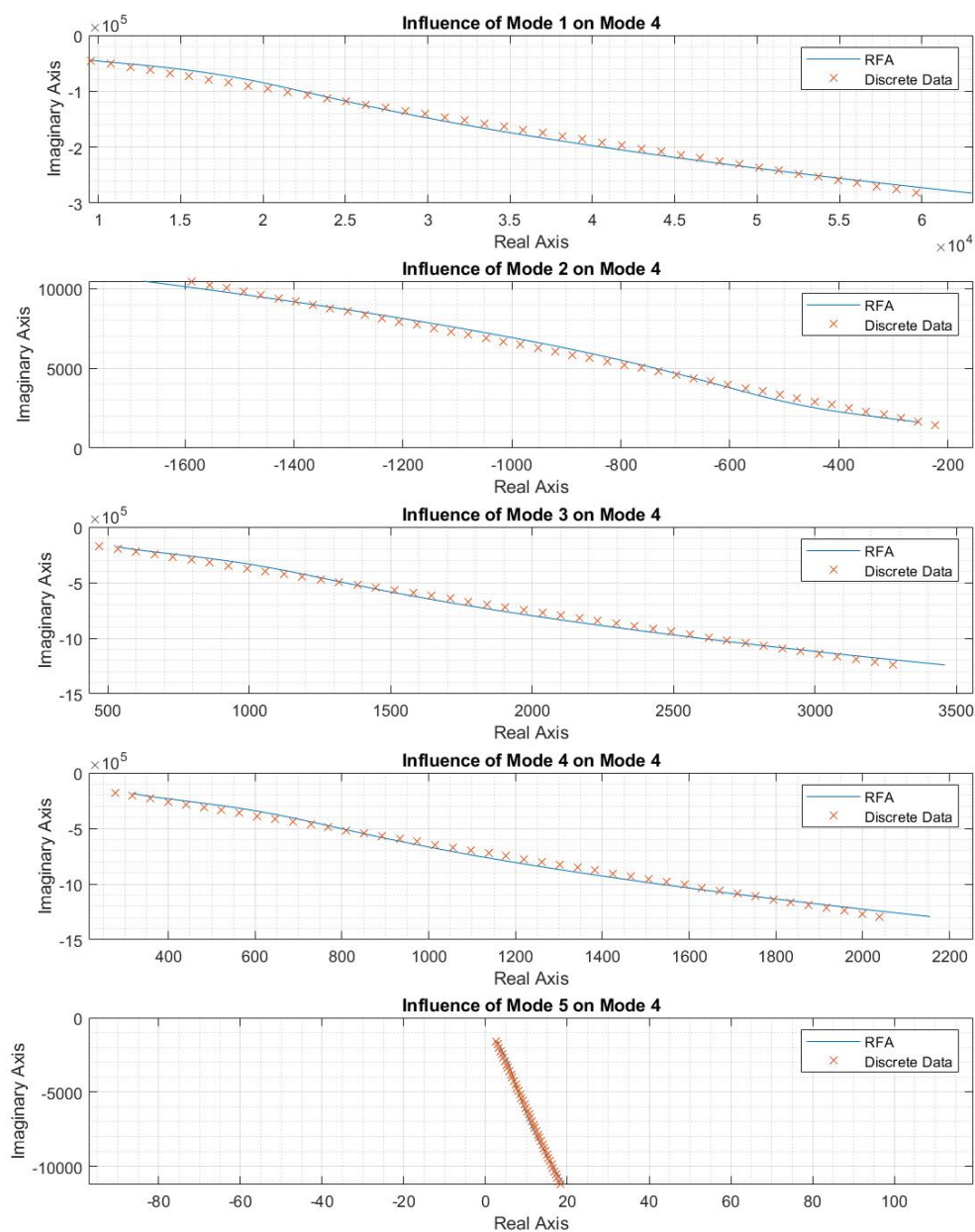
Figure C.3 Roger's Approximation for Mode 3 at Mach = 0.00
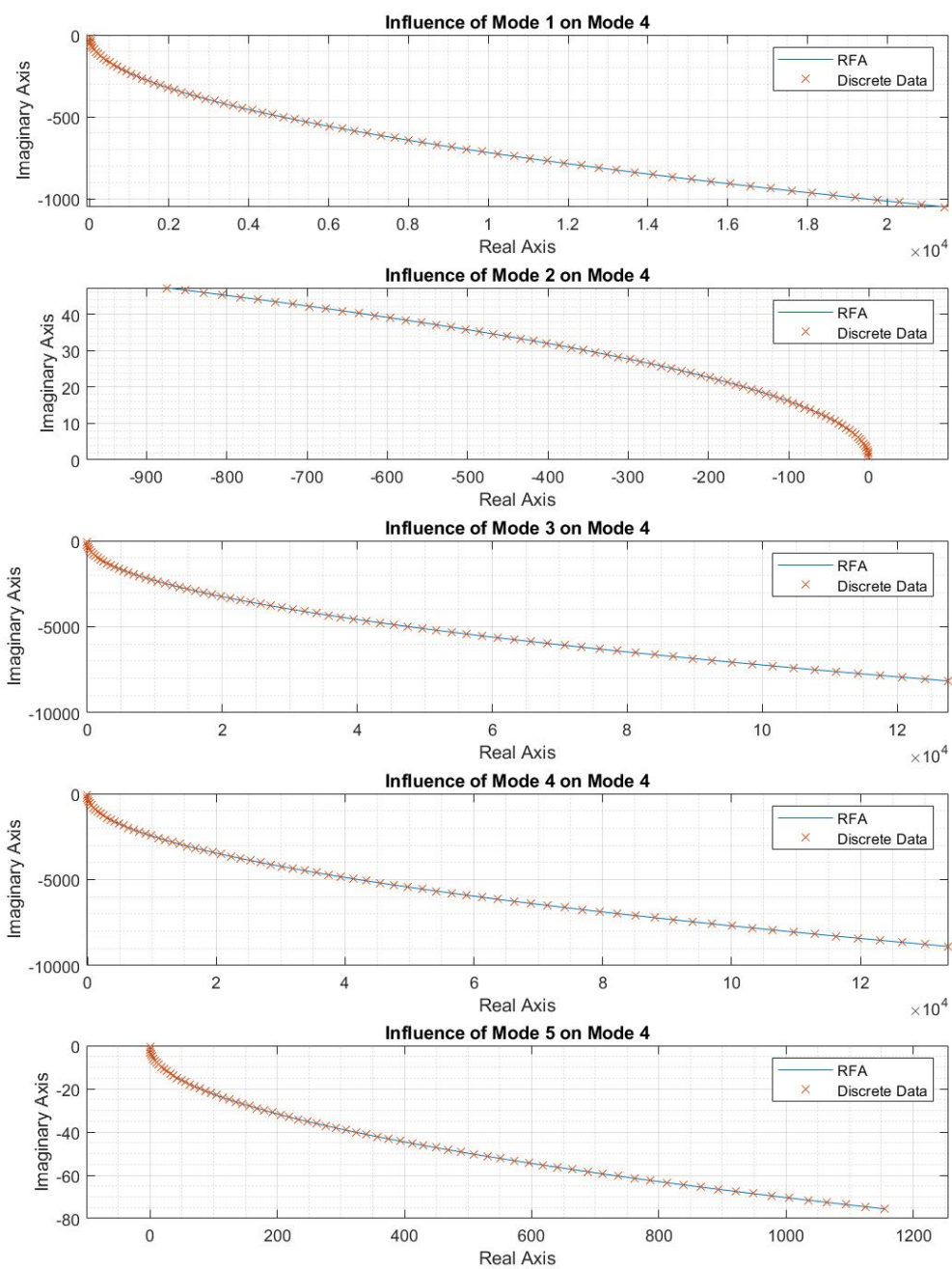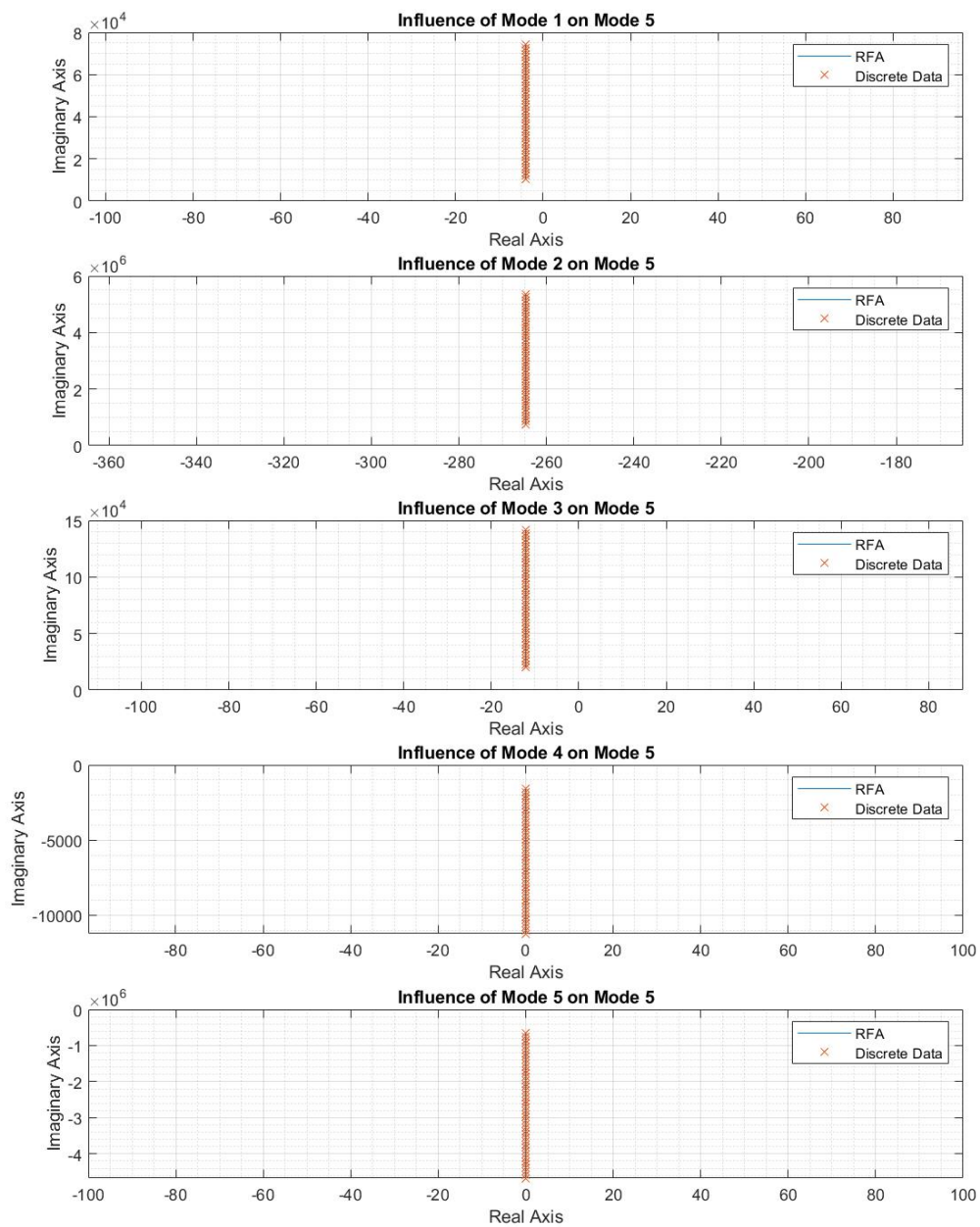
Figure C.4 Roger's Approximation for Mode 4 at Mach = 0.00
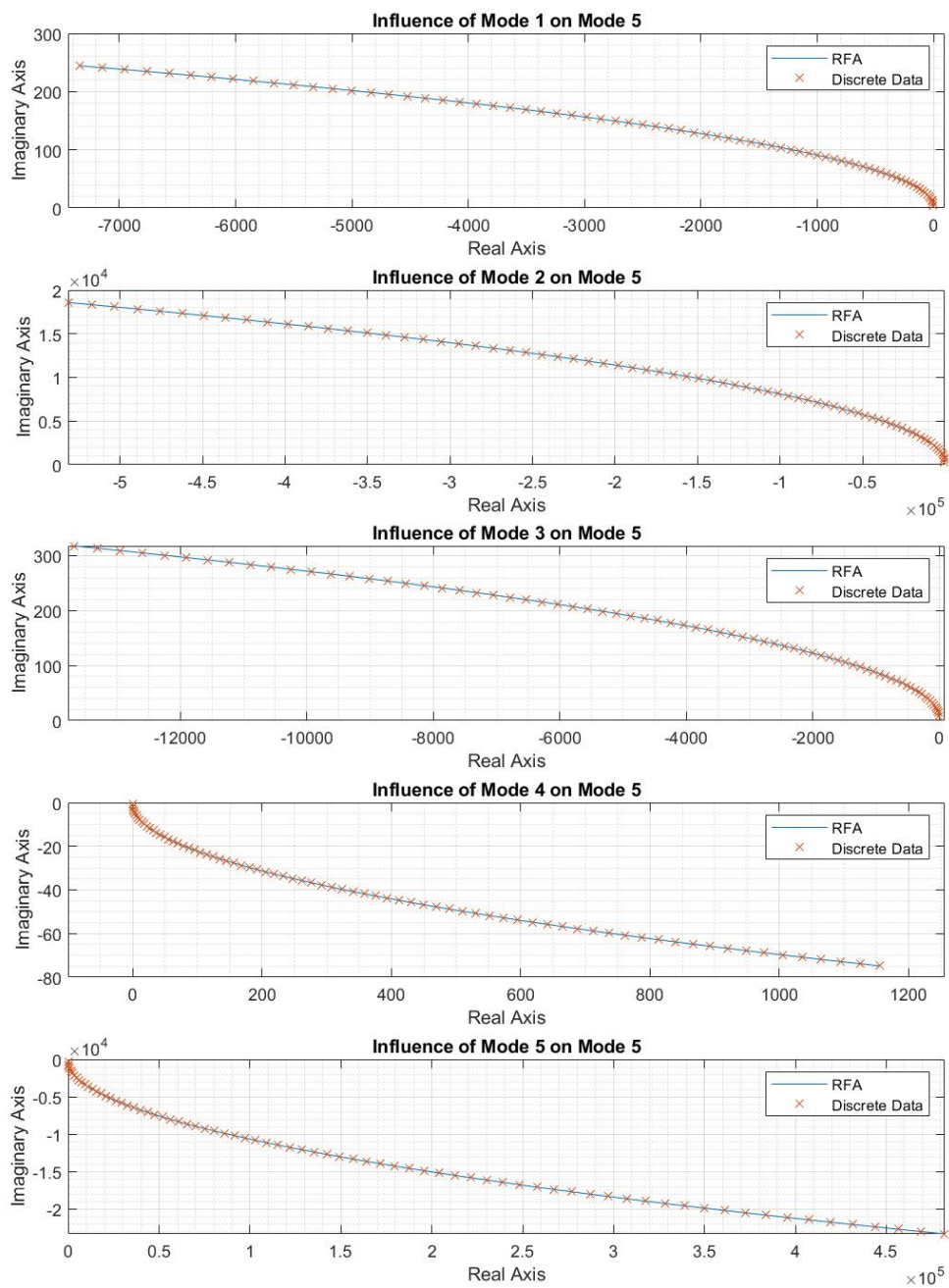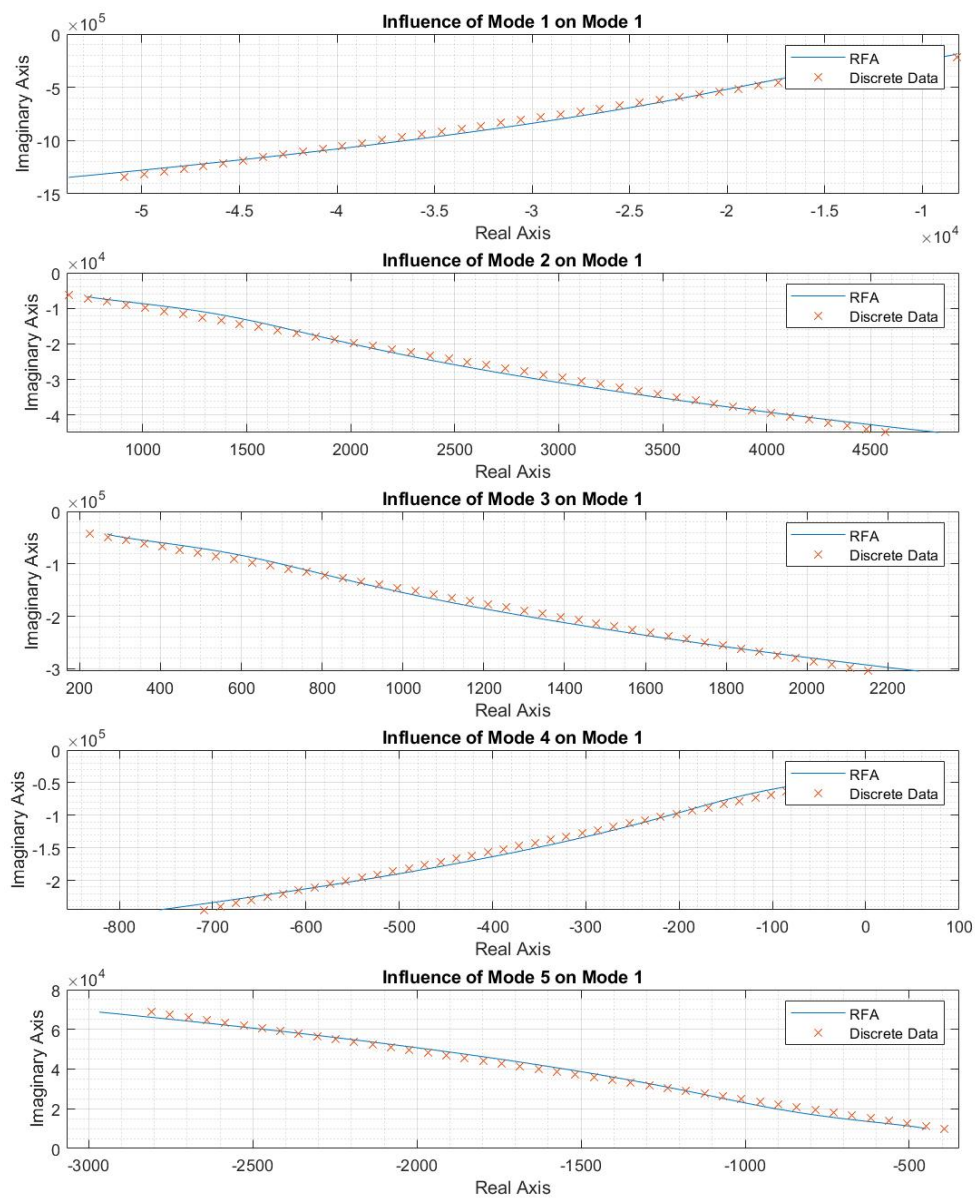
Figure C.5 Roger's Approximation for Mode 5 at Mach = 0.00
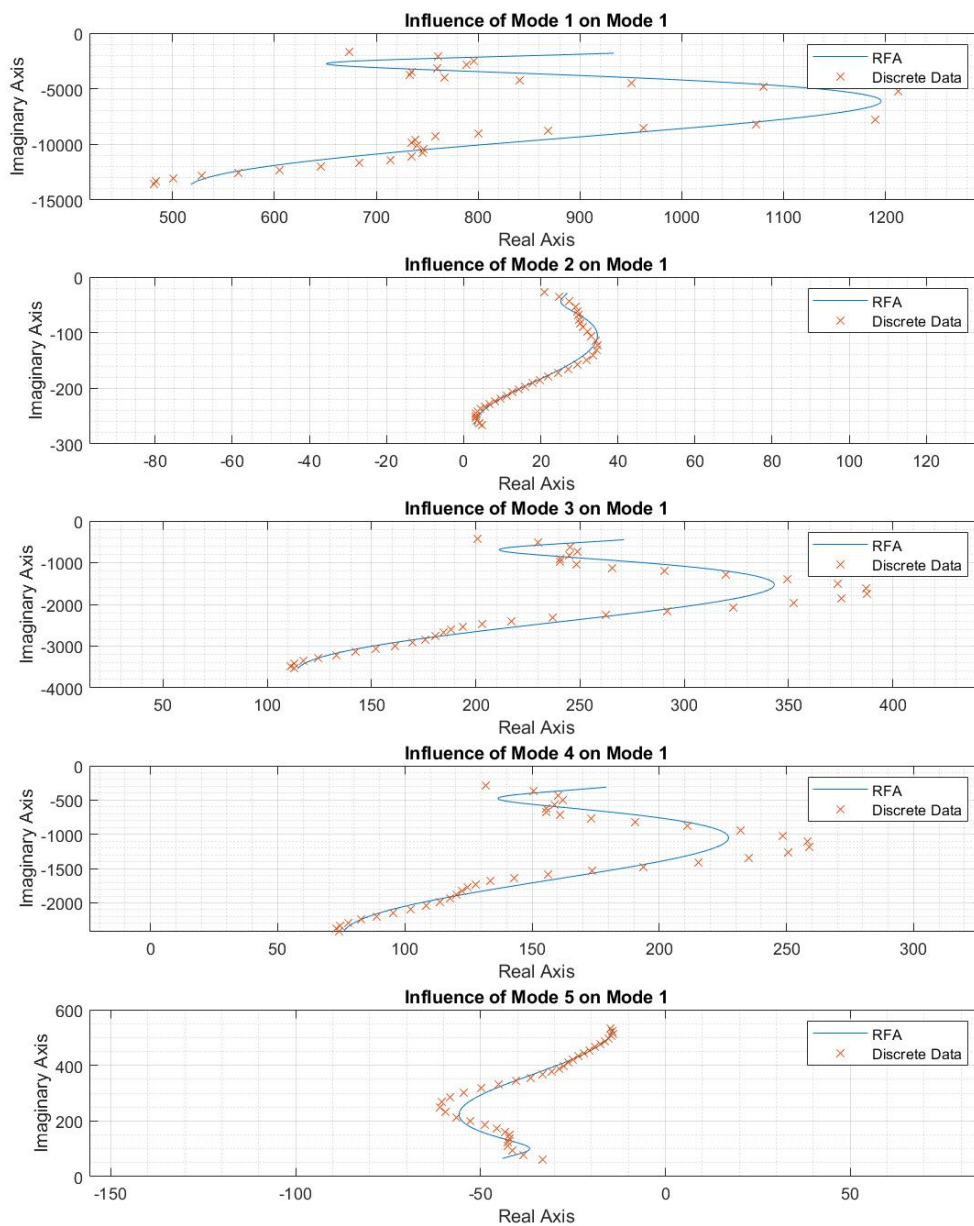
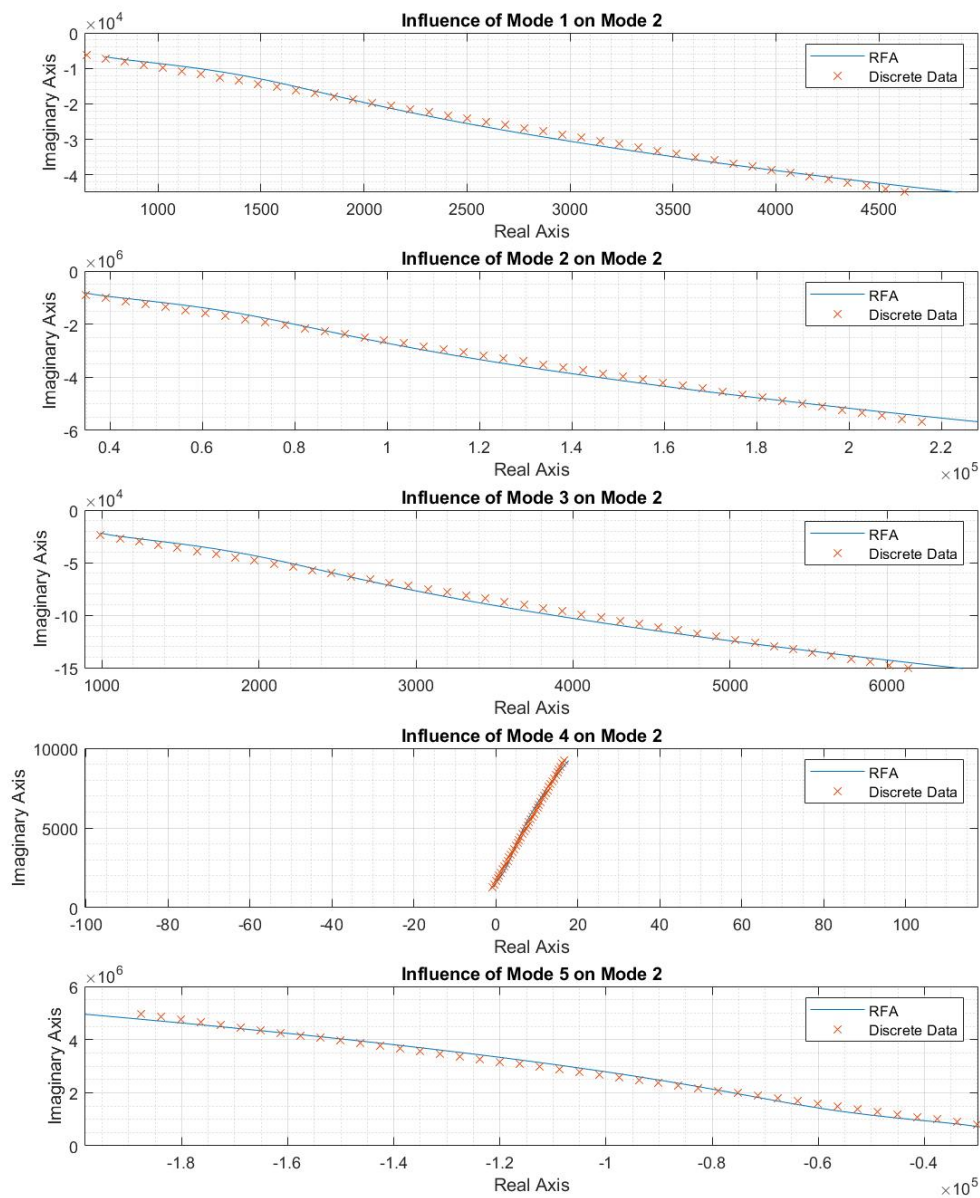*Figure C.6* Roger's Approximation for Mode 1 at Mach = 0.50
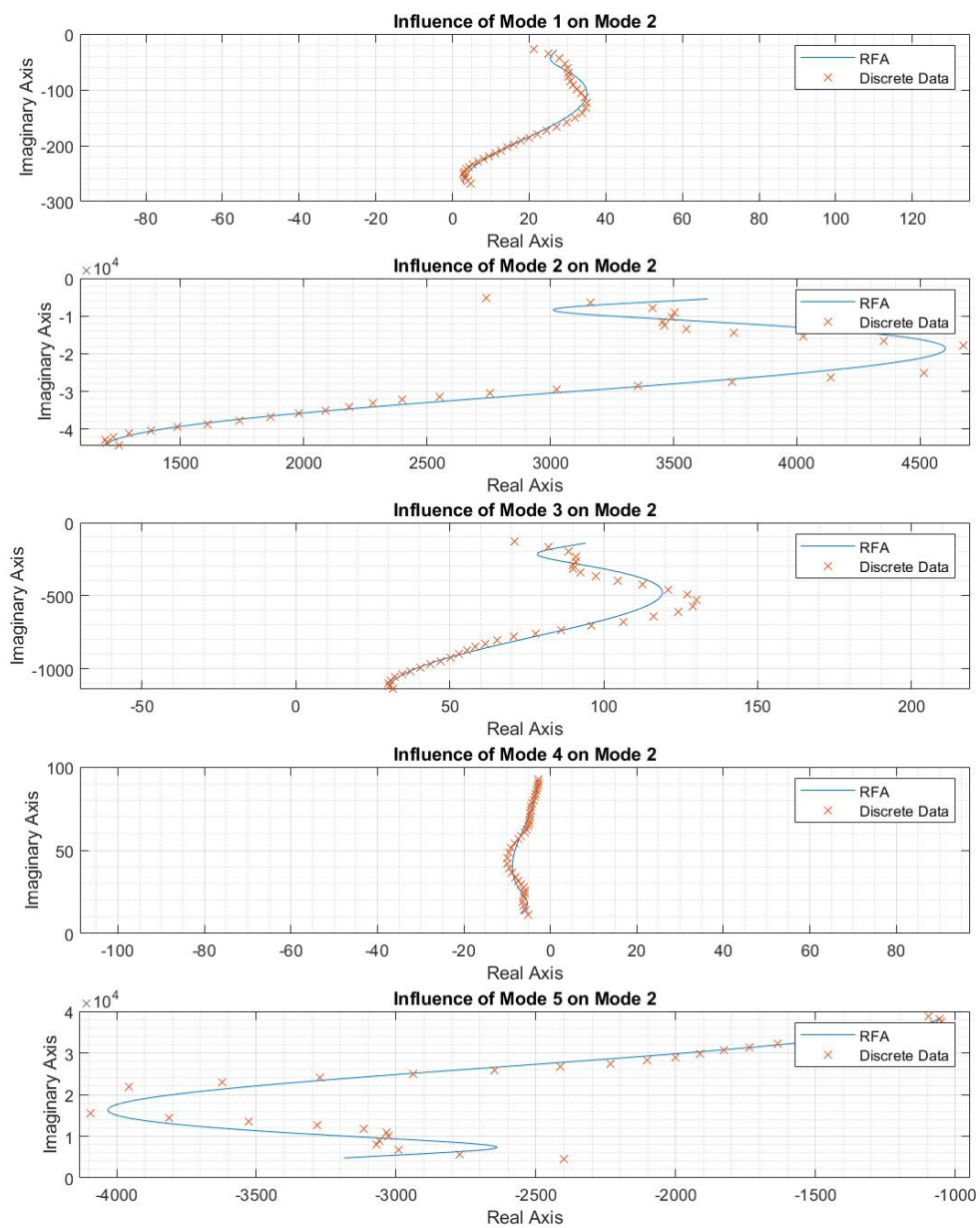
Figure C.7 Roger's Approximation for Mode 2 at Mach = 0.50
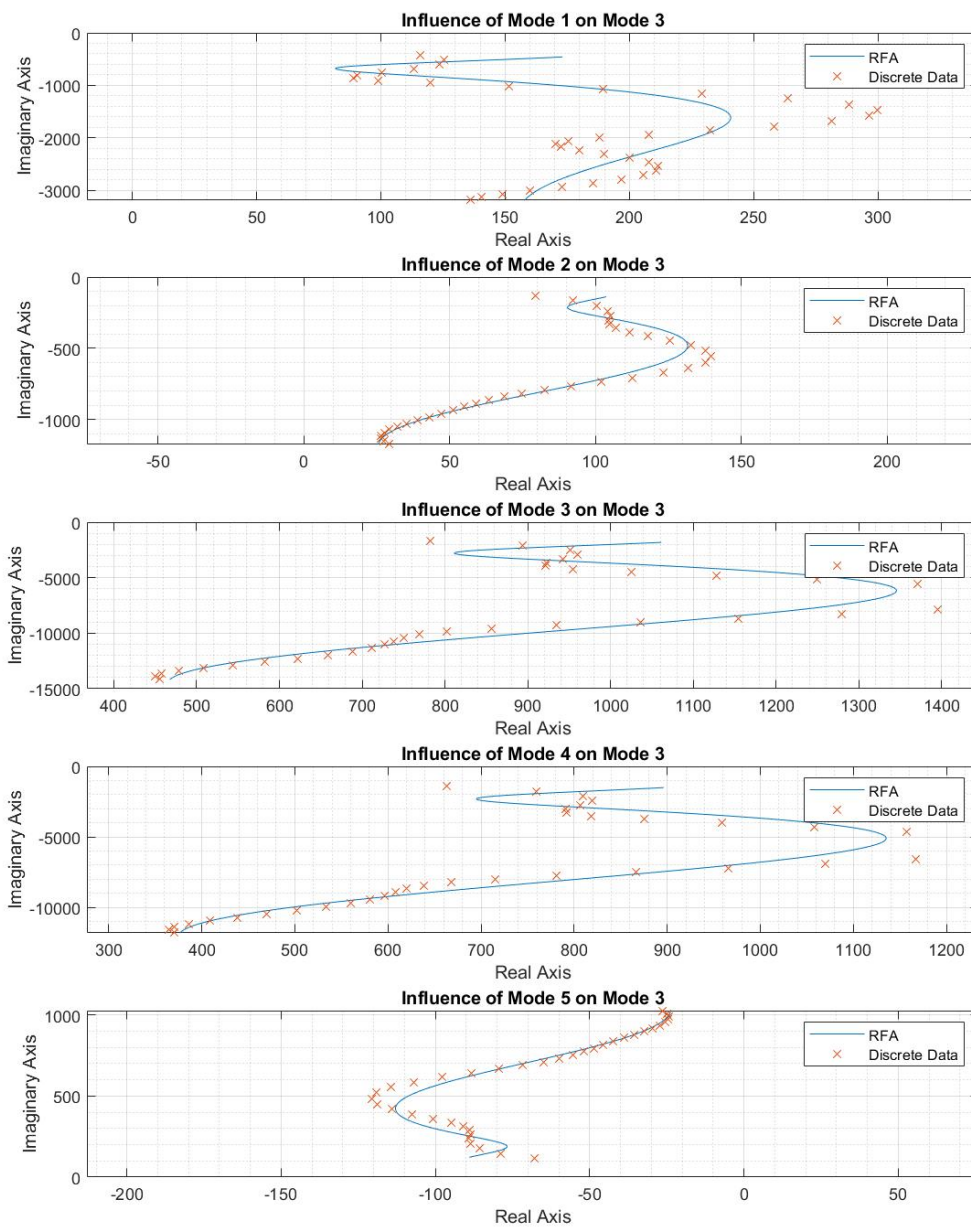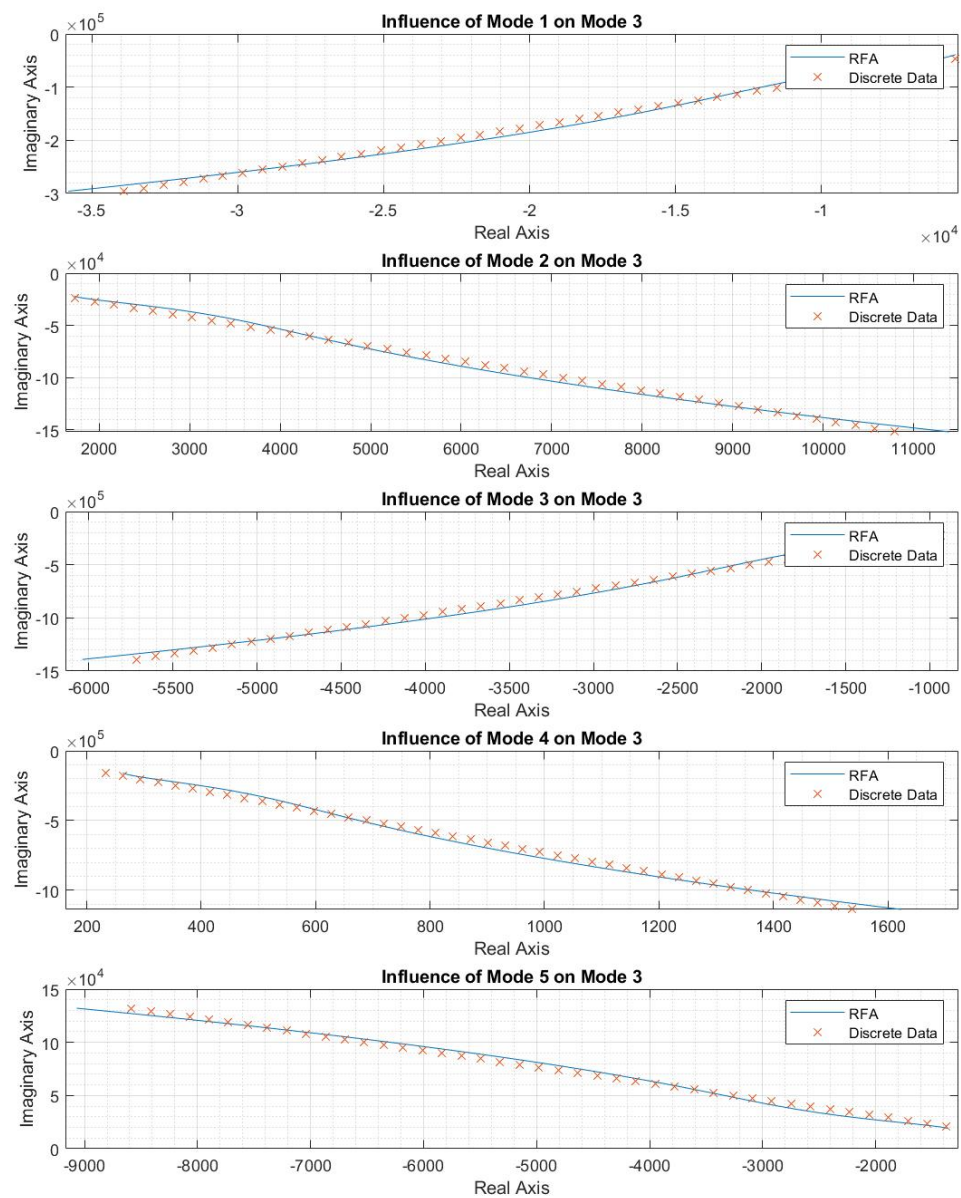
Figure C.8 Roger's Approximation for Mode 3 at Mach = 0.50
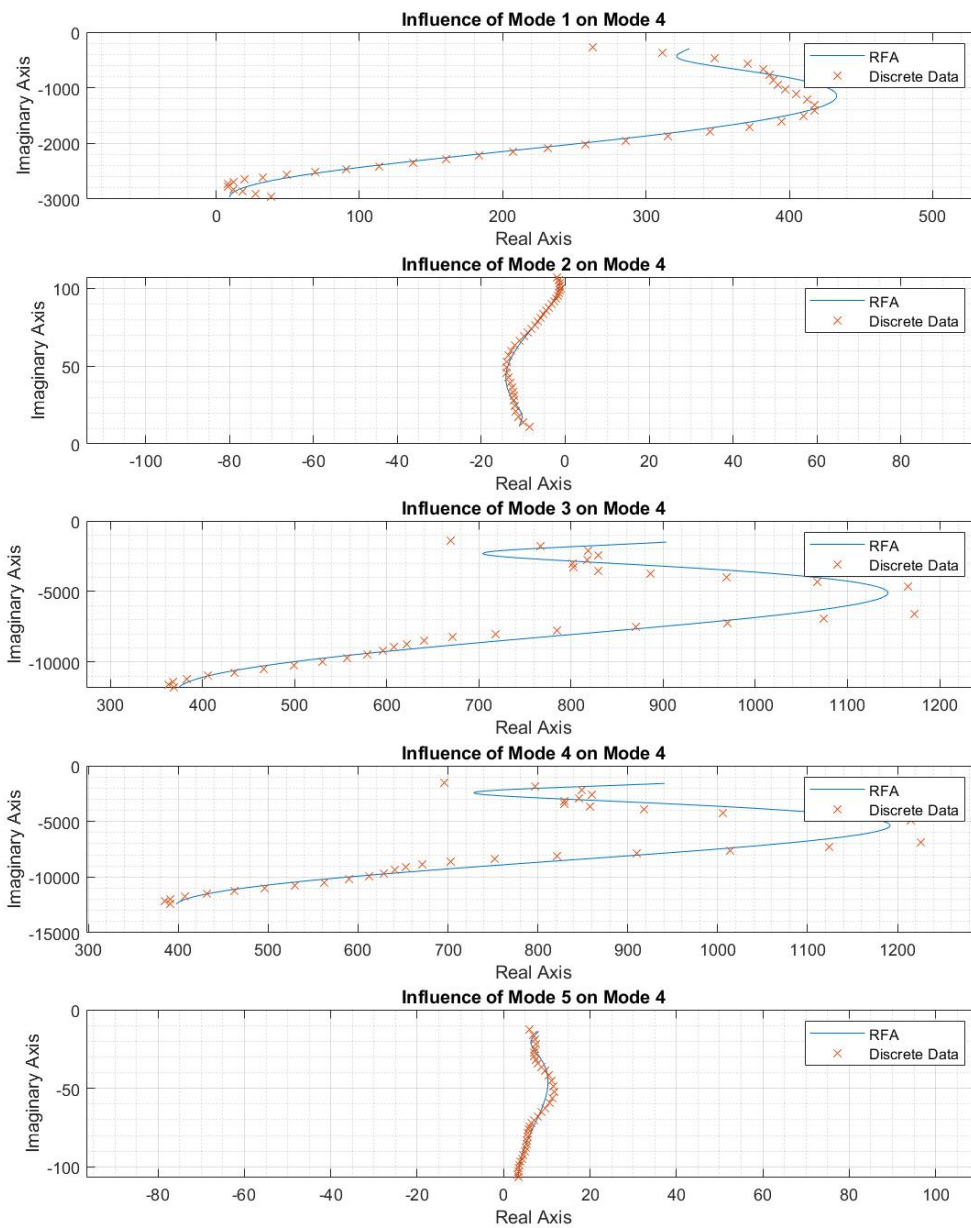
Figure C.9 Roger's Approximation for Mode 4 at Mach = 0.50
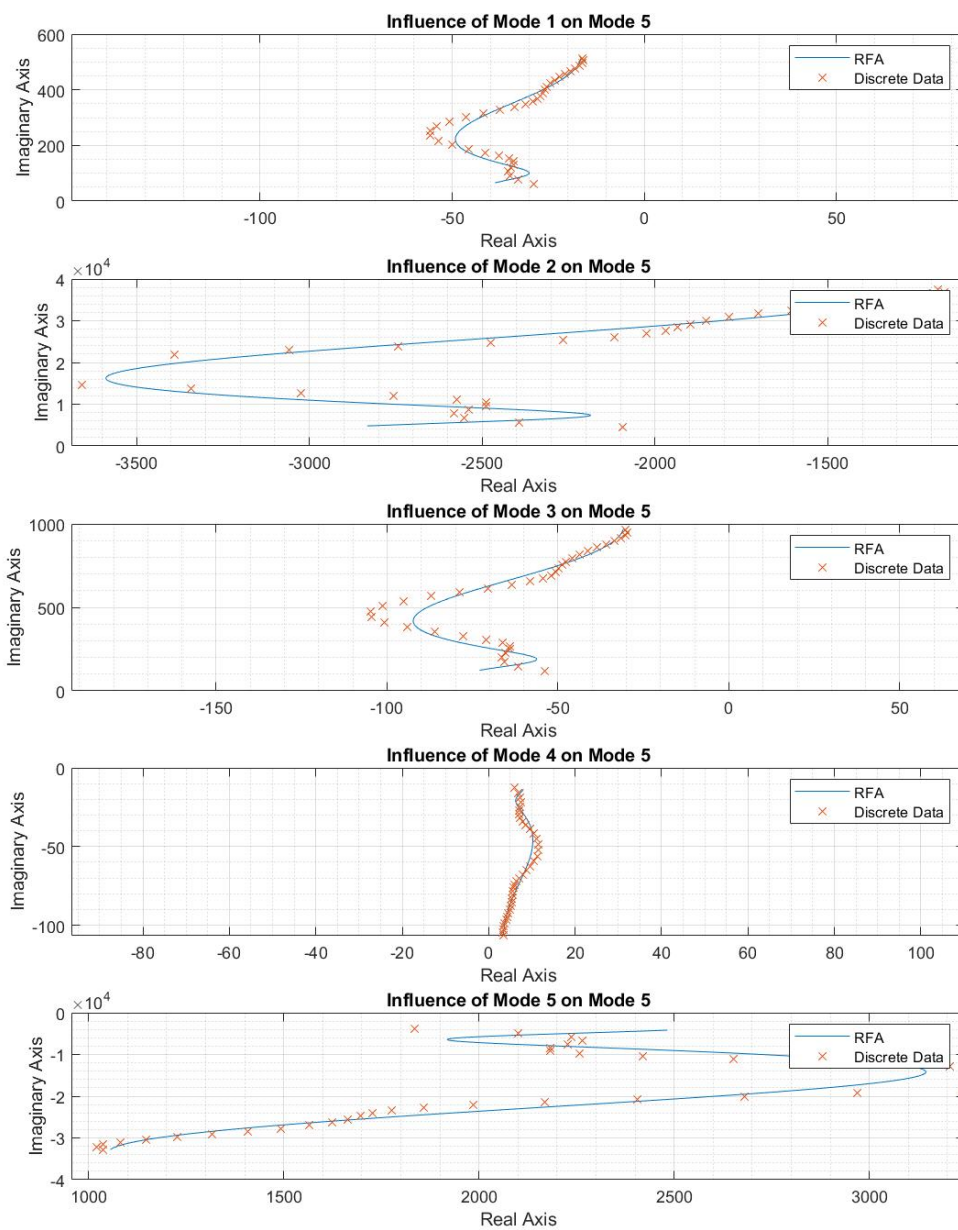
Figure C.10 Roger's Approximation for Mode 5 at Mach = 0.50
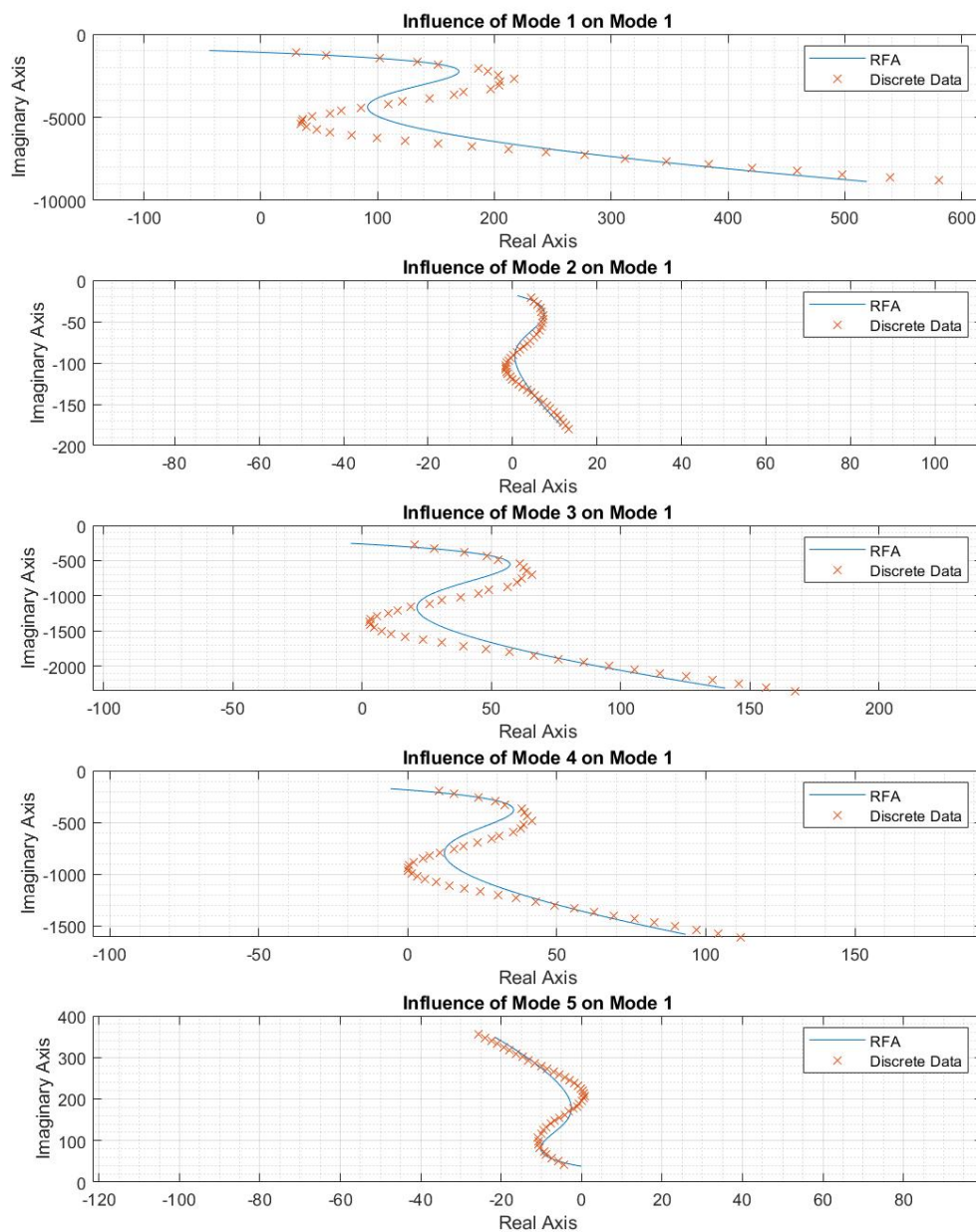
Figure C.11 Roger's Approximation for Mode 1 at Mach = 0.85
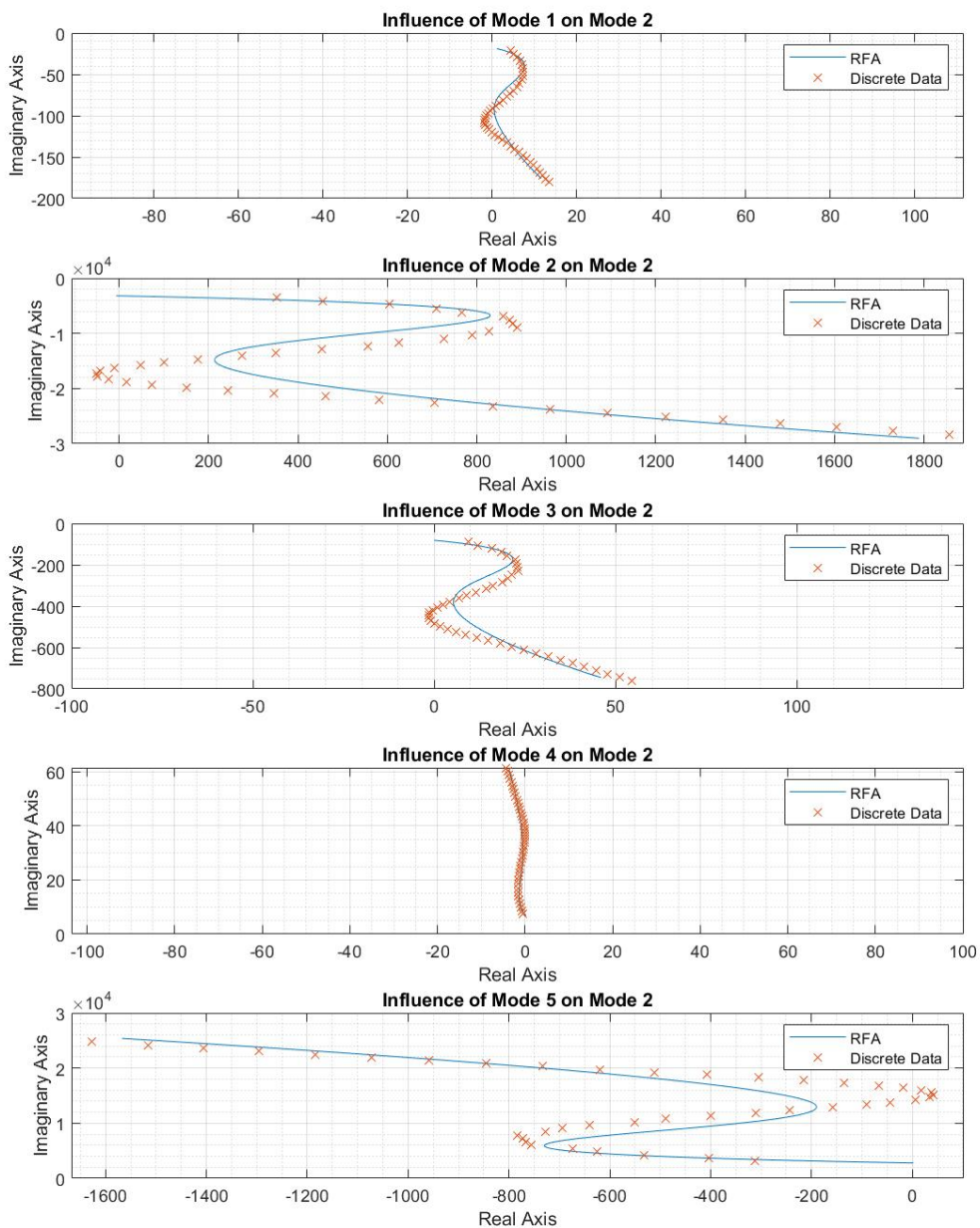
Figure C.12 Roger's Approximation for Mode 2 at Mach = 0.85
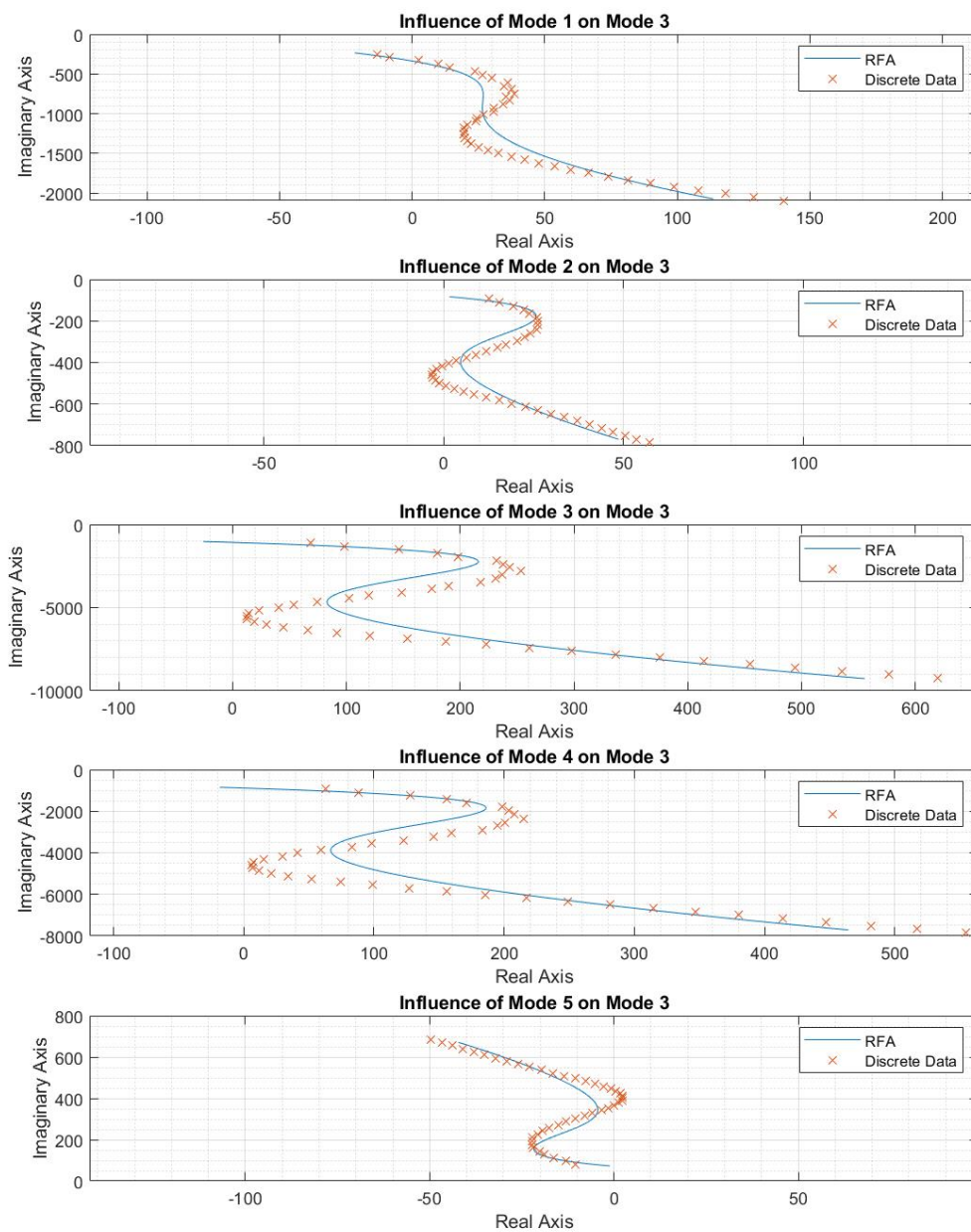
Figure C.13 Roger's Approximation for Mode 3 at Mach = 0.85
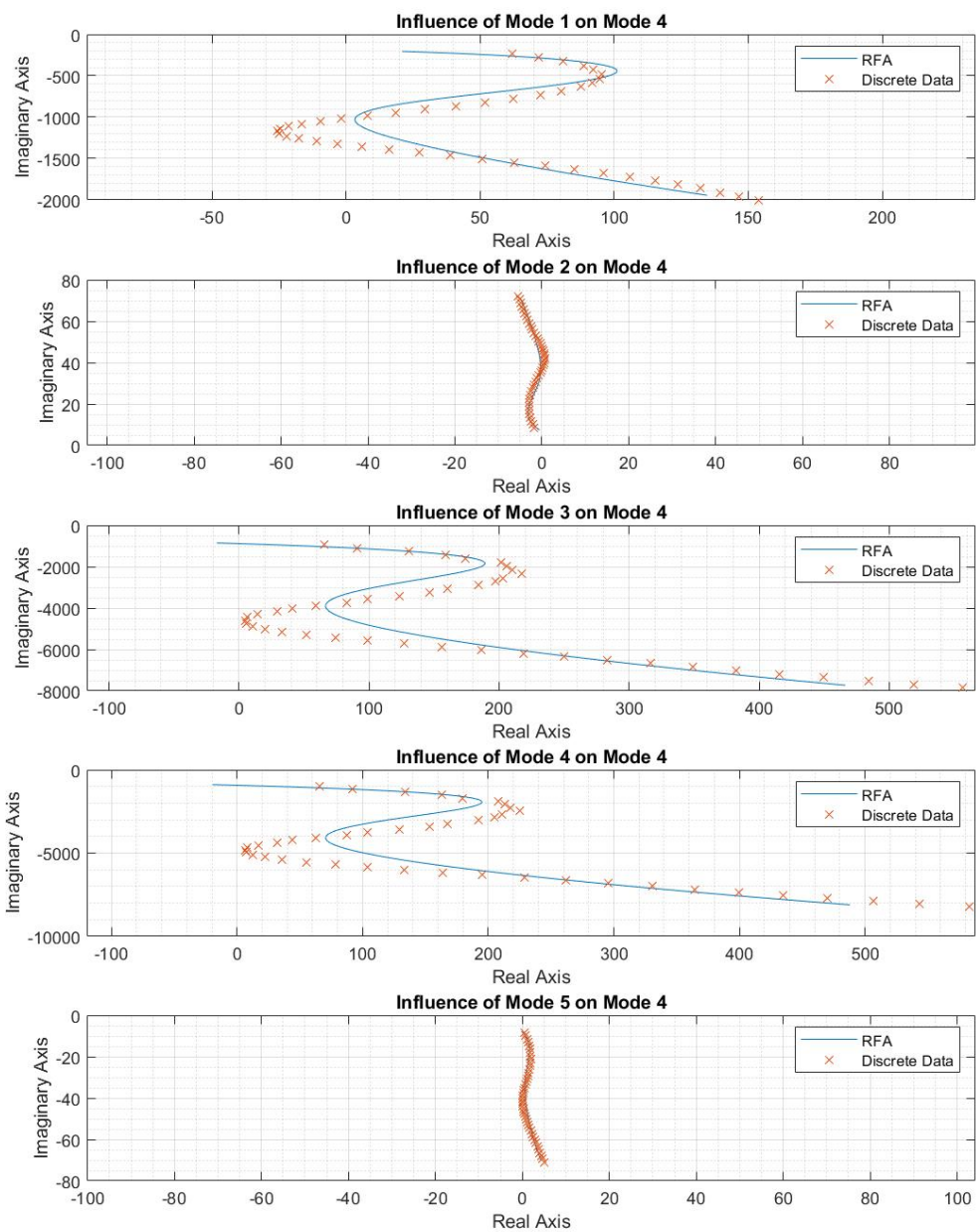
Figure C.14 Roger's Approximation for Mode 4 at Mach = 0.85
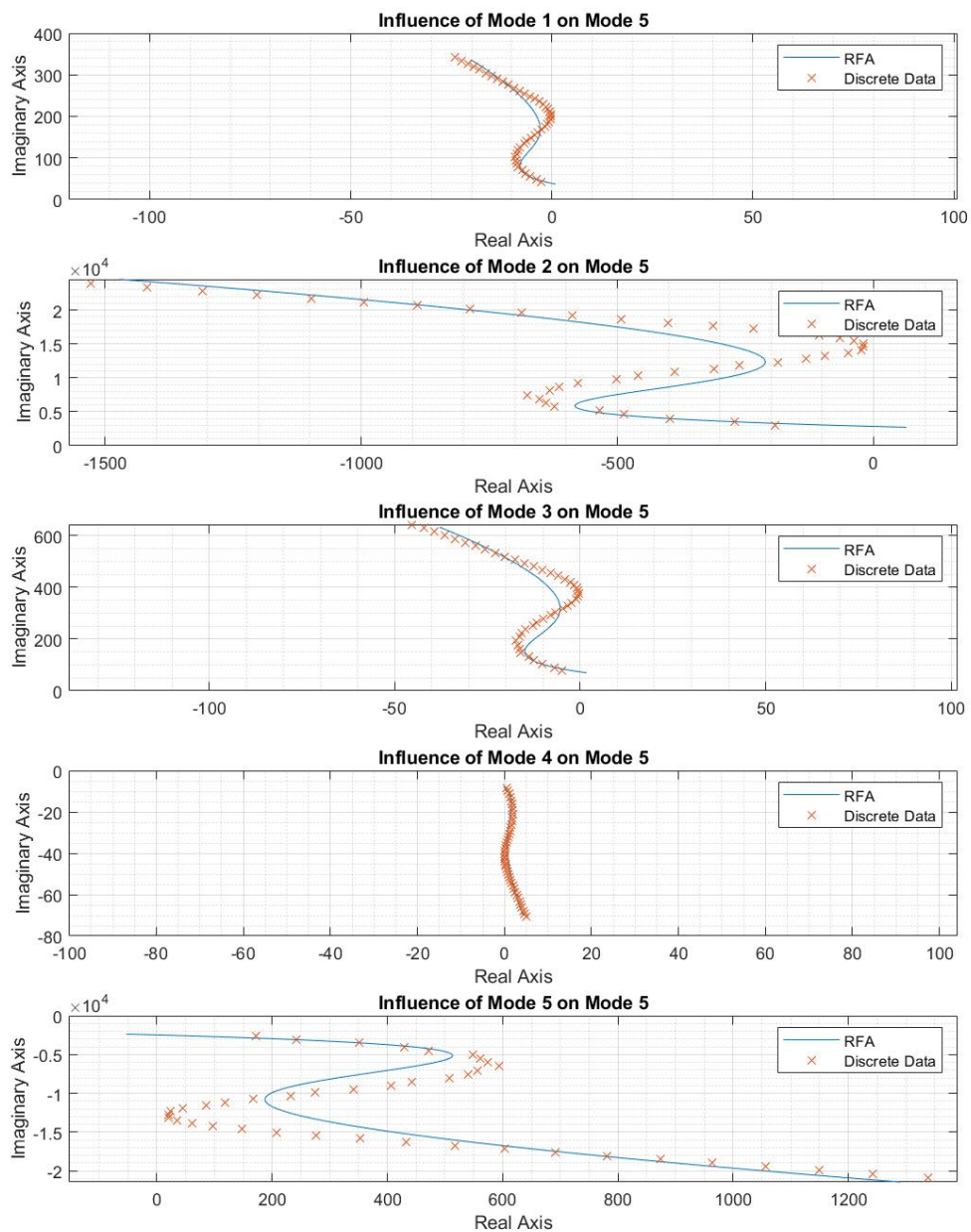
Figure C.15 Roger's Approximation for Mode 5 at Mach = 0.85
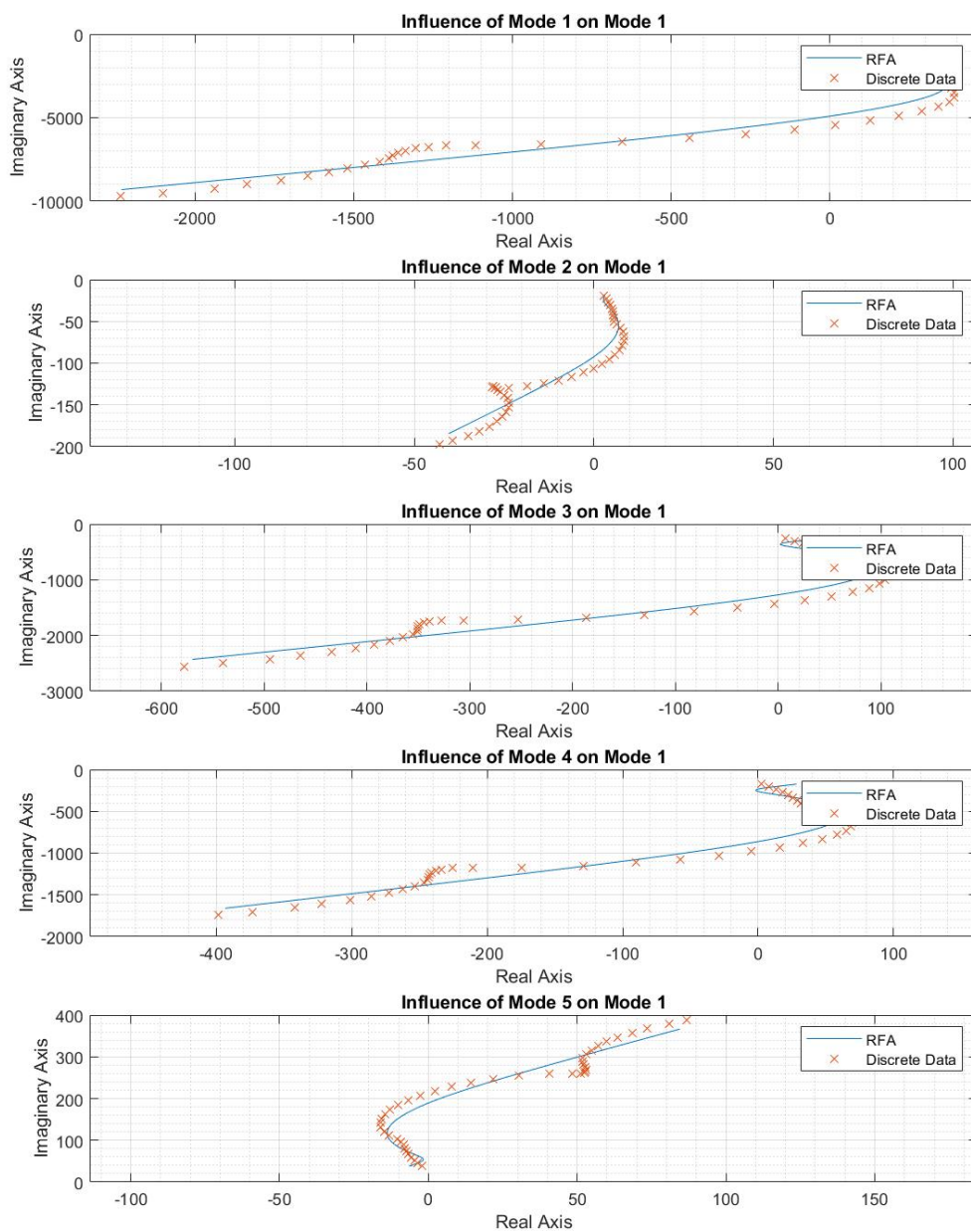
Figure C.16 Roger's Approximation for Mode 1 at Mach = 0.95
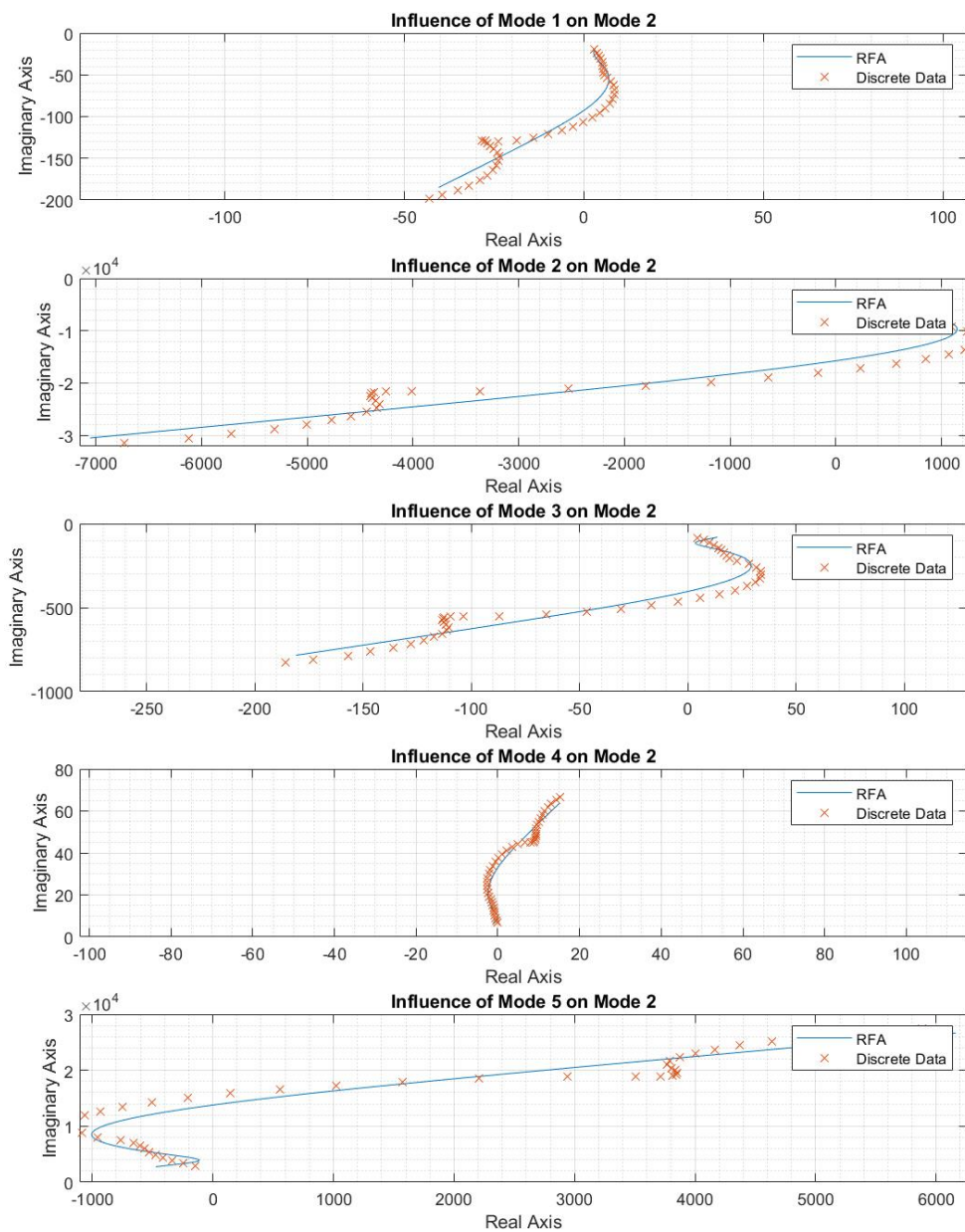
Figure C.17 Roger's Approximation for Mode 2 at Mach = 0.95
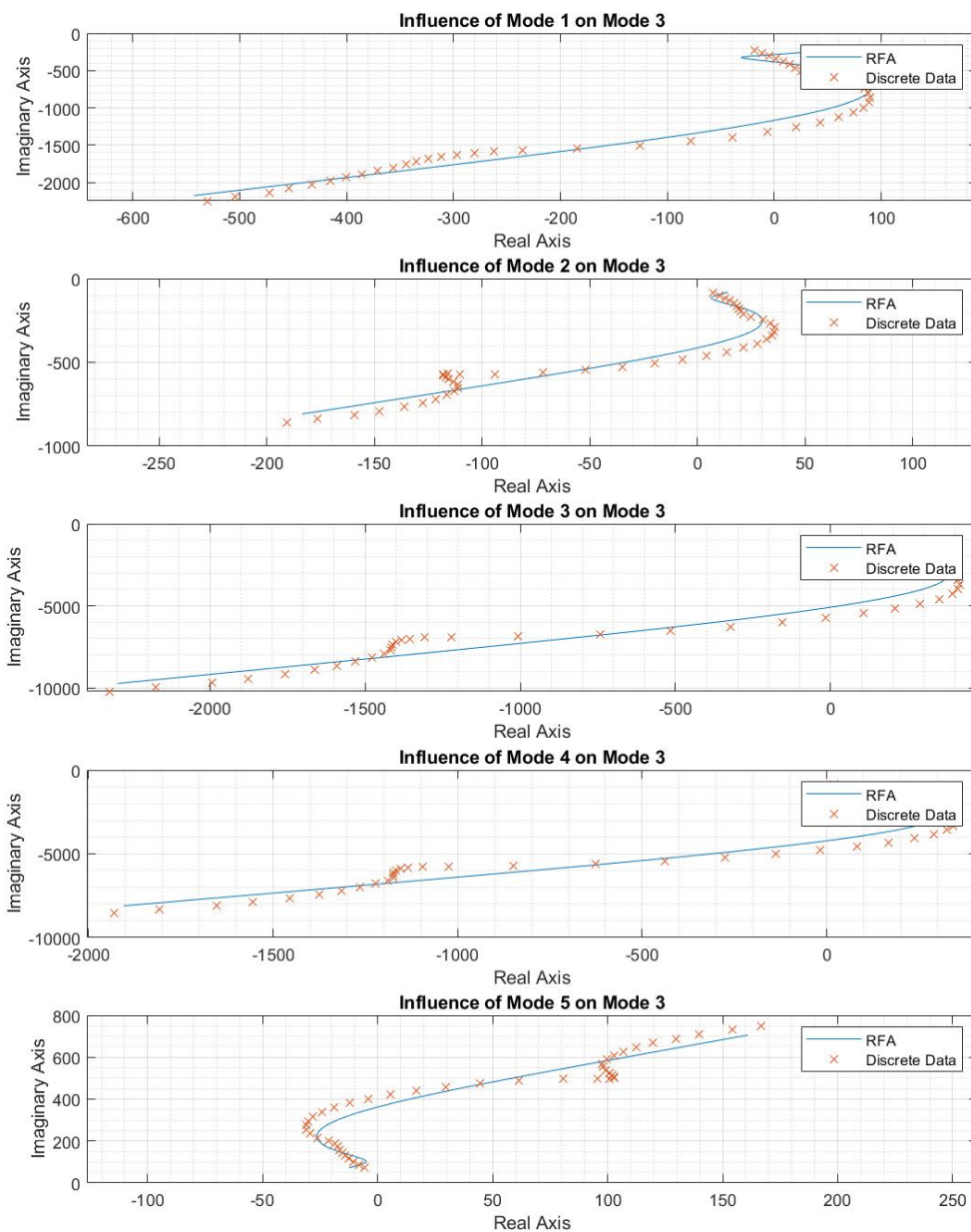
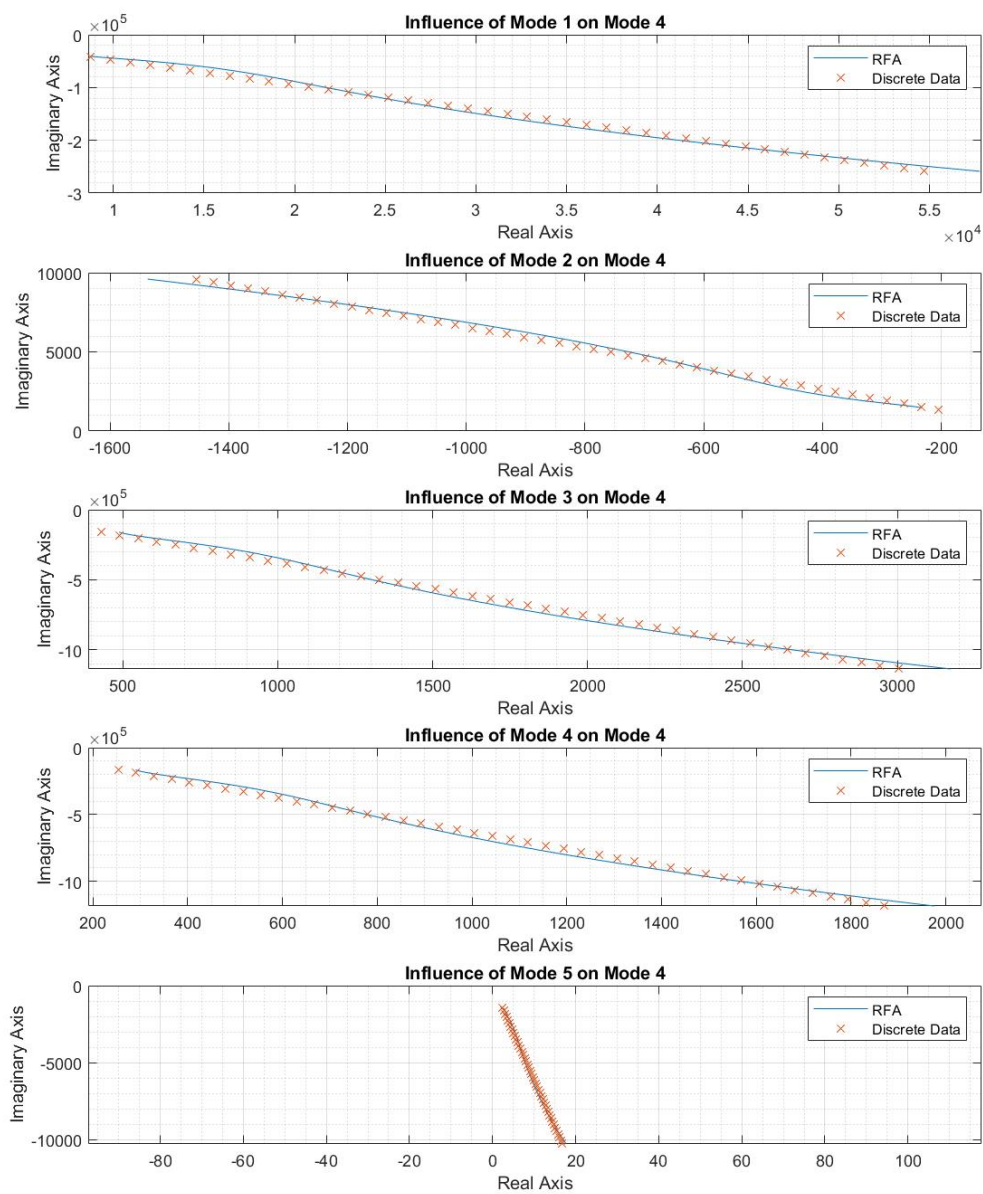*Figure C.18* Roger's Approximation for Mode 3 at Mach = 0.95
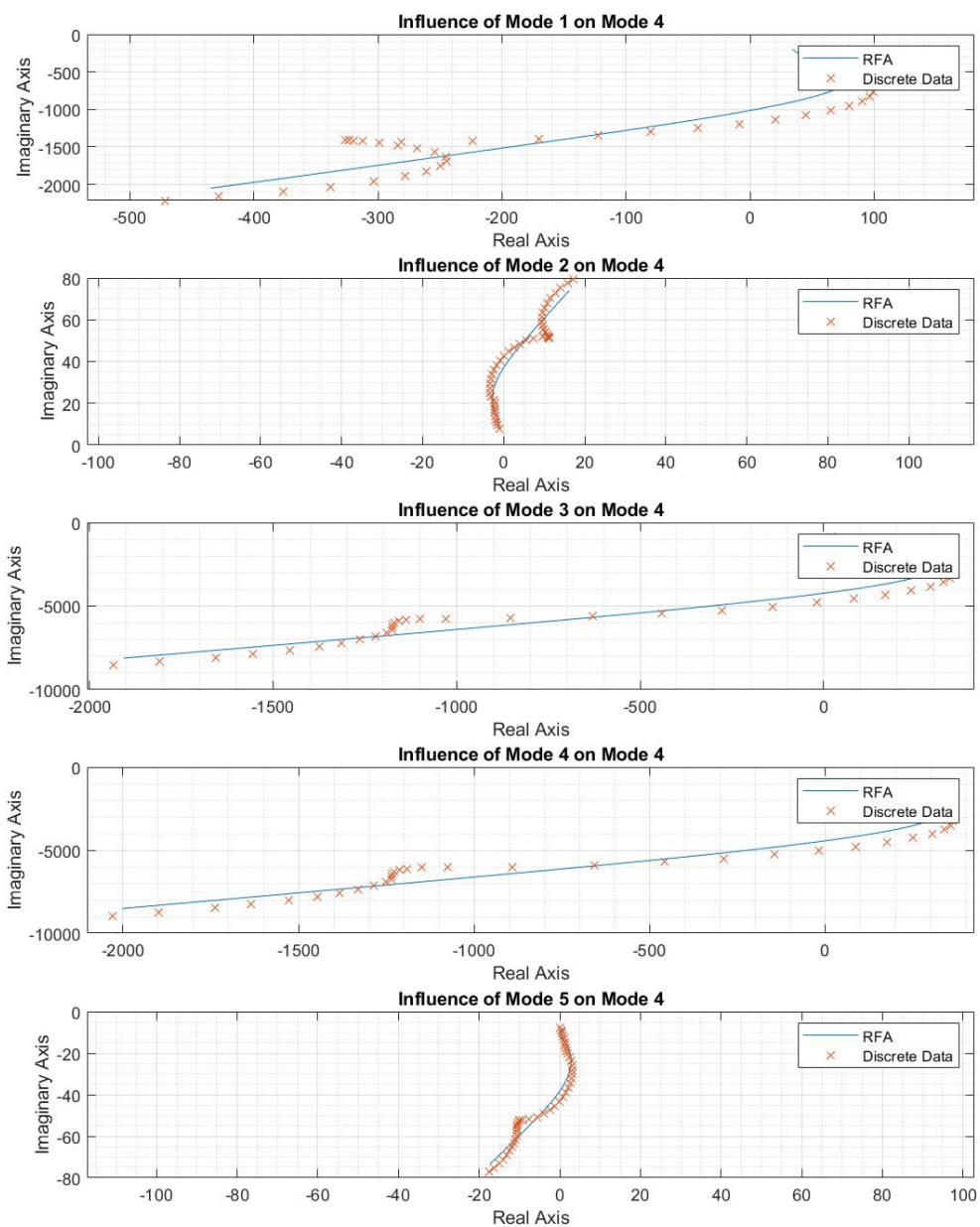
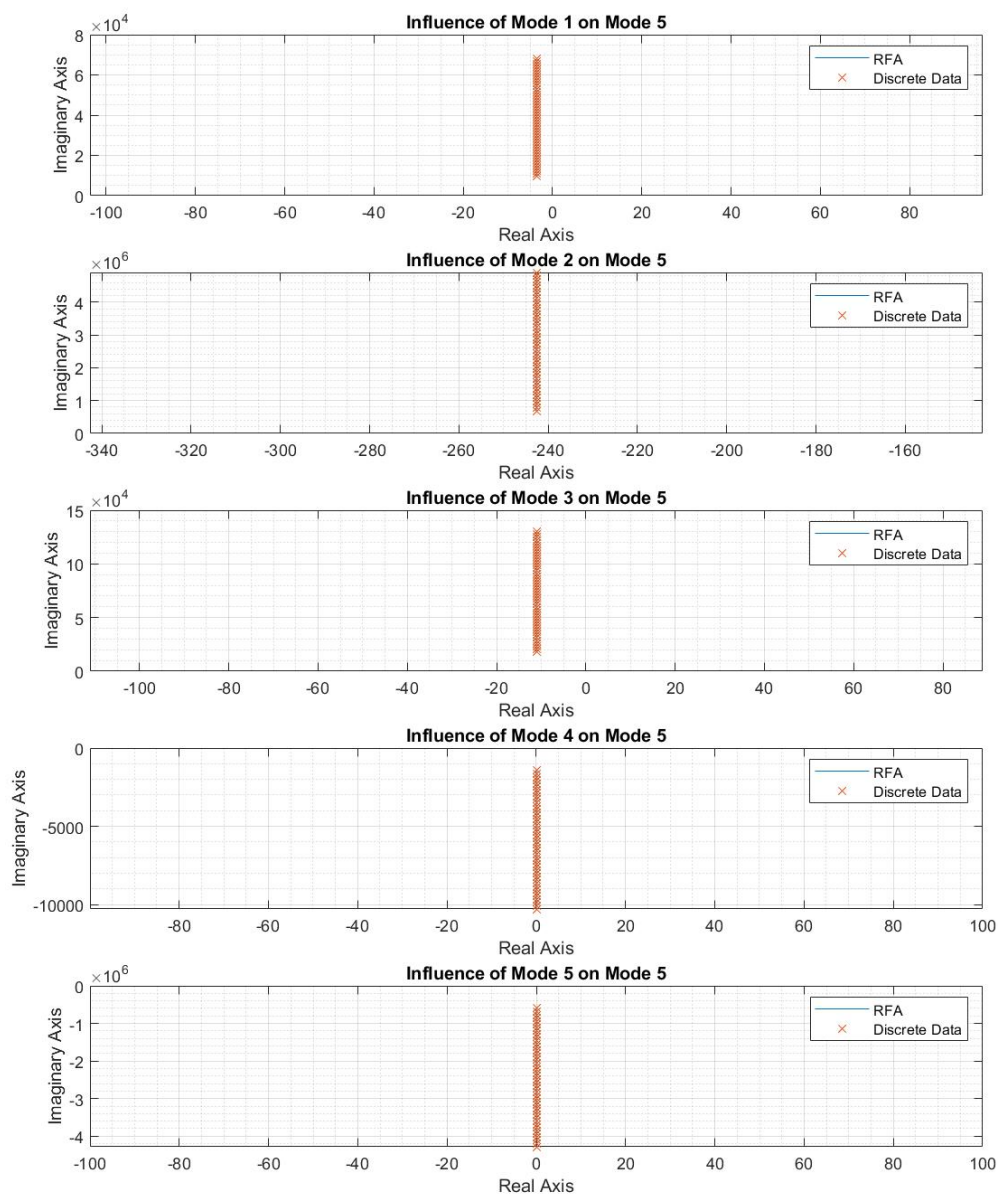*Figure C.19* Roger's Approximation for Mode 4 at Mach = 0.95
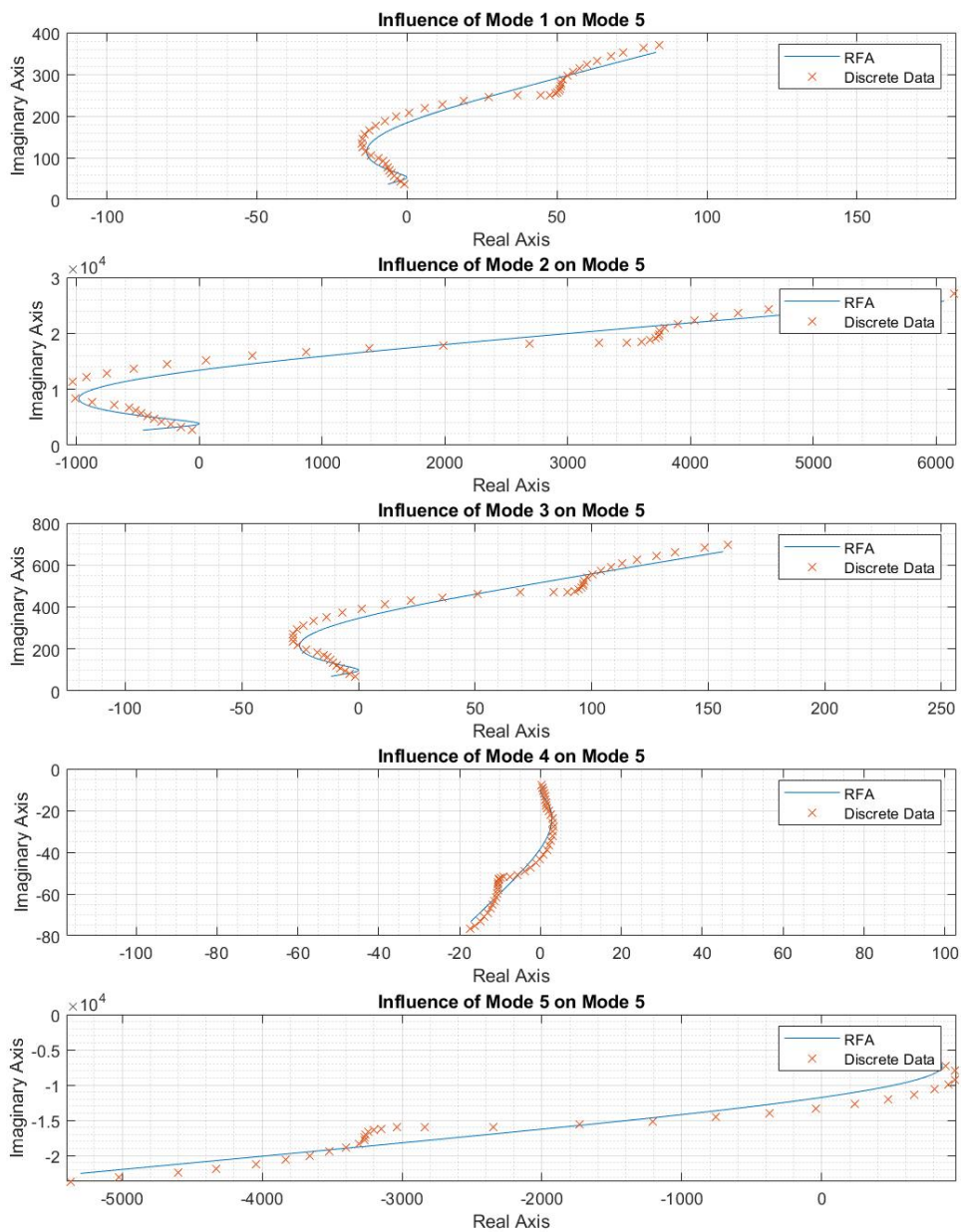
Figure C.20 Roger's Approximation for Mode 5 at Mach = 0.95

Figure C.21 Roger's Approximation for Mode 1 at Mach = 1.10

Figure C.22 Roger's Approximation for Mode 2 at Mach = 1.10

Figure C.23 Roger's Approximation for Mode 3 at Mach = 1.10

Figure C.24 Roger's Approximation for Mode 4 at Mach = 1.10

Figure C.25 Roger's Approximation for Mode 5 at Mach = 1.10

Figure C.26 Roger's Approximation for Mode 1 at Mach = 1.20

Figure C.27 Roger's Approximation for Mode 2 at Mach = 1.20

Figure C.28 Roger's Approximation for Mode 3 at Mach = 1.20

Figure C.29 Roger's Approximation for Mode 4 at Mach = 1.20

Figure C.30 Roger's Approximation for Mode 5 at Mach = 1.20

APPENDIX D - Summary of Nastran Results
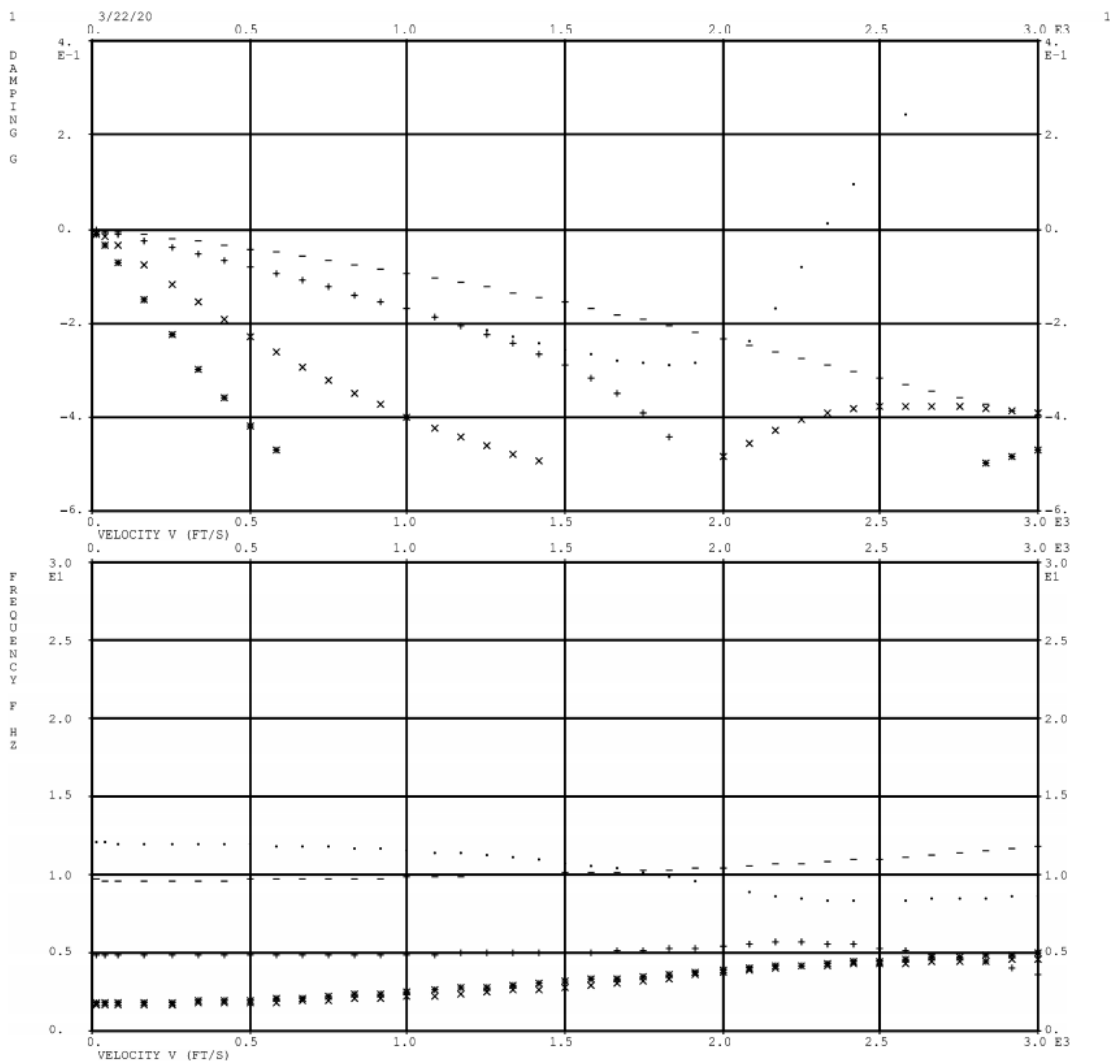
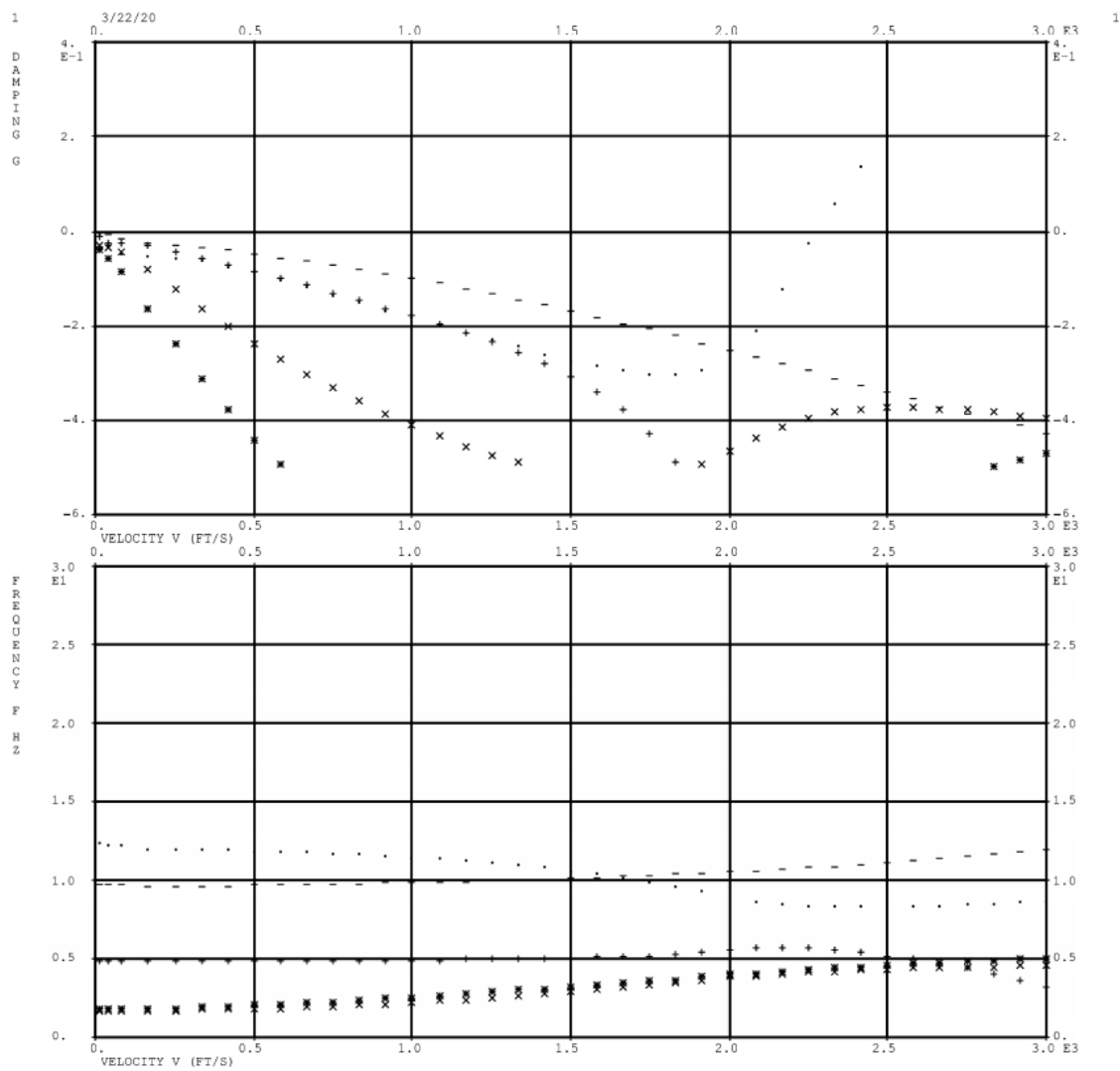*Figure D.1* V-g and V-ω curves for Mach = 0.00
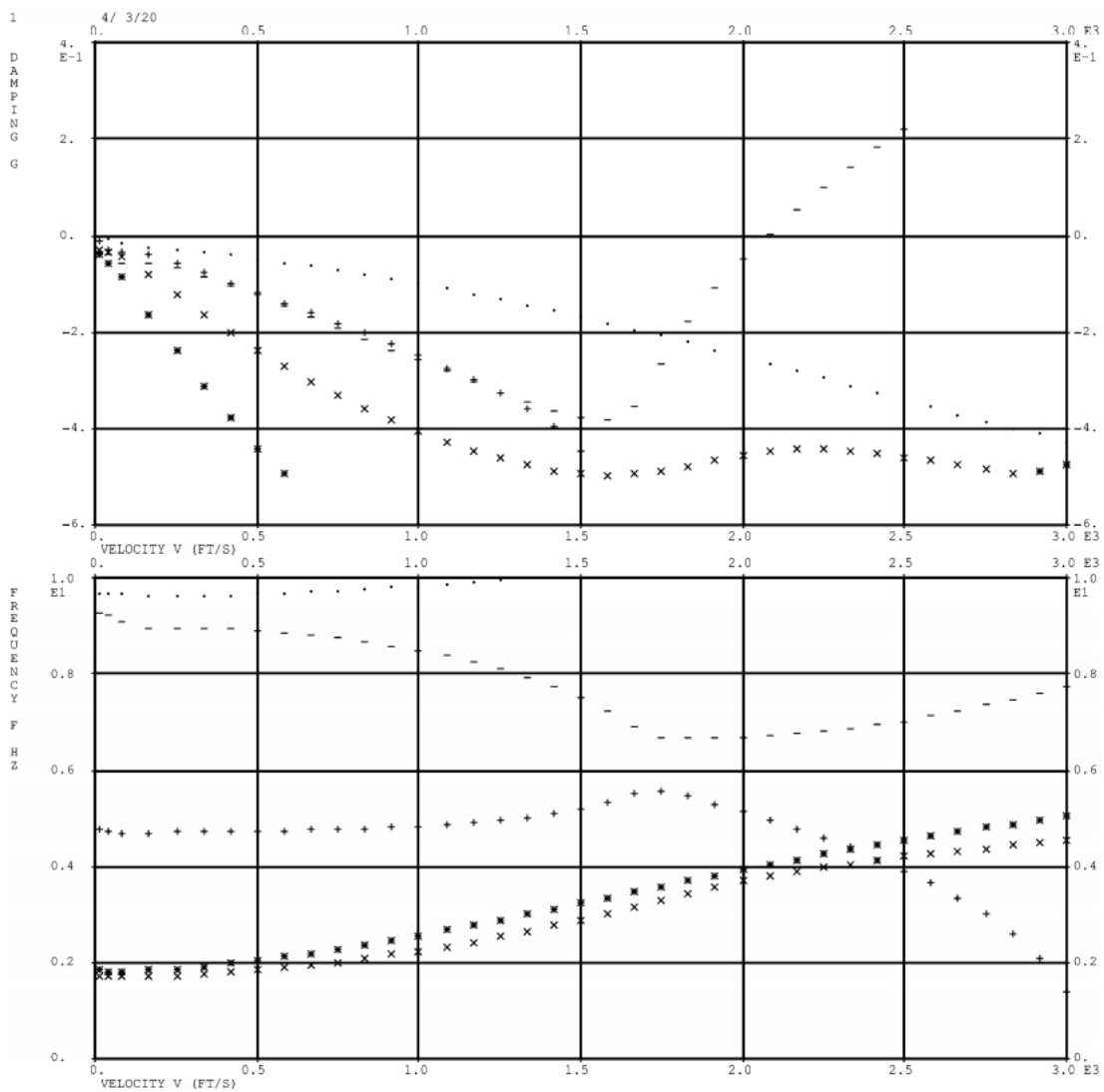
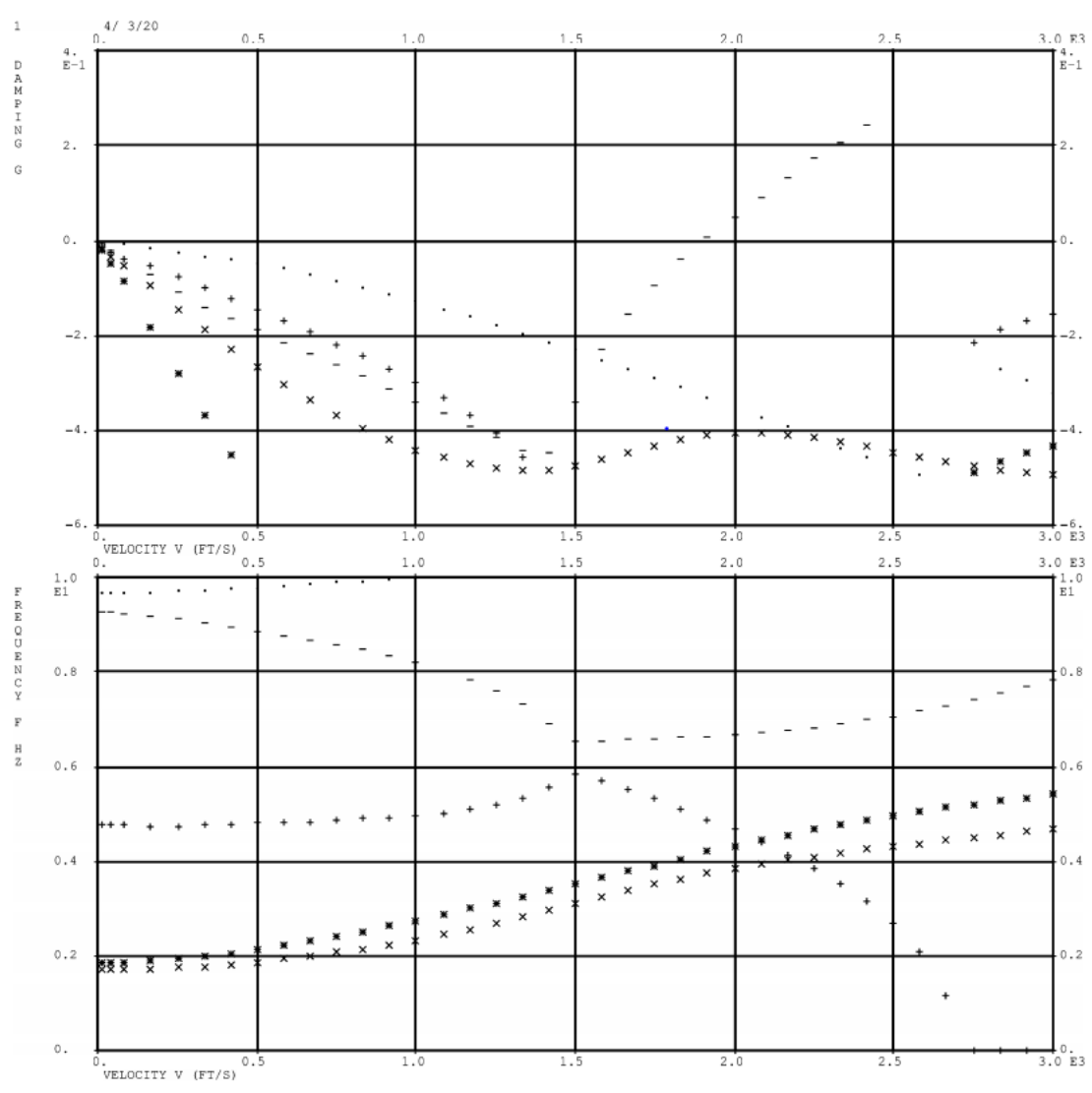*Figure D.2* V-g and V-ω curves for Mach = 0.50

Figure D.3 V-g and V-ω curves for Mach = 0.85

Figure D.4 V-g and V-ω curves for Mach = 0.95